Development and application of liquid chromatography-mass spectrometry for the analysis of nucleic acids

An-Wen Kung

A thesis submitted in partial fulfilment of the requirements for the degree of

Doctor of Philosophy

The University of Sheffield

Faculty of Engineering

Department of Chemical and Biological Engineering

November 2017

Acknowledgements

This thesis is the product of four years of hard work and perseverance, but I also owe a great debt to the many people who have generously supported me throughout my PhD.

First and foremost, this work would not have possible without the significant financial support from the Department of Chemical and Biological Engineering, the University of Sheffield as well as the generous contributions from the EPSRC HEFCE catalyst studentship co-sponsored by Syngenta UK.

I am forever indebted to my supervisor, Professor Mark Dickman for giving me the opportunity to work as part of his research group and for his unwavering support throughout my PhD and MSc, including training in the fundamentals of biomolecule analysis, guiding me on how to be an independent researcher, teaching me how to think critically when planning experiments or analysing data, as well as providing valuable feedback on my writing. Without his support, I would not be here today, nor would I have had the opportunity to work and learn so much, while collaborating with a world-class company like Syngenta.

I would like to express my deepest gratitude to my industrial supervisors Dr. David Portwood, and Dr. Peter Kilby for their considerable supervision and support during the HEFCE program and especially during my placement in Syngenta. Special thanks goes to Phil Clark who assisted me onsite during my time at Jealott's Hill.

I am fortunate to have gained experience in academic teaching, an opportunity facilitated by my mentor and friend, Dr. Mark Heslop has always been willing to lend an ear, even when dealing with personal issues. I can confidently say that my experience in teaching and marking has made my PhD a more productive, stimulating, and well-rounded experience.

I would like to give a big thank you to my colleagues: Dr. Alison Nwokeoji, for training me in important aspects of nucleic acid analysis during the initial stage of my PhD and also as a source of insight and discussion throughout; Dr. Phil Jackson and Dr. Caroline Evans, for their patience and generosity in teaching me the intricacies of mass spectrometry, such that I have gained skills and knowledge I would not have

otherwise; as well as all the members of my research group, especially Beata, Joby, and Tom, for their camaraderie and for fostering a joyful and cooperative work environment.

I owe a debt of gratitude to Dr. Esther Karunakaran who has given up many hours of her own free time to provide me with advice, both personal and academic, as well as moral support while acting as a mentor and successful role model for me to follow. I also thank Dr. Narciso Couto and Dr. Trong Khoa Pham for their help and technical guidance during the times I encountered roadblocks.

Another thank you goes to Dr. Clare Howarth from the University who acted as yet another one of my mentors and offered me advice and support during my writing up period.

During my PhD, I have encountered many tough periods, and I am grateful that I have had my best friends KYH, YC, and PZ by my side during those times. Their supports (emotional and otherwise) have been key motivators in helping me persevere, and I would not be here today if it were not for them.

Last but not least, I would like to thank my family, especially my mother, who has supported me in my PhD both emotionally and financially despite battling a major illness. Her insistence that I continue my studies and continued reassurance to not worry about her have been the greatest factors in helping me stay focused and motivated in achieving my goals. Thank you.

List of publication(s)

Publications arising from work presented in this PhD thesis.

An-Wen Kung, Peter M. Kilby, David E. Portwood, Mark J. Dickman. Quantification of dsRNA using stable isotope labeling dilution liquid chromatography mass spectrometry. Rapid communication in mass spectrometry. (2018), 15;32(7):590-596.

Alison O. Nwokeoji, An-Wen Kung, Peter M. Kilby, David E. Portwood, Mark J. Dickman. Purification and characterisation of dsRNA using ion-pair reversed-phase chromatography and mass spectrometry. Journal of Chromatography A, 1484 (2017) 14-25.

Manuscript(s) in preparation

Studying the effect of monolith porosity on the analysis of nucleic acids using ion-pair reversed-phase HPLC., An-Wen Kung, Phil Clarke, Peter M. Kilby, David E. Portwood, Mark J. Dickman.

Table of Contents

List of Figures

List of Tables

List of Abbreviations

Abbreviations	Full term
ACN	Acetonitrile
DC	Direct current
DIPA	Diisopropylamine
DNA	Deoxyribonucleic acid
DMSO	Dimethylsulfoxide
dsRNA	Double-stranded ribonucleic acid
EDTA	Ethylenediaminetetraacetic acid
ESI MS	Electrospray ionisation mass spectrometry
GuSCN	Guanidinium thiocyanate
GuHCl	Guanidine hydrochloride
HA	Hexylamine
HAA	N-hexylammonium acetate
HFIP	1,1,1,3,3,3,-Hexafluoro-2-propanol
HPLC	High-performance liquid phase chromatography
IPTG	Isopropyl-β-D-thiogalactopyranoside
IP RP HPLC	Ion-pair reversed-phase liquid phase chromatography
LC MS	Liquid chromatography mass spectrometry
LC ESI MS	Liquid chromatography electrospray ionisation mass spectrometry
NaCl	Sodium chloride
miRNA	Micro-ribonucleic acid
MS	Mass spectrometry
mRNA	Messenger ribonucleic acid
PCR	Polymerase chain reaction
Pre-mRNA	pre-messenger ribonucleic acid
RF	Radio frequency
RISC	RNA-induced silencing complex
RNA	Ribonucleic acids
RNAi	Ribonucleic acid interference
rRNA	Ribosomal ribonucleic acid
SELEX	Systematic evolution of ligands by exponential enrichment
SDS	Sodium dodecyl sulphate
shRNA	Small hairpin RNA
siRNA	Small interference ribonucleic acid
tRNA	Transfer ribonucleic acid

SPE	Solid-phase extraction
ssRNA	Single-stranded ribonucleic acid
TBA	Tributylamine
TBAA	Tetrabutylammonium acetate
TBAB	Tetrabutylammonium bromide
TEA	Triethylamine
TEAA	Triethylammonium acetate
TFE	Trifluoroethanol
TOF	Time of flight

Thesis abstract

There is currently a rise in demand for high throughput analytical tools that can readily purify, separate, and analyse nucleic acids. Recent discoveries on the pivotal functions of RNA in a wide range of biological systems have led to the potential application of RNA as therapeutic drugs to treat several serious diseases and as alternatives to chemical pesticides for insect management. This thesis focuses on the development and application of analytical approaches based on ion-pair-reverse-phase high-performance liquid chromatography (IP RP HPLC) and electrospray ionisation mass spectrometry (ESI-MS) for the analysis of RNA and oligonucleotides.

Buffer systems on ESI-MS were systematically tested by varying the concentrations of ion-pair reagents and organic modifiers to increase oligonucleotide ionisation efficiency. Optimal buffer systems were identified with respect to analyte type. Hydrophobic tags on oligonucleotides were tested to increase ESI-MS sensitivity. Different RNA extraction methods were compared and optimised based on extraction yields of dsRNA from engineered microbial cells. The performance, benefits, and drawbacks of various extraction methods were reported. LC-ESI-MS was also used in conjunction with *in vivo* and *in vitro* stable isotope labelling techniques for the quantitative analysis of dsRNA. The identification and absolute quantification of dsRNA in complex total RNA mixtures were performed.

The impact of porosity in monolithic columns on HPLC performance for nucleic acid analysis under both retentive (IP RP) and non-retentive HPLC modes was investigated. The RP-1S (standard porosity) and RP-2H (high porosity) columns achieved higher separation efficiencies for nucleic acids with larger molecular weights, while the RP-3U column (ultra-high porosity) showed optimum performance in analysing small oligonucleotides. High flow rates produced significant improvement in chromatographic resolutions regardless of column porosity. It was proposed from non-retentive mode analysis that micro, meso, and macropores exist within the RP-1S and RP-2H columns while only large channels or pores of limited accessibility exist in the RP-3U column.

Chapter I : Introduction

Ribonucleic acids (RNA) are one of the three major biological macromolecules involved in the central dogma of molecular biology, acting as an intermediary for genetic information between DNA and protein (Jacob and Monod, 1961). Research on RNA has been continuously growing with significant interest because of the essential roles it plays in many fundamental biological processes (Kruger et al., 1982; Guerrier-Takada et al., 1983; Fire et al., 1998a). Only recently, our understanding of the roles of RNA has been broadened to include a number of interesting functions such as the catalysis of biochemical reactions, the regulation of cellular processes, and gene functions (Guerrier-Takada et al., 1983; Fire et al., 1998a). In addition, it has been found that defective RNA and RNA viruses are involved in human diseases, further highlighting the importance of RNA in numerous biological processes and spurring extensive clinical research efforts for RNA-based drugs to cure these diseases (Melnikova, 2007). These drugs, which include small interfering RNA (siRNA) and antisense oligonucleotides have shown unprecedented versatility as biotherapeutic tools (Burnett and Rossi, 2012). Due to the important role that RNA plays in a variety of biological systems and its emerging industrial importance as bio-therapeutics and as alternatives to chemical pesticides (Mao et al., 2007; Baum et al., 2007), demand for the development of high-throughput analytical platforms such as liquid chromatography and mass spectrometry to characterise and quantify RNA have increased greatly.

1.1 Deoxyribonucleic acids (DNA)

Deoxyribonucleic acids comprise double strands of long polynucleotides, with individual strands called DNA strands. The two strands are held together via hydrogen binding between the base portions of nucleotides. The four nucleotide bases in DNA are adenine (A), cytosine (C), guanine (G), and thymine (T).

1.2 Ribonucleic acids (RNA)

Ribonucleic acids (RNA) are linear polynucleotide chains composed of four ribonucleotide bases namely, adenine (A), cytosine (C), guanine (G), and uracil (U), which are chemically attached via phosphodiester bonds (Figure I-1). A ribonucleotide is composed of a nitrogenous base, a phosphate group, and a ribose sugar. RNA are involved in the regulation of cellular functions in all living cells. Multiple types of RNA exist within cells, and the three major classes of cellular RNA involved in protein synthesis are protein-coding messenger RNA (mRNA), the non-protein-coding RNA such as transfer RNA (tRNA) and ribosomal RNA (rRNA). A class of small non-coding RNAs which includes siRNA and miRNA are responsible for regulating gene expression. All of these RNA types are described in the following sections.

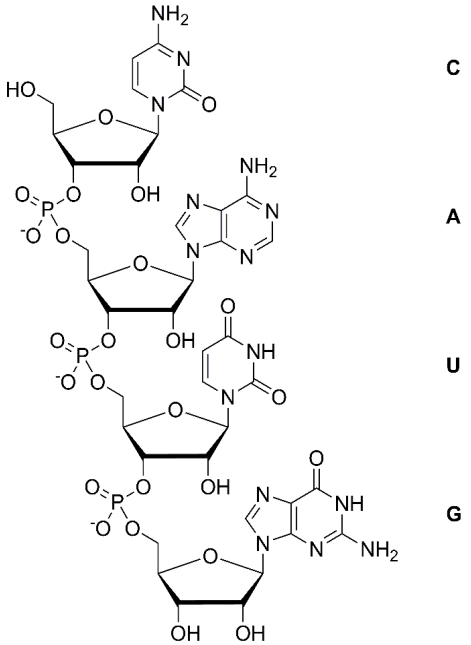

Figure I-1: Chemical structure of an RNA ribonucleotide (C: cytosine, A: adenine, U: uracil, G: guanine).

1.2.1 Messenger RNA (mRNA)

In the protein synthesis process, messenger RNA acts as an intermediary to convey genetic information from DNA to ribosomes (Jacob and Monod, 1961). The transcription of mRNA from DNA occurs through the copying of information encoded in a gene onto an RNA molecule called the precursor mRNA or pre-messenger RNA (pre-mRNA), which is subsequently processed into mature mRNA (Soller, 2006). These genetic codes are in the form of codons, each consisting of triplets of nucleotides. Codons begin with (AUG), which encodes for a specific amino acid. Each codon encodes for a different amino acid with the exception of three stop codons which terminate protein synthesis: UAA, UGA, and UAG, (Brenner et al., 1961; Brenner et al., 1965; Brenner et al., 1967).

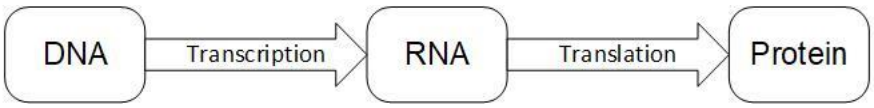

Figure I-2: The central dogma of molecular biology. Genetic information is transferred from the double strands of DNA onto a single strand of mRNA, where it is converted into a polypeptide amino sequence that folds to form a protein.

1.2.2 Ribosomal RNA (rRNA)

Ribosomal RNA (rRNA) is components of ribosomes (approximately 60%) which are transported to the cytoplasm to aid in the translation of information from mRNA into protein. They are synthesised in the nucleolus, which also contains the essential genes to encode rRNA. Encoded rRNA is differentiated by sizes, which are described as either large or small and all ribosomes contain at least one of each. In the nucleolus, the rRNA complex with ribosomal proteins to form two subunits: large subunits (LSU) (the 50s) and small subunits (SSU) (30S) of the ribosome in bacteria. During translation, the rRNA in LSU acts as an enzyme (ribozyme) which catalyses the linking of amino acids together to form polypeptides (Alberts et al., 1989).

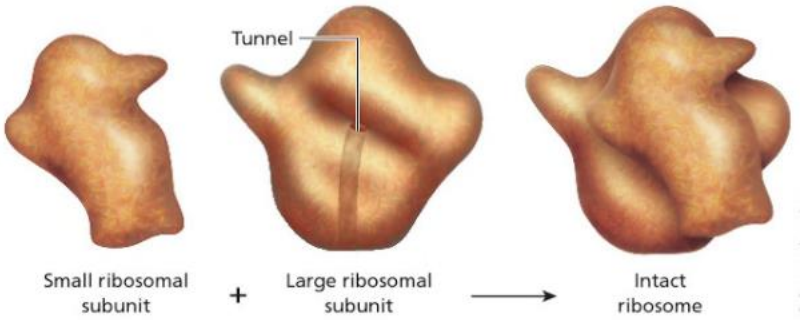

Figure I-3: Three-dimensional models of the small and large subunits of ribosomes. Each ribosomal subunit is made of proteins and ribosomal RNA (rRNA). Reprinted from *Human Heredity: Principles and Issues* (p. 201) by M. R. Cummings (2014), USA. Copyright 2014 by Brooks/Cole, Cengage Learning. Reprinted with permission.

1.2.3 Transfer RNA (tRNA)

Transfer RNA (tRNA) are a form of short-chain RNA, approximately 80 nucleotides in length, and serve as adaptors to link mRNA and amino acids (Sprinzl et al., 1976). During translation, tRNA recognises and binds to the specific codons of the mRNA and decodes them into specific amino acids at the ribosomal site (Sprinzl et al., 1976). In eukaryotic cells, tRNA is synthesised from a larger precursor tRNA by RNA polymerase III via splicing, folding, and chemical modifications, resulting in four, short double-helical segments resembling, a cloverleaf structure (Altman and Stark, 1974; Smith, 1975). The cloverleaf structure of the tRNA undertakes further folding, facilitating the formation of an L-shaped structure which is held together by hydrogen bonds between different regions of the molecule (Kim et al., 1974; Moras et al., 1980). This L-shaped tRNA structure has two regions of unpaired nucleotides located at each end. The first region contains three nucleotides (called the anticodon) complementary to a codon in an mRNA. The other is a short single-stranded region where the 3'-terminal for the corresponding amino acid attachment specified by that codon attaches to the tRNA (See Figure I-4) (Alberts et al., 2002).

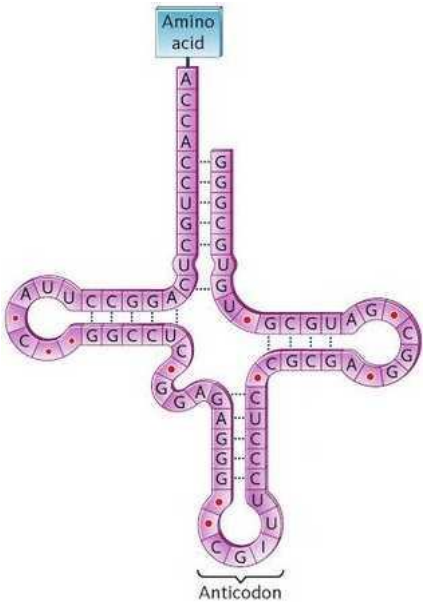

Figure I-4: A transfer RNA molecule (tRNA). tRNA contains two regions, an anticodon region (a three nucleotides sequence) which binds to the complementary codons of the mRNA, and a region on another end which binds to amino acids that correspond to the anticodon. Reprinted from *Human Genetics and Society* (p. 110) by R. Yashon and M. Cummings (2012), USA. Copyright 2012 by Brooks/Cole, Cengage Learning. Reprinted with permission.

1.2.4 Small non-coding RNA

Small non-coding RNA such as small interference RNA (siRNA) and microRNA (miRNA) are molecules that control gene expression in eukaryotic cells (Bernstein et al., 2001; Pasquinelli and Ruvkun, 2002). The siRNA molecule is a small double-stranded RNA molecule of approximately 20 base pairs in length (Figure I-5), is generated from the cleavage of dsRNA by the RNase III enzyme, Dicer, and targets perfectly matching mRNA for cleavage via a siRNA-protein complex (Bernstein et al., 2001). On the other hand, miRNA can target many different mRNA sequences due to the imperfect pairing, inhibiting translation, and is the result of a small hairpin precursor cleaved to the relevant size by Dicer (Pasquinelli and Ruvkun, 2002). The role that small non-coding RNA plays in inhibiting translation was first discovered through a short, double-stranded RNA in *C. elegans*. This molecule was complementary to the sense strand of mRNA, binging to its 3' untranslated region and resulting in specific degradation (Lee et al., 1993). This gene-specific degradation by small non-coding RNA is known today as RNA interference (RNAi), which is detailed in section 1.3.5.

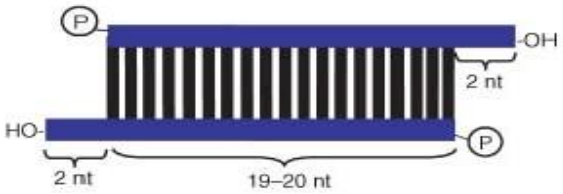

Figure I-5: Schematic illustration of siRNA. siRNA consists of two RNA nucleotides forming a duplex core (19-20 bp), with 2 nucleotide (nt) overhangs on both of the 3' ends. The 3' ends are hydroxyls (OH) and the 5' ends contain monophsphorylated (P). Reprinted from "Biogenesis and function of endogenous and exogenous siRNAs," by N. Snead and J. Rossi (n.d.), *Wiley Interdisciplinary Reviews: RNA*, 1(1), p. 117-131. Copyright 2003 by John Wiley and Sons. Reprinted with permission.

1.2.5 Double-stranded RNA

Double-stranded RNA (dsRNA) are molecules with an unique form appearing with two complementary strands, instead of the single-stranded structure which is more common for this type of genetic material. Molecules of dsRNA act as signals for gene-specific silencing in a phenomenon known as RNA interference (RNAi), leading to specific degradation of the targeted mRNA in eukaryotic cells or any organism that can respond to gene-specific dsRNA.

The occurrence of RNAi was first demonstrated after researchers attempted the injection of dsRNA into a worm (*Caenorhabditis elegans*) and observed the corresponding gene disappear (Fire et al., 1998). This phenomenon has also been demonstrated in many other eukaryotic cells by other researchers (Ngô et al., 1998; Kennerdell and Carthew, 1998; Voinnet et al., 1998; Waterhouse et al., 1998). This dsRNA-mediated interference has been generalised to another level of control over the gene regulation and expression.

Double-stranded RNA can be synthesised either in a bacterial system or through *in-vitro* transcription for the purpose of RNAi (Li et al., 2011; Palli, 2014). Timmons and Fire found that the use of short-length dsRNA can cause a restriction in penetrance and expressivity (Timmons and Fire, 1998); dsRNA engineered in an *E. coli* BL21 (DE3) strain showed degradation in some parts caused by endonuclease RNase III digestion (Timmons et al., 2001). Using an RNase III-deficient *E. coli* strain called HT115 to engineer dsRNA, they produced high quantities of specific dsRNA, which

activated effective interference when they were fed to cells of *C. elegans* (Timmons et al., 2001). This finding shows that exploiting *E. coli* cells which lack RNase III or using an *in-vitro* transactional process allows for the cost-effective production of large quantities of dsRNA, thus enabling the delivery of siRNAs to target organisms (Timmons and Fire, 1998; Aalto et al., 2007; Maori et al., 2009).

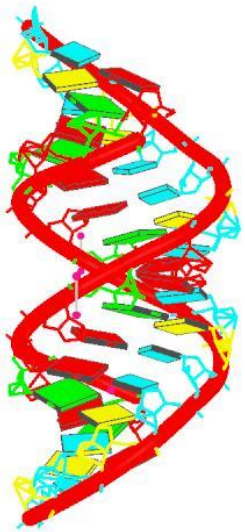

Figure I-6: Tertiary structure of a 16-mer dsRNA. The distinguishing feature between the structures of RNA and DNA is the presence of a hydroxyl group located at the 2' position of the ribose sugar of RNA, which constrains the helix to the A-form geometry. A consequence of the A-form geometry is that that the major grooves will be narrow and deep while the minor grooves will be wide and shallow. Image from the RCSB PDB (www.rcsb.org) of PDB ID 3ND4 by B. H. Mooers and A. Singh (2011) in "The crystal structure of an oligo(U):pre-mRNA duplex from a trypanosome RNA editing substrate." *RNA*, 17: 1870-1883. Reprinted with permission under RCSB PDB copyright policies.

1.3 Nucleic acid therapeutics

Recent discoveries of nucleic acid-based therapeutic drugs show great promise under clinical investigation for combating a wide variety of human major diseases including cardiovascular genetic disorders, AIDS infectious disease and various cancers (Burnett and Rossi, 2012).

The first oligonucleotide therapeutic drug to launch on the market was fomivirsen (Vitravene®, Isis Pharmaceuticals, CA, USA), an antisense therapy based drug that was approved in 1998 and was used to treat cytomegalovirus retinitis (Roehr, 1998). However, fomivirsen was discontinued in 2007 due to improvements in HIV medications. As of 2016, only two oligonucleotide drugs have reached the market besides fomivirsen, pegaptanib and mipomersen (

Table I-1) (Offord, 2016). Pegaptanib, which was approved in 2004 is an aptamer oligonucleotide that can block specific proteins and is used to treat age-related macular degeneration. It was quickly substituted by a more effective monoclonal antibody. Mipomersen is an antisense oligonucleotide designed for the treatment of a genetic form of high-cholesterol (Offord, 2016).

The slow advancement of nucleic acid-based drugs has not prevented more than 70 oligonucleotide therapeutics from reaching or even completing clinical testing for the treatment of cancers, viruses, and genetic disorders. RNA oligonucleotides hold both therapeutic and commercial promise as shown by a recent report estimating that the global antisense and RNAi therapeutics market will reach $ 4.58 billion by 2022 (Offord, 2016).

Table I-1 Commercialised oligonucleotide drug sequences of in 2016

Drug name	Sequence
Pegaptanib	5’-[40kD]-[HN-$(CH_2)_5$O]- $pC_fpG_mpGmpA_rpA_rpU_fpC_fpA_mpG_mpUfpG_mpA_mpA_m$ $pU_fpG_mpC_fpU_fpU_fpA_mpUfpA_mpC_fpAmpU_fpC_fpC_fpG_m$3’-p-dT
Mipomersen	2’MOE 2’Deoxy 2’MOE 5’-GCCTCAGTCTGCTTCGCACC Phosphorothioate backbone

1.3.1 The application of RNAi in agriculture improvement

In agriculture, insect pests incur significant costs and are a growing threat due to ever-present insecticide resistance, leading to efforts to research alternative pest-control

strategies. The RNA interference (RNAi) approach has been successfully demonstrated as a powerful tool in coleopteran and lepidopteran pests control (Mao et al., 2007; Baum et al., 2007), and can be used to engineer pathogen-resistant plants by altering plant gene expressions (Duan et al., 2012).

The RNAi defence mechanism can down-regulate any gene effectively driven by the induction of double-stranded RNA (dsRNA) (Fire et al., 1998), resulting in high- quality traits, such as combined resistance to biotic and abiotic stresses and improved of nutritional content in crops (Saurabh et al., 2014). The regulatory potential of RNAi is immense and has led to breakthroughs in agricultural improvement.

1.3.2 Classification of RNA based therapeutics

RNA-based therapeutics have unprecedented versatility as demonstrated by their multiple classifications based on mechanisms of action. These mechanisms include antisense, an mRNA translation inhibitor; siRNA, an agent involved in RNA interference; ribozymes, which are catalytically active RNA molecules; and aptamers, which are RNA molecules that bind to proteins and other specific ligands.

Table I-2: Specification of different type of RNA based therapeutics

Type	Structure	Target	Key action
Antisense oligonucleotide	Single-stranded DNA or RNA	Messenger RNA (mRNA) or pre-mRNA	Block ribosomal translation
Small interfering RNA (siRNA)	Double-stranded RNA	mRNA	siRNA to trigger target degradation
MicroRNA	Double-stranded RNA	mRNA	miRNA to inhibit translation
Ribozymes	Single-stranded RNA or transcribed therapeutic genes	Specific phosphodiester bonds	Catalyse site-specific self-cleavage of RNA
Aptamer	Single-stranded DNA or RNA	Small molecules, proteins, toxins, or whole cells	Inactivates or modifies targets

1.3.3 Antisense oligonucleotides

An antisense oligonucleotide is composed of short, single-stranded DNA or RNA oligonucleotide fragments of approximately 12-25 nucleotides in length that have undergone specific chemical modifications designed to increase stability (Crooke, 1999). The genetic sequences of antisense oligonucleotides are deliberately designed to be complementary to a target messenger RNA (mRNA). This complementarity allows antisense oligonucleotides to suppress targeted genes by inhibiting ribosomal translation of mRNA, disrupting a vital link in the protein synthesis process. In contrast, most conventional drug compounds are designed to interact with protein molecules by changing their structure and function, in order to restrain the causes of disease-potentiating or disease signalling pathways (Overington et al., 2006).

1.3.4 Antisense mechanism

The inhibition of RNA function following the binding of oligonucleotides to target RNA is a key feature of antisense oligonucleotides. Multiple antisense mechanisms exist for this purpose, and the best-characterised ones either result in the target RNA's cleavage by endonuclease such as RNase H or exploit nuclease association through a more elaborate pathway called RNA interference (RNAi) (Dean and Bennett, 2003).

1.3.4.1 RNase H Mechanism

RNase H is a ubiquitously expressed cellular enzyme which catalyses the hydrolysis of RNA strands from either an RNA or DNA heteroduplex. The RNase H mechanism is the most utilised method in clinical trials for antisense drugs due to its well-characterised pharmacology, toxicity, and pharmacokinetics (Dean and Bennett, 2003). Antisense oligonucleotides contain a continuous segment of approximately 5-7 DNA-like nucleotides that can inhibit gene expression via the RNase H-mechanism and support RNase H activity (Monia et al., 1993; Wu et al., 1999).

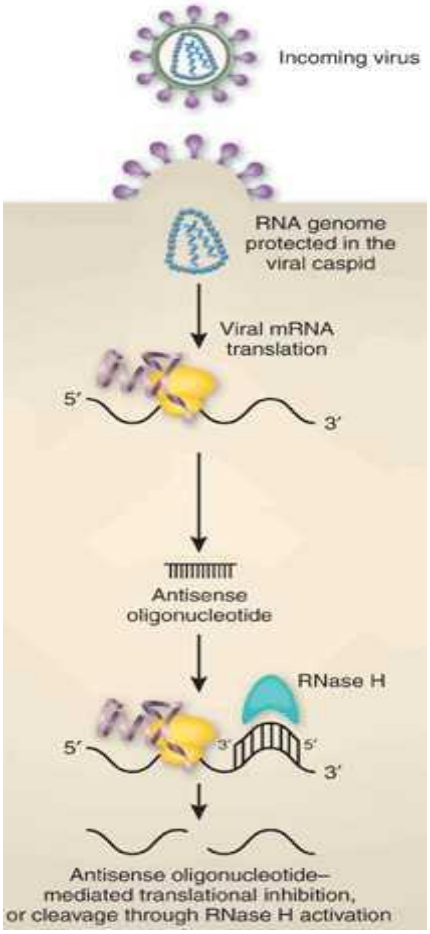

Figure I-7: The RNase H-dependent antisense pathway. Firstly, single-stranded oligonucleotides are transited through the plasma membrane, either through (poorly characterised) natural processes or by the utilisation cationic lipids as facilitators. After entering the cytoplasm, the oligonucleotides promptly accumulate in the cell nucleus. Once the oligonucleotides bind to their targeted mRNA within the cell nucleus, the oligonucleotide/RNA duplex would be "recognised" as a substrate by the enzyme RNase H. Finally, RNase H cleaves the RNA strand, thereby releasing the antisense oligonucleotide strand. Reprinted from “RNA interference against viruses: strike and counterstrike,” by J. Haasnoot, E. Westerhout, and B. Berkhout (2007), *Nature Biotechnology*, 25, p. 1435. Copyright 2007 by Springer Nature. Reprinted with permission.

1.3.5 siRNA therapeutics-RNA interference

Small interfering RNA (siRNA) are 21-23 nucleotides-long, double-stranded RNA with an antisense active strand that is exactly complementary to a sequence anywhere in the target mRNA. The RNAi process is initiated by RNase III enzymes (such as ‘Dicer’) which cleave either synthetic dsRNA or small hairpin RNA (shRNA) in order to produce small interference RNA (siRNA) and micro RNA (miRNA); small RNA molecules

central to the RNAi process (Dean and Bennett, 2003). Both molecules have the ability to bind with specific mRNA to either increase or decrease their activities by preventing the translation of that mRNA into a protein. The binding process is facilitated by the incorporation of siRNA and miRNA into an RNA-induced silencing complex (RISC), producing an siRNA-RISC complex or miRNA-RISC complex and leading to the degradation of its homologous target mRNA by endonucleases (see Figure I-8).

RNA-based therapeutics usually target mRNA, but may also target miRNA. An example of a miRNA-based drug is miravirsen (developed by Santaris Pharma A/S) which targets an endogenous miRNA in the liver necessary for Hepatitis C virus (HCV) infections (Lanford et al., 2010). In addition, an siRNA drug OPI-1007 has been developed by Quark Pharmaceuticals which targets caspase-2 to treat vision loss due to causes related to the optic nerve. Another example of an siRNA drug is SYL04002, which was developed by Sylentis to hinder the production of aqueous humor to ease intraocular hypertension (Guo et al., 2002).

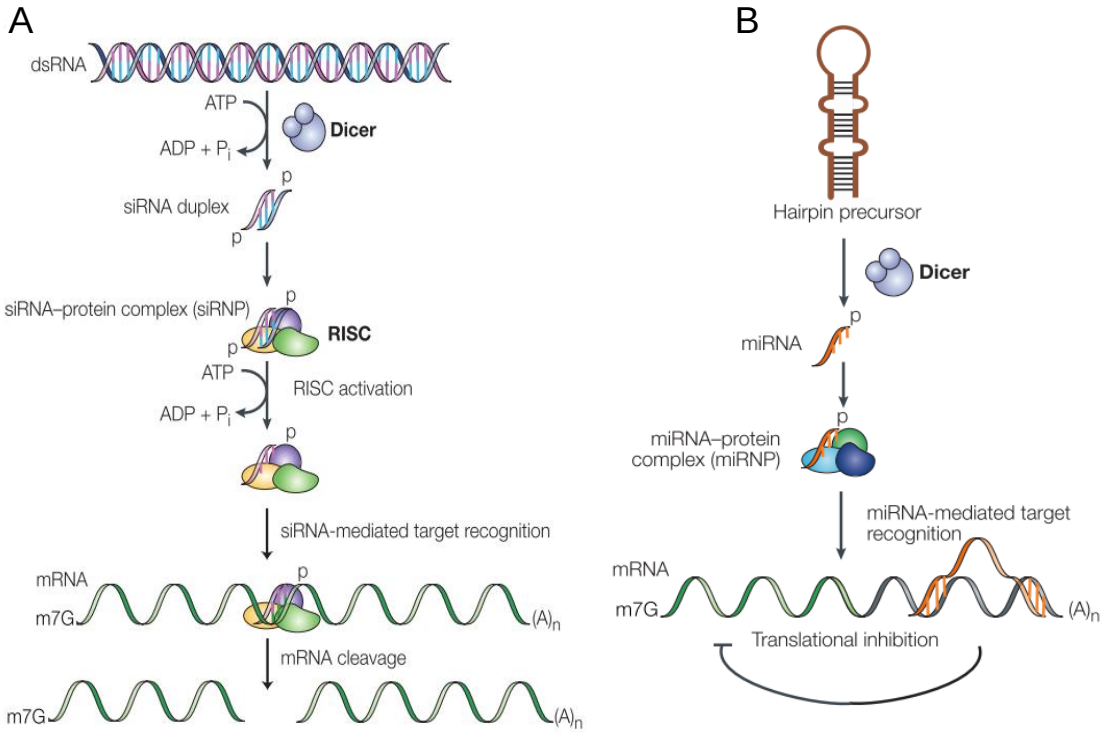

Figure I-8: The RNA interference antisense mechanism. The steps involved in the RNAi pathway: (A) Double-stranded RNA oligonucleotides enter through the plasma membrane via either (uncharacterised) natural processes or facilitators. The ATP-dependent RNase III enzyme “Dicer” initiates the process by cleaving the long double-stranded RNA (dsRNA). This results in a shorter double-stranded RNA, also known

as siRNA which contains 21-25 base pairs. Once it reaches the cytoplasm, siRNA are recognised and bound to the RISC, a protein complex. Next, the two RNA strands unwind (requiring ATP) and stimulate in the single-stranded antisense strand, serving to "guide" the RISC to bind to the target messenger RNA which has a complementary sequence. After the target mRNA are bound, they are cleaved by a ribonuclease, and the antisense strands are hydrolysed. (B) The microRNA pathway: the cleavage of the hairpin miRNA precursor (~70 nt) into a miRNA (~22 nt). miRNA is activated by Dicer. miRNA differs to siRNA, in which a single strand is incorporated into the miRNA-protein complex. The partial sequence of miRNA is complementary to the target mRNA, resulting in translational repression. Reprinted from “Killing the messenger: short RNAs that silence gene expression,” by D. M. Dykxhoorn, C. D. Novina, and P. A. Sharp (2003), *Nature Reviews Molecular Cell Biology*, 4(6), p. 457-467. Copyright 2003 by Springer Nature. Reprinted with permission.

1.3.6 Ribozymes

Ribozymes are self-processing catalytic RNA molecules that catalyse specific self-cleavage and ligation reactions (Burnett and Rossi, 2012). These reactions occur at specific phosphodiester bonds via base-pairing and interactions aligning the cleavage site within the ribozyme active site (Doudna and Cech, 2002).

The substrate that stimulates site-specific cleavage and recognises the domain of ribozymes can be engineered in *cis* (the same nucleic acid strand) or *trans* (a non-covalently linked nucleic acid) (Scherer and Rossi, 2003). Ribozymes enable gene expression through RNA site-specific cleavage; thus making ribozymes RNA therapeutics and diagnostic agents. In addition, ribozymes can be engineered as biosensors termed ‘riboswitches’, which are capable of switching on and off while being bound to small-molecule allosteric effectors (Wieland et al., 2010; Liang et al., 2011).

Ribozymes are similar to siRNA/shRNA therapeutics and can be delivered in RNA form to target cells or transcribed from therapeutic genes. Merck and Sirna currently holds a licensed for Angiozyme (RPI.4610), which is the first synthetic ribozyme to be tested clinically and which acts by targeting a specific mRNA related to angiogenesis and tumour growth in order to treat them (Kobayashi et al., 2005). Another target of ribozyme treatment is HIV; despite lack of success, there have been efforts to utilise CD4+T-cells or CD34+hematopoietic stem cells (HSCs) due to them being more

favourably infected by HIV-1 (Wong-Staal et al., 1998; Macpherson et al., 2005; Amado et al., 2004; Michienzi et al., 2003).

1.3.7 Aptamers

Therapeutic aptamers are short, single-stranded oligonucleotides (of 20-60 nucleotides) that are capable of binding to target molecular ligands. This capability terms from their specificity, which allows them to fold into a 3-dimensional structure, giving them high affinity and high specificity for the targeting of various molecules (Ellington and Szostak, 1990). Aptamers are engineered from multiple rounds of *in vitro* or *in vivo* selection through the process of SELEX (systematic evolution of ligands by exponential enrichment) with the desired characteristics. During SELEX, random nucleotides are selected from a large, initial oligonucleotide pool (IOP) for binding to a wide range of targeting molecules. The modulation of their functions is analogous to antibodies, which is why aptamers are often called nucleic acid antibodies (Keefe et al., 2010).

Aptamers are considerably easier and cheaper to produce than antibodies and are neither immunogenic nor toxic. These advantages are significant and have led to aptamers becoming an ideal candidate for numerous applications such as diagnostic and therapeutic tools as well as biosensors (Cibiel et al., 2012; Yang et al., 2011).

Several RNA-based aptamers have been developed and clinically tested. Pfizer/Eyetech have licensed an FDA-approved drug using a VEGF-specific modified RNA aptamer (sold as Macaugen) for the treatment of age-related macular degeneration (AMD) (Keefe et al., 2010; Thiel and Giangrande, 2009). Aptamers have also been modified to respond to other effector RNA, such as the REG1 dual-aptamer therapy developed by Regado Biosciences for acute coronary syndrome (ACS) (Cohen et al., 2010).

1.4 Oligonucleotide synthesis

1.4.1 Synthesis methods

Clinical research on oligonucleotides requires ranging amounts of material (from a few grams up to several kilograms) depending on the application. While small-scale synthesis of oligonucleotides is relatively attainable, large-scale production of a sufficient quality remains a challenge due to the high costs of the required reagents and chemicals, environmental safety regulations, and the scarcity of raw materials (Sinha et al., 2006). To improve the situation, synthetic techniques are being researched to manage large-scale synthesis at high throughput levels (Murgha et al., 2014).

Phosphoramidite chemistry has become the most widely applied solid phase synthesis technique, allowing convenient synthesis of oligonucleotides using nucleoside phosphoramidites as building blocks (Wei, 2013). Its advantages include easy implementation, efficient separation of end products and sufficiently high yields (Amarnath and Broom, 1977; Beaucage and Caruthers, 1981).

Despite these advantages, purification remains a necessary step due to the impurities generated by the synthesis process (Huber et al., 1993). To that end, the use of liquid chromatography methods such as anion exchange chromatography (with improved protocols) are convenient and effective separation and purification techniques which can enhance the yield and quality of oligonucleotide products (Wincott et al., 1995).

This solid phase synthesis of oligonucleotides involves four stages. A controlled pore glass (CPG) support is used to immobilise and protect the initial base the sequence. The protecting group is removed to release a free 5'-terminal hydroxyl of ribose sugar on the oligonucleotides precursor during the first stage of detritylation, following which, the nucleoside readily reacts with additional phosphoramidite nucleosides formed in the coupling stage for chain extension. The small amount of uncoupled 5-hydroxyl group remaining on the oligonucleotides chains is coupled with subsequent bases in the sequence by acetylation during the capping stage. Finally, the unstable phosphite triester (P (III)) linkage is converted to the stable phosphate triester (P (V)) linkage using an oxidation agent (iodine) to treat the developed oligonucleotide chains. The phosphoramidite synthesis cycle is shown in Figure I-9.

The critical step in the overall synthesis cycle is coupling, which is the limiting reaction. Thus, it should be quick and close to the quantitative position, and any serious side-reactions should be avoided. In order to efficiently couple, an appropriate coupling activator is needed so that the phosphoramidites are in a highly activated mode (Wei, 2013).

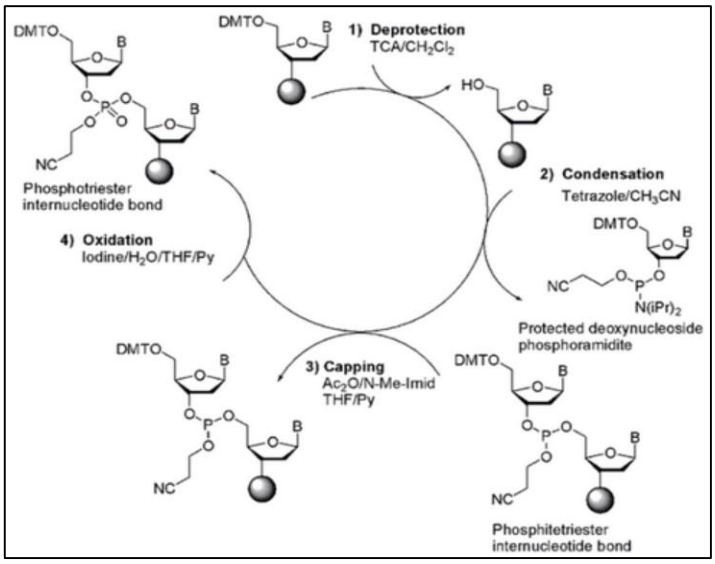

Figure I-9: The oligonucleotide chemical synthesis cycle via phosphoramidite chemistry. Reprinted from Synthesis of DNA Using a New Two-Step Cycle, in: *Oligonucleotide Synthesis*, (pp. 1–16), Methods in Molecular Biology by D. J. Dellinger, J. R. Betley, T. K. Wyrzykiewicz, and M. H. Caruthers (2005). Copyright 2005 by Springer Science and Bus Media B V. Reprinted with permission.

1.5 Oligonucleotide modification

1.5.1 Types of modifications

Oligonucleotides can be chemically modified in order to increase nuclease stability, modify structural preferences, increase binding affinity, determine knockdown specificity, improve cellular uptake, and/or overcome immune stimulation (Nolte et al., 2013) (Deleavey and Damha, 2012; Watts and Corey, 2012). In particular, improved nuclease stability is crucial to avoid degradation of the oligonucleotides upon entry to cells due to the presence of nuclease enzymes. Chemical modifications of oligonucleotides can be broadly classified into three categories: Internucleotide linkage modifications (backbone), sugar modifications, and nucleobase modifications.

These modifications can be located at varying positions, for example at the 3'-end or 5'-end of the backbone, internally within the sugar-phosphate or at nucleobases of the oligonucleotide sequence (Corey, 2007). Common examples of oligonucleotide modifications are shown in Figure I-10. Finally, it is worth noting that modifications involving RNase H-dependent mRNA cleavage require the modified oligonucleotide to preserve a polyanionic character (Sheehan et al., 2003).

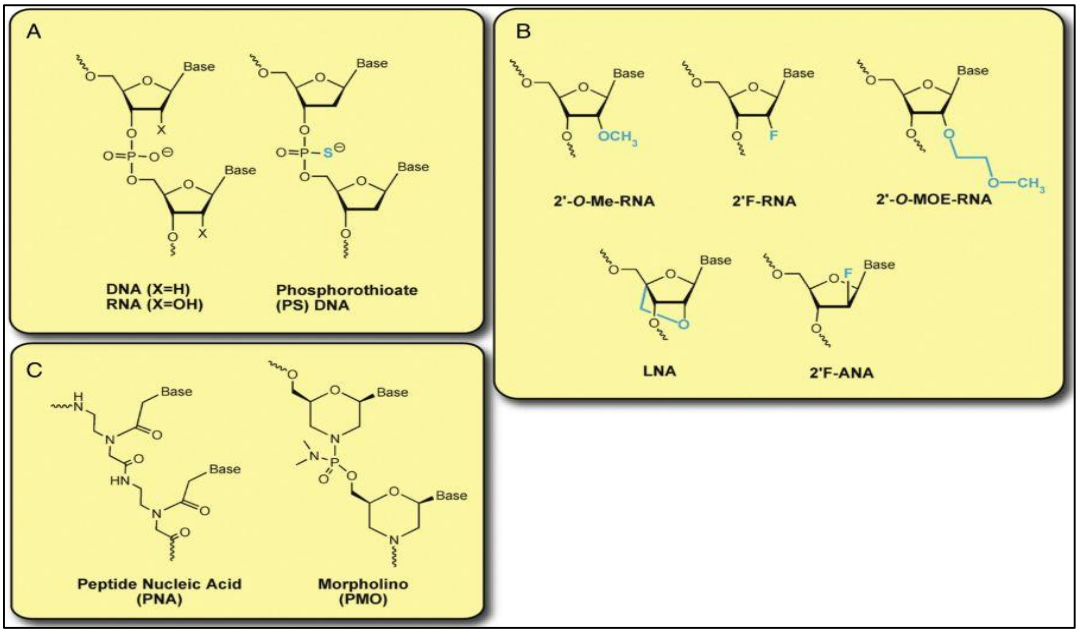

Figure I-10: Structures of commonly used chemical modifications. Reprinted from "Silencing disease genes in the laboratory and the clinic," by J. Watts and D. Corey (2012), *The Journal of Pathology*, 226(2), p. 365-379. Copyright 2012 by John Wiley and Sons. Reprinted with permission.

Phosphorothioate (PS) linkages are a common type of internucleotide linkage modification, providing greatly improved nuclease resistance (Watts and Corey, 2012). They are mainly represented by first-generation antisense therapeutic oligonucleotides, such as Fomivirsen (Deleavey and Damha, 2012). The key feature of the PS linkage modification is the substitution of sulfur with a single non-bridging phosphate oxygen (Deleavey and Damha, 2012). PS modifications are a cost-effective and easily implemented method to increase the nuclease resistance of oligonucleotides using typical solid-phase oligonucleotide synthesis procedures (Sanghvi, 2011).

Sugar modifications are frequently combined with internucleotide linkage modifications to exert additional control over oligonucleotide properties. Together, they feature heavily in second and third generation oligonucleotides. The key physical property manipulated by sugar modifications is the “nucleotide sugar puckering preference”, which is of interest because of its relation to oligonucleotide binding affinities, among other parameters (Deleavey and Damha, 2012).

Most sugar modifications involve changing the 2’ position of RNA and replacing the hydroxyl with various other groups. Commonly used sugar modifications include 2’-O-MOE (2’-O-(2-methoxyethyl)), locked nucleic acid (LNA), 2’-O-Me, 2’F-ANA, and 2’F-RNA, with 2’-O-MOE featured through the drug Mipomersen (Deleavey and Damha, 2012). Mipomersen, a second-generation oligonucleotide, was recently approved by the FDA (Pollack, 2013). A “gapmer” is commonly utilised for second and third generation sugar modifications, and features sugar-modified nucleotides on the oligonucleotide ends, adjoining a central DNA core (Deleavey and Damha, 2012).

Finally, nucleobase modifications are less common than internucleotide linkage and sugar modifications, but are still numerous and can be used to improve thermal stability, in addition to the other properties mentioned above. Nucleobase modifications are usually performed to increase duplex stability while preserving and improving base pairing recognition as well as hydrogen bonding (Deleavey and Damha, 2012).

1.6 Analytical approaches for the analysis of RNA

The need for advanced knowledge and understanding of intracellular RNA functions has prompted the development of numerous approaches which address the different stages of large biomolecular RNA analysis, from upstream cell synthesis and extraction to downstream analysis.

Unfortunately, in comparison to other macromolecules such as DNA and proteins, the development of a highly efficient approach for nucleic acid analysis has been hampered by the challenging nature of RNA which refuses to yield to conventional analytical techniques. These difficulties are primarily due to the chemically labile

structure of RNA leading to difficulties in extracting, storing, and transferring it to downstream analysis. Moreover, the presence of a polyanionic phosphate backbone in the RNA structure leads to a high tendency to form stable cation adducts during downstream characterisation of RNA, hindering mass spectrometry analysis. In addition, due to the similarity of the nucleic acid product to potential impurities (such as n-1 or single base conversions) separation of the oligonucleotide therapeutic from related impurities is challenging. To effectively analyse RNA, a wide variety of analytical approaches which specifically address these issues have been developed and are discussed in the following sections.

1.7 RNA purification technology

1.7.1 Solid-phase extraction

Historically, nucleic acid solid phase extraction involved the use of chaotropic agents: either guanidinium thiocyanate (GuSCN) or guanidine hydrochloride (GuHCl) in conjunction with a solid membrane silica column. In general, following cell lysis in GuSCN, DNA/RNA is purified by directly loading it onto the solid phase column prior to centrifugation and ethanol wash (Boom et al., 1990). Under the induced hydrophilic conditions, nucleic acids are attracted to the silica membrane surface via specific binding. The other non-selected materials do not undergo such an attraction to the surface and can be removed with an additional ethanol wash.

Solid phase extraction has some similarities to the classical liquid chromatography approach. Both methods involve dissolving the samples in solvents before passing the mixture through a solid phase containing column. The primary difference between SPE and chromatography is that SPE does not rely on partitioning phenomena, which is described as on and off separation procedure. The resulting materials from SPE are crude compared to the ones obtained from chromatography (Gjerde et al., 2009). A number of commercially available kits often use silica or glass spin columns for their quick selectivity of the nucleic acid of interest from prokaryotic and eukaryotic cells.

1.7.2 Agarose gel electrophoresis

Gel electrophoresis has become the standard method for the characterisation and separation of charged macromolecules, including nucleic acids (Ylmaz et al., 2012). During electrophoresis, a voltage gradient is applied across the gel; the negatively charged phosphate backbone of RNA/DNA has a strong affinity to the positive electrode in an electric field and migrates towards it. Frictional forces in the pores of the gel slow down this migration process at rates dependent on the hydrodynamic size and shape of RNA molecules, thus enabling separation based on size (Lehrach et al., 1977).

The charaterisation and quantification of RNA are usually determined using standards of known molecular weights and concentrations while performing traditional agarose gel analysis. However, RNA might migrate in a folded or semi-folded form, and the resultant smearing bands lead to the imprecise measurement of RNA (Lehrach et al., 1977). In response, denaturing agarose gel electrophoresis conditions are often employed with the aim of improving these smearing issues (Lehrach et al., 1977). Unfortunately, many of these denaturing methods either require complicated procedures or utilise toxic, carcinogenic chemicals, such as the glyoxal/dimethyl sulfoxide and methyl mercury hydroxide (Bailey and Davidson, 1976, McMaster and Carmichael, 1977). To avoid the use of these hazardous chemicals, other denaturants have been proposed such as urea, guanidine thiocyanate, DMSO, formamide, and formaldehyde (Floyd et al., 1974, Pinder et al., 1974, Skopp and Lane, 1988, Goda and Minton, 1995). Although these methods were an improvement over previous ones, they were still imperfect due to the involvement of extensive washing before staining with ethidium bromide as well as interference with the electrophoretic mobility of RNA molecules (Tsang et al., 1993). In addition, following gel electrophoresis, RNA requires further extraction from the gel matrix, (a process that is done by cutting out the band and re-extracting the material), leading to a high potential for RNase contamination.

Drawbacks of gel electrophoresis include the required use of hazardous denaturants, risks of RNase contamination, difficulty in automation and less than accurate quantification. These caveats limit the performance of gel electrophoresis for the analysis of nucleic acids.

1.8 High-performance liquid chromatography

High-performance liquid chromatography (HPLC) is a widely used separation technique based on the specific interaction between analytes and a stationary phase (a column). During its process, the analyte is dissolved in a solvent and carried through a column in a liquid phase (known as the 'mobile phase'). The separation rate of each compound depends on its affinity to the column. The difference in affinity between different compounds allows the separation of the constituents of a sample (Gjerde et al., 2009).

The use of HPLC for nucleic acid analysis has been proposed as an alternative to conventional methods such as gel electrophoresis. The superior capabilities of HPLC become apparent when it is used for the identification, separation, and quantification of nucleic acids. Some of these advantages include sample automation, fraction collection, and data reporting functions, which promote higher sample analysis throughput and recovery rates (Huber, 1998). Thus far, a variety of HPLC approaches have been employed for the analysis and purification of RNA, with the ion-pair reverse-phase high-performance liquid chromatography (IP RP HPLC) mode being the most widely utilised technique for this purpose (Huber and Krajete, 1999; Premstaller et al., 2000; Dickman, 2011).

1.8.1 Ion-pair reverse-phase chromatography (IP RP HPLC)

IP RP HPLC has been defined by numerous alternate names in literature, each depending on the suggested mechanism and application (Wittmer et al., 1975; Kraak and Bijster, 1977; Bidlingmeyer et al., 1979; Bidlingmeyer, 1980; Hoffman and Liao, 1977; Knox and Jurand, 1976). The ion-pair model proposes the use of ion-pair reagents in the mobile phase due to their tendency to interact with solute ions to form neutral ions, which are retained on the hydrophobic column with an improved retention time (Wittmer et al., 1975; Knox and Jurand, 1976). An alternate dynamic ion exchange model suggests that the adsorption of ion-pair reagents first occurs on the surface of the hydrophobic column, which then provides the exchange sites for solute ions (Kraak and Bijster, 1977; Hoffman and Liao, 1977; Bidlingmeyer et al., 1979). A third model combines the previous two models, proposing that both ion-pairing and

dynamic ion exchange processes occur and that the degree of significance of each process depends on experimental conditions (Knox and Jurand, 1976; Wittmer et al., 1975). Bidlingmeyer et al., (1979) indicated that an electrical double layer is formed once the ion-pair reagent binds via the dynamic adsorption onto the hydrophobic stationary phase (Bidlingmeyer et al., 1979; Bidlingmeyer, 1980).

IP RP HPLC is the principal HPLC mode for nucleic acid separations, and was first demonstrated by Huber et al., (1995) through the unique separation properties of an alkylated polystyrene-divinylbenzene (PS-DVB) polymer bead stationary phase with a nonporous surface (Huber et al., 1992). Their technique facilitated rapid and high-resolution separation of single-stranded (ss) and double-stranded (ds) DNA. In addition, a resolution of the fragments differing by only a single base pair in length was achieved in very short analysis times (Huber et al., 1995). The C18 PS-DVB column was later commercialised by Transgenomic (USA) as the “DNAsep column,” which contributed significantly to the development of nucleic acid chromatography. Subsequently, a few monolithic, polymer-based materials have been extensively reviewed to prove their potential as alternatives to particle-packed columns, and have shown results demonstrating their capacity for high-resolution separation of nucleic acids (Premstaller et al., 2000; Huber and Oberacher, 2002; Oberacher and Huber, 2002; Nwokeoji et al., 2016).

Results from recent studies using IP RP HPLC to analyse and purify RNA indicate its capability to perform in a wide range of RNA applications, from the purification of synthetic oligoribonucleotides to the analysis of more complex RNAs (Murray et al., 1994; Hölzl et al., 2005; McCarthy et al., 2009; Farand and Gosselin, 2009; Ivleva et al., 2010; Nwokeoji et al., 2016).

1.8.2 Mechanism of ion-pair reverse-phase chromatography for nucleic acid analysis

Nucleic acids are naturally hydrophilic and are negatively charged due to the presence of a phosphate backbone, which cannot interact with the hydrophobic stationary phase for chromatographic separation without pre-treatment. Thus, an ion-pair reagent (organic alkylammonium cation salt) is necessarily added into the eluent to form a

nonpolar hydrophobic ion-pair with the phosphate anion group of nucleic acids, increasing its hydrophobicity and allowing it to interact with the stationary phase. In general, triethylammonium acetate (TEAA) is the most commonly used amine cation salt for this purpose, as nonpolar ion-pairs (N^+A^-) are formed when a nucleic acid sample is introduced, allowing subsequent adsorption of the TEAA/ nucleic acid ion-pair fragments onto the non-anionic and hydrophobic surface column. Acetonitrile (ACN) is another additive that is frequently added to the mobile phase in a gradual manner according to a specific gradient to reduce the polarity of the mobile phase: a prerequisite for successful separation. Once the nucleic acid ion-pair fragments desorb from the column, the fragments will elute in the order of increasing size as the concentration of acetonitrile is increased. For instance, the smaller fragments will be eluted first, followed by the larger fragments. Figure I-11 illustrates the mechanism of the IP RP HPLC separation process for nucleic acids.

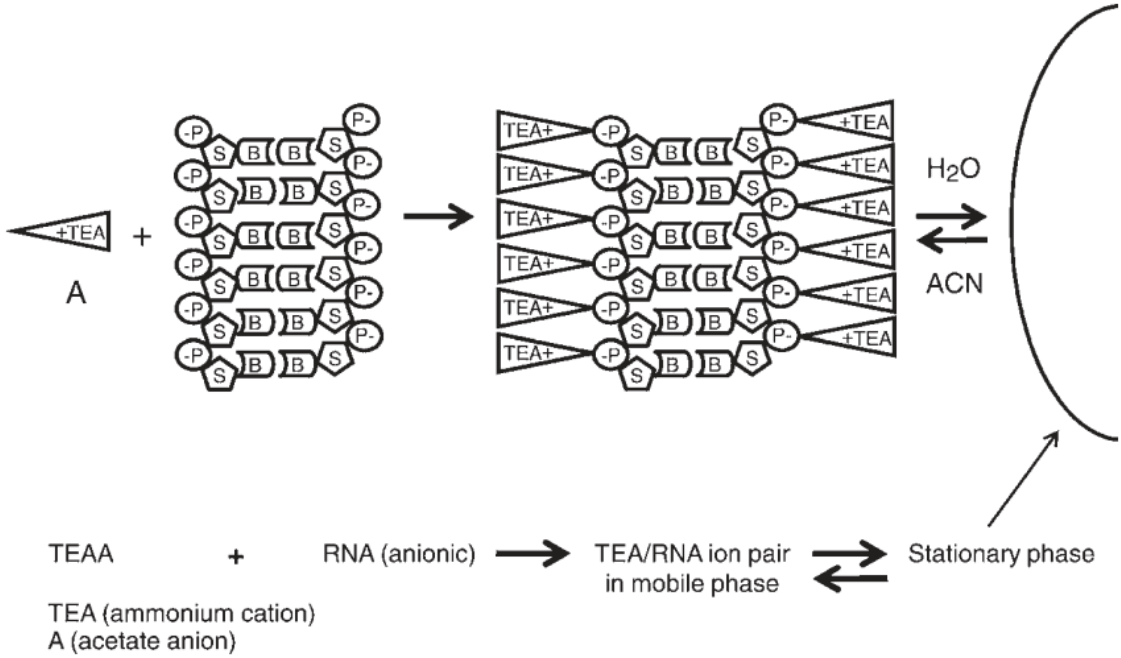

Figure I-11: Schematic illustration of the mechanism of the IP RP HPLC separation process for nucleic acids. TEA=Triethylammonium; A= acetate; P= phosphate; B= nitrogenous base. The ion-pairing reagent, triethylammonium acetate (TEAA) is prepared by mixing triethylamine with acetic acid to make a final solution with pH 7.0. The positively charged hydrophobic TEAA ions interact with the negatively charged polyanionic backbone of nucleic acid fragments to form neutral ion-pairs. Thus, TEA/ nucleic acid ion-pairing complexes become hydrophobic and can interact with the hydrophobic stationary phase. The separation process is size-based as the

acetonitrile percentage rises larger nucleic acids are able to desorb. Reprinted from *RNA Purification and Analysis* (p. 55) by D. T. Gjerde, L. Hoang, and D. Hornby (2009), USA. Copyright 2009 by John Wiley and Sons. Reprinted with permission.

1.8.3 Separation of RNA using IP RP HPLC

The chromatographic separation of RNA using IP RP HPLC is dependent on the choice of the mobile phase as well as the particular properties of the RNA being analysed. For instance, the separation of single-stranded nucleic acid is heavily influenced by differences in size, sequence hydrophobicity, and conformation. However, in some cases, different molecules may exhibit relatively similar separation behaviours, such as that of short oligodeoxynucleotides (from DNA) and oligoribonucleotides (from RNA).

The presence of polar phosphodiester groups in nucleic acids have a greater effect on retention time due to their interaction with non-polar ion-pairing ions. For example, ssRNA which is smaller than dsRNA and has half the amount phosphodiester groups only interacts with half the amount of ion-pairing ions, leading to shorter retention times (Gjerde et al., 2009).

The hydrophobic properties of the stationary phase are directly correlated to the number of methyl groups present in the alkyl chain of the ion-pair reagent. In TEAA, these short alkyl chains, only manage to retain the stationary phase in a partially hydrophobic state due to partial coverage. Under such conditions, the separation process depends on both size and base composition.

The effect of base composition is a result of all four bases of RNA being different in their relative hydrophobicity: adenine (A) and uracil (U) are more hydrophobic compared to cytosine (C) and guanine (G). Thus, sequences rich in C- and G will elute prior to sequence rich in A and U. This effect has been found to be more pronounced if the C and G nucleotides are positioned at the end of the fragment (Huber et al., 1992; Huber et al., 1993). In the case of ssRNA separation, replacing the less hydrophobic TEAA with a more hydrophobic ion-pairing reagent such as tetrabutylammonium bromide (TBAB) or N-hexylammonium acetate (HAA) may reduce or eliminate this sequence dependency (Dickman et al., 2002; Dickman, 2005). This is because the

longer alkyl chains contained in TBAB and HAA are able completely to cover the stationary phase, causing the dynamic anion-exchange process to dominate in size-dependent separation.

1.8.4 Reversed-phase stationary phases

1.8.4.1 Silica-based stationary phases

Initially, conventional silica-based C_{18} resins and polymeric reversed-phase stationary phases were widely adopted for nucleic acid separation (Swiderski et al., 1994). The porous stationary phases were shown to successfully separate small-sized molecules, but were ineffective for biopolymers, thus limiting their application. This limitation was explained by the small pores of the chromatographic support restricting access to large biomolecules (Unger et al., 1987).

Subsequently, advanced silica packing media with a wide range of pore sizes from normal to large (300-4000 Å) were developed. The large pores provided macro-biomolecules with sufficient access to the functional surface of stationary phase, removing a crucial limitation and proliferating the use of HPLC in the field of biotechnology (Jilge et al., 1989). Despite this advancement, researchers found that the large macropores in the stationary phase support considerably slowed down the mass transfer of small molecules, causing poor resolutions and low sample recovery rates (Rozing and Goetz, 1989). In addition, low molecular diffusion rates of biopolymers in porous stationary phase meant that only low flow rates and shallow gradients were feasible, resulting in time-consuming separations (Huber, 1998). Overall, the described disadvantages of conventional C18 silica-based columns make them unsuitable for nucleic acid research where high throughputs are needed.

1.8.4.2 Polymeric stationary phases

Polymeric reversed-phase resins are made of polystyrene divinylbenzene (PS-DVB) and are formed through crosslinking of several polymer chains. Porous and non-porous variants exist, and both forms have been used for IP RP HPLC separations. The porous variant consists of small pores, which suffer from the same issues as

small-pore silica-based columns (Unger and Janzen, 1986). The non-porous variant was introduced as 2 µm, C18 non-porous polymeric media and was a breakthrough at the time, revolutionising nucleic acid separation with its significant advantages (Huber et al., 1992; Oefner and Huber, 2002).

1.8.4.3 Monolithic stationary phases

Most recently, the use of monolith columns as part of separation processes has been the subject of much research. A wide variety of monolith polymeric materials has been employed for high-efficiency nucleic acid separation including the poly-(styrene/divinylbenzene) PS-DVB monolith (Premstaller et al., 2000) and one made from poly (p-methylstyrene-co-bis (p-vinylbenzyl) dimethylsilane) MS/BVBDMS. These polymeric columns have a wide range of internal pore sizes, going from micro- (< 2 nm) to meso- (2-50 nm) and macro scales (> 50 nm) (Tanaka et al., 2001; Unger et al., 2008).

Premstaller et al., (2000), in their seminal paper, used a PS-DVB monolithic particle to demonstrate its capacity for high-efficiency separation and its potential in both proteomic and genomic research. This promising particle shows significant improvement in terms of large biomolecule mass transfer rates, which is a result of its micropellicular monolith configuration. The monolithic bed consists of a single porous polymer rod with internal porosity (consisting of macropores and mesopores) which facilitates convective flow while lacking interstitial volume (Horvath et al., 1977).

The morphology of monolith column consists of interconnected network structure links throughout the inner capillary wall (Eeltink et al., 2017). As a result of the high interconnectivity of its channels, diffusional distances in a monolithic column are significantly reduced, resulting in higher chromatographic efficiencies. The same interconnectivity which provides its mass transfer capabilities is also responsible for its structural robustness. The durability of monolith columns was demonstrated by Škeříková and Urban (2013) who reported over 10,000 chromatographic injections performed using a single monolith column.

Stationary phases built with polymer-based materials are favoured for nucleic acid separation, because of their excellent chemical and mechanical stabilities. They are resilient toward acidic, alkaline, and hydro-organic conditions, and are also able to withstand extreme temperature conditions. A high degree of polymeric crosslinking in a monolith column minimises the swelling of packed materials in an organic solvent, resulting in mechanical stability and allowing for operation under high pressures (Maa and Horvath, 1988). Its high permeability avoids the loss of column efficiency and resolution normally associated with high flow velocities. Overall, monolithic columns can achieve high efficiencies comparable to conventional non-porous media while also delivering higher yields (Huck and Bonn, 2005).

Finally, the features of monolith materials mean that they can be readily used in miniature scale experiments: for example, in capillary and microfluidic liquid chromatography. Coincidentally, these techniques are also preferable for direct coupling to ESI-MS for the online analysis of structure and the identification of separated compounds, as only small amounts of sample are required.

In summary, the unique characteristics of monolith materials make them ideally positioned to tackle the unique and often difficult requirements of nucleic acid separation, which has led to their increasing attractiveness as the column material of choice for many researchers.

1.9 Mass spectrometry

1.9.1 Mass spectrometry of RNA analysis

Mass spectrometers measure the mass to charge ratio (m/z) of ions, in the gas phase. One of the key components of mass spectrometers are ion sources, whose basic function is to convert the sample from a liquid phase to a gaseous phase and to channel the resulting gaseous ions into the mass spectrometer. In the case of nucleic acids, their ionisation and delivery into the gas phase can be achieved by several different MS ion sources such as matrix-assisted laser desorption ionisation (MALDI) or electrospray ionisation (ESI) via an online high-performance liquid chromatography system (HPLC).

Both ioniser and mass analyser technologies have undergone multiple innovative improvements over the years. Some of the developed ioniser technologies include electrospray ionisation (ESI), matrix-assisted laser desorption ionisation (MALDI), fast atom/ion bombardment (FAB), electron ionisation (EI) and chemical ionisation (CI) (Fenn et al., 1989; Karas and Hillenkamp, 1988; Karas, 1996). Meanwhile, the advancement of analysers has significantly contributed to the power of MS analysis. Analysers currently available include quadrupole, quadrupole ion trap, time-of-flight (ToF), time of flight reflectron, quad-ToF and Fourier transform ion cyclotron resonance (FT-ICR) mass spectrometers. In this PhD project, ESI-MS using Q-ToF and 3D ion trap instrument were used for the analysis of RNA and oligonucleotides.

1.9.2 Ion source

1.9.2.1 Electrospray ionisation source

Electrospray ionisation converts a solution sample into gas-phase ions using an electrospray at atmospheric pressures, a process which preserves the analytes' integrity, resulting in intact, ionised molecular species with multiple charge states. This feature of the ESI is why it is described as a "soft" ionisation method in the sense that only a small degree of fragmentation occurs upon ionisation (Fenn et al., 1989). In addition, the multiple charge states of the ions cause lower mass ranges (m/z values) and allow them to be detected by all common mass analysers. Unsurprisingly, ESI has become a key tool for subsequent mass spectrometric analysis of important biological macromolecules such as proteins and nucleic acids, revealing structural characteristics and identifying basic molecular features. Its revolutionary impact on the analysis of important classes of large biomolecules led to the inventor of ESI-MS, Fenn, being awarded the Nobel Prize in Chemistry in 2002 for his breakthrough.

The overall ESI process consists of three consecutive stages: droplet formation (dispersion), droplet fission, and desolvated ion production, which are shown graphically in (Figure I-12 B). In the first stage, the solution analyte flows through the metal capillary, which is retained at a high-voltage (2-6 kV). The polarity of the applied voltage results in the counter electrode producing either positive or negative ion. This strong electric field induces electrophoretic movement of ions, causing dispersion of

the sample solution and forming an aerosol of highly charged droplets from the electrospray. A heated, inert gas (e.g. nitrogen) flows around the capillary to enhance the nebulisation. Solvent evaporation (desolvation), which is the precursor to droplet fission, reduces droplet sizes and increases the surface tension of the droplets until they reach the Rayleigh limit, ultimately resulting in Coulomb fission (Rayleigh, 1882). The fission process creates smaller droplets (called “progeny” droplets), which are enriched with the ions surrounding the “parent” droplet. Repeated fission leads to smaller and smaller droplets, eventually creating charged nanodroplets, with the end result being multi-charged analyte molecules in a gas-phase (Figure I-12 B).

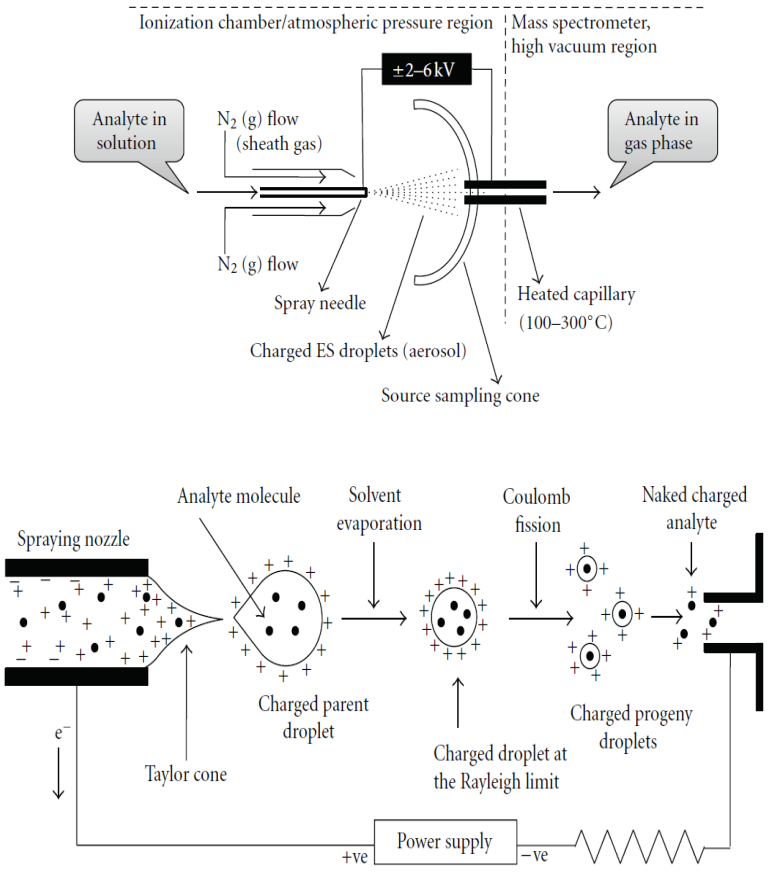

Figure I-12: Diagrammatic representation of Electrospray ionisation. (A) An ESI-ion source. (B) The Electrospray ionisation process. Reprinted from “Electrospray Ionization Mass Spectrometry: A Technique to Access the Information beyond the Molecular Weight of the Analyte,” by S. Banerjee and S. Mazumdar (2012), *International Journal of Analytical Chemistry*, 2012, p. 1-40. Copyright 2012 by Shibdas Banerjee and Shyamalava Mazumdar. Reprinted with permission under the Creative Commons Attribution License.

1.9.3 Mass analysers

1.9.3.1 Quadrupole analysers

A quadrupole analyser operates based on the stability of the trajectories of ions in oscillating electric fields and separates them according to their mass-to-charge ratio (m/z). Two and three-dimensional ion traps operate on the same basic principle. Quadrupole analysers consist of four parallel cylindrical metal rods, with each opposing pair connected by an electrical constant such as a direct current (DC) voltages and radio frequency (RF).

The stability of the trajectory of the ions that travel to the mass filter is dependent on the oscillation of the RF voltage applied. Only ions of a selected m/z range are stable enough to reach the detector via the supplied voltages, while ions with unstable trajectories will collide with the rods. The selectivity of ions according to their m/z allows continuous scanning across a range of m/z values through the variation of voltages.

1.9.3.2 Time-of-flight mass analysers

The time of flight (TOF) analyser contains a long metal tube and operates based on the acceleration of ions through a high electric field. In a TOF analyser, the mass-to-charge ratio is measured from the velocity of the ions and the time taken for an ion to travel down a flight tube until they reach the detector. This acceleration (V_s) of ions is such that provided they have equal kinetic energy (E_k) (which is converted from the potential energies E_{el}) and the same charge (q=ze), their velocities will depend on only mass (m) (equation 1)(Hoffmann and Stroobant, 2007).

$$E_k = \frac{mv^2}{2} = qVs = zeV_s = E_{el}$$

Equation 1

Once these ions pass through the field, they will be separated based on velocity, which itself is a function of mass-to-charge-ratio. The time (t) needed to cover the distance (L) is given by equation 2; Using equation 3 and a measurement of t^2 mass-to-charge

ratio can be calculated, with the terms in parentheses being constant, and all other factors being equal. As a result, given the same charge, heavier ions will travel to the detector at lower speeds.

$$t = \frac{L}{v}$$

Equation 2

$$t^2 = \frac{m}{z}\left(\frac{L^2}{2_e V_s}\right)$$

Equation 3

The TOF analyser suffers from limited mass resolutions due to the range of kinetic energies required for ions, resulting in a widening effect on the ion packet. In addition, other factors such as variability in flight times also contribute to the poor resolution, resulting in a distribution of ions with identical m/z ratios.

A reflectron is a series of electrostatic mirrors of equal charge and is utilised to improve the resolution of TOF analysers (Mamyrin et al., 1973). In principle, the reflectron is applied at one end of the flight tube and the field effect decelerates ions flying towards the end of the tube. The ions are then reflected out of the mirror into the detector, which is offset from the source. Ions with higher kinetic energies will decelerate since they penetrate deeply into the field, rendering them unable to quickly reflect back to the detector (ions with lower kinetic energy will reflect quicker)(Larsen and McEwen, 1998). The advantages of replacing the third quadrupole (Q2) with a TOF mass spectrometer are higher mass accuracy, sensitivity, and mass resolution (Morris et al., 1996; Shevchenko et al., 1997).

The Q-TOF is a configuration of the triple quadrupole (Q0, Q1, and Q2) interfaced with a TOF mass analyser instrument. The first quadrupole mass filter (Q0) serves mainly in transmission mode, focusing on transmitting the ions generated across the whole m/z range from the ESI to the next quadrupole (Q1). Application of both constant and RF voltages allows scanning of a range of m/z values along the axis of the poles. Thus,

only a narrow band of m/z values are selected (precursor ions) and transmitted to the third quadrupole (Q2). The ions that move to Q2 are collision cells and are bombarded into fragment ions through collision-induced dissociation (CID). The information gathered from the sequence of the precursor ions permits identification based on the resulting fragment ions and the analysis of fragmentation patterns.

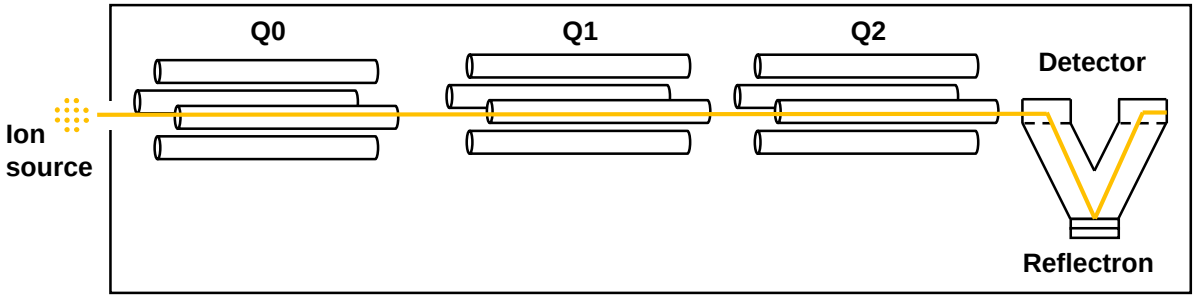

Figure I-13: Schematic diagram of a Q-TOF mass spectrometer. The mass spectrometer has a triple quadrupole (Q0, Q1, and Q2), and the last quadrupole section is replaced with a TOF analyser.

1.9.4 Three-dimensional ion trap analysers

The three-dimensional (3D) ion trap consists of a circular electrode with two ellipsoid end caps which form a 3D quadrupolar field. An oscillating electric field operating at a radio frequency (RF) and a direct current (DC) voltage is subsequently applied to the ring electrodes, trapping incoming ions which fall under a specific m/z mass range within the 3D quadrupolar electrostatic field. Once the trap is filled with ions the mass analysis process begins (see Figure I-14).

The stability of the ions (maintains by the RF signal) is perturbed by ramping the RF signal to destabilise them in trap one after the other. This causes the ions to eject from the trap based on their m/z ratio; a scan of the trapped masses is created as a spectrum on the basis of these values when they are detected.

Moreover, specific precursor ions can be isolated in the trap by the exiting voltage with the inert gas supplied to the trap to induce fragmentation. Over time the ions' trajectories in the trap expand, resulting in some ion losses. This is countered by

having a damping gas (e.g. helium) in the trap to remove excess energy and reduce collisions (Paul, 1990; Hoffmann and Stroobant, 2007).

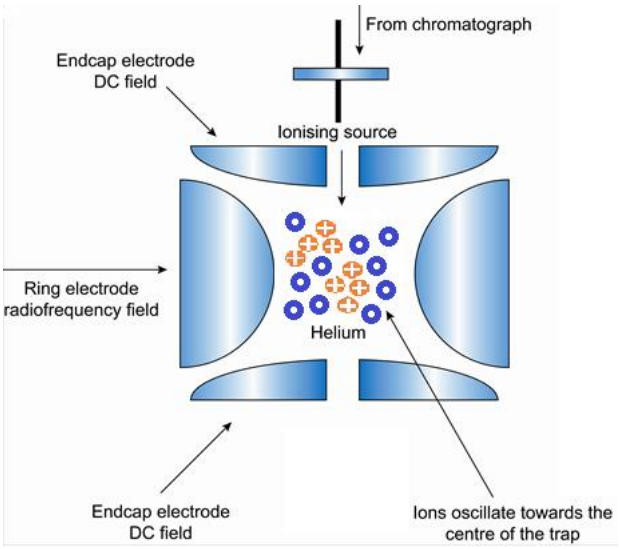

Figure I-14: Schematic of a 3-dimensional ion trap mass analyser. After being formed in the capillary, the ions are directed through an ion trap device where an oscillating electric field operates at a radio frequency (RF) and a direct current (DC) voltage, trapping them for subsequent mass measurement.

1.10 Interfacing IP RP chromatography with mass spectrometry

Interfacing IP RP HPLC with ESI MS has proven to be an effective strategy, increasing the power of assessments such as the identification and characterisation of nucleic acids. The efficiency of this combination depends heavily on the choice of an appropriate mobile phase, yet it is known that both systems have individually optimised mobile phases, which do not perform well on the other system. Specifically, the optimised HPLC mobile phase suffers from weak ESI-MS signals, while the optimised ESI mobile phase (with high volatility, low conductivity, and surface tension designed to minimise adduct formation) is not suitable to be applied on the HPLC (Apffel et al., 1997). For instance, TEAA or TBAB enable high-resolution nucleic acid separation but both are not considered fully volatile and result in significant ion suppression. In addition, reducing the concentration of the ion-pair reagent in the mobile phase is often attempted to enhance MS sensitivity but it significantly lowers chromatographic performance at the same time. In an attempt to solve this dichotomy, Apffel et al.,

(1997) introduced an advanced mobile phase containing 1,1,1,3,3,3- hexafluoro-2-propanol (HFIP) as an additive to triethylamine (TEA), which was LC-MS compatible. Their findings have been successfully extended and applied in a wide variety of applications within nucleic acid research (Gilar, 2001; Fountain et al., 2003; Taoka et al., 2009; Emmerechts et al., 2007; Emmerechts et al., 2008).

Alternatives to the TEA ion-pair reagent aimed at improving LC ESI MS compatibility with higher volatilities such as triethylammonium bicarbonate (TEAB) (Premstaller et al., 2000), butyldimethylammonium bicarbonate (BDMAB)/butyldimethylammonium acetate (Hölzl et al., 2005) and Cyclohexyldimethylammonium acetate (CycHDMAA)(Oberacher and Pitterl, 2009), have demonstrated positive results in LC separation interfaced with online mass spectrometry for nucleic acid analysis. Enhancement of the LC ESI MS analysis for nucleic acids remains a challenge and is an active area of research today.

Another dimension of study in addition to mobile phase choice is the utilisation of monolithic capillary columns in conjunction with the aforementioned MS-compatible mobile phases for a wide range of LC-MS analyses on nucleic acids (Oberacher and Huber, 2002). This approach has enabled the extraction of oligonucleotide sequence information from either synthetic siRNA or small RNA (tRNA and 5S rRNA) at low concentration quantities (down to picomole/L levels)(Hölzl et al., 2005). Recently, the analysis and sequencing of synthetic oligonucleotides using IP RP UHPLC interfaced with MS and a TEA/HFIP buffer in conjunction with UPLC OST C_{18} columns was demonstrated (Ivleva et al., 2010).

1.10.1 Problems associated with RNA mass spectrometry

Inherent to the structure of RNA is the presence of a polyanionic phosphate backbone which leads to a high tendency to form stable cation adducts, i.e. with Na^+ and K^+ as a countermeasure to stabilise their secondary and tertiary structures (Wacker, 1969; Misra and Draper, 1998). These metal ions often exist in analyte solutions, associating with RNA molecules and impeding the ability of ESI-MS to detect and characterise oligonucleotides (Huber and Krajete, 1999). This has become one of the most major issues in RNA mass spectrometry.

A wide variety of approaches (either off-line or on-line prior to RNA ESI-MS analysis) have been attempted to remove these metal ions, including cation ion exchange (Huber and Buchmeiser, 1998; Limbach et al., 1995) ,ethanol precipitation with ammonium salts (Limbach et al., 1995), addition of organic bases (triethylamine) (Greig and Griffey, 1995; Limbach et al., 1995) and denaturing gel electrophoresis (Berhane and Limbach, 2003). These approaches have also been combined with different methods in various combinations to overcome the problem associated with cation adduct formation. The pairing of the LC system with MS, with the LC acting as an on-line sample separation system, is a demonstrably successful method of desalting while reducing cation adducts, which directly improves oligonucleotide analysis (Oberacher et al., 2004).

1.11 Aim of the study

Recent advancements in the understanding of the functions of RNA in different biological systems have raised the potential of RNA to be applied as therapeutic drugs for serious diseases and innovative tools to replace chemical pesticides in insect management strategies. This has resulted in an increase in the demand for analytical tools which can efficiently purify, quantify, and characterise these analytes. For instance, an important aspect of drug quality control involves validating purity levels as well as identifying impurities to determine whether the drug will function effectively while simultaneously avoiding side-effects such as unwanted off-target gene silencing.

The overall aim of this thesis is to develop a high throughput analytical platform based on ion-pair reversed-phase chromatography (IP RP HPLC) and electrospray ionisation mass spectrometry (ESI-MS) for the analysis of nucleic acids including RNA therapeutics and dsRNA. The successful development of an effective platform will be an important step towards clearing another roadblock in drug analysis. The first step in achieving these aims will focus on examining the effect of the mobile phase composition on the performance of ESI-MS of oligonucleotides, specifically comparing their different physiochemical properties. The analyses will aim to optimise signal intensities while reducing cation adduct formation, which often limits the sensitivity and accuracy of oligonucleotide analysis.

The second part of this study aims to fulfil the need for a method which produces large-quantities of high-quality dsRNA for use in RNAi applications, as recent discoveries show that RNAi holds great potential as therapeutic drugs as well as in insect management strategies by serving as an alternative to chemical pesticides. To that end, it is proposed to develop a method capable of isolating, purifying, and quantifying of dsRNA extracted from microbial cells. Techniques such as metabolic and genetic engineering *in vitro* stable isotope labelling of RNA will be explored in conjunction with LC-ESI-MS analysis to characterise and quantify of dsRNA.

Monolithic porous columns have demonstrated their capability for highly efficient separation of large-biomolecules. However, their behaviour in relation to nucleic acids has not been fully characterised. A part of this study will aim to compare the performance of monolithic columns of different pore sizes in combination with retentive and non-retentive HPLC modes for the analysis of nucleic acids.

Chapter II: Materials and methods

2.1 Materials

2.1.1 Equipment

Equipment	Company
Automatic Pipettes (P10, P100, P100)	Gilson, Eppendorf
Weighing balance	Kern
Heating Block	Techne
Heated ultrasonic bath	Fisher Scientific
Centrifuge	Eppendorf
Nanodrop Spectrophotometer	Fisher Scientific
Ultrospec 1100 Pro Spectrophotometer	Amersham Bioscience
UV transilluminator	UVP
Cell disruptor	scientific industries
Vortex mixer	Fisher Scientific
pH meter	Mettler Toledo
Real Time PCR	Applied Biosystems
Horizontal gel apparatus	Bio-rad
Power supplies	Bio-rad
Autoclave	Prioclave
Incubator Shaker	SciQuip
Transgenomic HPLC	Transgenomic
HPLC Ultimate 3000	Dionex
HPLC Agilent 1100	Agilent
HTC Ultra PTM Discovery System	Bruker Daltonics
maXis UHR ToF MS	Bruker Daltonics
Corning® syringe filters (0.2 µm)	Sigma

2.1.2 Chemicals and reagents

Chemicals, reagents, kits, and samples	**Company**
Acetic Acid	VWR
Acetonitrile	Fluka
Agarose	Bioline
Ammonium acetate	Sigma
Ammonium sulfate	Sigma
^{15}N ammonium sulfate	CK gas products LTD
Ampicillin sodium salt	Sigma
Chloroform	Thermo fisher
Diisopropylamine (DIPA)	Sigma
Dimethylsulfoxide (DMSO)	Sigma
DNA primers	MWG
DNAzol reagent	Life technologies, GeneArt
Enpresso B Defined Nitrogen-Free pack	BioSilta
Ethanol	Fluka
Ethylenediaminetetraacetic acid (EDTA)	Sigma
Ethidium Bromide	Sigma
Formamide (RNA grade)	Sigma
Guanosine-$^{13}C_{10}$, and $^{15}N_5$ 5'-triphosphate sodium salt solution	Sigma
Hexylamine (HA)	Sigma
HiScribe™ T7 High Yield RNA Synthesis Kit	Sigma
HyperLadder™ 1kb	New England Bioabs
Isopropyl-β-D-thiogalactopyranoside (IPTG)	Bioline
Isopropanol	Fluka
Nuclease-free water	Life Technologies
2-mercaptoethanol	Life Technologies
Mix and Go transformation kit	Zymo research
MS2 RNA	Sigma

Oligonucleotides	Sigma
PCR mix master	MWG Eurofins
Phosphate buffered saline	Thermo Fisher
Purelink™ Genomic DNA Mini Kit	Life Technologies (Invitrogen)
Proteinase K	Thermo Fisher
pUC18 DNA *Hae* III digest ladder	Sigma
RiboPure kit	Sigma
RNA loading dye 2x	Ambion
RNase A	New England Biolabs
RNAzol reagent	Life Technologies (Ambion-Invitrogen)
Sodium chloride (NaCl)	Sigma
Sodium dodecyl sulphate	Thermo Fisher
Sodium hydroxide reagent grade, ≥98%, pellets (anhydrous)	Sigma
Tributylamine (TBA)	Sigma
Tetrabutylammonium acetate (TBAA)	Sigma
Tetracycline hydrochloride	Sigma
Tris	Sigma
Triethylamine	VWR
Triethylammonium acetate	Sigma
Trifluoroethanol (TFE)	Sigma
TRIzol max bacterial RNA isolation kit	Sigma
1,1,1,3,3,3,-Hexafluoro-2-propanol (HFIP)	Sigma
Urea solution, BioUltra ~8M in H2O	Life Technologies (Ambion-Invitrogen)

2.1.3 Oligonucleotides

Oligonucleotide	**Sequence**
BC2	5'-CAAAAGTCCGTGAGA-3'
BC2b C6 (amino-link C6)	5'-C6CAAAAGTCCGTGAGA-3'
BC2b C12 (spacer C12)	5'-C12CAAAAGTCCGTGAGA-3'

2.1.4 Oligonucleotide sample preparation

Oligonucleotide samples (listed in section 2.1.3) were received dry and re-suspended in 200 µL of nuclease-free water. Each sample was dissolved into the mobile phase system to reach a final MS direct-infused oligonucleotide concentration of 2 µM.

2.1.5 DNA primers

The designed forward and reverse primers were obtained from MWG Eurofins

Details	**Sequence**
Forward-T7+Spacer	TAATACGACTCACTATAGGGTGGCGCCCCTAGATG
Forward-Spacer+linker	GGTGGCGCCCCTAGATGGATATCGGACATCTTGCG GT
Reverse-T7+Spacer	TAATACGACTCACTATAGGGCGACGCCCGCTGATA
Reverse-Spacer+linker	GGCGACGCCCGCTGATACGGGCAGGAACCTATCCT AT

2.1.6 Double-stranded RNA gene sequence

Details	**Sequence**
COIV PMA Length: 765 bp	TAATACGACTCACTATAGGGAGCAAAAAACCCCGCGAGACC CCCGAAGAGGCCCCGCGGGGTTAATGGCCCTGCGACTACT CAACAGTGCTGTGCTCCGCCAGCTGGCCTCTCAGCTGCCCA AGAGTGCCCAGGTGGGCAGCGTGGCCGCCGTCCACACACT GGACAAGATCGGCAAGCGGGAGATCGTTGGCTACGGCTGG AACGGCACCGCCTGCTACGCGGATCGCGTGGACTACCCTCT GCCCGCCGTGCGCTTCCGTGAGCCCACCAACGAGATCAAC GCTCTGCGCGCCAAGGAGCAGGGAGACTGGAAGAAGCTCA GCACCCAGGAGATCAAGGCCCTGTACCGCGCCAGCTTCTG CCAGACTATCGCCGAGGTCCAGGCTGGAAGCGGGGAGTGG AAGCTCCACCTGGGCGTTTCACTCCTCTTCTGCGCCGCCGC CATCTGGGTGGCCGTACTGATGAACATCTTCGTGTACGATG AGCTGCCCGTTACCTTCGATGAGGAGCACCAGAAGGCGCA

	GCTGCAGCGCATCATCGACCTGGAAATCAACCCCGTCACCG GATTGACCTCCAAGTGGGACTACGAGAACAAGAAGTGGAAG AACCTGGAATTGCTCATGGTGGAGCTTCAGTTCCGCAAGGG CATGAACGATCTGCTGGGTAAAACCCCGCGGGGCCTCTTCG GGGGTCTCGCGGGGTTTTTTGCTCCCTATAGTGAGTCGTAT TA

Details	**Sequence**
Dome 11 Length: 401 bp	GATATCGGACATCTTGCGGTATTTCTTGTACACGAGGTAGAA GATGACGCCCAGCACGAGAATCGCCACGGTCACCTCAATGG TCTGGTACATGGCCTTCACGCTGTGCGTGTCCGGTGTACAG ATGAATCCGTAGATGCCCCAATCGGATCTGTAGAGCCGGTA GGCGGTCATGTTGGCAGCGTAGGCCTCGAACTGCAGCCGC TCCTCTTCGCCGAGCGCATCGGTGCGTGCCTCGCATCCCTT GCCGTTGGTCGACATAAGCAAAACGGCACCTTCCGCTGCAT CCGCTCCGTTCAACTGCGGATGCTGCTCCACGTTGATGGCA CGCACCGCTAGCTGGAAGGGATTGTGGCTGGTGCAGCGCG GCGTGGCCATCACATAGGATAGGTTCCTGCCCG

2.2 Buffer compositions

2.2.1 RNA extraction buffers

RNAsnap Solution	
EDTA	18 mM
SDS	0.025 %
2-mercaptoethanol	1 %
Formamide	95 %

20% SDS	**100 mL**
SDS	20 g
HPLC grade water	80 mL

RNAswift Lysis Buffer	
SDS	4%
NaCl	5M
Tris Ethanol Wash Buffer	
Tris (pH 7.5)	10 mM
Ethanol	80 %

IPD Buffer	
Isopropanol	33 %
DMSO	33 %
HPLC grade water	33 %

2.2.2 Gel electrophoresis buffer

Tri-Acetate-EDTA (TAE) buffer	**1L of 50X**
Tris base	242 g
Glacial acetic acid	57.1 mL
0.5 M EDTA (pH 8.0)	100 mL

The working buffer (1X of TAE) was made by diluting the stock solution with 50X deionised water.

2.3 Amplification of DNA template using polymerase chain reaction (PCR)

Drosophila S2R^{+} cells were extracted using the Purelink^{TM} Genomic DNA mini Kit (following the protocol for animal culture cells) to obtain the genomic DNA used for PCR amplification. The PCR process was carried out using specific primers. The PCR mixture consisted of 13 µL of PCR master mix (10 × reaction buffer, MgCl2, dNTP mix and Taq DNA polymerase) (Thermo Fisher), 1 µL of genomic DNA, 1 µL each of the forward and reverse primers (see Section 2.1.5), and 34 µL of PCR grade water (Sigma Aldrich). For the second round of PCR, 1µL of the genomic DNA from the first

round of product was used (1:20 dilution) and added to the same PCR mixture components stated above.

PCR parameters for the first round were as follows: 94°C for 3 min, 35 cycles at 94°C for 30 s, a gradient from 54 to 58°C over 30 s, a cycle at 72°C for 30 s; and a final step at 72°C held for 5 min. PCR parameters for the second round were: 94°C for 3 min, 35 cycles at 94°C for 30 s, a gradient from 49 to 60°C over 30 s, and 72°C for 30 s, and a final step at 72°C held 5 min. The DNA template containing 401 bp sequence flanked the T7 promoter sequence on both ends.

The final PCR products were purified using a QIAquick PCR Purification Kit (QIAGEN, Germany) and were analysed using electrophoresis on 1% agarose gel in 1× TAE buffer (contained ethidium bromide).

2.4 Bacterial transformation, induction, and culture growth

2.4.1 List of bacterial strains used

In this study, the *E. coli* strand HT115 (DE3) was engineered with two different plasmids to generate a specific length of dsRNA.

Bacterial strand	Plasmid	Antibiotic resistance	Source
HT115 (DE3) (Tetracycline)	COIV PMA	Ampicillin	Cold spring harbor laboratory, NY, USA
	DOME 11	Kanamycin	

2.4.2 Culture media and antibiotics

The optimal *E. coli* growth conditions were produced using Luria-Bertani (LB) and Enpresso media (consisting ^{14}N and ^{15}N ammonium sulfate) to generate ^{14}N and ^{15}N labelled materials. The LB medium was sterilised by autoclaving it at 121°C for 20 min prior to use. The culture media were contained with the appropriate antibiotics at the

required working concentrations. The stock antibiotics used were prepared with water and sterilised by filtration using a 0.2 µM syringe filter.

LB medium (pH 7.5)	**1L**
Bacto-tryptone	10 g
Yeast extract	5 g
NaCl	10g

Enpresso B Defined Nitrogen Free media (^{15}N growth media)	
Sterile water	45 mL
Enpresso B Defined Nitrogen Free tablets	2 tablets
$^{15}NH_4Cl$ (40g/L, final concentration 2.5 g/L)	3 mL

Antibiotic	**Stock concentration**	**Working concentration**
Ampicillin	100 mg mL^{-1}	100 µg mL^{-1}
Tetracycline	10 mg mL^{-1}	10 µg mL^{-1}
Kanamycin	50 mg mL^{-1}	50 µg mL^{-1}

2.4.3 Plasmid transformation

The HT115 (DE3) bacterial strain (described in Section 2.4.1) was used for the transformation of COIV PMA and DOME 11 plasmids. The transformations were performed according to the manufacturer's (Zymo research) instructions to obtain competent HT115 (DE3) cells. 1 µL of plasmid DNA was added to HT115 competent cells and they were gently suspended for few seconds. 100 µL of the cell suspension was spread onto a pre-warmed agar plate (containing appropriate antibiotic) for each plasmid. The plate was incubated at 37°C overnight.

2.4.4 Double-strand RNA culture growth in LB media

Pre-culture for the HT115 cells engineered with 765 bp dsRNA was prepared by inoculating a single colony of the transformed cells from a fresh plate (described in

2.4.3) into 5 mL of LB medium, which contained tetracycline (10 µg/mL) and ampicillin (100 µg/mL). The procedure for the preparation of HT115 cells engineered with 401 bp dsRNA was identical to that of the 765 bp cells except that the medium contained tetracycline (10 µg/mL) and kanamycin (50 µg/mL). Both cultures were incubated with vigorous shaking at 37°C until the OD600 nm reached 0.6.

In a separate experiment (Chapter IV, dsRNA extraction study), the culture for HT115 cells expressed with 765 bp dsRNA was prepared with the procedure described above, dsRNA expression was performed by adding IPTG (1 mM final concentration), and the culture was further incubated for 2 hours.

2.4.5 Metabolic isotope labelling of HT115 dsRNA

A single colony from the HT115 (DE3) cells expressing the 765 bp dsRNA in the LB culture (see Section 2.4.4) (without IPTG induction) was inoculated into both ^{14}N and ^{15}N media (see Section 0). The culture was supplemented with 10 µg/mL of tetracycline and 100 µg/mL Ampicillin. Reagent A (final concentration 1.5 U/L) was added to the culture before it was incubated at 37°C under continuous shaking conditions until an OD600 of 0.6 was achieved. Then, IPTG (1 mM final concentration) was added to the cultures to express the dsRNA, followed by a further 2 hours of incubation. The same procedure as described above was used to prepare the ^{14}N HT115 expressing 401 bp dsRNA culture supplemented with tetracycline (10 µg/mL) and kanamycin (50 µg/mL).

2.4.6 *In vitro* transcription of $^{13}C_{10}$, $^{15}N_5$ guanosine containing dsRNA

The amplified DNA (described in section 2.3) was used as the template for subsequent in vitro transcription in conjunction with HiScribe™ T7 High Yield RNA Synthesis Kit (New England Biolabs). To perform *in vitro* labelling, 2.0 µL of each the NTPs (10 mM) except for the GTP were replaced with GTP-$^{13}C_{10}$, $^{15}N_5$ 5'-triphosphate (Sigma-Aldrich). Next, 2µL of 10 x reaction buffer, 1µg DNA template and 2µL HiScribe™ T7 polymerase were added into in 20µL RNase-free water; the mixture was incubated at 37 °C for 4 hours.

The IVT reaction product was further subjected to solid phase spin column purification (see Section 2.5.1.8).

2.5 RNA preparation

2.5.1 Double-stranded RNA extraction

For the comparison of dsRNA extraction methods, $1x10^9$ HT115 *E. coli*. cells expressed with COIV PMA 765 bp dsRNA were used and each method was performed in three independent biological replicates as well as three technical replicates. Five different bacterial RNA extraction methods were evaluated: TRIzol Max, Ribopure kit, DNAzol, RNAzol, and RNAsnap. TRIzol max and Ribopure kit extractions were performed using the manufacturer's protocol with slight modifications in the procedures to improve the extraction yield.

2.5.1.1 Ribopure kit™ extraction

The sample was extracted according to the Ribopure Kit™ manufacturer's protocol to extract total RNA from the aqueous phase. The interphase was retained and re-extracted with the TRIzol max™ method. The new aqueous phase resulting from TRIzol max™ re-extraction was subjected to a one-time sample volume of isopropanol precipitation as well as an additional QIAGEN column purification method. To induce precipitation, the new organic phase (in which no interphase could be clearly identified) was subjected to a one-time sample volume of isopropanol.

2.5.1.2 RNAsnap extraction

The original protocol for RNA extraction proposed by Stead et al (2012) was followed except for some modifications: instead of using just one 100 µL of RNAsnap solution (see section 2.2.1) as suggested, three separate amounts of RNAsnap extraction solutions (100 µL 200 µL, and 300 µL respectively) were used. For each amount, the cell pellets were resuspended by adding the extraction solution and the mixture was vortexed vigorously. The samples were placed into a heating block set at 95°C and

incubated for 7 min to lyse the cells; the samples were then centrifuged at 16,000 rpm for 5 min at room temperature. The supernatant containing the RNA was carefully transferred to a fresh tube without disturbing the clean gelatinous pellet.

2.5.1.3 RNAsnap ethanol precipitation and solid phase extraction

The RNAsnap method was followed by both ethanol precipitation and QIAGEN solid phase extraction clean-up procedures to compare extraction yields. For the ethanol precipitation step, 1 mL of ethanol was added to the RNAsnap extracted sample and the mixture was incubated for 10 min, followed centrifugation at 20,238 rpm for 7 min. The supernatant was discarded, and the RNA pellet was washed with 1ml of 75% ethanol. Next, the sample was centrifuged for 5 min at 7,500 rpm. The supernatant was carefully removed without disturbing the RNA pellet. Lastly, the RNA pellet was air dried and resuspended in 100 µL of nuclease-free water.

For the QIAGEN solid phase extraction (clean-up) method, 500 µL of PB, 25 µL of isopropanol, and 50 µL of 5M NaCl was added to the sample, and the contents were mixed well by pipetting up-and-down. The mixture was applied to a QIAGEN silica membrane column with 2 mL collection tube and centrifuged at 13,000 rpm for 1 min before discarding the flow from the collection tube. Next, 750 µL of PE was applied to the column and the mixture was centrifuged at 13,000 rpm for 1 min with the flow being discarded. This was followed by centrifugation at 13,000 rpm again for 1 min. The silica column was transferred to a new tube and added with 100 µL of nuclease-free water. Subsequently, the sample was left at room temperature for 1 min before being centrifuged at 13,000 rpm for 1 min.

2.5.1.4 TRIzol Max™ extraction with different pH values

The TRIzol max™ reagent was neutralised by adding Tris-HCl to reach a pH of 7.5; this was compared with the original TRIzol solution (pH 4.5) according to the manufacturer's instructions for dsRNA extraction.

2.5.1.5 DNAzol® isolation method

Initially, 200 µL of TRIzol max bacterial enhancement reagent were preheated at 95°C, and the *E. coli.* pellet was resuspended in the reagent. The tube was then incubated at 95°C using a heating block for 4 min. Next, 1 mL of DNAzol® reagent was added to the lysate and the contents mixed well by repeated pipetting. After 4 min of incubating the homogenised samples, the RNA present in the aqueous phase were precipitated with 500 µL of pure ethanol. The mixture was incubated for 10 min and centrifuged at 20,308 rpm for 7 min at room temperature. After the RNA precipitate formed as a white pellet along the side and bottom of the tube, the supernatant was discarded carefully in order to not disrupt the RNA pellet. Then, the RNA pellet was washed with 1 mL of 75% ethanol, before being centrifuged at 7,500 rpm for 5 min at room temperature. The flow was discarded and the sample centrifuged at 7,500 rpm again. A micropipette was used to remove any remaining ethanol in the tube. The RNA pellet was left out in the air to dry for 1 min, before being resuspended in 100 µL of RNase-free water.

2.5.1.6 RNAzol® isolation method

Firstly, the sample was resuspended in 162.5 µL of RNase free water before adding 25 µL of 10 X phosphate buffered saline (PBS) and 6.25 µL of 20% SDS for homogenisation. The sample was mixed by, several times of tube inversion. The mixture was then incubated at 100°C for 5 min while flicking the tube several times to mix the contents. Next, 6.25 µL of proteinase K (Ambion) solution at 20 mg/mL was added and the mixture was incubated at 58°C for 30 min while mixing the contents as described above. Then, 625 µL of RNAzol® RT extraction solution was added and the contents were mixed with a pipette before being incubated for 10 min at room temperature. The mixture was centrifuged at 12,000 rpm for 15 min at room temperature. The supernatant (at least 805 µL) was transferred to a new tube leaving a layer of the supernatant above the DNA/protein pellet. An equal volume (805 µL) of isopropanol was added and the contents mixed by tube inversion to precipitate the RNA. The mixture was left to stand for 10 min before being centrifuged at 12,000 rpm for 10 min at room temperature. The RNA pellet was observed to be along the side and bottom of the tube. The RNA pellet was washed with 1.0 mL of 75% ethanol three

times, mixed well, and centrifuged at 8,000 rpm for 3 min at room temperature. After discarding the flow through and centrifuging again, the residual ethanol were carefully removed with a micropipette. The pellet was air-dried for a minute before it was resuspended in 100 µL of RNase free water.

2.5.1.7 RNAswift total RNA isolation method

The RNAswift protocol (A. O Nwokeoji et al., 2016) was used to extract total RNA from $1x10^9$ ^{14}N and ^{15}N HT115 cells expressing 765 bp dsRNA and ^{14}N HT115 cells expressing 401 bp dsRNA. To lyse the cells, 200 µL of lysis buffer (described in Section 2.2.1) was preheated at 95°C and used to resuspend the cells. The suspended cells were incubated at 90°C for 4 min. After cell lysis, 100 µL of 5M NaCl was added to the lysate and the mixture was homogenised by inverting the tube up to 6 times before incubating it for 3 min. The lysate was then centrifuged for 10 min at 13,000 rpm. The supernatant was collected and transferred to a fresh Eppendorf tube. RNA precipitation was performed by adding 500 µL of isopropanol and incubating for 5 min. The mixture was centrifuged for 5 min at 13,000 rpm and the flow-through was discarded. To wash the RNA pellet, 1 mL of 75% ethanol was used to resuspend the pellet prior to 5 min centrifugation. The ethanol was discarded and the RNA pellet allowed to air dry for 1 min. Finally, the pellet was resuspended in 100 µL of nuclease-free water.

2.5.1.8 ^{15}N in vivo and ^{13}C ^{15}N in vitro transcribed dsRNA purification

For the purification of ^{15}N HT115 cells expressed with 765 bp dsRNA, the same RNAswift method described in section 2.5.1.7 was followed, up to the supernatant collection step. Approximately 400 µL of supernatant was taken, and 0.1 µg of RNase A was added, followed by incubation at 37°C for 10 min. Prior to silica membrane column (Invitrogen) purification, 300 µL of IPD buffer (see Section 2.2.1) was added to the mixture. After loading the column, centrifugation was performed at 13,000 rpm for 1 min. The flow-through was discarded and 700 µL of wash buffer was added (see Section 2.2.1). Centrifugation was performed for 1 min and repeated once. The

purified dsRNA were eluted by adding 80 µL of nuclease-free water (QIAGEN, Germany). Membrane solid phase purification was also applied to clean up any possible impurities from the $^{13}C^{15}N$ GTP labelled in vitro transcript 401 bp dsRNA.

2.5.2 Enzymatic digestion of dsRNA

Purified, heavy isotopic-labelled dsRNA were mixed with light-labelled total RNA (expressed dsRNA) in a range of different amounts prior to RNase A enzymatic digestion. For digestion, 0.1µg RNase A was added to 1 µg of RNA sample. Digestion was performed for an hour at 37°C.

2.5.3 Determination of nucleic acid concentration

A NanoDrop 2000 UV visible spectrophotometer (Thermo Scientific) was used to determine the concentration of nucleic acids. The concentration of DNA/RNA was measured by using 10 µL of sample, diluting it with 490 µL of distilled water, and recording absorbance at 260 nm. The molar extinction coefficients (Table II-1) were used for the calculation of DNA/RNA concentrations.

Table II-1: Extinction Coefficient and Concentration by Nucleic Acid Type

Nucleic Acid Type	**Extinction Coefficient $(\mu g/mL)^{-1}$ cm^{-1}**	**Concentration (µg/mL) If A_{260} value = 1**
ssDNA	0.027	37
dsDNA	0.020	50
ssRNA	0.025	40

Using the conversion of molar extinction coefficients, the equations used to determine the concentrations of nucleic acid were as follows:

ssDNA (µg/mL)=Dilution factor × Absorption × 37

dsDNA (µg/mL)=Dilution factor × Absorption × 50

ssRNA (µg/mL)=Dilution factor × Absorption × 40

2.6 Liquid chromatography

2.6.1 Ion-pair reversed-phase chromatography

All procedures involving IP RP HPLC were performed on an Ultimate 3000 HPLC, a Transgenomic HPLC, or an Agilent 1100 HPLC using the columns listed in section 2.6.3 and the mobile phases listed in section 0, throughout the experiments, column temperature was maintained at 50°C (except for Section 5.3.3 was performed at both 50°C and 75°C) and the data were recorded at a UV wavelength of 260 nm.

All oligonucleotide quantification analyses (see Section 2.6.2) were performed using an Ultimate 3000 HPLC with an Accucore-150-C18 (50 mm x 2.1 mm) column.

2.6.2 Verification of oligonucleotide concentration using IP RP HPLC

To verify the quantification of the oligonucleotides based on NanoDrop measurements, individual oligonucleotides (see Section 2.1.3) at concentrations of 20 and 50 pmol were used. The samples were analysed in partial loop injection mode with an injection volume of 10 µl using standard IP RP HPLC buffers (listed in the 0).

2.6.2.1 Quantification of oligonucleotides using IP RP HPLC

To achieve accurate quantification of oligonucleotides, each sample was analysed at concentrations of 10, 20, and 50 pmol in full-loop injection mode with an injection volume of 84 µl. All analyses were performed using TBAA buffer systems.

2.6.2.2 Determination of oligonucleotide hydrophobicity

The three oligonucleotides listed in 2.1.3 were analysed at a concentration of 20 pmol using the standard IP RP HPLC buffers listed in 2.6.4.

2.6.3 Stationary phases

Columns	Company
ProSwift Monolith RP-1S (4.6 mm i.d. × 50 mm)	Thermo Fisher
ProSwift Monolith RP-2H (4.6 mm i.d. × 50 mm)	Thermo Fisher
ProSwift Monolith RP-3U (4.6 mm i.d. × 50 mm)	Thermo Fisher
Accucore C18 column (150 mm i.d × 2.1 mm)	Thermo Fisher
Accucore C18 column (50 mm i.d × 2.1 mm)	Thermo Fisher

2.6.4 Mobile phase compositions

Standard IP RP HPLC buffer A	
Triethylammonium acetate (TEAA)	100 mM
Acetonitrile	0.01%

Standard IP RP HPLC buffer B	
Triethylammonium acetate (TEAA)	100 mM
Acetonitrile	25%

TEAA+Urea IP RP HPLC buffer A	
Triethylammonium acetate (TEAA)	100 mM
Urea	10%
Acetonitrile	0.01%

TEAA+Urea IP RP HPLC buffer B	
Triethylammonium acetate (TEAA)	100 mM
Urea	10%
Acetonitrile	25%

TBAA IP RP HPLC buffer A	
Tetrabutylammonium acetate	5 mM
EDTA	1 mM
Acetonitrile	10%

TBAA IP RP HPLC buffer B	
Tetrabutylammonium acetate	5 mM
EDTA	1 mM
Acetonitrile	80%

Non-retentive HPLC Buffer A	
HPLC water	100%

Non-retentive HPLC Buffer B	
Acetonitrile	100%

2.6.5 Gradient conditions

2.6.5.1 IP RP HPLC gradient conditions

Gradient condition (1): Starting at 20% buffer B followed by a linear extension to 57.5% buffer B in 8 min at a flow rate of 0.4 mL min^{-1}, performed on Ultimate 3000 HPLC (see Section 2.6.4 for compositions of standard IP RP HPLC buffer systems A and B).

Gradient condition (2): Starting at 40% buffer B followed by a linear extension to 70% buffer B in 10 min at a flow rate of 0.4 mL min^{-1}, performed on Ultimate 3000 HPLC (see Section 2.6.4 for the compositions of TBAA IP RP HPLC buffer systems A and B).

Gradient condition (3): Starting at 20% buffer B followed by a linear extension to 57.5% buffer B in 15 min at a flow rate of 0.4 mL min^{-1}, performed on Ultimate 3000 HPLC (see Section 2.6.4 for the compositions of TBAA IP RP HPLC buffer systems A and B)..

Gradient condition (4): Starting at 25% buffer B followed by an increase to 40% buffer B in 3 min, followed by a linear extension to 50% buffer B over 10 min at a flow rate of 0.75 mL min^{-1}, performed on Agilent 1100 HPLC (see Section 2.6.4 for compositions of standard IP RP HPLC buffer systems A and B).

Gradient condition (5): Starting at 30% buffer B followed by an increase to 45% buffer B in 3 min, followed by a linear extension to 55% buffer B over 10 min at a flow rate of 0.75 mL min^{-1}, performed on Agilent 1100 HPLC (see Section 2.6.4 for compositions of standard IP RP HPLC buffer systems A and B).

Gradient condition (6): Starting at 22% buffer B followed by a linear extension to 62% buffer B over 17 min, then further extended to73% buffer B in 19.5 min at a flow rate of 1 mL min^{-1}, performed on Agilent 1100 HPLC (see Section 2.6.4 for compositions of standard IP RP HPLC buffer systems A and B for 5.3.1 experiment; TEAA+Urea IP RP HPLC buffer systems A and B for 5.3.3 experiment).

Gradient condition (7): Starting at 5% buffer B followed by an increase to 10% buffer B in 2 min, followed by a linear extension to 45% buffer B over 17 min, further extended to 60% buffer B in 19.5 min at a flow rate of 1 mL min^{-1}, performed on Transgenomic HPLC (see Section 2.6.4 for compositions of standard IP RP HPLC buffer systems A and B).

Gradient condition (8): Starting at 10% buffer B followed by an increase to 20% buffer B in 10 min, followed by a linear extension to 52% buffer B over 17 min, further extended to 63% buffer B in 19.5 min at a flow rate of 1 mL min^{-1}, performed on Agilent 1100 HPLC (see Section 2.6.4 for compositions of standard IP RP HPLC buffer systems A and B for 5.3.1 experiment; TEAA+Urea IP RP HPLC buffer systems A and B for 5.3.3 experiment).

Gradient condition (9): Starting at 25% buffer B followed by an increase to 50% buffer B in 3 min, followed by a linear extension to 60% buffer B over 10 min, applied at flow rates from 0.4 to 1.2 mL min^{-1} in 0.2 mL min^{-1} increments, performed on Transgenomic HPLC (see Section 2.6.4 for compositions of standard IP RP HPLC buffer systems A and B).

Gradient condition (10): Starting at 30% buffer B followed by an increase to 55% buffer B in 3 min, followed by a linear extension to 65% buffer B over 10 min, applied

at flow rates from 0.4 to 1.2 mL min-1 in 0.2 mL min^{-1} increments, performed on Transgenomic HPLC (see Section 2.6.4 for compositions of standard IP RP HPLC buffer systems A and B).

Gradient condition (11): Starting at 25% buffer B followed by an increase to 30% buffer B in 2 min, followed by a linear extension to 65% buffer B over 17 min, and then further extended to 80% buffer B in 19.5 min at a flow rate of 1 mL min^{-1}, performed on Transgenomic HPLC (see Section 2.6.4 for compositions of standard IP RP HPLC buffer systems A and B).

Gradient condition (12): Starting at 32% buffer B followed by an increase to 37% buffer B in 2 min, followed by a linear extension to 72% buffer B over 17 min, then further extended to 83% buffer B in 19.5 min at a flow rate of 1 mL min^{-1}, performed on Transgenomic HPLC (see Section 2.6.4 for compositions of standard IP RP HPLC buffer systems A and B).

2.6.6 Non-retentive HPLC

Non-retentive conditions refer the absence of the absorption at the surface media of the column. All non-retentive analyses were performed on the Ultimate 3000 HPLC using the columns listed in section 2.6.3 and the mobile phases listed in Section 2.6.4.

2.6.6.1 Non-retentive HPLC gradient condition

Gradient condition (13): 20% buffer B held for 2 min, applied at flow rates from 0.75 to 1.25 mL min^{-1} with 0.25 mL increments (see Section 2.6.4 for compositions of non-retentive buffer systems A and B).

Gradient condition (14): 50% buffer B held for 2 min, applied at flow rates from 0.75 to 1.25 mL min^{-1} with 0.25 mL increments (see Section 2.6.4 for compositions of non-retentive buffer systems A and B).

Gradient condition (15): 80% buffer B held for 2 min, applied at flow rates from 0.75 to 1.25 mL min^{-1} with 0.25 mL increments (see Section 2.6.4 for compositions of non-retentive buffer systems A and B).

2.7 Mass spectrometry analysis

2.7.1 Ion trap mass spectrometry

The development of a high-throughput analytical platform for the analysis of therapeutic oligonucleotides was performed using an ion trap mass spectrometer (HCT Ultra PTM Discovery System, Bruker Daltonics). All analyses were performed with different buffer systems (listed in section 2.7.2) and in full scan negative ion mode to data acquisition.

The ESI ionization voltage was set to -2000 V, the high-flow nebuliser was operated in a standard manner with nitrogen as the nebulising gas (1.51 L/min) and the injected drying gas flow rate was 6.0 L/min at 300° C. Mass range was selected from 300-1800 m/z, and the average of 3 spectra, as well as highest accumulated time, were maintained at 200,000 µs.

2.7.2 Mass spectrometry mobile phase components

A variety of ion-pair (IP) reagents in conjunction with different types of organic modifiers were tested at various concentrations. The pH values of the IP reagents were also adjusted to improve ESI-MS sensitivity and suppress cation adduct formations, so that enhanced signal intensities could be achieved.

The combinations of mobile phase systems are listed in the table below. All buffers were prepared with 50% acetonitrile and 50% HPLC grade water. For every experiment, each run was performed in technical triplicate on the same day to ensure consistent results (except for experiment 1). Experiments were then compared to determine which buffer had the greatest enhancement effect.

Description of experiment	Experimental Conditions	
	Mobile Phase System(s) Used	pH
BC2 oligonucleotide vs IP reagents	20 mM TEA with 0, 20, 50, & 80 mM HFIP 15 mM HA with 0, 20, 50, & 80 mM HFIP 5 mM TBA with 0, 20, 50, & 80 mM HFIP 20 mM DIPA with 0, 20, 50, & 80 mM HFIP	N/A
BC2 oligonucleotide vs Organic Modifiers HFIP, TFE, DMSO	5 mM TBAA with 0, 20, 50, & 80 mM HFIP 5 mM TBAA with 0, 20, 50, & 80 mM TFE 15 mM HAA with 0, 20, 50, & 80 mM HFIP 15 mM HAA with 0, 20, 50, & 80 mM TFE	pH = 7.4
	15 mM HA with 0,1, 5,10 & 20 % DMSO 5 mM TBA with 0,1, 5,10 & 20 % DMSO	N/A
BC2 oligonucleotide vs pH	5 mM TBA with 50 mM HFIP 15 mM HA with 50 mM HFIP	pH = 8.0 pH = 9.0 pH =10.0 pH =11.0
BC2, BC2b C6, and BC2b C12 oligonucleotide vs IP reagents	20 mM TEA with 0, 20, 50, & 80 mM HFIP 15 mM HA with 0, 20, 50, & 80 mM HFIP 5 mM TBA with 0, 20, 50, & 80 mM HFIP 20 mM DIPA with 0, 20, 50, & 80 mM HFIP	N/A

2.7.2.1 Mass spectrometry mobile phase pH value

The pH values of mobile phases with the IP reagents TBA and HA were dynamically adjusted by adding acetic acid as a counter ion. Acetic acid was used to bring the pH values in the mobile phase to neutral. The pH of both TBA and HA reagents started at 8.0 and were increased to their respective maximum pH points: 10.0 and 11.0.

2.7.3 Liquid chromatography and electrospray mass spectrometry

The RNase digestion products from stable isotopic labelled RNA were analysed on ESI-MS with maXis ultra-high-resolution time-of-flight (UHR-TOF) (Bruker, Daltonics) interfaced with a capillary liquid chromatography system (U3000, Dionex) and an Accucore C18 column (150 mm × 2.1 mm ID, Thermo Fisher). The buffer systems and gradient conditions for oligoribonucleotide separation are listed in the table below.

LC ESI MS Buffer A	
Triethylammonium acetate (TEAA)	20 mM
1,1,1,3,3,3,-Hexafluoro-2-propanol (HFIP)	80 mM

LC ESI MS Buffer B	
Triethylammonium acetate (TEAA)	20 mM
1,1,1,3,3,3,-Hexafluoro-2-propanol (HFIP)	80 mM
Acetonitrile	50%

Gradient condition (14): 10% buffer B held for 2 min, followed by a linear increase to 20% B in 20 min, followed by a linear extension to 25% B over 10 min, and finally a linear extension to 80% B in 2 min.

2.7.4 Ultra high-resolution time-of-flight mass spectrometry

Ultra high-resolution time-of-flight (UHR-TOF) mass spectrometry (Bruker, Daltonics) was performed in negative ion mode with a mass range selected from 300-2500 m/z for data acquisition. ESI Ionization voltage was set to -2000 V, capillary temperature was maintained at 300°C, N_2 nebuliser gas pressure was set at 0.4 bar and a flow rate of 6.0 L/h was used.

2.7.5 Data processing

The molecular weight and electrospray charge series of the oligonucleotides and oligoribonucleotide fragments obtained from an *in silico* RNase A digestion were calculated using the Mongo Oligo Mass Calculator (available at http://Library.med.utah.edu/masspec/mongo.htm).

A list of theoretical monoisotopic masses of the light version of RNase A digested oligoribonucleotides fragments was obtained by compiling all possible chemical terminals selected during data processing, including 5'-OH, 5'-phosphate, 5'-cyclic phosphate and 3'-OH 3'-phosphate, 3'-cyclic phosphate. The resulting theoretical monoisotopic masses were utilised to calculate the mass of heavy isotope oligoribonucleotide based on the number of nitrogen atoms contained in base compositions or the number of heavy labelled G present in the oligoribonucleotide sequences. The Isopro 3.1 software was used to calculate the theoretical monoisotopic mass spectrum peak distribution as well as the relative abundance peak in an isotopic series.

Data acquired by the ion trap mass spectrometer (HCT Ultra PTM Discovery System, Bruker Daltonics) from varying MS buffer systems were processed using total ion chromatograms (TIC) and deconvolution procedures from the software package Bruker Compass DataAnalysis (version 4.1, Build 317) as follows: 1) The desired dataset and spectra were opened. 2) Spectrum view to the Compound Spectra was copied using the command, “Copy to Compound Spectra and Deconvolute”. 3) The “Charge State Ruler” was activated. 4) The ruler for the Adduct Ion was set to –H 1 (which corresponds to negative mode ESI). 5) The ruler was moved until the Charge Series aligned with the corresponding oligonucleotide component mass (the correct peak was determined using Mongo). 6) Deconvoluted results were viewed using “Spectrum Data”, which included the mass and abundance of the component.

The TIC procedure was the same with the deconvolution procedure except at the end, where the electrospray series mass peak values were manually chosen to match exactly with the charge series. The sum of the values was obtained resulting in the total ion count for the sample.

2.7.6 Characterisation and quantification of oligoribonucleotides using stable isotope labelling in conjunction with LC ESI MS

To quantify oligoribonucleotide fragments using metabolic and *in vitro* stable isotope labelling, stable isotope labelled dsRNA were synthesised under both in vivo (^{15}N) and in vitro ($^{13}C_5{}^{15}N_{10}$ Guanosine containing dsRNA) conditions. Different amounts of heavy isotope-labelled dsRNA standards (with known concentrations) were subsequently spiked into light isotope- labelled total RNA (expressed dsRNA).

Prior to the experiment, all samples were quantified using UV spectrophotometry (see Section 2.5.3) followed by LC ESI MS analysis. Values of the ion abundance for the digested oligoribonucleotides were obtained from extracted ion chromatograms (XIC). Mass mapping approaches were subsequently used for the characterisation and absolute quantification of the dsRNA by identifying the same oligoribonucleotide in both light and heavy versions and measuring the ratio and peak areas for both light and heavy samples. This was done using Data Analysis (Bruker Daltonics) for ten identified oligoribonucleotides (from both the sense and antisense strands) in the ToF-MS scans to obtain sufficient statistical evidence.

2.8 Agarose gel electrophoresis analysis of nucleic acids

Gel electrophoresis analysis was performed on a horizontal gel apparatus (Bio-rad). 1% agarose powder was mixed with 100 mL of 1× Tris-Acetate-EDTA buffer (TAE) (described in Section 2.2.2). The mixture was dissolved using a microwave and swirled in a flask to ensure thorough mixing before allowing it to cool down. Ethidium bromide (0.5 µg mL^{-1}) was added to the agarose solution for staining. The agarose was poured into a gel tray, and a gel comb was inserted. After the gel was constructed, the gel comb was removed. The gel electrophoresis was set in the tank which was then filled up with TAE to cover the gel. Prior to the analysis, samples were prepared with appropriate volumes of loading Dye and loaded into the wells. Following sample loading, the gels were run at 100V for 45 min. Gel images were captured using a UV illuminator. The size and intensity of each sample were classified via comparison with the HyperLadder™ 1kb.

Chapter III : Optimisation of electrospray-ionisation mass spectrometry for the analysis of oligonucleotides

3.1 Abstract

The development of therapeutic oligonucleotides has led to an associated rise in demand for analytical tools to efficiently characterise these drug agents. Liquid chromatography electrospray ionisation mass spectrometry (LC-ESI-MS) is the most widely used analytical technique for the analysis of therapeutic oligonucleotides (Huber and Krajete, 1999). A key parameter in LC-ESI-MS performance is the physiochemical composition of the mobile phase, which has a critical impact on the efficiency of oligonucleotide ionisation (McGinnis et al., 2013; Chen et al., 2013; Gong and McCullagh, 2014).

The overall aim of the chapter is to focus on the development and optimisation of ESI-MS-methods for the analysis of oligonucleotides. Initial work focused on the optimisation of ESI-MS buffers and the relationship between oligonucleotide hydrophobicity and ESI-MS sensitivity. A range of ion-pair reagents and organic modifiers were evaluated in an attempt to optimise of oligonucleotide analysis. The results showed that a composition containing 5 mM tributylamine (TBA) with 80 mM hexafluoro-2-propanol (HFIP) produced the highest signal intensity with minimal cation adduct formation. Furthermore, the effects of various alkylamines on oligonucleotide charge state distributions were studied. In particular, HA and TBA produced lower higher charge state distributions respectively. Together, the results show that both the desorption efficiency of oligonucleotides and the resulting charge state distribution are correlated with the Henry's law constant of volatile alkylamines. Finally, the effects of oligonucleotide hydrophobicity and ESI-MS sensitivity was studied using oligonucleotides with C6 and C12 alkyl linkers. It was found that altering the oligonucleotides hydrophobicity did not significantly affect ESI-MS sensitivity under the experimental conditions.

3.2 Introduction

The application of analytical techniques is an important part of the development of antisense drugs, which includes the identification and quantification of oligonucleotides as well as their related impurities. Impure antisense drugs may cause detrimental effects such as off-target silencing of unwanted genes (Ivleva et al., 2008). Electrospray-Ionisation Mass-Spectrometry (ESI-MS) is a powerful technique for the study of oligonucleotides as it is compatible with online separation while preserving the solution phase for the conversion of macromolecules to gaseous ion form, which provides further specificity and structural characterisation ability (Huber and Krajete, 1999; Apffel et al., 1997).

Despite these advantages, the use of LC-ESI-MS for oligonucleotide analysis is hindered by the conflict between LC resolution and MS sensitivity, the formation of RNA-metal ion adducts which impede accurate analysis, and performance issues with larger oligonucleotides (Huber and Krajete, 1999).

Tremendous efforts have been made to develop an analytical platform capable of analysing therapeutic oligonucleotides in the presence of alkylamine ion-pairing reagents due to the fact that solution composition has a considerable effect on the magnitude of both signal enhancement and suppression (McGinnis et al., 2013; Chen et al., 2013; Gong and McCullagh, 2014).

3.2.1 ESI-MS mobile phases containing HFIP

Apffel et al. (1997a) first introduced a mobile phase for ESI-MS oligonucleotide analysis containing hexafluoro-2-propanol (HFIP) with triethylamine (TEA) (pH of 7.0), in which the TEA acts as an ion-pairing reagent while the HFIP acts a counter ion. Although the mechanism is not fully understood, it is proposed that HFIP rapidly evaporates from the electrospray droplet due to its high volatility and low boiling point (57°C), raising the droplet's pH value to 10.0. Then, oligonucleotide-TEA ion-pairs dissociate and enter the gas phase for desorption, resulting in enhanced ionisation of the oligonucleotides. The mechanism behind this mobile phase system was described by dynamically adjusted droplet pH values during the electrospray process, is a key

process in the selective removal of the anionic counter ion from the droplet via evaporation.

Moreover, Apffel et al. (Apffel et al., 1997) stated that the pH value of 10 promoted optimal oligonucleotide negative ion formation since it is critical for analytes to exist present as ions in a solution. Finally, the presence of a strong organic base such as TEA can successfully inhibit adduct formation. More recent work presented in this thesis demonstrates that a small amount of additional HFIP in the IP reagent greatly enhances oligonucleotide ionisation due to the availability of free protons for electrochemical reduction (Chen et al., 2013). Meanwhile, the competition for ionisation at the droplet surface occurs between the additional amounts of deprotonated HFIP ions from the mobile phase and oligonucleotide molecules.

3.2.2 Different mobile phase compositions

For the past 20 years, the TEA/HFIP combination has been the standard mobile phase for LC-ESI-MS analysis of oligonucleotides, while other IP reagents (shown in Table III-1) have been proposed as alternatives to TEA/TEAA. These alternative reagents were tested at different concentrations and pH values to reach the optimal conditions stated for both LC and MS.

Table III-1: IP reagents used in different studies

IP Reagent	Study
Tripropylamine (TPA)	(Huang et al., 2013)
N,N-dimethylbutylamine (DMBA)	(Oberacher, Parson, et al., 2001)
Hexylamine (HA)	(McCarthy et al., 2009)
N,N-diisopropylethylamine(DIEA)	(Chen and Bartlett, 2013)
Dibutylamine (DBA)	(Levin et al., 2011)
Tributylamine (TBA)	(McGinnis et al., 2013)

Recently, Basiri et al., (2017) systemically tested 15 different physiochemical IP reagents alongside 11 oligonucleotide sequences to determine which parameters influence the ESI ionisation of the oligonucleotide. They observed that TEA was not the ideal IP reagent compared to other IP reagents for all of the oligonucleotide

sequences tested as it considerably decreased the ESI-MS process sensitivity. This result suggests that alternative alkylamine IP reagents are necessary to improve the ESI-MS sensitivity of oligonucleotides. Another implication is that the choice of IP reagent should be considered on a case by case basis as its effectiveness would be strongly influenced by the oligonucleotide sequence being analysed. Unfortunately, this means that the optimal IP reagent for a given oligonucleotide has to be determined each time prior to the ESI-MS analysis, an additional step which encumbers method development.

Recently, McGinnis et al. (2013) systematically examined 13 IP reagents at different concentrations to compare the ionisation of oligonucleotides. The IP reagents with better signal intensity were selected for further testing with HFIP at a range of concentrations from 0-100 mM. It was found that the optimised mobile phase systems were 10 mM DIPA and 25 mM HFIP with methanol and 15 mM TPA and 50 mM HFIP for hydrophilic samples and modestly hydrophobic samples respectively.

The combination of HAA with HFIP has been previously reported as an effective mobile phase system for LC separation of both single- and double-stranded oligonucleotides (Gilar et al. 2003; McCarthy et al. 2009). However, Noll et al. (2011) highlighted that an HAA system was significantly less mass-sensitive than buffer systems containing HFIP. Even so, the use of a low mass-sensitive system like HAA has been suggested because of the role that acetate can play as a buffering acid (Apffel et al. 1997a: Bleicher, and Bayer 1994). On the other hand, combining HA as the IP reagent with HFIP has been proposed, as HFIP performs better compared to acetate due to its higher volatility and constant evaporation through the electrospray (Huber and Oberacher 2001). This is supported by work showing that 15 mM HA and 50 mM HFIP outperformed other IP reagents including TEA for oligonucleotide analysis (Gong and McCullagh, 2014).

3.2.3 Alternative to hexafluoro-2-propanol: Trifluoroethanol

Trifluoroethanol (TFE) has been proposed as an alternate organic modifier to HFIP (Cech and Enke, 2001), since it can produce deprotonated anions with stability, thus improving ESI response. Additionally, TFE is a solvent with weak acidity that does not

affect the pH regardless of concentration (Wu et al., 2004). This facilitates the electrochemical reaction by producing trifluoroethoxide and hydrogen (Cech and Enke, 2001), which is the dominant reaction in negative-ion ESI (Chen et al., 2013). Moreover, Wu et al. (2014) pointed out that TFE is more responsive to hydrophobic samples compared to hydrophilic ones.

Similar to HFIP, the boiling point (74.0°C) of TFE is also lower than that of TEA (88.0°C). Chen et al. (Chen et al., 2013) tested the impact of TFE on oligonucleotides and showed that TFE did not alter the charge state regardless of concentration and could not evaporate fast enough to avoid the suppression and deprotonation of oligonucleotides. In summary, although TFE may substitute HFIP, the lack of studies supporting it and the combined benefits of medium acidity and volatility of HFIP makes HFIP a better acidic modifier over TFE.

3.2.4 Influence of mobile phase pH values on ESI-MS Ionisation

Due to the importance of pH, Gong and McCullagh (2014) proposed that increasing IP reagent concentration elevates the pH value of the mobile phase. When near its pKa value, an IP reagent, becomes less dissociated, directly affecting protonation and IP efficiency.

Bleicher and Bayer (1994) reported that raising the solution pH and the percentage of organic solvent significantly increased droplet charge during ionisation. However, it should be noted that even mild variations in pH concentration can have a significant effect on ionisation, selectivity, capacity factor, and resolution. Therefore, pH values should be carefully controlled to ensure sufficient experimental reproducibility. Optimal pH values have been suggested for a mobile phase containing a mixture of buffer and acid to resist change when the sample and ionisable analytes enter the column (Mannur et al., 2011).

3.2.5 Effect of analyte hydrophobicity on ESI-MS performance

Studies show that the hydrophobicity of oligonucleotides has a strong correlation with electrospray ionisation efficiency (Null et al., 2003; McGinnis et al., 2013). The contribution of hydrophobicity and the correlated free energy with solvation on the ESI-MS spectrum of nucleic acids was evaluated (Null et al. 2003). An improved correlation between higher signal intensity and increasing hydrophobicity was observed, by adding an alkyl chain to the 5' terminus on a 20-mer oligonucleotide.

In summary, the available literature suggests that the choice of alkylamine ion-pairing reagents in ESI-MS has the most significant effect on oligonucleotide signal intensity. The main parameters to be considered for an IP reagent are its boiling point, proton affinity, water solubility, Henry's law constant, as well as the hydrophobicity content of the oligonucleotides. However, a range of contrasting data and theories are evident in the literature. (Apffel et al., 1997; Null et al., 2003; Huber and Oberacher, 2002; Chen et al., 2013; McGinnis et al., 2013; Gong and McCullagh, 2014; Basiri and Bartlett, 2014; Basiri et al., 2017).

This chapter describes approaches to the development and optimisation of ESI-MS for oligonucleotides analysis. In addition, the aim was to study the effect of different hydrophobic tags on oligonucleotides on ESI-MS sensitivity. Initial work focused on the optimisation of an ESI-MS mobile phase. Six ion-pairing reagents of interest (TBA, TBAA, TEA, HA, HAA and DIPA) were systematically examined in combination with various types of organic modifiers and pH values.

3.3 Results and discussion

Part A

3.3.1 Effect of different IP reagents on ESI-MS analysis of oligonucleotides

The experimental objective was to determine how different IP reagents in combination with varying concentrations of HFIP affect the ESI-MS analysis (ESI signal) of oligonucleotides, which were 2 µM infusions of a 15 mer oligonucleotide (BC2 see materials and methods). The IP reagents tested were TEA, HA, TBA, and DIPA while HFIP concentrations ranged from 0 mM to 80 mM. A typical MS spectrum of the oligonucleotide obtained in negative ion mode is shown in Figure III-1 with its different charge states highlighted. Following data acquisition, the signal intensity of all corresponding charge states for the oligonucleotide (i.e. total ion chromatogram) was recorded for each of the different buffer compositions (see Figure III-2).

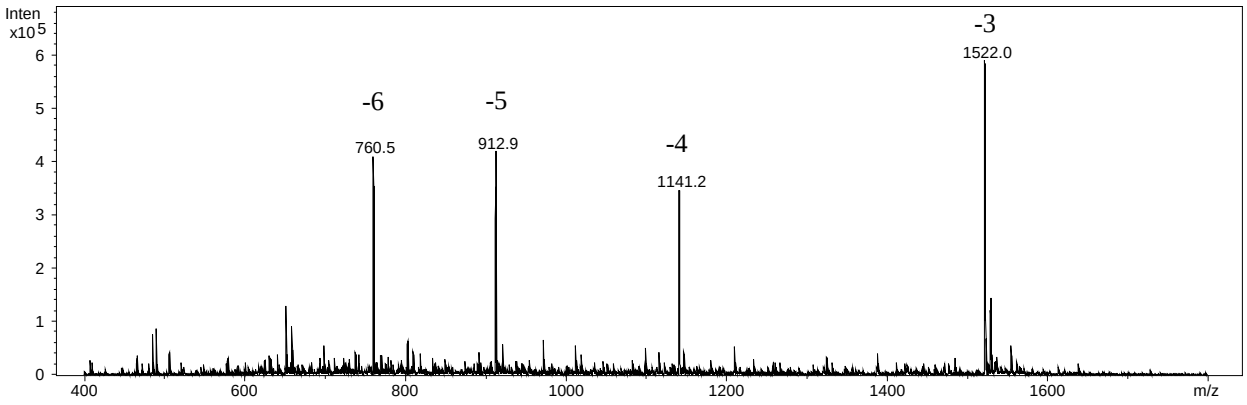

Figure III-1: A typical MS spectrum of the 15 mer oligonucleotides obtained in negative ion mode. The range of different charge states from -3 to -6 are highlighted.

Table III-2: Physiochemical properties of the ion-pair reagents in this study

IP agent	Boiling point (°C)	Proton affinity (kcal/mol)	Water Solubility (g/L)	$k_{H,cc}$ (aq/gas)	pKa
HA	130.00	221.70	20.57	1.57	10.56
DIPA	83.90	232.30	75.31	0.42	11.05
TEA	89.70	234.70	68.30	0.35	10.78
TBA	216.50	238.60	0.08	0.08	10.90

*HA=Hexylamine, DIPA= Diisopropylamine, TEA= Triethylamine, TBA= Tributylamine

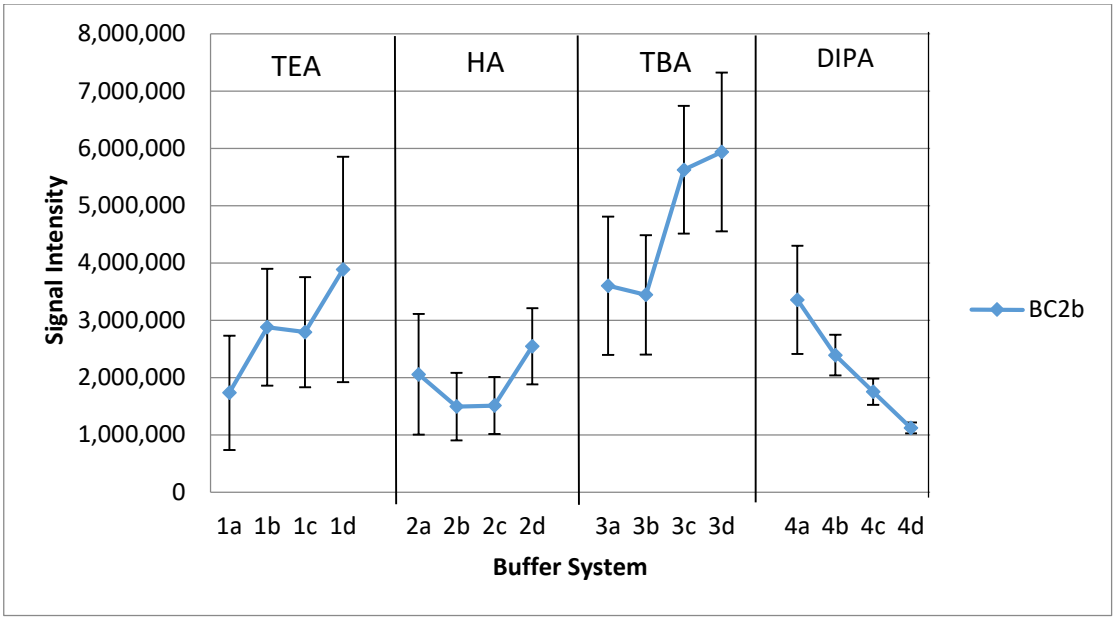

Figure III-2: ESI-MS signal intensity of unmodified 15 mer (5'-CAAAAGTCCGTGAGA-3') oligonucleotide, with concentration at 2 µM. Samples were infused with 4 sets of buffers; Set 1 (a,b,c,d) 20 mM TEA with 0, 20, 50, 80 mM HFIP respectively; Set 2 (a,b,c,d) 15 mM HA with 0, 20, 50, 80 mM HFIP respectively; Set 3 (a,b,c,d) 5 mM TBA with 0, 20, 50, 80 mM HFIP respectively; Set 4 (a,b,c,d) 20 mM DIPA with 0, 20, 50, 80 mM HFIP respectively, were studied on ESI-MS in negative ion mode. The signal intensity (total ion chromatogram) for each buffer composition was recorded for three minutes and performed in triplicates. The means and standard deviations for each triplicate were calculated.

Firstly, TEA (Figure III-2, 1a-1d,) displayed a general increase in signal intensity with increasing amounts of HFIP. The highest signal (~4 x 10^6) was obtained with 80 mM HFIP, which is twice as high compared to TEA without HFIP. Secondly, with HA (Figure III-2, 2a-2d), a U-shaped trend can be observed, with signal intensities dropping after initial addition of HFIP before increasing again when 80 mM HFIP was added. In this case, only a small increase in intensity was observed through the addition of HFIP.

Thirdly, TBA (Figure III-2, 3a-3d) produced the greatest effect of signal enhancement, with a maximum value at 80 mM of HFIP (3d), an almost 100% improvement over 0 mM HFIP (3a). Furthermore, this value was the highest recorded among all buffer combinations, suggesting that it is the optimum combination for the oligonucleotide studied. Finally, for DIPA (Figure III-2, 4a-4d), a downward trend was observed when the HFIP concentration was increased. DIPA with 80 mM HFIP (4d) produced the

lowest signal intensity among all buffer combinations, implying that DIPA performs better without any HFIP added.

Overall, it appears that for the analysis of the 15 mer oligonucleotide (BC2), a combination of 5 mM TBA with 80 mM HFIP provides the highest signal intensity across all buffers, followed by 20 mM TEA, 20 mM DIPA and 15 mM HA. These results may be related to the Henry's Law constant as the IP reagent with the lowest $k_{H,cc}$ (aq/gas) produced the highest ESI-MS signal. This conclusion is supported by Chen et al. (2013) who proposed that IP reagents with lower $k_{H,cc}$ (aq/gas) result in an increase of the oligonucleotide concentration at the droplet surface, thus leading to more effective ionisation. However, the positive effect of the Henry's Law constant may be dependent on the sequence of the oligonucleotide used, as a recent study has shown conflicting results (Basiri et al., 2017)

Unfortunately, the results of this experiment could not confirm a link between increasing concentration of HFIP and enhancement of oligonucleotides signal intensity. It is possible that certain IP reagents respond adversely to HFIP which explains the negative correlation in the case of HA and DIPA. It has been suggested that the complex interaction between the physiochemical properties of the buffer components and the solubility of IP reagents in HFIP may have an effect (Gong et al. 2014).

3.3.2 Effect of varying alkylamines on cation formation and charge state distribution

In addition to signal intensity, the effect of different IP reagents with varying HFIP concentrations on cation adduct formation and charge state distribution were investigated. The ESI-MS spectra of the oligonucleotide in the presence of TEA is shown in Figure III-3, where the charge state distribution and the sodium adducts observed in the 3- charge state are highlighted. Analysis of the charge state distribution revealed a range of values from 7- to 3- under these conditions, with the 3- charge state as the most abundant especially in the presence of 80 mM HFIP.

The ESI-MS spectra of the oligonucleotide analysed in the presence of HA displayed low levels of cation adduction as shown in Figure III-4. However, when HFIP was added to the system, a few observations were noted: (1) the charge state distribution

was reduced and the 7- charge state was no longer observable; (2) the extent of sodium adduction was reduced; (3) the spectral pattern shifted, with the most intense signal moving from the higher charge states 5- and 6- to the lower charge state 3- (i.e., the charge state was reduced). Hence, the addition of HFIP (a weak acidic modifier), is predicted to lower the solution's pH value and provide additional protons to the oligonucleotides, leading to a shift in the observed charge state distribution, consistent with previous observations (McGinnis et al., 2013).

The ESI-MS spectra of the oligonucleotide analysed in the presence of TBA is shown in Figure III-5. The combination of TBA and HFIP led to improved spectral quality, while a small amount of cation adduction was observed. For TBA, the most abundant charge state was 6- across all HFIP concentrations (20-80 mM) while the absence of HFIP showed a similar effect as with HA without HFIP. The highest intensity switched the charge state from 5- to 6- after HFIP was added. Interestingly, the results show significant differences compared to the addition of HFIP to HA. The ESI-MS spectra of the oligonucleotide analysed in the presence of DIPA is shown in Figure III-6 Charge state distribution analysis revealed that for DIPA without HFIP, the most intense charge states were 5- and 6-. In general, increased abundance of the 3- charge state was observed with the addition of HFIP in a similar manner to that observed for TEA and HA. The mobile phase systems consisting of DIPA and HFIP showed a small reduction in cation adduction with increasing HFIP, suggesting a positive correlation between higher HFIP concentration and reduced cation adduction.

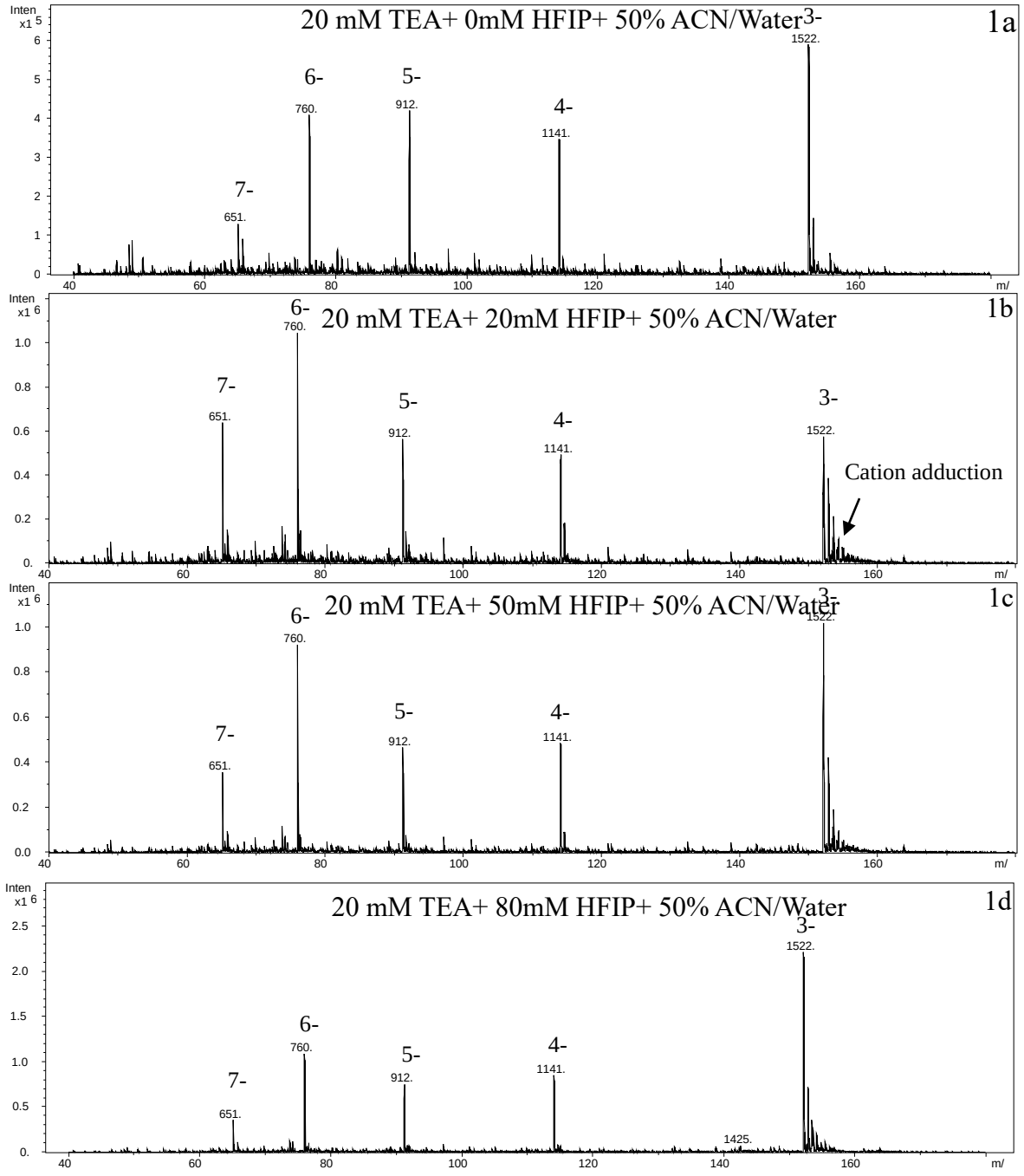

Figure III-3: Spectrum of 15 mer (5'-CAAAAGTCCGTGAGA-3') oligonucleotide at a concentration of 2 µM infused with 20 mM of TEA and 0 - 80 mM HFIP: studied using ESI-MS negative mode. The spectrum shows cation adduction and charge state distribution. Data were recorded for three minutes.

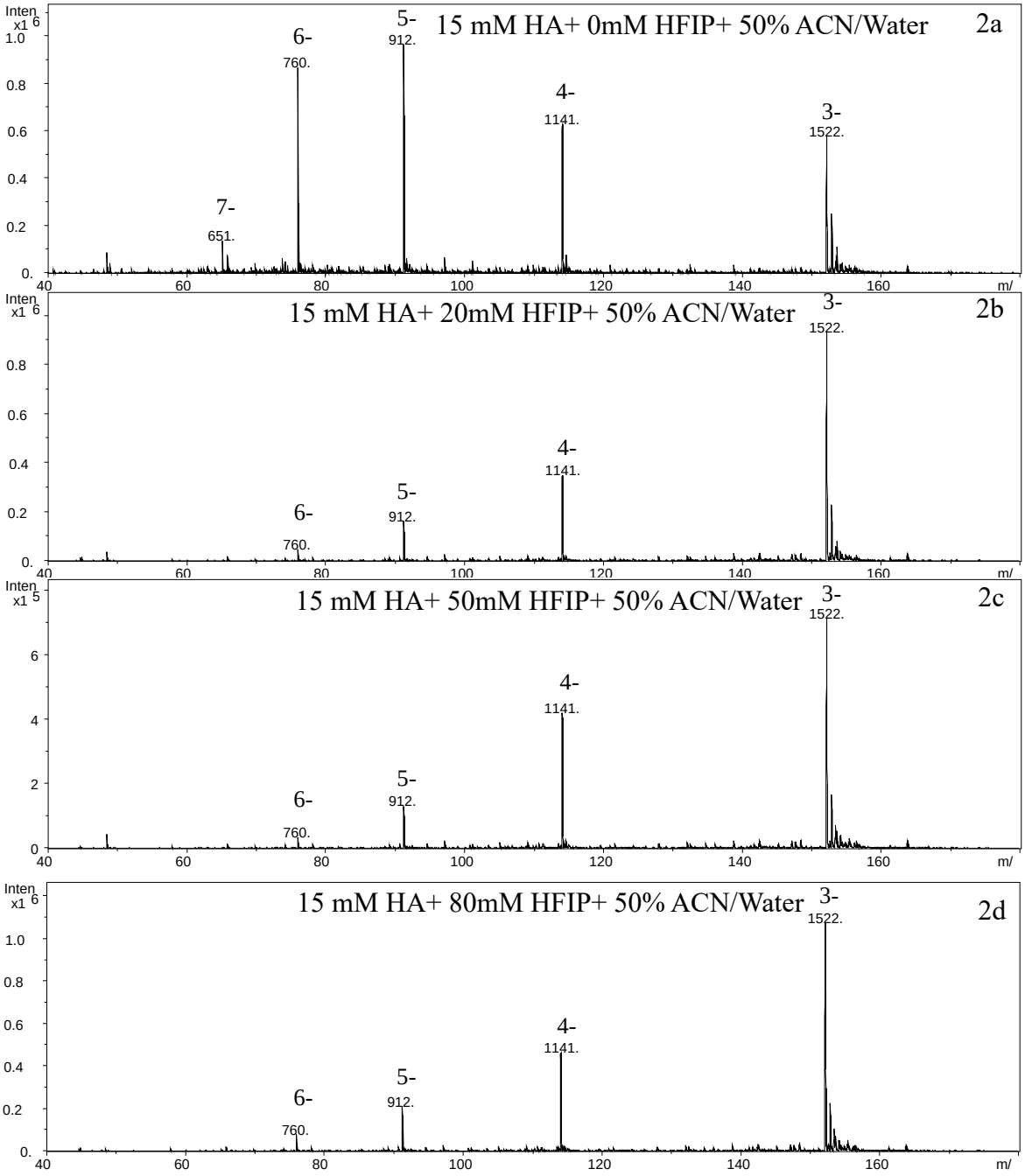

Figure III-4: Spectrum of 15 mer (5'-CAAAAGTCCGTGAGA-3') oligonucleotide at a concentration of 2 µM infused with 15 mM of HA and 0 - 80 mM HFIP: studied using ESI-MS negative mode. The spectrum shows cation adduction and charge state distribution. Data were recorded for three minutes.

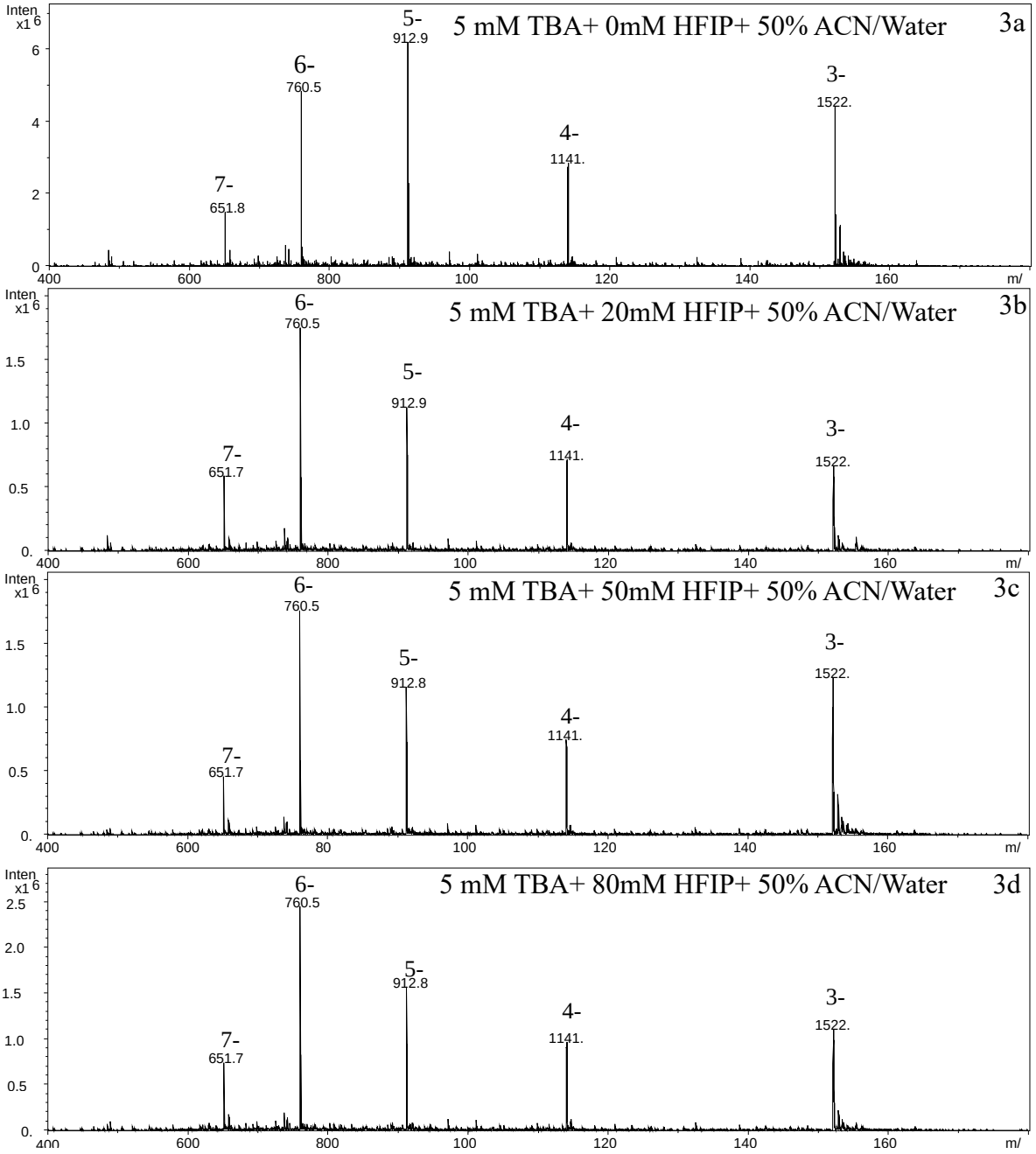

Figure III-5: Spectrum of 15 mer (5′-CAAAAGTCCGTGAGA-3′) oligonucleotide at a concentration of 2 µM infused with 5 mM of TBA and 0 - 80 mM HFIP: studied using ESI-MS negative mode. The spectrum shows cation adduction and charge state distribution. Data were recorded for three minutes.

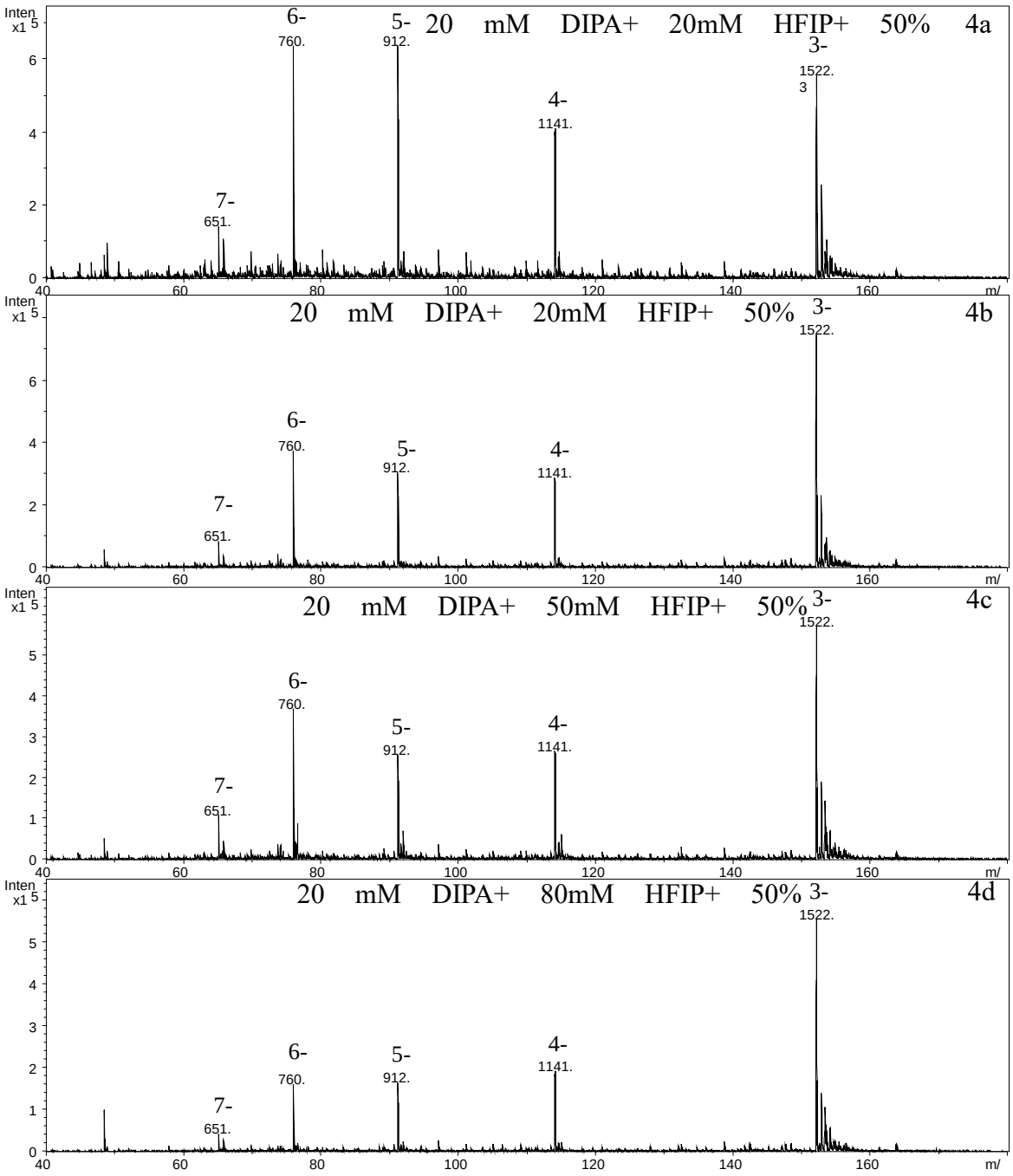

Figure III-6: Spectrum 15 mer (5'-CAAAAGTCCGTGAGA-3') oligonucleotide at a concentration of 2 µM infused with 20 mM of DIPA and 0 - 80 mM HFIP: studied using ESI-MS negative mode. The spectrum showed cation adduction and charge state distribution. Data were recorded for three minutes.

3.3.3 Charge state distribution of different alkylamine ion-pair reagents

A comparison of the charge state distribution of the 15-mer oligonucleotide across 4 different IP reagents with 20 mM HFIP is shown in Figure III-7. Significant charge reduction was observed on the 15 mM HA buffer system, which could be explained using either Henry's law or the effect of the pKa value.

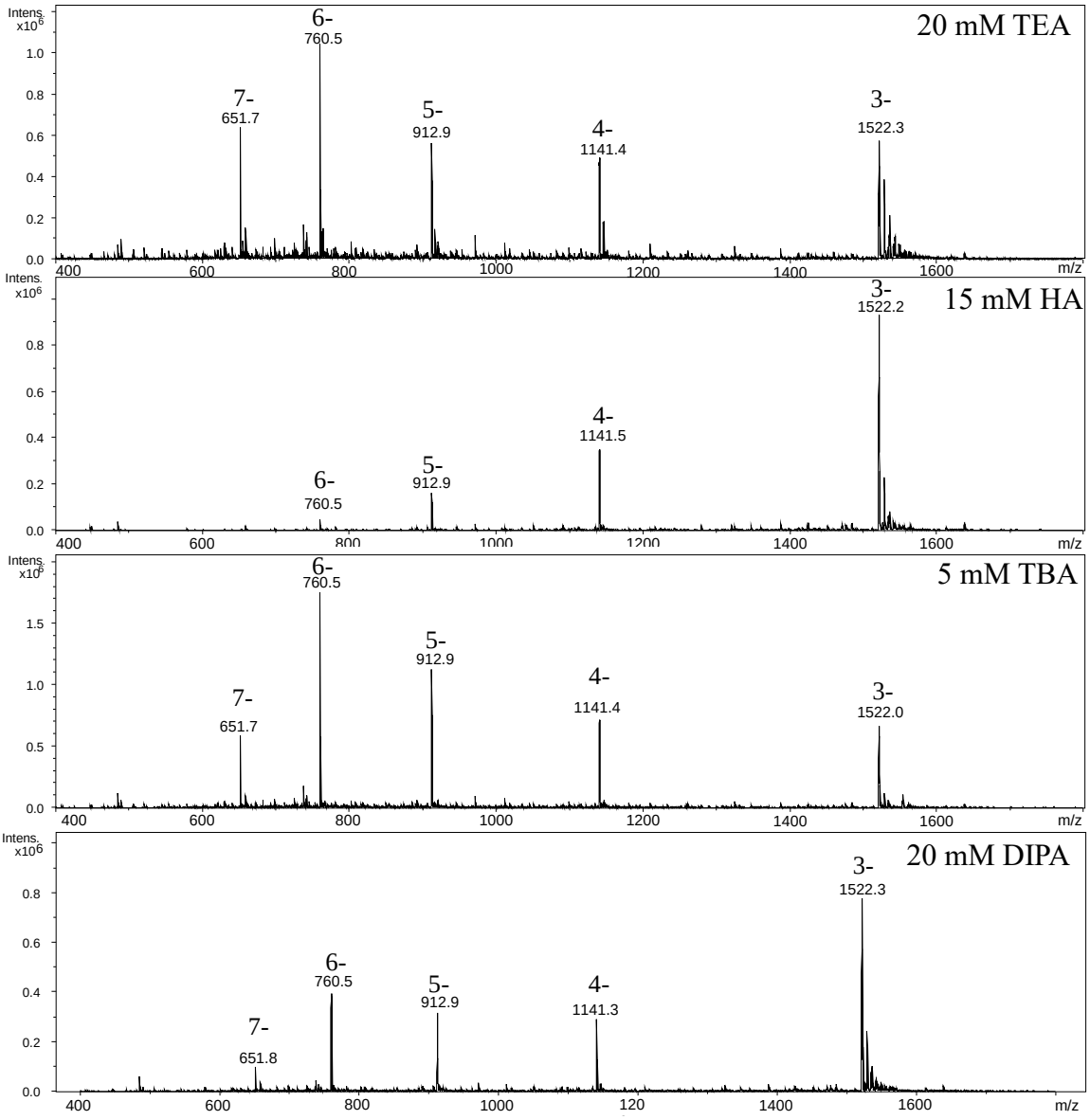

Figure III-7: MS spectrum of the oligonucleotides in negative mode showing the observed charge state distribution of the 15 mer (5'-CAAAAGTCCGTGAGA-3') oligonucleotide at a concentration of 2 µM was infused within TEA, HA, TBA and 20 mM HFIP+50% ACN/Water. Data were recorded for three minutes.

Figure III-7 show that HA which has the highest $k_{H,cc}$(aq/gas) also has the lowest charge state distribution (predominantly 3-) while TBA which has the lowest $k_{H,cc}$(aq/gas) has the highest charge state distribution (predominantly 6-). Constants for other IP reagents used in the experiment are given in Table III-2. These results are consistent with the conclusions drawn by Chen et al. (2013) the $k_{H,cc}$(aq/gas) has the effect of reducing the charge state distribution as the higher the reagent's $k_{H,cc}$(aq/gas) (such as HA), the more likely it is to remain in solution with the analyte to form a complex before separating from the analyte during the subsequent droplet evaporation process. The pKa value is another factor which may have influenced the results. It was observed that HA having the lowest pKa (10.56) out of all the IP reagents and, in the presence of 20 mM of acidic modifier HFIP resulted in the lowest charge state reduction across all the IP reagents evaluated.

3.3.4 Effect of pH on the ESI-MS mobile phase for the analysis of oligonucleotides

The present work evaluated the influence of the pH values of the IP reagents: hexylamine (HA) and tributylamine (TBA) on ESI-MS response in negative ion mode. Acetic acid was added to the alkylamines to generate buffers with the desired pH. The evaluation was done by comparing the signal intensities at pH values of 8, 9, 10, and 11 with a 15 mer (5'-CAAAAGTCCGTGAGA-3') oligonucleotide at a concentration of 2 µM. Each buffer composition was analysed to obtain the oligonucleotide signal intensity (total ion chromatogram) for three minutes. From Figure III-8, it can be seen that for HA, signal intensity increased with pH up to a maximum of 11.0 (Figure III-8). In the case of mobile phases with higher pH values, acetic acid was added to convert the solution to neutral. It follows that the solution containing more acetic acid has lowered ionisation efficiency due to competition between acetate ions and the oligonucleotides, an inference that is supported by results in literature (Apffel et al. (1997a). For TBA, the greatest signal intensity was observed at pH 9 rather than the expected pH of 10. However, as with HA, the lowest signal intensity was observed with the most acetic acid present (pH 8.0).

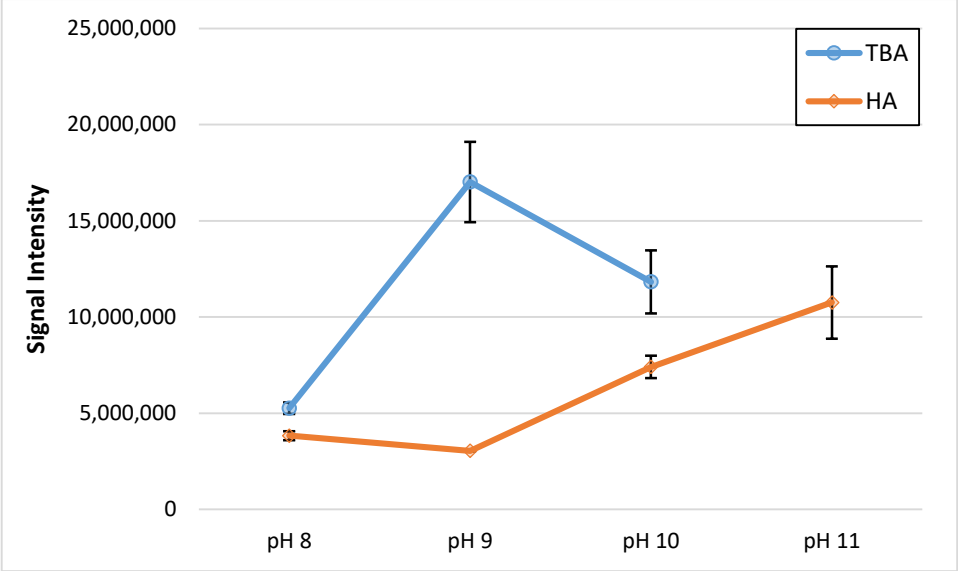

Figure III-8: The effect of pH values on signal intensity using 5 mM TBA and 15 mM HAA.

3.3.5 Effect of pH on the charge state distribution of IP reagents TBA and HA

The effect of varying pH values on the charge state distribution of buffers with TBA and HA was also investigated. The pH of the buffer systems was adjusted by lowering the pH using acetic acid to form the IP-acetate ions. TBA buffer was tested in the pH range of 10.0 to 8.0 (Figure III-9). As the pH was lowered from 10.0 to 8.0, the most intense signal shifted from the higher charge states of -6 and -5 to the lower charge state of -3. In addition, the signal intensity at the higher charge states (-7) weakened considerably. The pattern of the charge state distribution at pH 9.0 was similar to that at pH 10.0 but with stronger intensities at most charge states except -3. These observations suggest a relationship between the amount of acetic acid added and the degree of charge state reduction.

Previous experiments showed that HA might have an effect on charge state reduction when compared with other IP reagents. In this experiment using HA, it was observed that the -4 charge state was more intense at pH 8.0 than at pH 9.0 (Figure III-10). In addition, from Figure III-12. The total ion count signal intensities were higher at pH 10.0/11.0, further demonstrating that increasingly adding acetic acid as a counter ion results in signal suppression. A similar pattern of charge state distribution was observed between pH 9.0 and pH 10.0.

Interestingly, at pH 11.0 (i.e. without any acetic acid added), additional charge states of -7 and -8 appeared (Figure III-10). This finding is supported by Muddiman et al., (1996) who reported that the addition of acetic acid to the solution resulted in charge state reduction. As can be seen from pH 8.0 to11.0, higher amounts of acetic acid weakened the signal intensities at the higher charge states. In other words, depending on whether the IP reagent is contained in a more acidic or basic solution, the charge states will decrease or increase respectively.

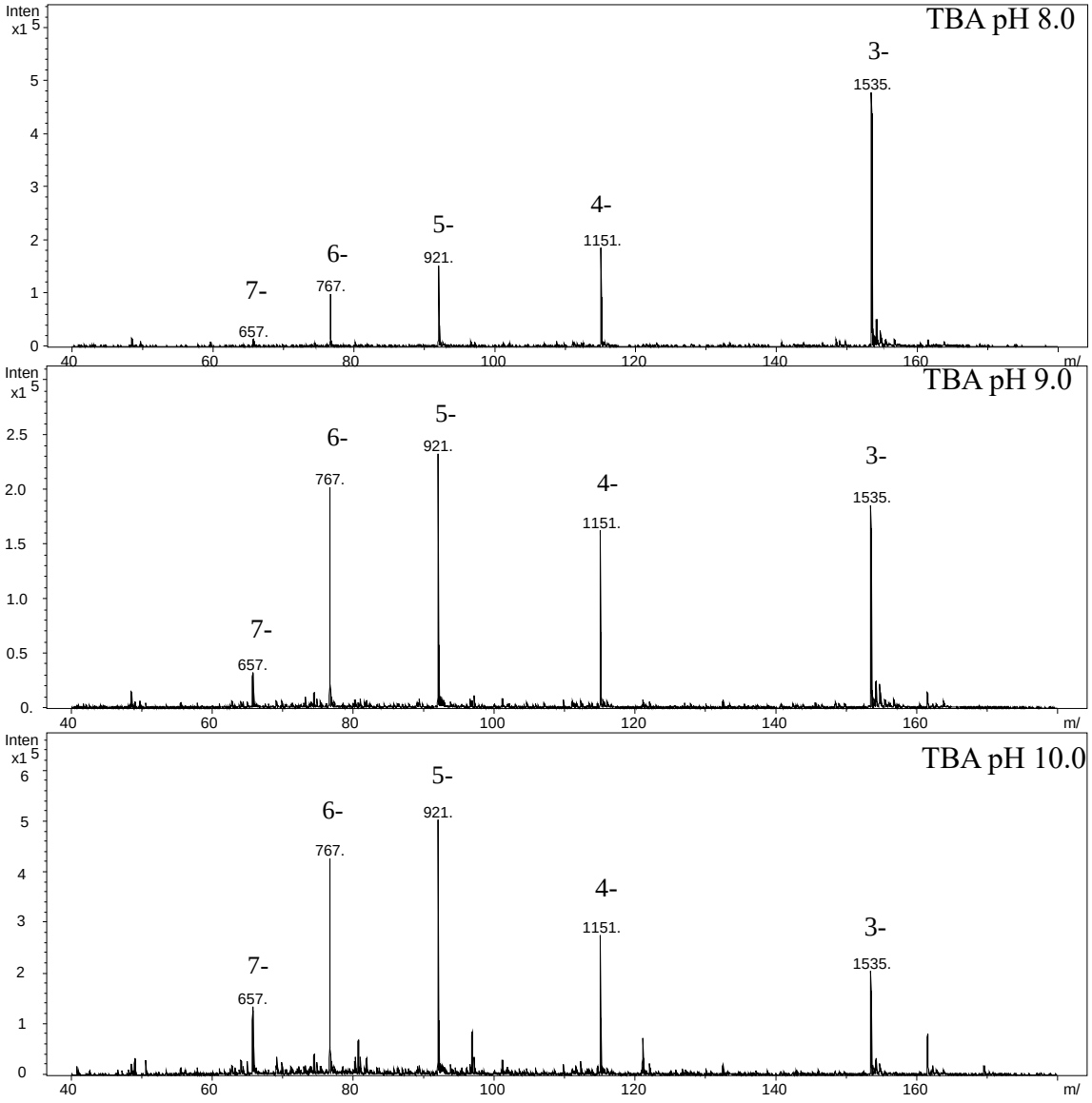

Figure III-9: MS spectrum showing the effect of pH values on the charge distribution of the 15 mer (5'-CAAAAGTCCGTGAGA-3') oligonucleotide at a concentration of 2 µM with 5 mM TBA. Data were recorded for three minutes.

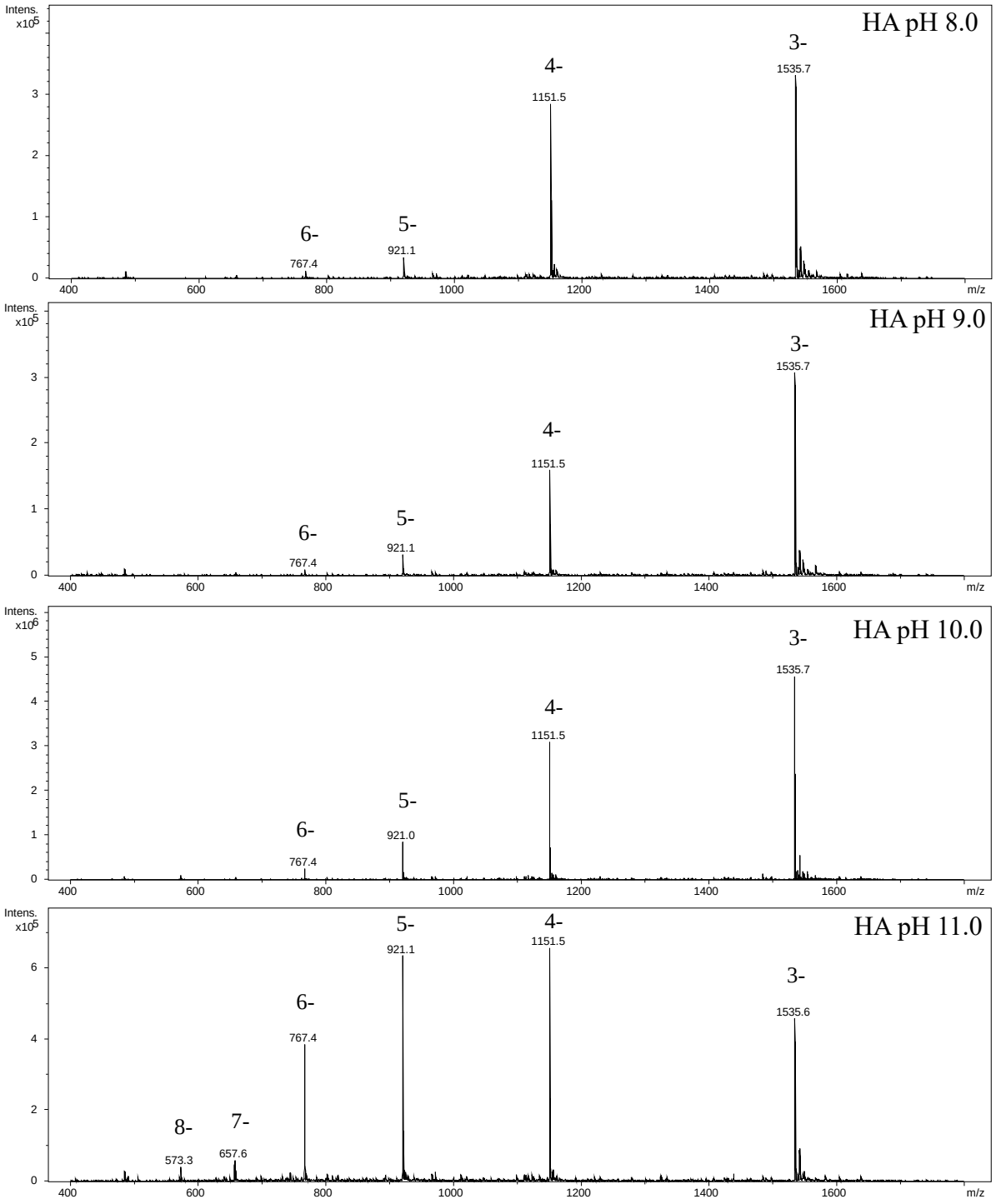

Figure III-10: MS spectrum showing the effect of pH values on the charge distribution of the 15 mer (5'-CAAAAGTCCGTGAGA-3') oligonucleotide at a concentration of 2 µM with 15 mM HA. The data were recorded for three minutes.

3.3.6 Effect of organic modifiers HFIP, TFE and DMSO in the mobile phase

In this experiment, HAA and TBAA were used as buffers instead of HA and TBA to study how the addition of ammonium acetate affects oligonucleotide ESI-MS ionisation. HAA and TBAA were chosen in particular due to their large relative differences in $k_{H,cc}$ (aq/gas). In addition, the effect of different organic modifiers was studied using HFIP, TFE and, DMSO with 5 mM TBAA and 15 mM HAA for the analysis of oligonucleotides using ESI-MS. It was hypothesised that each of these organic modifiers would have a specific magnitude of enhancement effect on ESI-MS performance.

The experiment was performed with 15-mer (CAAAAGTCCGTGAGA) oligonucleotides at a concentration of 2 µM. The oligonucleotides were infused with either 5 mM TBAA or 15 mM HAA in combination with HFIP or TFE in the range of 0-80 mM. The samples were studied on ESI-MS using negative-ion mode. The signal intensity (i.e. total ion chromatogram) was recorded for three minutes for each buffer composition, and the results are summarised in Figure III-11.

The data show that for 5 mM TBAA, the optimal concentration of HFIP was 10 mM, which produced the highest signal intensity (total ion count, TIC) (see Figure III-11). It is notable that further increasing the concentration of HFIP to 80 mM significantly reduced signal intensity to approximately 5,000,000 counts, but high concentrations of TFE did not critically suppress the signal intensity. At 10 mM and 20 mM of HFIP and TFE, similar effects were observed, resulting in approximately equal values for signal intensity. Finally, whereas 80 mM of HFIP induced ion suppression, 80 mM of TFE appeared to boost signal intensity, though the signal intensity was still almost equal to that at 0 mM TFE.

Based on Figure III-11 B and Figure III-12 B, the standard deviations for each dataset are relatively low, except for the 20 mM TFE and 0 mM HFIP and 20 mM TFE datasets, which were likely due to instrument instability. The experiment was run in instrument triplicate on the same day. When HAA was used as the IP reagent (Figure III-12 A), a similar trend to TBAA was observed. No significant changes in ESI intensity were observed between 0-20 mM HFIP/TFE. At 80 mM of HFIP, more suppression occurred, with the signal intensity below the original value without HFIP. The results for TFE

were unexpectedly similar to HFIP at concentrations of 10 mM and 20 mM. At 80 mM the results diverged with TFE and showed a slightly increased signal intensity. The findings of this experiment are consistent with the conclusions of Wu et al. (2004) who found that high concentrations of TFE (>100 mM) improved signal intensity. In addition, McGinnis et al. (2013) noted that lower HFIP concentrations (25 - 50 mM) are more effective than higher HFIP concentrations (100 mM).

Overall, at the same concentration of organic modifier, 15 mM HAA performed better than 5 mM TBAA at enhancing signal intensities. On the other hand, the HAA and TFE combination did not show significant improvement in signal intensity with increasing TFE concentration. Thus far, published details on the use of the combination of HAA and TFE and its effects on signal intensity have been scarce, thus motivating this study. Based on the results, this combination may have potential as a signal-enhancing mobile phase system.

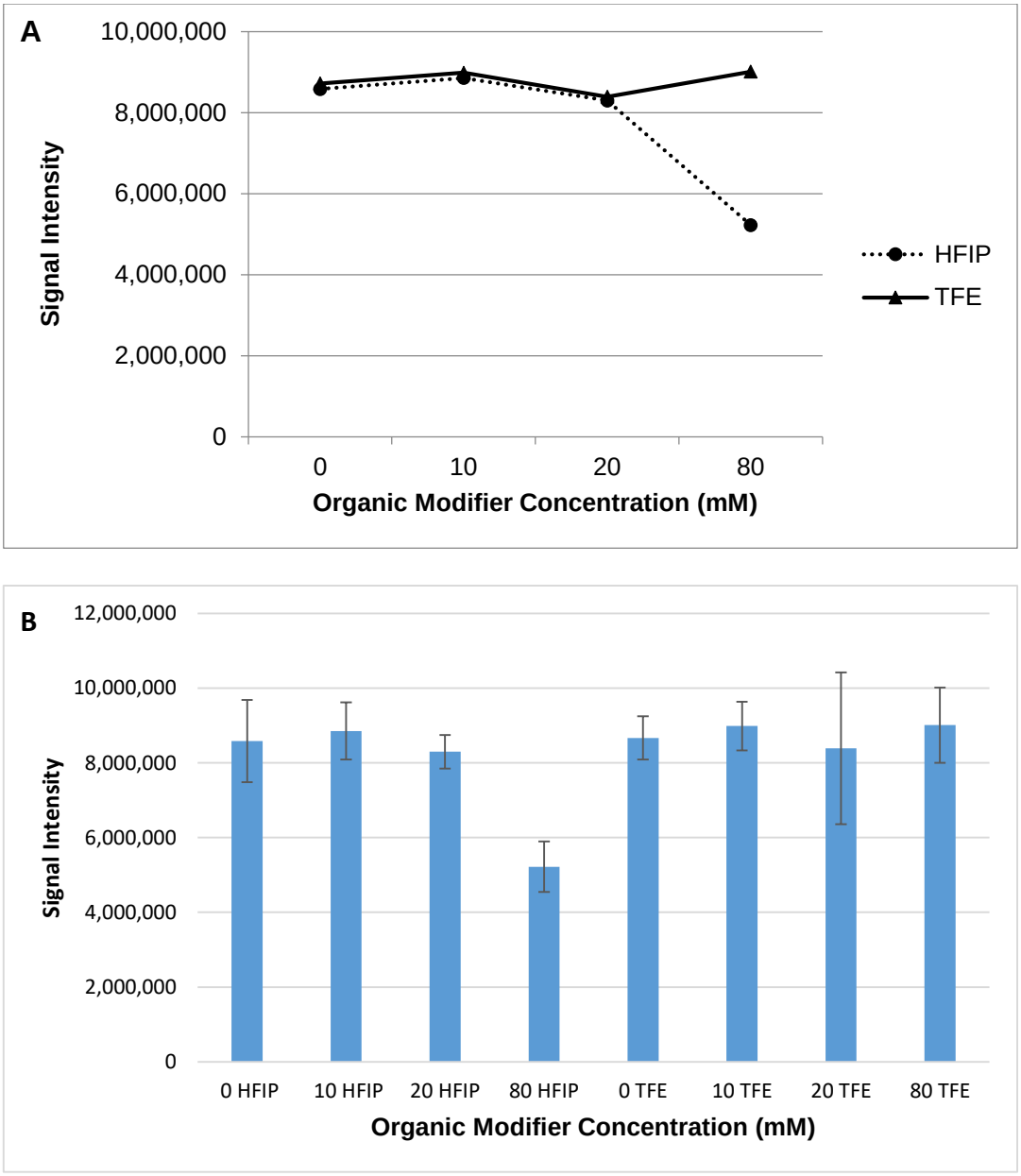

Figure III-11: The effect of organic modifier in a TBAA containing mobile phase. (A) Signal intensity of the 15 mer oligonucleotide in 5 mM of TBAA with 0 - 80 mM HFIP vs. with 0 - 80 mM TFE. The signal intensity (total ion chromatogram) for each buffer composition was recorded for three minutes and performed in triplicates. (B) 5 mM TBAA with various concentrations of HFIP and TFE, the means and standard deviations for each triplicate were calculated.

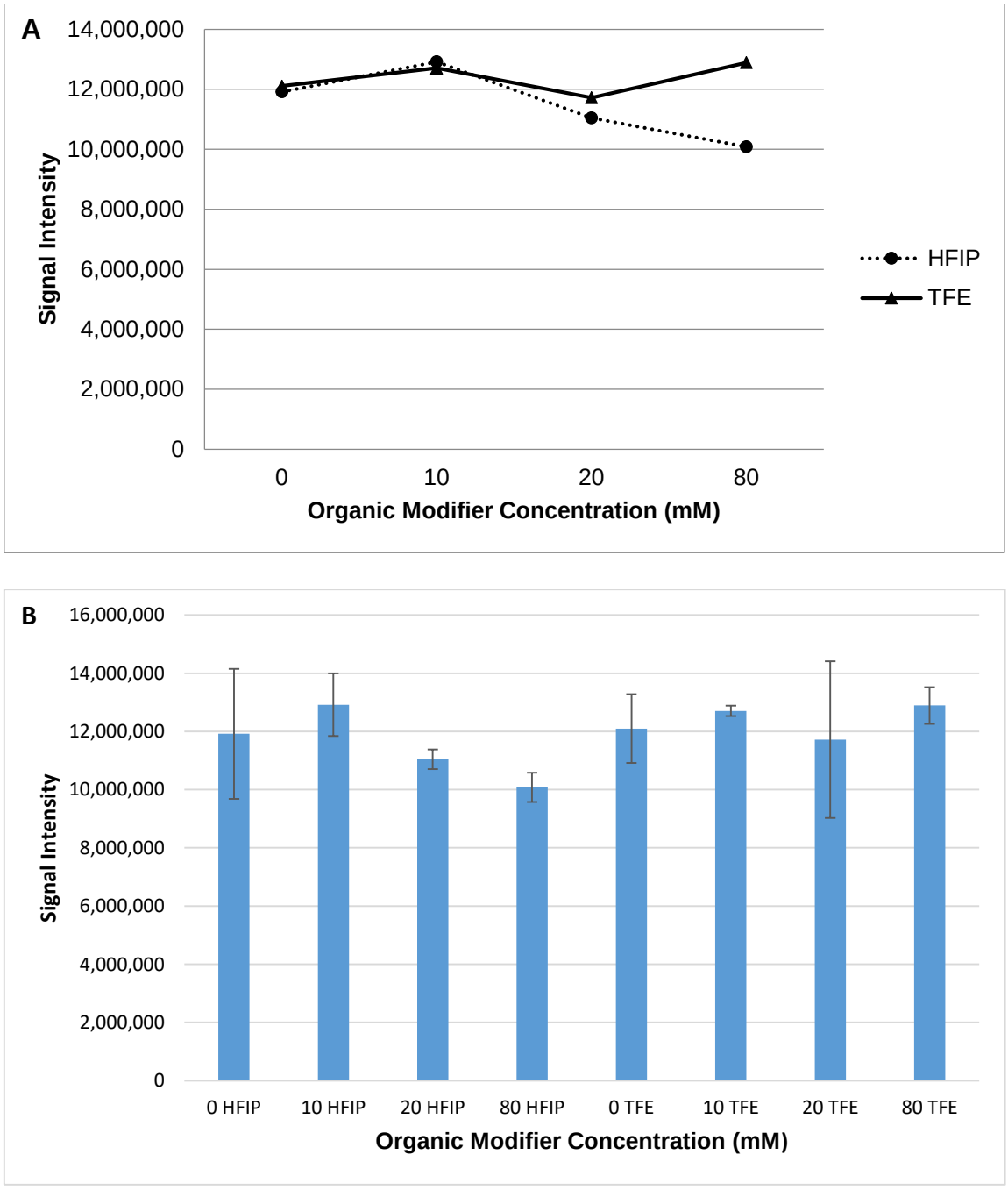

Figure III-12: The effect of organic modifier in an HAA containing mobile phase. (A) Signal intensity ratio of the 15-mer oligonucleotide in 15 mM of HAA with 0 - 80 mM HFIP with 0 - 80 mM TFE. The signal intensity (total ion chromatogram) for each buffer composition was recorded for three minutes and performed in triplicates. (B) 15 mM HAA with various concentrations of HFIP and TFE, the means and standard deviations for each triplicate were calculated.

Part B

3.3.7 Effect of analyte hydrophobicity on ESI-MS

Increased oligonucleotide hydrophobicity has been suggested to result in enhanced ESI-MS signal intensity (Null et al. 2003). To test this hypothesis, the following synthetic oligonucleotides were used: unmodified BC2b, modified hydrophobic BC2b with a C6 amino linkage (used to couple the amine-reactive to the oligonucleotide), and BC2b with C12 spacer linkage (which is a 12-carbon spacer used to insert a long spacer arm into the oligonucleotide) (See Figure III-13). The aim of this experiment was to compare the ESI MS signal intensity of the unmodified sample (BC2) with that of the modified samples (BC6 and BC12) using four different IP reagents (TEA, TBA, HA, and DIPA) in combination with different concentrations of HFIP.

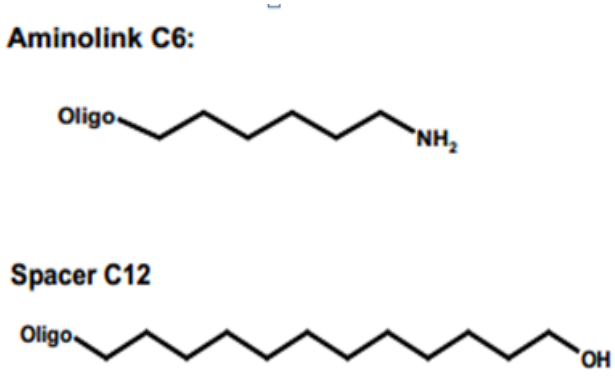

Figure III-13: Structure of oligonucleotide modifications. (A) Amino-link C6, (B) Spacer C12 modification.

The various alkylamine IP reagents used in this experiment paired with the hydrophobic oligonucleotide sample backbone may make it more hydrophobic (Null et al. 2003). As a result, the signal intensity may increase by promoting oligonucleotide desorption while the alkylamines evaporate and dissociate from the oligonucleotide in the gas phase.

Following quantification of the different oligonucleotides using the NanoDrop spectrophotometer, a solution of 2 µM oligonucleotide was infused for ESI-MS

analysis. The typical ESI-MS spectrum for each oligonucleotide with their associated molecular weights confirming the applied modifications is shown in Figure III-14. The results show no significant change in the charge state distribution to the hydrophobic tag.

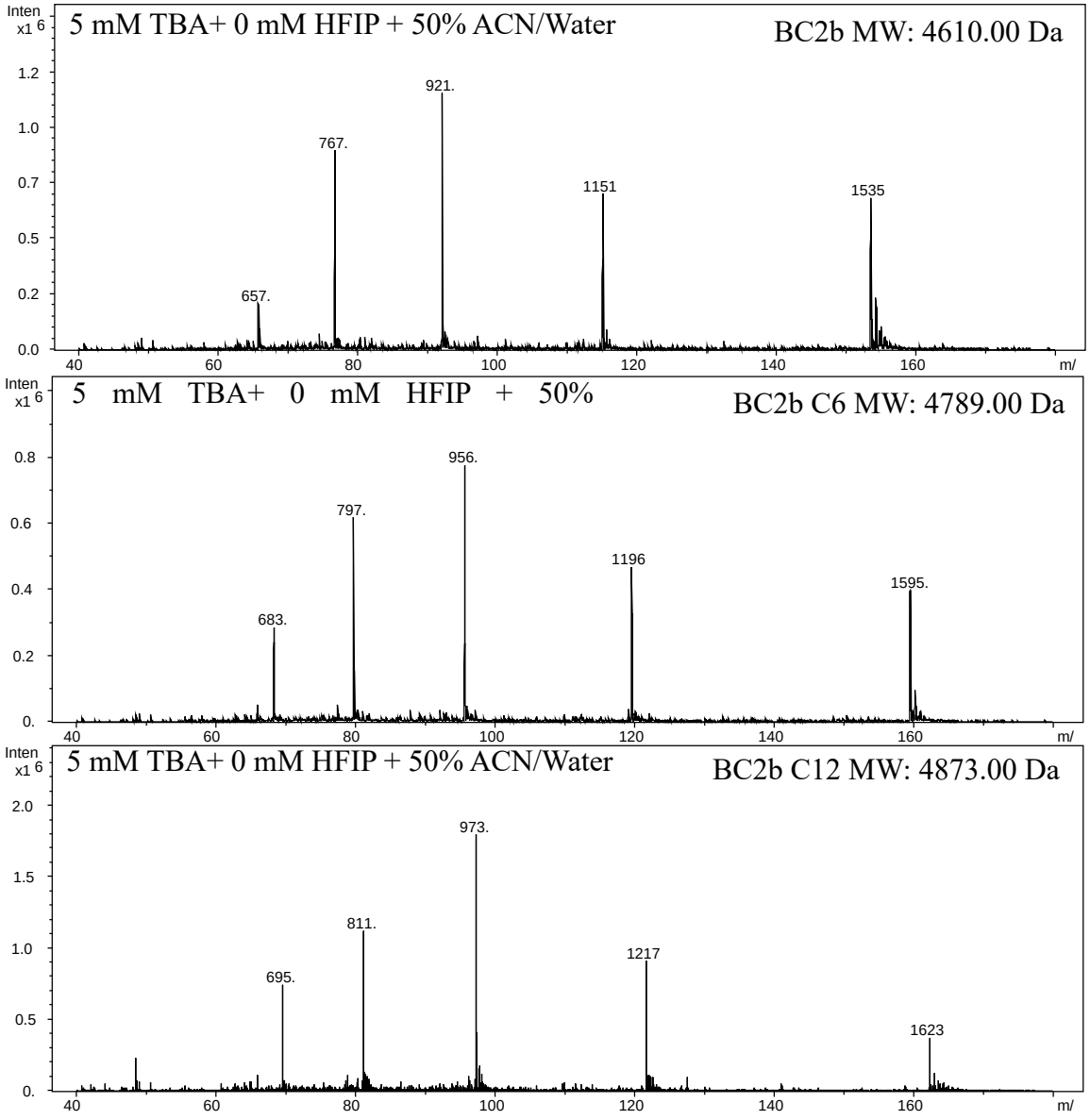

Figure III-14: Mass spectrum of BC2, BC6, BC12 oligonucleotides at a concentration of 2 µM (infused in a buffer system containing 5 mM TBA and 0 mM HFIP on ESI-MS). Data were recorded in negative mode for three minutes.

3.3.8 Verification of NanoDrop measurement of oligonucleotides using HPLC

For a comparative analysis of each oligonucleotide, accurate quantification is important to ensure that equal amounts are analysed each time in the MS. To verify the quantification of the oligonucleotides from the NanoDrop spectrophotometer, HPLC analysis of the individual oligonucleotides with concentrations of 20, and 50 pmol were analysed using UV absorbance measurements (260 nm). Each sample was injected in triplicate under partial loop mode (Figure III-15). A comparison using the same gradient demonstrates a significant increase in the retention time of the C12 modified oligonucleotide, which was not observed for the C6 modified oligonucleotide. The results also show an increase in hydrophobicity of the C12 oligonucleotide when analysed using the weak ion-pair reagent.

Additionally, unmodified BC2b was found to have the highest intensities while modified BC2b C6 and BC2b C12 showed much lower intensities across the two different concentrations. Due to the possibility of inaccurate concentration measurements from the NanoDrop, normalisation was performed based on the peak areas obtained from the HPLC (Table III-3).

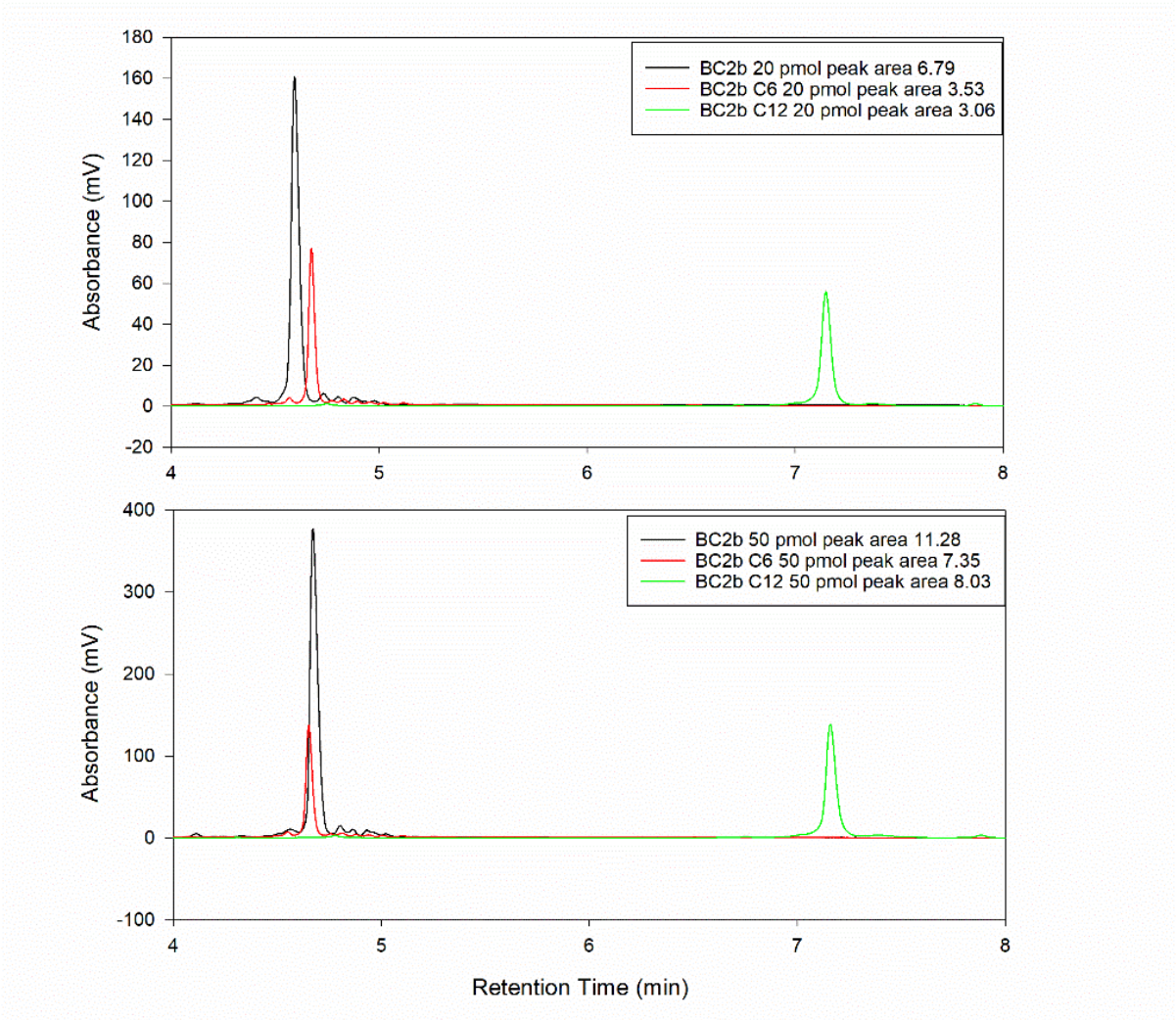

Figure III-15: IP RP HPLC quantitative analysis of BC2b, BC2b C6 and BC2b C12. Concentrations of 20 pmol and 50 pmol were analysed using a weak ion-paring reagent (TEAA) in conjunction with an Accucore C18 column (150 mm i.d × 2.1 mm) under gradient condition 1 (see chapter 2.6.5.1).

3.3.9 Quantification of oligonucleotides based on synthesis yields

In addition to quantification using the NanoDrop spectrophotometer, synthesis reports from the oligonucleotide supplier were also used for the calculation of sample concentrations. Further verification was subsequently performed through HPLC analysis (UV absorbance 260 nm) of individual oligonucleotides at concentrations of 10, 20, and 50 pmol. Each sample was injected in triplicate using full loop injection to ensure high reproducibility for the quantification. The resulting chromatogram (shown in Figure III-16) indicates that very similar peak areas were obtained, demonstrating improved accuracy of the initial quantification compared to the NanoDrop

spectrophotometer. However, the BC2 oligonucleotide had an increased intensity compared to the other oligonucleotides for the same amount of oligonucleotide analysed. Similar retention times were observed for all the oligonucleotides (Figure III-16), which was a consequence of using a strong ion-pairing reagent (TBAA), causing the dynamic anion-exchange process to dominate in size-dependent separation (Dickman, 2011).

The results summarised in Table III-4 show that the NanoDrop concentrations differed from that obtained from the synthesis reports. Nevertheless, in each case normalisation based on the accurate HPLC analysis can be used to ensure equal concentrations of the oligonucleotide are analysed using ESI-MS.

Table III-3: Calculation steps for the normalisation of oligonucleotide concentrations measured by NanoDrop UV spectrophotometer.

Concentration	Calculation
20 pmol	$BC6/BC2 = \frac{3.53}{6.79} = 0.52$ $BC12/BC2 = \frac{3.06}{6.79} = 0.45$
50 pmol	$BC6/BC2 = \frac{7.35}{11.28} = 0.65$ $BC12/BC2 = \frac{8.03}{11.28} = 0.71$
Overall	$BC6/BC2_{overall} = \frac{0.52 + 0.65}{2} = 0.59$
	$BC12/BC2_{overall} = \frac{0.45 + 0.71}{2} = 0.58$

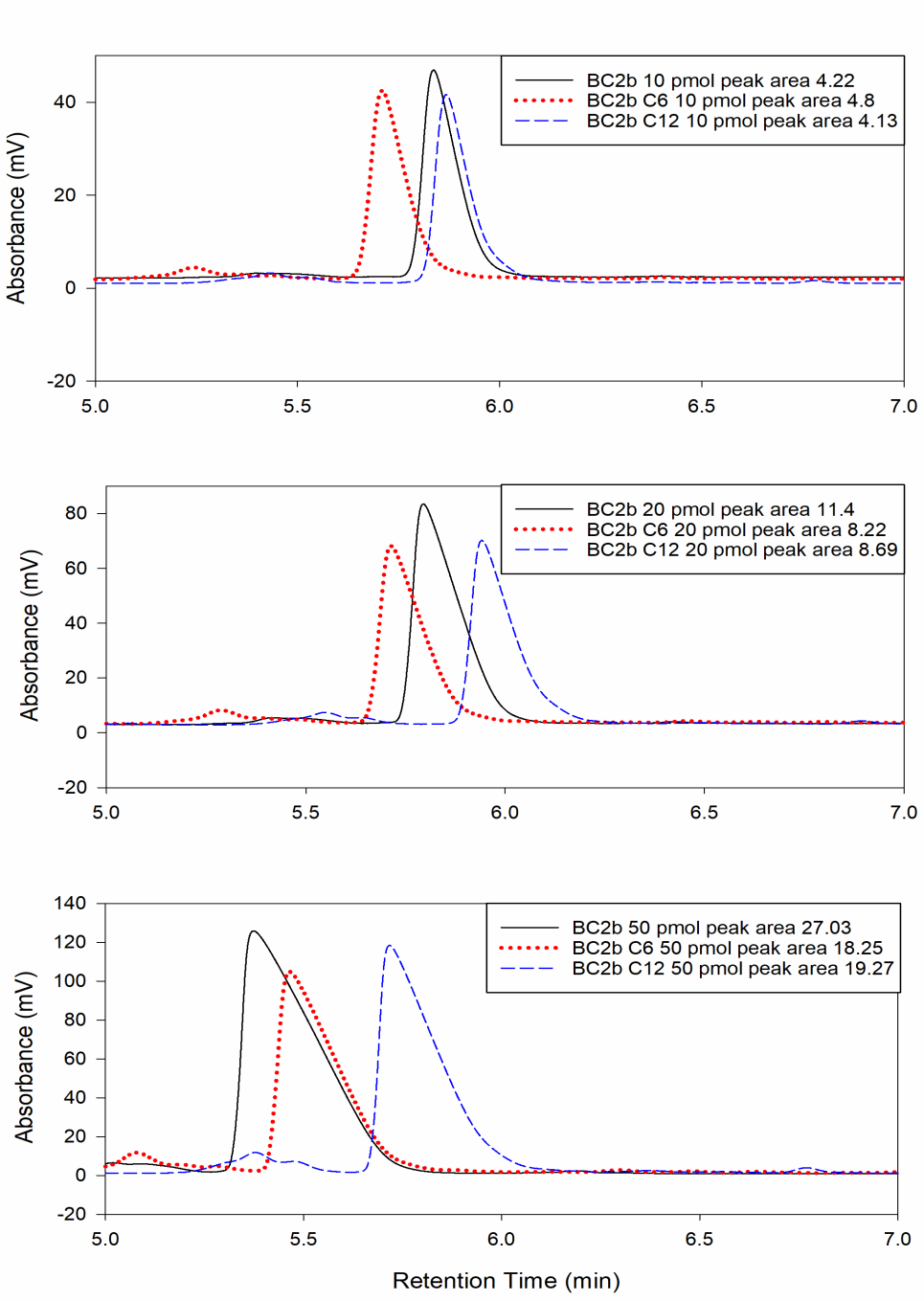

Figure III-16: Results from IP RP HPLC analysis of BC2b, BC2b C6 and BC2b C12 at concentrations of 10 pmol, 20 pmol, and 50 pmol. Analysis was based on synthesis reports (from the oligonucleotide supplier) using a strong ion-pairing reagent (TBAA) in conjunction with an Accucore C18 column (150 mm i.d × 50 mm) under gradient condition 2 (see chapter 2.6.5.1).

Table III-4: Results from different methods of measuring oligonucleotide sample concentration.

Sample	Nanodrop	Synthesis Report
BC2b	1260 µM	1320 µM
C6	479 µM	846 µM
C12	914 µM	486 µM

Table III-5: Calculation steps for the normalisation of oligonucleotide concentrations, calculated from the synthesis report.

Concentration	Calculation
10 pmol	$\mathrm{BC6}/_{BC2} = \frac{4.8}{4.22} = 1.14$ $\mathrm{BC12}/_{BC2} = \frac{4.13}{4.22} = 0.98$
20 pmol	$\mathrm{BC6}/_{BC2} = \frac{8.22}{11.4} = 0.72$ $\mathrm{BC12}/_{BC2} = \frac{8.69}{11.4} = 0.76$
50 pmol	$\mathrm{BC6}/_{BC2} = \frac{18.25}{27.03} = 0.68$ $\mathrm{BC12}/_{BC2} = \frac{19.27}{27.03} = 0.71$
Overall	$\mathrm{BC6}/_{BC2_{overall}} = \frac{1.14 + 0.72 + 0.68}{3} = 0.85$
	$\mathrm{BC12}/_{BC2_{overall}} = \frac{0.98 + 0.76 + 0.71}{3} = 0.82$

3.3.10 ESI-MS analysis of oligonucleotides with varying hydrophobicities using different alkylamines

To study the effect of oligonucleotide hydrophobicity on ESI-MS sensitivity, 2 µM of direct infusions of oligonucleotides were used in the presence of different ion-pair reagents. The overall ESI-MS signal intensities were measured and normalised based on the data in Table III-3. Experimental results show that for TEA, HA, and TBA the oligonucleotide with the C6 tag had the highest ESI-MS signal compared to that with a C12 tag and the oligonucleotides without any tags. However, the most hydrophobic oligonucleotide with the C12 tag did not result in the highest ESI-MS signal as should be expected. Replicate analysis was also performed normalising the quantification of the three oligonucleotides based on the HPLC Absorbance 260 nm prior to direct infusion as previously described. This approach ensured that equal amounts of oligonucleotides were analysed before ESI-MS analysis (Figure III-16).

The results show that similar ESI-MS intensities were obtained for each oligonucleotide modification (Figure III-17 B) in contrast to data obtained from literature (Null et al. 2003). Despite performing two normalisations (one based on initial NanoDrop measurements and one based on the synthesis report), the unmodified oligonucleotides still showed higher signal intensities compared to the oligonucleotide with the C12 tag. Hence, it may be surmised that the overall hydrophobicity of the oligonucleotides does not enhance ESI-MS intensity based on results in this study. These results appear to contradict previous observations by Null et al. (2003) where the use of a 20 mer oligonucleotide with an additional amino-C12 modification (which resulted in a four-fold increase in hydrophobicity relative to its unmodified state) resulted in improved signal intensities. However, it should be noted that no direct evidence for the accurate quantification of the oligonucleotide prior to LC-ESI-MS analysis was provided in their study.

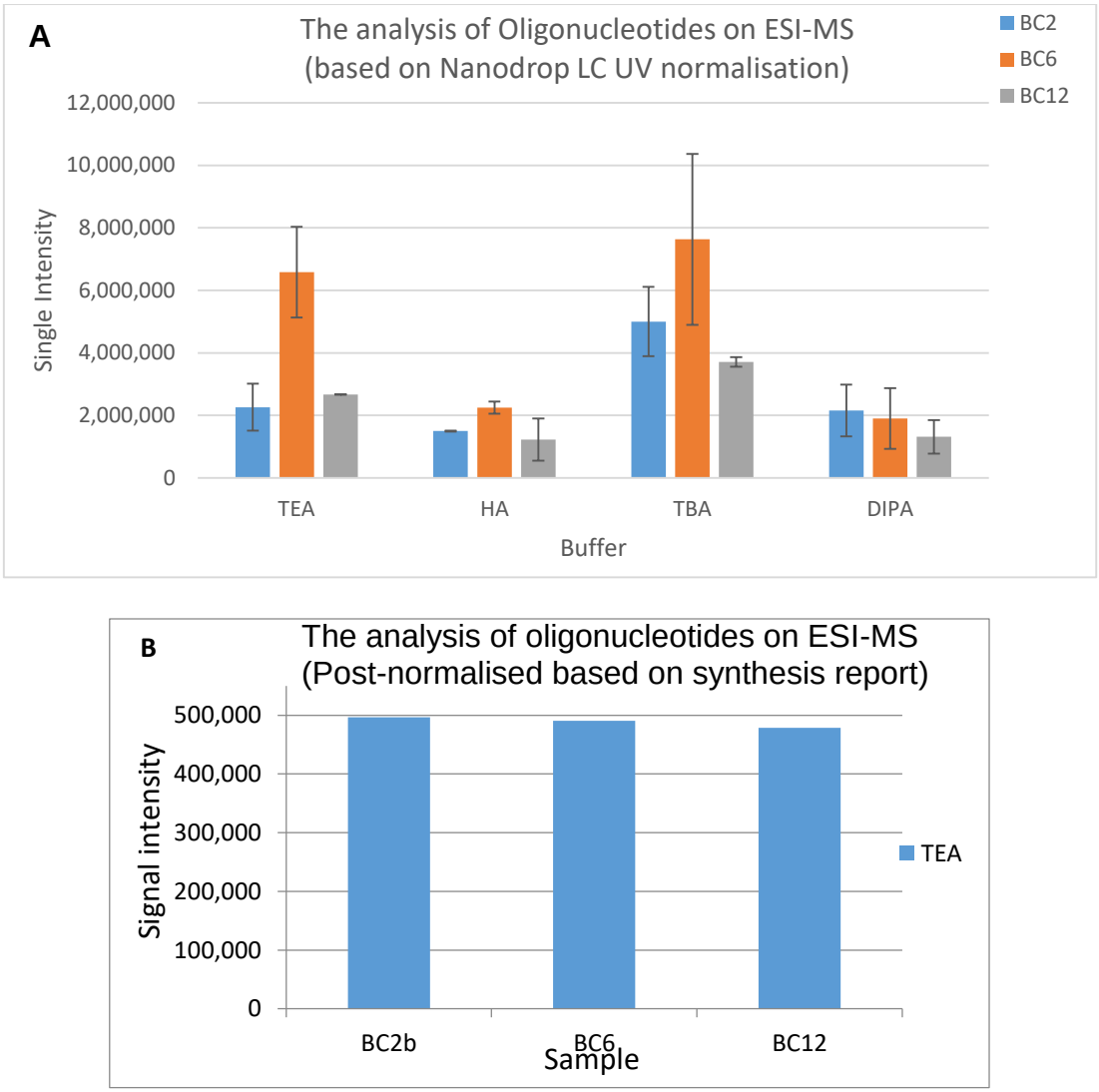

Figure III-17: The effect of oligonucleotide hydrophobicity on ESI-MS mass signal intensity with various buffer systems. (A) Samples used were unmodified 15 mer (5'-CAAAAGTCCGTGAGA-3') oligonucleotide, modified C6 15 mer oligonucleotide, and modified C12 15 mer oligonucleotide at a concentration of 2 µM. Samples were infused with 4 sets of buffers; Set 1 20 mM TEA; Set 2 15 mM HA; Set 3 5 mM TBA; Set 4 20 mM DIPA, HFIP was used in conjunction with all the buffer sets, the analyses were studied on ESI-MS in negative ion mode. Signal intensities (the results of total ion chromatogram were further normalised based on NanoDrop LC UV analysis). Data for each buffer composition were recorded for three minutes. The means and standard deviations for each triplicate were calculated. (B) Signal intensity of the 15 mer unmodified BC2 oligonucleotide, modified BC2b C6, and BC2b C12 oligonucleotide. The injected concentration 2 µM was based on the synthesis report, which was post-normalised prior to the ESI-MS analysis in 20 mM of TEA with 20 mM HFIP.

3.4 Conclusions

Analysis of a wide range of IP reagents and organic modifiers were performed to optimise ESI-MS conditions for the analysis of 15 mer oligonucleotides (CAAAAGTCCGTGAGA). It was shown that 5 mM TBA produced the highest signal intensity while also responding positively to increasing HFIP concentration. This result is consistent with recent studies where TBA was shown to be one of the best performing IP reagents in terms of signal intensity over various concentrations 5 mM -15 mM (McGinnis et al. 2013). It was further demonstrated that utilising an IP reagent with a high Henry's law constant resulted in a low charge state distribution of the oligonucleotide, while low Henry's law constants resulted in higher charge states distributions.

The investigation into the effects of HFIP from 0-80 mM for varying IP reagents was inconclusive as no consistent trend of either improvement or reduction of ESI-MS signal intensity could be observed. Nevertheless, the highest ESI-MS signal intensities were observed using 5 mM TBA in combination with 80mM HFIP in this study.

A comparison between HAA and TBAA showed that HAA benefitted more from increasing amounts of either HFIP or TFE with increased signal intensities. Comparing the organic modifiers TFE and HFIP, TFE was generally better at enhancing ESI-MS signals, especially at higher concentrations; demonstrating potential benefits as an alternative in comparison to the expensive and hazardous HFIP.

The optimal pH conditions were found to depend on the IP reagents used: pH 9.0 and pH 11.0 for TBA and HA respectively. The charge state distribution did not seem to be affected by pH in the case of TBA but was altered when using HA within a pH of 8.0 to11.0.

The effects of oligonucleotide hydrophobicity were studied using a range of modified oligonucleotides with either a C6 tag or C12 tag at the 5'-end of the oligonucleotide. Following accurate quantification of the modified oligonucleotides using HPLC UV analysis, no significant increase in ESI-MS signal intensity was observed from higher hydrophobicity. These results are in contrast to observations in literature where the utilisation of a 20 mer oligonucleotide with an additional amino-C12 modification

(resulting in a four-fold increase in hydrophobicity relative to the unmodified state) demonstrated improved signal intensities (Null et al., 2003).

Chapter IV : Purification and quantification of dsRNA extracted from microbial cells

4.1 Abstract

RNA interference (RNAi) is a powerful technique used to down-regulate specific target gene expression. It is widely employed in the study of gene functions in eukaryotic organisms and holds potential for many promising applications in both medicine and insect management strategies. The application of RNAi requires high quantities of quality dsRNA, which is currently challenging to produce. The production of large-scale dsRNA has led to a need for analytical techniques capable of rapidly isolating, purifying, and analysing dsRNA.

Extraction of dsRNA is critical for downstream applications of RNAi; this chapter aims to study five different RNA extraction methods currently available on the market (including a number of variations using the guanidine isothiocyanate-phenol/chloroform procedure) for the high-throughput extractions of dsRNA from microbial cells. Experimental results based on extraction from 10^9 *E. coli* cells show that the DNAzol method yielded the highest amount of dsRNA extracted, despite the presence of genomic DNA in the extracted samples.

In addition, the successful utilisation and development of stable isotopic labelling to characterise and quantify dsRNA in complex RNA mixtures, specifically using metabolic labelling and *in vitro* labelling of dsRNA in conjunction with mass spectrometry has been reported (Kung et al., 2018). Reference dsRNA was synthesised (^{15}N and $^{13}C^{15}N$ dsRNA), both *in vivo* and *in vitro* prior to purification and quantification. The reference dsRNA was subsequently mixed into RNA extracted from *E. coli* that were engineered to express dsRNA. Following isolation of the total RNA (including dsRNA), known amounts of isotope-labelled dsRNA standard were added, and the mixture digested with a ribonuclease prior to MS analysis and quantification of dsRNA. It was demonstrated that isotope labelling of reference dsRNA simplifies the characterisation and mass mapping of dsRNA fragments based on the significant mass shift between light and heavy oligonucleotides.

4.2 Introduction

4.2.1 RNAi and dsRNA extraction

Exploitation of the RNAi pathway to block the expression of specific genes holds considerable promise for the development of novel RNAi-based insect management strategies (Gordon and Waterhouse, 2007). Many potential applications of RNAi exist such as the control agricultural-insect pests and the engineering of pathogen-resistant plants (Mao et al., 2007; Baum et al., 2007; Duan et al., 2012). Recent developments in RNA interference (RNAi) have created a need for cost-effective, large-scale synthesis of dsRNA, which in turn requires effective analytical techniques to purify, characterise and accurately quantify dsRNA prior to RNAi application. A wide range of dsRNA products can be generated either via bacterial expression systems or *in vitro* transcription for RNAi application. The development of suitable analytical methods to characterise the dsRNA products produced from both *in vitro* and in microbial systems remains a significant challenge.

Double-stranded RNA (dsRNA) is the key initiator in the RNAi mechanism. Large quantities of dsRNA can be synthesised for the use of RNAi applications either in bacterial systems or through *in-vitro* transcription (Li et al., 2011; Palli, 2014). Nevertheless, the synthesis process is hampered by difficulties in isolating and enriching RNA (Phongsisay et al., 2007). These difficulties arise due to the highly labile structure of RNA, making it susceptible to endonuclease and exonuclease degradation while requiring a complicated procedure to isolate RNA (Nwokeoji et al., 2016).

A number of methods have been developed and evaluated for the extraction of RNA from *E. coli* cells. The total RNA extracted from these methods, however, suffered from low yield and poor quality (Phongsisay et al., 2007). For example, during the developmental stage of RNA extraction technology, guanidium isothiocyanate was the primary detergent used to lyse cells and denature proteins. It was used with a caesium chloride cushion to isolate RNA; this method involved long hours of centrifugation (Glisin et al., 1974). Even though undegraded RNA could be effectively separated from DNA, this method was still relatively time-consuming (Chirgwin et al, 1979).

Difficulties with its use eventually led to the substitution of the caesium chloride cushion gradients with phenol isolation (Lin-Chao and Bremer 1986). However,

significant issues have been reported when phenol was used for RNA extractions. Firstly, phenol is highly toxic; secondly, it is difficult to be removed from the extracted RNA completely: finally, despite high quality and high integrity RNA produced from phenol, it is often irreproducible (Donovan and Kushner, 1986). Subsequently, guanidium isothiocyanate was used in combination with phenol-chloroform to improve extraction quality. This improved protocol included an additional phenol-chloroform phase separation step before centrifugation, which allowed the total RNAs to be soluble in the top acidic aqueous phase, without any contamination from DNA and proteins, resulting in extracted RNA of consistently high quality (Chomczynski and Sacchi, 1987). The method above was eventually commercialised by Life Technologies as "TRIzol®". A schematic illustration of the extraction/phase separation employed for RNA extractions is shown in Figure IV-1.

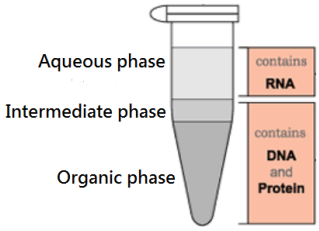

Figure IV-1: Phase separation during guanidium thiocyanate-phenol/chloroform extraction. Acidic phenol retains RNA in the upper aqueous phase (bases and phosphate groups remain charged under acidic conditions, positively and negatively respectively, therefore retaining water solubility), while DNA is moved into either the interphase or lower organic phase due to differences in the overall polarity of ssRNA compared to dsDNA at acidic pH values.

More recently, several RNA extraction kits have been developed to make it simpler for most laboratories to isolate RNAs of interest with high yield and purity levels (Stead et al., 2012; Nwokeoji et al., 2016). The principles behind these RNA extraction kits are similar to each other and are all based on either chemical or mechanical mechanisms to lyse cells while removing protein to extract RNA.

Effective implementation of RNAi requires high-quality dsRNA at sufficiently high yields. While there are currently a number of methods used for the purification of total RNA (i.e. single-stranded RNA), their application in dsRNA purification has not been reported. Therefore, the experiments in this chapter analysed five RNA isolation

methods: Ribopure, RNAsnap, TRIzol Max, DNAzol, and RNAzol by utilising their corresponding reagents to extract dsRNA and performing a quantitative and qualitative comparison on the results.

4.3 Results and discussion

Part A

4.3.1 Comparative analysis of different extraction methods for the isolation of dsRNA

The current experiment aimed to compare a range of RNA extraction methods (listed in Table IV-1) for the extraction and purification of dsRNA from microbial cells. Following RNA extraction, gel electrophoresis and ion-pair reversed-phase liquid chromatography were utilised to analyse the integrity of the extracted RNA. Quantification of dsRNA was performed by combining the quantification from NanoDrop™ spectrophotometer A_{260}, with measured peak areas to calculate the amount of dsRNA present in the total RNA from IP RP HPLC. Final quantities of dsRNA were calculated by multiplying total RNA concentration with the dsRNA percentage for each sample.

Table IV-1: Specification of RNA extraction reagents

Reagent	Main component	SPE	Precipitation
TRIzol Max™	Phenol, guanidine isothiocyanate, ammonium thiocyanate	N/A	Isopropanol
Ribopure™ (RNAwiz)	Phenol/guanidine thiocyanate	Glass-fiber filter purification	Ethanol
RNAzol®	Phenol, potassium thiocyanate	N/A	Ethanol
RNAsnap	Formamide	QIAGEN Spin column	Ethanol
DNAzol	Guanidine isothiocyanate	N/A	Ethanol precipitation

4.3.1.1 Extraction of dsRNA using Ribopure™ Kit

Initially, RNA extractions were performed using Ribopure kits on 10^9 *E. coli* cells (expressing 765 bp dsRNA). High-quality total RNA were extracted as observed by the abundant yields of ribosomal RNAs with minimal RNA degradation (see Figure IV-2 A). However, no dsRNA were observed in the chromatograms or gel electrophoresis (see Figure IV-2 A and C). Based on the assumption that dsRNA were not present in the aqueous phase, further experiments were performed to re-extract the RNA from the remaining intermediate and organic phases using the TRIzol reagent (Figure IV-2A, B, and C respectively). The results showed no dsRNA in any of the phases. Thus, it is concluded that the Ribopure kit is only suitable for the extraction of rRNA, (for which it can generate high-quality total RNA with minimal degradation) but not for dsRNA.

4.3.1.2 Extraction of dsRNA using the RNAsnap method

Stead et al. (2012) demonstrated a new extraction method called 'RNAsnap' which is based on the use of formamide. This single-step method is able to efficiently recover all species of intracellular RNA compared to commercial kits (guanidinium isothiocyanate and phenol-chloroform based methods), yielding approximately 60 µg of total RNA from 10^8 *E. coli.* cells. Therefore, it was desired to test the RNAsnap method on its ability to extract dsRNA.

Initial attempts at using the RNAsnap method for dsRNA extraction while following the original protocol resulted in a highly viscous sample. This observed change in sample viscosity suggested that the RNAsnap samples might not be compatible with direct, downstream analysis. In subsequent attempts, the extracted samples were analysed in conjunction with gel electrophoresis. Figure IV-3 A shows that the formamide extracted sample caused significant smearing on all bands of the gel. Despite that, the region of expected rRNA and dsRNA bands were still visible.

To improve the RNAsnap method, the amount of RNAsnap lysis solution used for RNA extraction was increased from 200 µL to 300 µL. In addition, ethanol precipitation and solid phase extraction (silica membrane spin column) were performed on the

RNAsnap extracted samples (Figure IV-3 B) to reduce sample viscosity as well as to clean up the remaining lysis solution.

It was found that using ethanol precipitation (Figure IV-3 B, lanes 5-7) did not significantly lessen the smearing issues when compared to the first attempt observed on the gel (Figure IV-3 B, lanes 2-4). Therefore, the RNAsnap method was further tested with SPE clean-up. Although the inclusion of SPE clean-up improved gel quality, significant amounts of RNA were lost (Figure IV-3 B, lanes 8-10).

Following optimisation, the RNAsnap samples were further purified using both solid phase extraction and ethanol precipitation for dsRNA extraction (Figure IV-3 C). The additional SPE clean-up step effectively reduced the previously encountered smearing issues (Figure IV-3 C, lanes 6-7). Next, the optimised samples (Figure IV-3 C) were further analysed using IP RP HPLC (D-G). The results are shown in the chromatograms from the IP RP HPLC analysis of RNAsnap total RNA extraction. Comparing the extraction materials on the gel and HPLC (Figure IV-3 C and D-G), the amount of dsRNA observed from the HPLC was unexpectedly lower.

In a separate issue, RNAsnap samples appear to have affected the performance of the stationary phase on the HPLC after the analysis; a loss of resolution was observed on a control pUC 18 DNA Hae III digested ladder analysis (data not shown). Overall, the yield of rRNA was higher than that of dsRNA, as shown on the chromatograms (Figure IV-3 E).

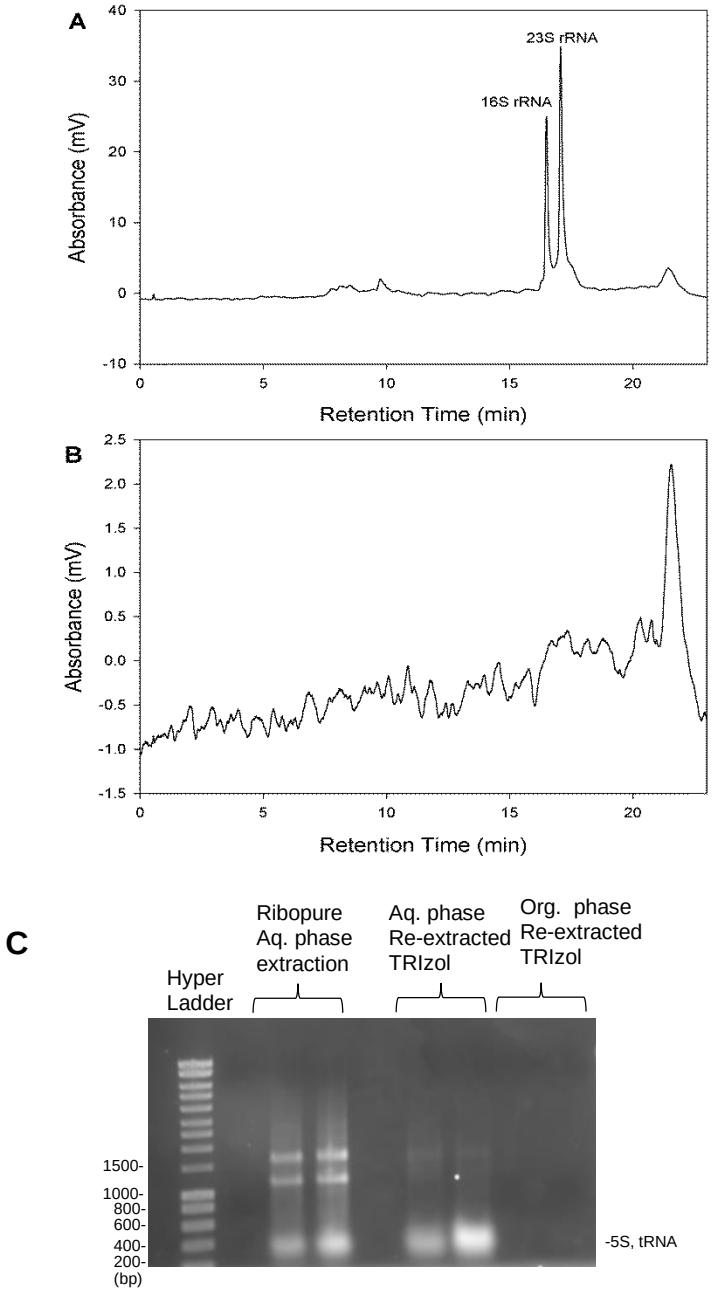

Figure IV-2: Results from IP RP HPLC analysis of total RNA extracted from *E. coli*. (expressing 765 bp dsRNA) using Ribopure™. (A) Ribosomal RNA extracted from the Ribopure aqueous phase (B) The resulting Ribopure interphase re-extracted by TRIzol max using gradient condition 11 (see Chapter 2.6.5) (C) The gel electrophoresis analysis of all the different phases of Ribopure extraction.

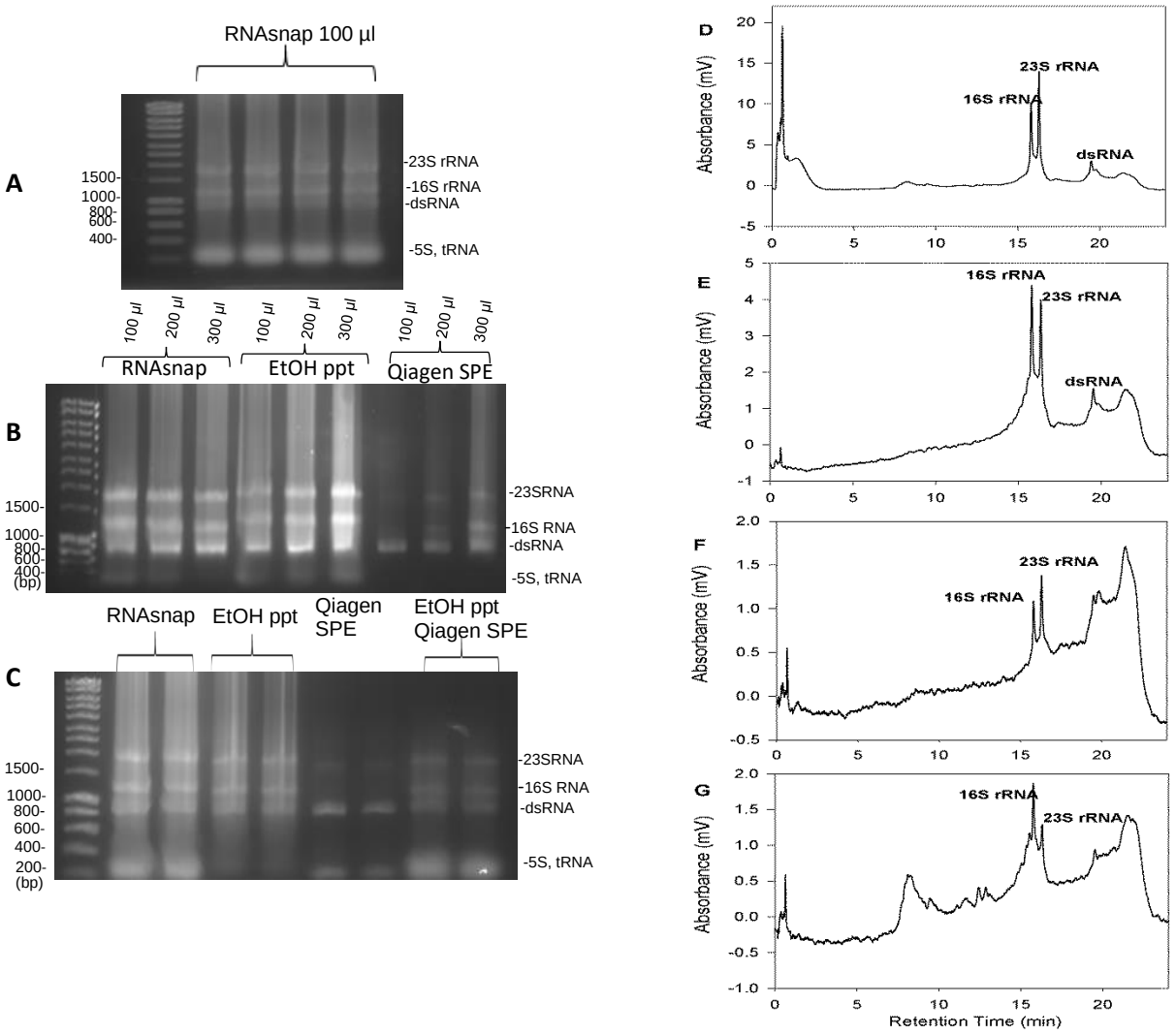

Figure IV-3: Quality assessment of RNAsnap samples analysed on agarose gel electrophoresis and IP RP HPLC analysis. (A) using the unmodified RNAsnap method (B) extracted with 100-300 µL of extraction solution and ethanol precipitation using the Qiagen SPE method (C) extracted with 100 µL of extraction solution and ethanol precipitation using the Qiagen SPE method. IP RP HPLC analysis of RNAsnap extractions (D) RNAsnap (E) RNAsnap with EtOH precipitation (F) RNAsnap and SPE (G) EtOH precipitation with SPE. All samples were analysed using IP RP HPLC gradient condition 11 (see Chapter 2.6.5).

4.3.2 Comparative analysis of guanidine isothiocyanate-phenol/chloroform based methods for the isolation of dsRNA

The TRIzol Max™, RNAzol®, and DNAzol™ methods (see Table IV-1) were selected for a comparative analysis of dsRNA extraction. Samples containing $1x10^9$ of *E coli.* cells expressing 765 bp dsRNA were used for all RNA extractions. Analyses were performed using both gel electrophoresis and IP RP HPLC (Figure IV-4 A-D) and runs were performed with three independent biological replicates for each method (see appendix A1-A3).

In each case, successful extraction of the dsRNA was observed, although it should be noted that degradation of the rRNA occurred in each of these samples on IP RP HPLC analysis (Figure IV-4 A-C). Results from gel electrophoresis showed similar yields for dsRNA from the three extraction methods Figure IV-4 D. The results also show that additional purification of the genomic DNA occurred only from DNAzol samples. In order to further verify the quality and quantities of extracted dsRNA, further analysis of the IP RP HPLC chromatogram was performed.

The amount of dsRNA present in the total RNA was quantified by combining the peak areas from IP RP HPLC analysis, with the quantification results from NanoDrop™ spectrophotometer A_{260}. Then, multiplication of total RNA concentration with the percentage of dsRNA provided the final quantities of dsRNA in each sample (see Table 4.3.2-1). The results show that out of all the methods tested the DNAzol method was the optimal dsRNA extraction method in terms of dsRNA isolation yield.

With respect to absolute values, the TRIzol Max method produced the least amount of both total RNA and dsRNA. Although, although, the RNAzol/proteinase K method produced the highest yield of total RNA (nearly three times as much compared to the TRIzol Max), the ratio of dsRNA extracted by TRIzol Max was still higher in contrast to RNAzol. The DNAzol method managed to produce a higher amount of dsRNA (almost twice as much compared to the TRIzol method and one and a half times more compared to RNAzol). It was found that these three methods were similar in the degree of degradation observed for ssRNA (16S and 23S rRNA) (Figure IV-4 A-C), although this did not affect the quality of the dsRNA of interest.

The results revealed some unexpected properties of the DNAzol method. Despite being designed specifically for DNA purification and not RNA, it was able to quickly and efficiently extract dsRNA compared to the other methods tested. It is also important to note that the aqueous phase pH values were 7.5 for DNAzol and 4.5 for TRIzol and RNAzol.

It is hypothesised that the results may be a consequence of dsRNA having a duplex form, allowing it to behave similarly to dsDNA rather than to ssRNA. For instance, in the presence of acids (aqueous phase: pH 4.5), the duplex is considered neutralised and preferentially partitions in the organic phase (although DNA surface is surrounded by negative charges, the isoelectric point of phosphate backbones is greater than 4.5 and thereby these charges are wiped out due to full protonation) (Avison, 2008). However, under acidic pH conditions, ssRNA remains charged due to the presence of both the positively charged of exposed bases and the negatively charged phosphate backbone, which when mediated through hydrogen bonding via the exposed nitrogenous bases, makes ssRNA water soluble. Thus, ssRNA is partitioned into the aqueous phase, a process which is not possible for dsDNA. Hence, using phenol at a neutral pH ensures that duplex nucleic acids are fully partitioned in the aqueous phase.

The hypothesis above may help explain why a high yield of dsRNA was extracted under pH conditions higher than acidic (i.e. neutral conditions). Further evidence to support this hypothesis was found by using Tris-HCl to adjust the pH of the TRIzol aqueous phase from 4.5 to 7.5 (Figure IV-5 A and B). This produced an improved dsRNA yield of 45 µg, versus 19 µg when the pH was at 4.5. It can be inferred from the combined results that higher pH conditions result in significantly higher dsRNA yields compared to acidic conditions.

It should be noted that the existence of genomic DNA was revealed from the total RNA profiles during IP RP HPLC analysis of the samples extracted using both the DNAzol and TRIzol max methods at pH 7.5 (Figure IV-4 B and Figure IV-5 B respectively). The presence of genomic DNA further suggests that the pH value influenced the type of nucleic acid isolated. In other words, neutral pH conditions (pH of 7-8), caused the partitioning of both genomic DNA and dsRNA into the aqueous phase. Meanwhile, under acidic pH conditions, only RNA could be partitioned into an aqueous phase. This postulate is supported by previously obtained results and recent data observed with

the TRIzol max method at pH 4.5 (Figure IV-4 A and Figure IV-5 A), where only total RNA was successfully extracted.

In summary, both the DNAzol and TRIzol max methods (Figure IV-4 B and Figure IV-5 B) had increased yields of dsRNA under pH 7.5 compared to under pH 4.5 (see Table 4.3.2-2). Despite the presence of genomic DNA (a problem easily solved by removal via SPE-column clean-up, (Figure IV-5 C)), the amount of dsRNA extracted by the DNAzol and TRIzol max (pH 7.5) methods were still the highest out of all the methods compared.

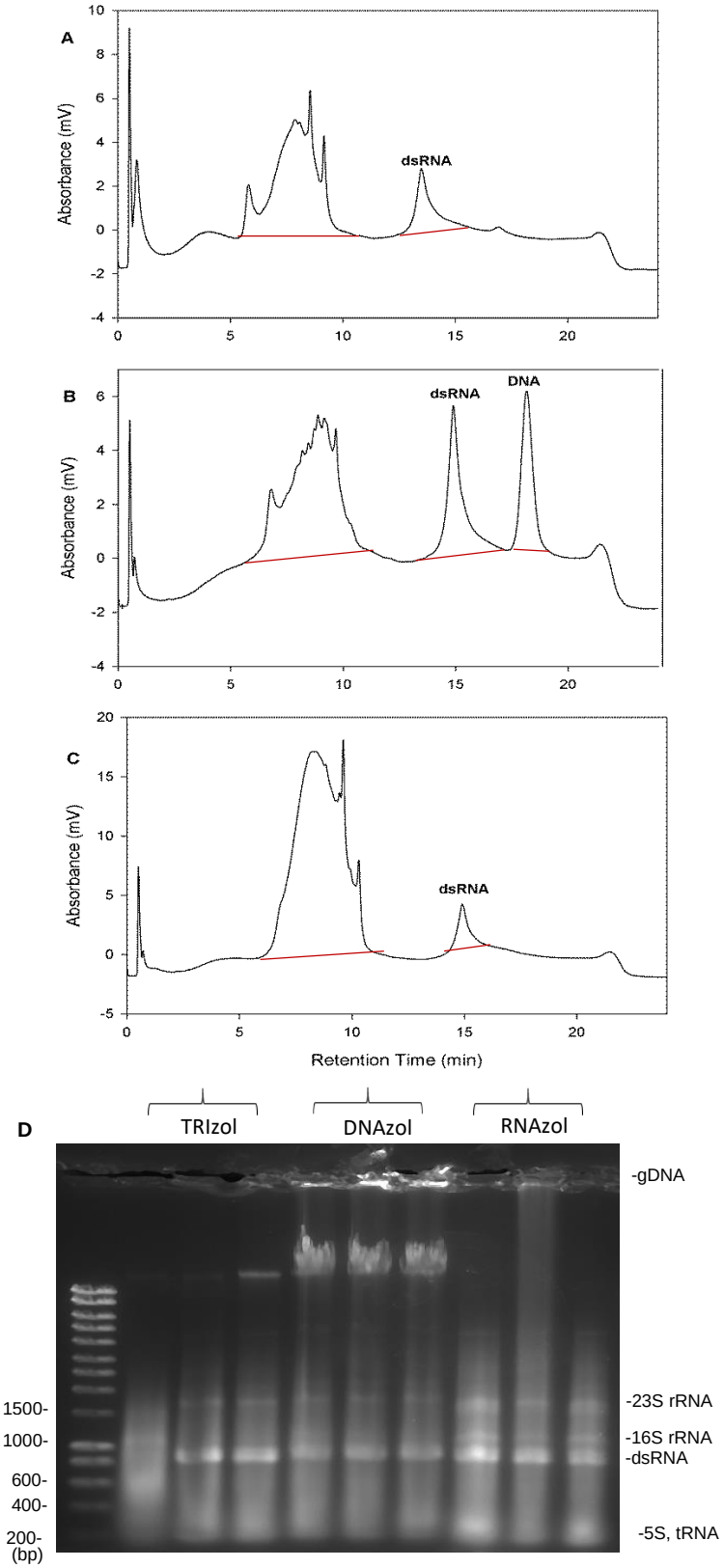

Figure IV-4: The extraction analysis of *E. coli* expressed with 765 bp dsRNA. Extracted using (A) TRIzol Max (B) DNAzol and (C) RNAzol and proteinase K using IP RP HPLC under gradient condition 12 (see Chapter 2.6.5), peak areas were measured as highlighted (D) Agarose gel electrophoresis analysis of total RNA samples from the three extraction methods.

Table IV-2: Quantitative results (yields) from the analysis using different RNA isolation methods. Extractions were performed in triplicate and shown with the mean and standard deviations.

Metric	RNA extraction method					
	RNAzol	DNAzol	TRIzol (pH 4.5)	TRIzol (pH 7.5)	Ribopure	RNAsnap
Yield (µg) per 10^9 cells	180 ±7.07	135 ±7.07	65 ± 7.07	120± 8.02	19±1.08	232±14.1
dsRNA (µg) in total RNA	29.5±4.95	49.5±12.02	18.8±4.52	45.3±10.1	0	N/A

*Ribopure kit was unable to extract any dsRNA.
*RNAsnap was not directly compatible with downstream analysis, and its dsRNA extraction yield was relatively low. Therefore, it was not included in this comparison.

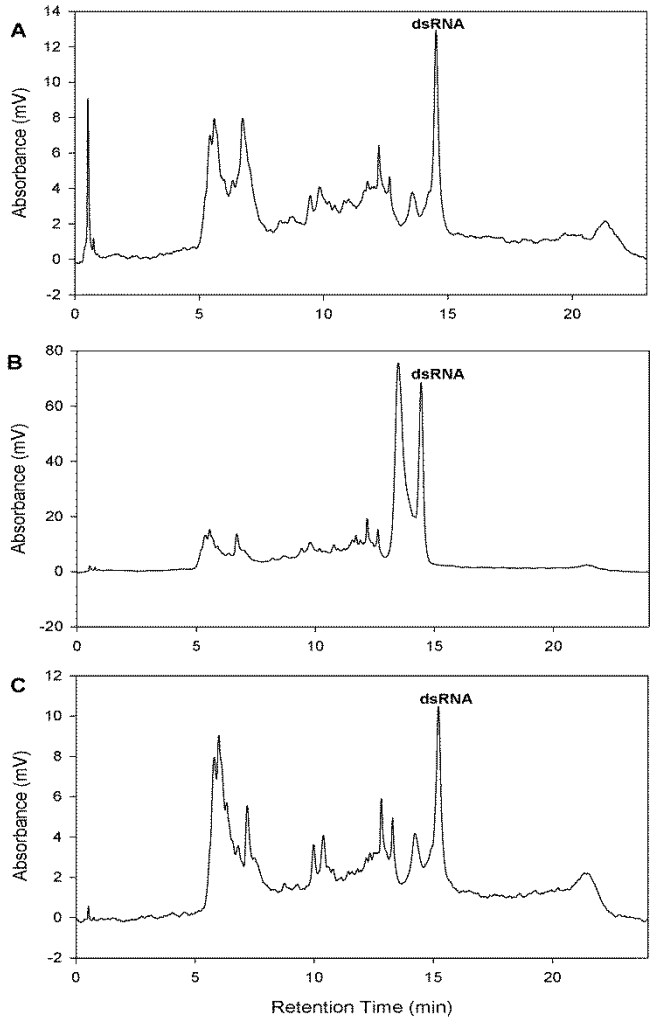

Figure IV-5: Results from the IP RP HPLC analysis of total RNA extracted using TRIzol Max under different pH conditions. (A) The total RNA extraction using TRIzol at pH 4.5 and (B) pH 7.5 (C) TRIzol pH 7.5 total RNA extraction in conjunction with SPE column to remove genomic DNA contamination under gradient condition 12 (see Chapter 2.6.5).

4.3.3 Conclusions

The choice of extraction method directly affects the species and quality of the RNA extracted. Thus, these factors need to be carefully considered before selecting a suitable RNA extraction method. This study demonstrated a rapid dsRNA extraction method which uses the DNAzol solution in conjunction with an optimised procedure. Experimental times were less than 30 minutes, and no additional phenol-chloroform is needed for further phase separation. Based on extraction from 10^9 *E. coli.* cells, the DNAzol method and the TRIzol method at pH 7.5 had similar yields (49.5 µg dsRNA), which were higher compared to all the other methods considered. Despite both methods resulting in the presence of contaminating genomic DNA, they were easily removed using either solid phase extraction or DNase treatment.

The other methods studied had a number of major drawbacks: Ribopure kits can only extract rRNA and was not suitable for the purification of dsRNA. The TRIzol Max method suffered from long experimental times despite high amounts of dsRNA extracted (at pH 7.5); the RNAzoL/proteinase K method only managed to extract a low amount of dsRNA despite a high amount of total RNA extracted; finally, the RNAzol method appears to be effective only for the extraction of small RNA such as rRNAs. These drawbacks further support the use of the modified DNAzol method as the method of choice for dsRNA extraction.

Part B

4.3.4 Characterisation and quantification of dsRNA using stable isotope labelling in conjunction with LC-MS analysis

Mass spectrometry is a powerful tool for the direct identification and characterisation of nucleic acids (Kowalak et al., 1993). Prior to mass spectrometry analysis, purification of the RNA of interest using HPLC is an essential step. For further LC-MS analysis, specific RNA enzymatic digestion (RNase) is required in the case of large RNA molecules in order to produce smaller oligoribonucleotide fragments, which are then amenable for direct on-line LC separation and MS measurement. RNase mapping is the main approach used with MS for the characterisation and location of individual RNA from sequences (Kowalak et al., 1993; Hossain and Limbach, 2007).

Although a wide number of MS-based technologies have been employed for RNA studies, the analysis remains challenging due to limited sensitivity and resolution in contrast to proteomics MS analysis. In fact, when oligoribonucleotides are cleaved via RNase digestion a heterogeneous mixture is produced which makes MS analysis more complex because of the presence of the 2'3'- cyclic phosphate intermediate and 3-phosphate from digestion products (Waghmare and Dickman, 2011).

More recently, research has focused on developing more quantitative methods in conjunction with RNase mass mapping methods. Initial studies focused on the development of incorporating a quantitative approach by using isotopic labelling in conjunction with RNase mapping. Waghmare and Dickman (2011) first introduced the use of metabolic labelling in *E. coli* culture growths to generate both light and heavy labelled RNA, combining them for the purpose of rRNA isolation, and using LC-MS for the identification and quantification of oligoribonucleotides and RNA modification. Their approach facilitates RNA application in both qualitative and quantitative analysis while allowing the rapid determination of potential oligoribonucleotides and compositional isomers. Popova and Williamson (2014) adapted Waghmare and Dickman's method using a reference mature ^{15}N labelled rRNA from *E. coli* in their study to understand the roles that rRNA modifications play inside the living cells (Popova and Williamson, 2014).

In addition to isotope labelling (metabolic labelling), *in vitro* transcribed RNAs with chemical isotopic labelling, such as $^{13}C_{10}$-guanosine triphosphate (GTP), have been used as an internal reference to quantitatively characterise rRNA post-transcriptional modification from *Schizosaccharomyces pombe* and *Saccharomyces cerevisiae* (Taoka et al., 2015; Taoka et al., 2016). Incorporating isotopic quantification technology by either *in vivo* or *in vitro* transcribed strategies increases the utility of an MS-based approach to absolute quantification.

A similar approach to isotopic labelling termed ‘‘comparative analysis of RNA digests (CARD)’’ extends isotopic labelling to tRNA sequencing by labelling the known sequence with $H_2{}^{16}O$, and the unknown sequence with $H_2{}^{18}O$ in order to distinguish an unknown sequence by a mass increase of 2 Da (Li and Limbach, 2013). The use of this method to achieve tRNA quantification has been challenged (Castleberry and Limbach, 2010). Issues were reported by the authors due to difficulties in determining only 2 Da mass shift from complex change states; these were addressed only through use of a high mass accuracy MS. Attempts have been made to modify the method published by Taoka et al (2015) using stable isotopic labelling *in vitro* transcribed as an internal standard in order to improve the CARD approach for characterising tRNA; this new method is called SIL-CARD (Paulines and Limbach, 2017).

New advancements in RNA interference (RNAi) have led to a need for economical and large-scale production of dsRNA, which in turn necessitates effective analytical techniques for full characterisation and accurate quantification of dsRNA before RNAi application. In this study, two stable isotopic labelling techniques: metabolic labelling and *in vitro* labelling were used on reference dsRNA in conjunction with mass spectrometry. The techniques were shown to successfully characterise and quantify dsRNA in complex total RNA mixtures produced from *E. coli.*

4.3.5 Synthesis of stable isotope labelled dsRNA

In this study, metabolic labelling in *E. coli* HT115 (DE3) cells (transformed with plasmids to express either 765bp or 401 bp dsRNA) was performed in conjunction with light (^{14}N) and heavy (^{15}N) isotope media. Following cell growth, the ^{15}N dsRNA was extracted and purified in conjunction with RNase A to remove the background

rRNA/tRNA (Nwokeoji et al., 2017). The results of the purification from the ^{15}N HT115 expressing a 765 bp dsRNA are shown in Figure IV-6 A. In addition to the purification of a dsRNA generated *in vivo* using metabolic labelling *in vitro* transcribed $13C_{10}{}^{15}N_5$ (GTP) dsRNA (401 bp) were also synthesised and purified using solid phase extraction prior to IP RP HPLC Figure IV-6 B. The results the successful synthesis and purification of the stable isotope labelled dsRNA standards generated both *in vivo* and *in vitro*. Following purification and analysis using IP RP HPLC, quantification of each sample was performed using UV spectrophotometry.

These results highlight the importance of analysing purified dsRNA samples prior to downstream dsRNA application. Using IP RP HPLC for total RNA analysis: (1) enables the determination of the purity of the product; (2) provides information on the proportion of dsRNA present; (3) provides a level of confidence regarding the NanoDrop measurements as well as the approximate amount of dsRNA labelled sample required when spiking into an unknown amount of ^{14}N total RNA.

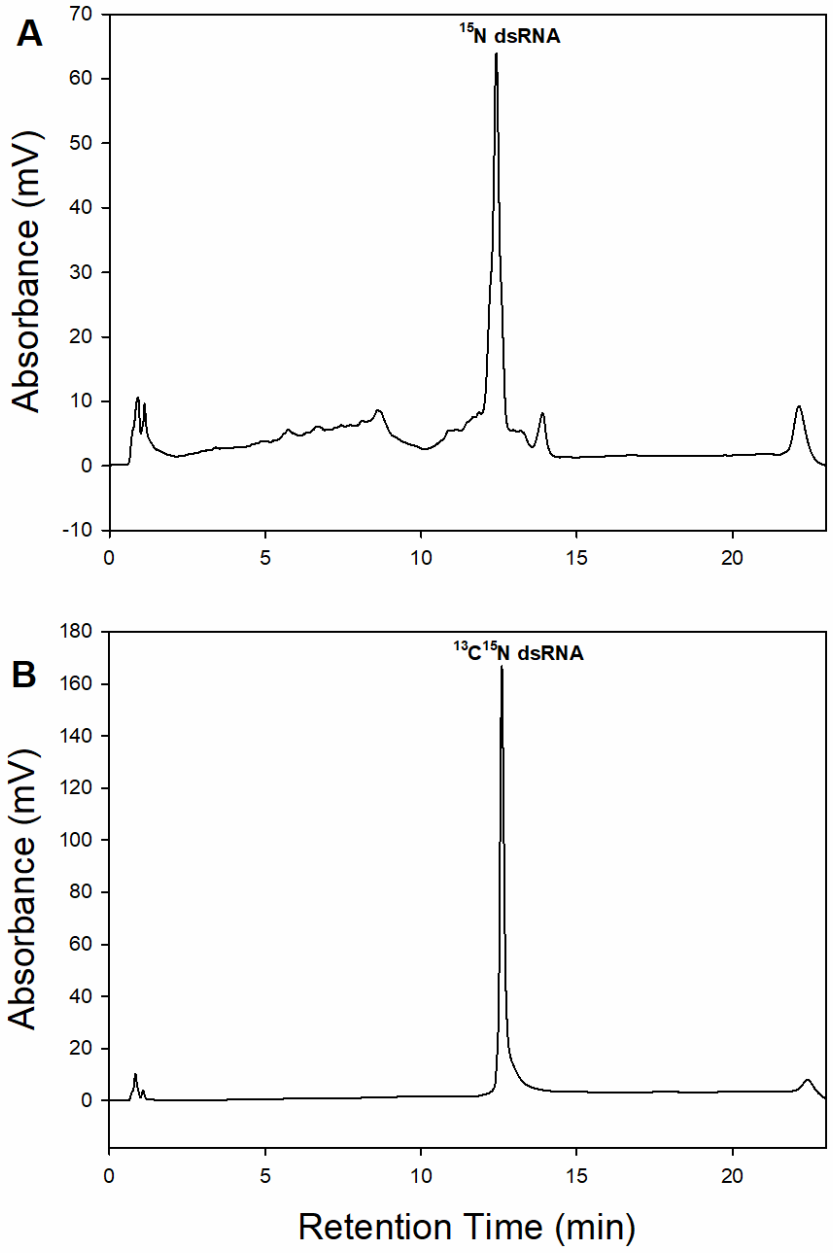

Figure IV-6: Results from IP RP HPLC analysis of *in vivo* and *in vitro* purified heavy stable isotope labelled dsRNA reported in terms of absorbance and retention time. (A) Purified metabolic isotopically labelled ^{15}N 765 bp dsRNA from *E. coli* HT115 (DE3), approximately 1.9 µg of dsRNA was injected (B) Purified *in vitro* transcribed 401 bp dsRNA isotopically labelled with enriched ^{13}C^{15}N guanosine triphosphate, 2 µg of dsRNA was injected. The analysis was performed using gradient condition 6 (see chapter 2, 2.6.5.1).

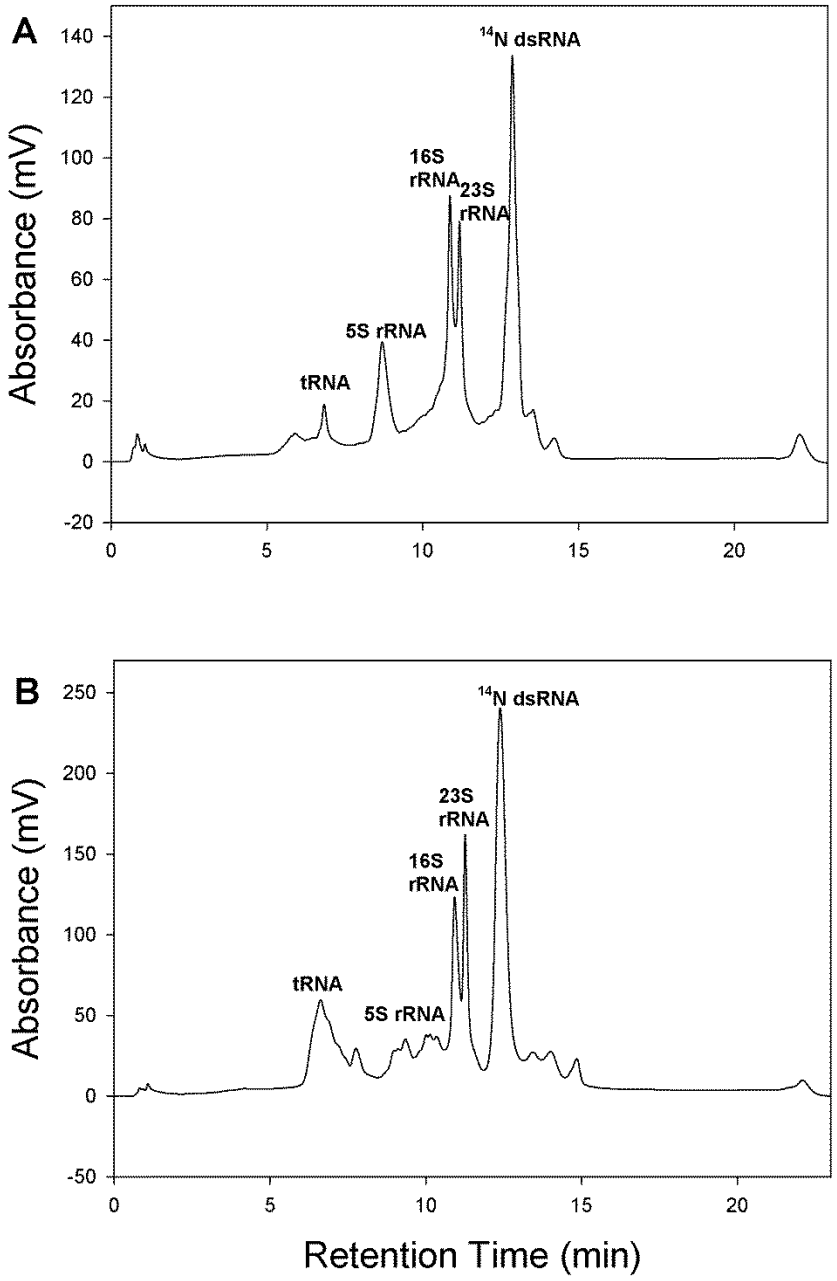

Figure IV-7: IP RP HPLC analysis of ^{14}N metabolic labelling total RNA extracted from *E. coli* (DE3) cells expressing dsRNA, reported in terms of absorbance and retention time. (A) ^{14} N Total RNA extracted from *E. coli* expressing 765 bp dsRNA, with approximately 7 µg of total RNA injected. (B) ^{14}N Total RNA extracted from *E. coli* expressing 401 bp dsRNA, with approximately 11 µg of total RNA injected and analysed using gradient condition 6 (see chapter 2, 2.6.5.1).

4.3.6 Characterisation of dsRNA using stable isotopic labelling in conjunction with RNase mass mapping for LC-MS analysis

To characterise and quantify the dsRNA expressed in *E. coli* total RNA two different strategies were employed: illustrated workflows are shown in Figure IV-8. ^{15}N dsRNA generated *in vivo* was used as the reference standard (Figure IV-8 A). In addition, $^{13}C^{15}N$ guanosine labelled dsRNA were prepared via *in vitro* transcription also used as a reference standard, prior to RNase mass mapping in conjunction with mass spectrometry analysis (Figure IV-8 B).

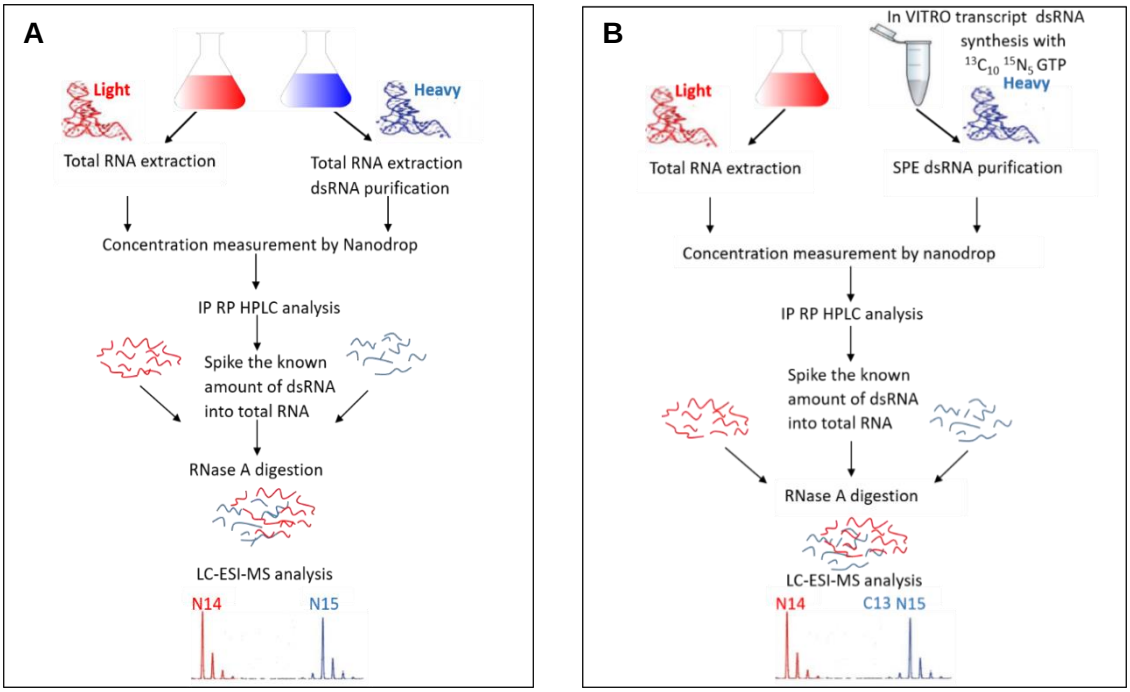

Figure IV-8: Schematic of the stable isotope labelling process in conjunction with LC-ESI-MS analysis. (A) The metabolic labelled ^{15}N dsRNA produced from *E. coli* cells is the reference RNA and is combined with ^{14}N total RNA containing 765 bp dsRNA for RNase A digestion. The mass spectrum will reveal a number of pairs ^{14}N and ^{15}N oligoribonucleotides; the differences in mass correspond to the number of nitrogen atoms. (B) *In vitro* transcribed dsRNA synthesised with $^{13}C^{15}N$ guanosine triphosphates were used as the reference RNA, and combined with ^{14}N total RNA containing 401 bp dsRNA for RNase A digestion. The mass spectrum reveals a number of pairs of ^{14}N and $^{13}C^{15}N$ oligoribonucleotides, the differences in mass correspond to the number of C and N atoms per guanosine on the oligoribonucleotides.

To characterise and quantify the dsRNA expressed in *E. coli*, total RNA were extracted from HT115 cells expressing 765 bp dsRNA and 401 bp dsRNA and analysed using IP RP HPLC (Figure IV-7 A-B.). The results show the expected chromatogram highlighting the presence of the abundant tRNA/rRNA in conjunction with dsRNA. Direct analysis using UV spectrophotometry cannot accurately determine the amount of dsRNA present in these complex mixtures. Therefore, following validation of the expression and extraction of the dsRNA in complex RNA mixtures extracted from *E. coli*, the 15N dsRNA standard previously generated were spiked into these samples.

Approximately equal amounts of reference dsRNA (^{15}N 765 bp dsRNA generated via metabolic isotopic labelling) were mixed with unlabelled dsRNA present in the complex RNA mixture followed by RNase A enzymatic digestion, in order to generate a series of oligoribonucleotides. The digested oligoribonucleotides were analysed using online ion-pair LC interfaced with ESI-MS (LC-ESI-MS). The ESI-MS was performed using an ultrahigh resolution time-of-flight (UHR-TOF) mass analyser instrument. Following LC-ESI-MS analysis, fragments of five different dsRNA oligoribonucleotides were chosen exclusively in the sense and antisense strands from total RNA and identified and characterised using the metabolic isotope labelling approach (Table IV-3 and Table IV-4). Due to the complexity of the sample, oligoribonucleotides which were less than 3 mers long were not considered.

The application of stable isotope labelling enables rapid identification of oligoribonucleotides generated from the dsRNA as they appear as light and heavy pairs in contrast to the oligonucleotides generated from the background rRNA and tRNA in the total RNA extraction. The theoretical monoisotopic masses of the light version of oligoribonucleotides were obtained using an *in silico* RNase A digest of the dsRNA, which were then utilised for comparison with the experimental monoisotopic masses. Based on the theoretical monoisotopic of light oligoribonucleotides, the amount of heavy isotope oligoribonucleotide can be calculated from the number of nitrogen atoms in the base compositions. A representative mass spectrum of the isotope labelled pair identified from the dsRNA is shown in Figure IV-9. The oligoribonucleotide AAGAUp light (827.013 m/z -2 charge) and heavy (837.985 m/z, -2 charge) is shown in (Figure IV-9 A). As there are 22 nitrogen atoms on the oligoribonucleotide, this resulted in a 21.94 Da mass shift on the heavy isotope

labelled oligoribonucleotide. A single unique oligoribonucleotide GGAGGUp from the antisense strand was distinguished in both light (1015.508 m/z) and heavy (1028.969, m/z) versions of isotopic labelling (Figure IV-9 B). As there are 27 nitrogen atoms in the oligoribonucleotide, this resulted in a 26.92 Da mass shift.

Furthermore, using the predicted monoisotopic masses for mass mapping will typically result in a number of potential base compositions in the sense or antisense strands. An example of the theoretical light (2032.292 m/z) and heavy (2060.292 m/z) oligoribonucleotides detected with two possible base compositions which could be related to the experimental masses are shown (Table IV-5). This is commonly found in RNA digestion products which generate a range of isobaric isomers and is difficult to distinguish because of the small mass difference (1 Da) between cytidine (243.2166 g/mol) and uridine (244.2014 g/mol). However, according to the base composition assignment along with the heavy isotope experimental mass, only the base composition ($G_4A_1U_1$) corresponded to 27 nitrogen atoms with the experimental masses (light, 2033.032 Da) and (heavy, 2059.955 Da), thus an oligoribonucleotide GGAGGUp in the antisense strand could be assigned (Table IV-5). Similar base compositions from either the sense or antisense strands were able to be identified using base composition assignment in conjunction with RNase predicted masses.

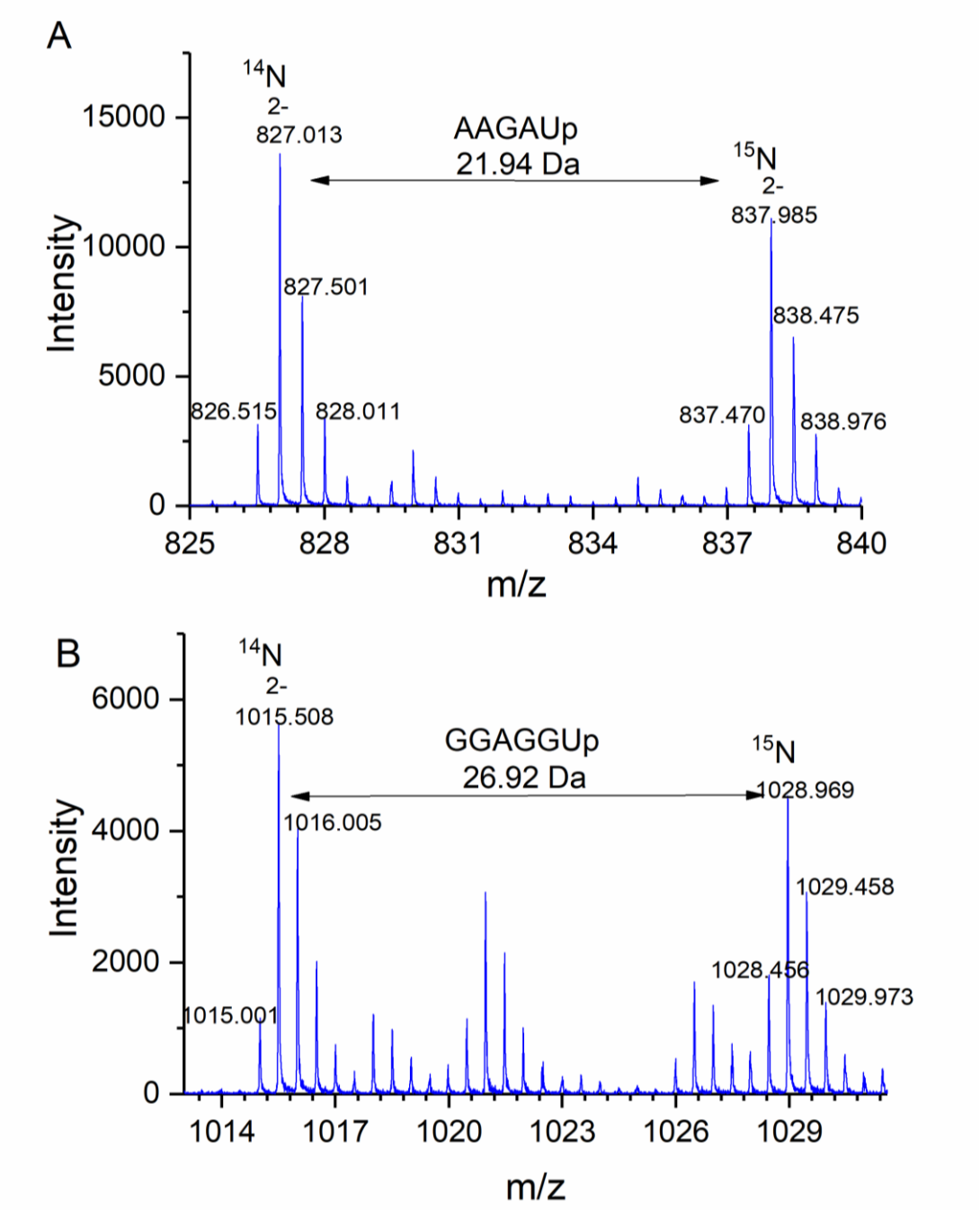

Figure IV-9: Mass spectrum of the identification of *E. coli* expressed dsRNA (765 bp) using metabolic isotopic labelling in conjunction with an RNase A digestion. The same digested oligoribonucleotides from the heavy isotope labelled will appear with increased mass compared to the light isotope labelled, depending on the number of nitrogen atoms present in the oligoribonucleotide. (A) Two pairs of isotopically labelled oligoribonucleotides were identified in the dsRNA sense strand. Oligoribonucleotides: AAGAUp (light, 827.013 m/z, -2 charged) (heavy, 837.985 m/z, -2 charged) (B) A pair of light versus heavy oligoribonucleotides, GGAAGCp (light, 1007.511 m/z) and (heavy, 1020.971 m/z) were identified from the digested dsRNA anti-sense strand, with the expected mass differences.

Table IV-3: Comparison of the light and heavy monoisotopic masses of the sense strand oligoribonucleotides.

Sequence	^{14}N Theoretical mass	^{14}N Experimental mass	^{15}N Theoretical mass	^{15}N Experimental mass	^{14}N Δ Da	^{15}N Δ Da
AAGAUp	1656.239	1656.018	1678.239	1677.991	-0.221	-0.248
GAGAUp	1672.234	1672.041	1694.234	1693.985	-0.193	-0.249
GGAAGAAGCp	3019.449	3019.077	3062.148	3061.946	-0.372	-0.202
AGGAGAUp	2346.333	2346.058	2378.333	2378.502	-0.275	+0.169
AAGGCp	1671.249	1671.048	1694.249	1693.983	-0.201	-0.266

Table IV-4: Comparison of the light and heavy monoisotopic masses of the antisense strand oligoribonucleotides.

Sequence	^{14}N Theoretical mass	^{14}N Experimental mass	^{15}N Theoretical mass	^{15}N Experimental mass	^{14}N Δ Da	^{15}N Δ Da
GGAGGUp	2033.276	2033.272	2060.276	2060.209	-0.004	-0.067
GAAGGUp	2017.281	2017.299	2044.281	2044.229	-0.018	-0.051
AGAAGAGGAGUp	3694.532	3694.286	3746.523	3746.443	-0.246	-0.079
AGAGGGUp	2362.328	2362.049	2394.328	2393.953	-0.279	-0.375
GAGAGGCp	2361.344	2361.007	2394.344	2393.950	-0.337	-0.394

Comparison of the theoretical and experimental masses of the dsRNA (765 bp) digested oligoribonucleotides shown in heavy and light monoisotopic masses. The oligoribonucleotides were generated from RNase A digestion. Grey highlight represents a single predicted unique oligoribonucleotide sequence which is only in either the sense or anti-sense strand. Bold represents a number of unique theoretical monoisotopic isomers in either the sense or antisense strand. The prediction of oligoribonucleotide base composition corresponds to the theoretical monoisotopic masses of light 2033.276 Da and heavy 2060.276 Da, and the number of nitrogen atoms present.

Table IV-5: Two potential base compositions were found, the $G_4A_1U_1p$ consisted of 27 nitrogen atoms which match the experimental masses (light, 2033.032 Da, and heavy, 2059.955 Da). This confirms that the sequence of oligoribonucleotide GGAGGUp is from the antisense strand.

C	G	A	U	p	^{14}Nmonoisotpic mass Da	^{15}N monoisotopic mass Da	Δ 14N	Δ 15N	Nitrogen atoms
1	4	1	0	1	2033.0328	2059.9552	-0.7409	0.3367	28
0	4	1	1	1	2033.0324	2059.9550	0.2436	0.3210	27

In addition to providing further evidence and assisting in the identification of oligoribonucleotides generated from the dsRNA product by identifying light and heavy isotope pairs, the analysis also enables distinguishing between those oligoribonucleotides generated from rRNA. An example is shown in Figure IV-10 here a single ^{14}N labelled mass (no isotope pair) was identified, confirming that a different species of RNA was identified instead of dsRNA. Based on the theoretical digestion list of the total RNA, the isolated mass fragment was matched to the 16S ribosomal RNA oligoribonucleotide, AAAGAGAAGCp and shows up in 1109.690 m/z, -3 charge state.

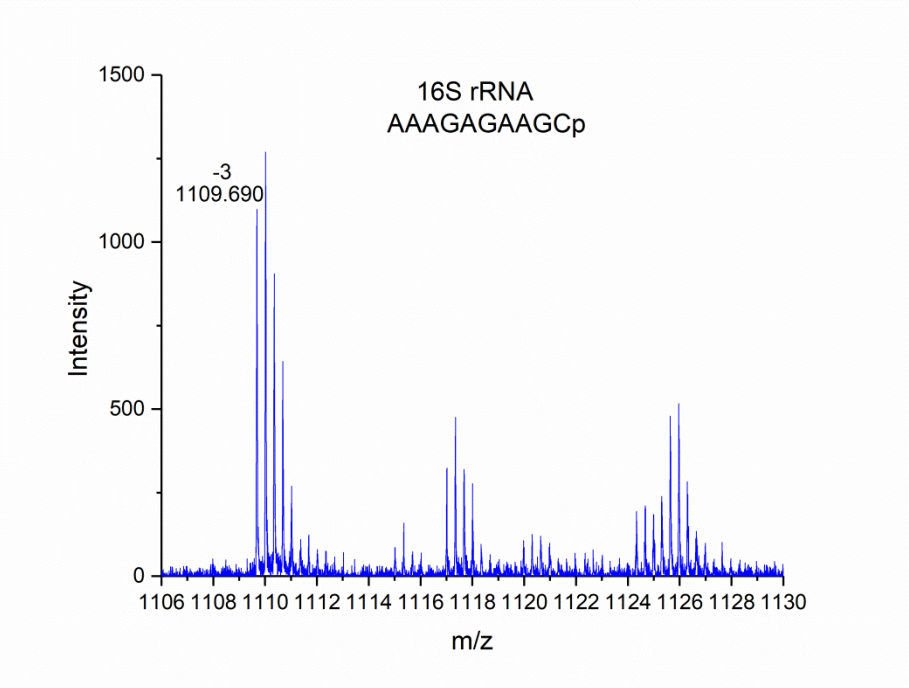

Figure IV-10: Identification of the 16S ribosomal RNA oligoribonucleotide MS spectra, AAAGAGAAGCp in total RNA (expressed 765 bp dsRNA). Observed by identifying the ^{14}N isotopic labelling (light, 1109.690 m/z, -3 charged) without a corresponding ^{15}N isotope pair (heavy, 1125.827 m/z, -3 charged).

4.3.7 Characterisation of dsRNA using *in vitro* transcribed dsRNA as an internal reference

Following analysis of dsRNA using the metabolic isotopic labelling approach in conjunction with LC-MS, the use of *in vitro* labelled dsRNA ($^{13}C^{15}N$ guanosine dsRNA) was further demonstrated as the internal standard to characterise and quantify dsRNA expressed in *E. coli*. The use of stable isotope labelled *in vitro* transcripts as internal standards was initially demonstrated by Taoka et al (2015). Total RNA were extracted from *E. coli* HT115 cells expressing 401 bp dsRNA and analysed using IP RP HPLC (Figure IV-7 B). A range of amounts of $^{13}C^{15}N$ guanidine dsRNA (401 bp) were added prior to RNase A enzymatic digestion and analysis of the oligoribonucleotide using LC-ESI-MS as previously described.

Theoretical monoisotopic masses were obtained from the RNase A digest of the dsRNA sequence prediction and were compared with the experimental monoisotopic masses. Five digested dsRNA oligoribonucleotides from both sense and anti-sense strands were assigned from the complex mixture of ^{14}N labelled total RNA using the isotopic labelled guanosine dsRNA approach (Table IV-6 and Table IV-7). A range of monoisotopic masses corresponding to unique dsRNA oligoribonucleotides were identified from the sense and antisense strands, including GGACp, AGAAGAUp, and GAGAAUp (Table IV-6). Meanwhile, the unique oligoribonucleotides; GGGCp, GGAAGGUp, AAGGGAUp, GAGGCp, and AAGAUp were also assigned to the anti-sense strand (Table IV-7).

Figure IV-11 shows a representative mass spectrum of *E. coli.* dsRNA characterisation in total RNA (^{14}N) using the *in vitro* transcript dsRNA ($^{13}C^{15}N$) method. The expected oligoribonucleotide in the sense strand AGAAGAUp was identified with the corresponding masses, light (1164.0187 m/z, -2 charge) and heavy (1179.0351 m/z, -2 charge) with a mass tolerance of ± 0.5 Da. The 30.03 Da mass difference between the light and heavy oligoribonucleotide fragments was expected due to the two $^{13}C^{15}N$ labelled guanosines present in the reference RNA (Figure IV-11 A). Another example which highlights the benefit of using dsRNA *in vitro* transcripts as the internal reference during the identification of dsRNA oligoribonucleotide fragments. GGAAGGUp oligoribonucleotide was identified (light, 1180.0116 m/z -2 charged) from the reference (heavy, 1210.0421 m/z -2 charged) in the antisense strand (Figure IV-11 B): The

results show the expected mass shift of 60 Da from the oligoribonucleotide fragment which contains 4 guanosines residues.

Table IV-6: Comparison of the light and heavy monoisotopic masses of the sense strand oligoribonucleotides.

Sequence	^{14}N Theoretical mass	$^{13}C^{15}N$ Theoretical mass	^{14}N Experimental mass	$^{13}C^{15}N$ Experimental mass	^{14}N Δ Da	$^{13}C^{15}N$ Δ Da
GGACp	1342.197	1372.197	1342.030	1372.061	-0.166	-0.135
GAGGUp	1688.228	1733.228	1688.031	1372.081	-0.196	-1.147
AGAAGAUp	2330.338	2360.338	2330.051	2360.087	-0.286	-0.250
GAGAAUp	2001.286	2031.286	2001.046	2031.075	-0.240	-0.210
AGAUp	1327.186	1342.186	1327.035	1342.355	-0.150	+0.169

Table IV-7: Comparison of the light and heavy monoisotopic masses of the anti-sense strand oligoribonucleotides.

Sequence	^{14}N Theoretical mass	$^{13}C^{15}N$ Theoretical mass	^{14}N Experimental mass	$^{13}C^{15}N$ Experimental mass	^{14}N Δ Da	$^{13}C^{15}N$ Δ Da
GGGCp	1358.192	1403.192	1358.031	1403.069	-0.160	-0.122
GGAAGGUp	2362.328	2422.328	2362.039	2422.100	-0.288	-0.227
AAGGGAUp	2346.333	2391.333	2346.042	2391.086	-0.290	-0.246
GAGGCp	1687.244	1732.244	1687.038	1732.084	-0.205	-0.159
AAGAUp	1656.239	1671.239	1656.039	1671.054	-0.199	-0.184

Comparison of the theoretical and experimental masses of the dsRNA (401 bp) RNase A digested oligoribonucleotides shown in light and heavy monoisotopic masses. The oligoribonucleotides were generated from RNase A digestion. Grey highlighting represents a unique oligoribonucleotide sequence which is only in the sense or anti-sense strand. Underlined bold represents the number of theoretical isomers in either the sense or antisense strand.

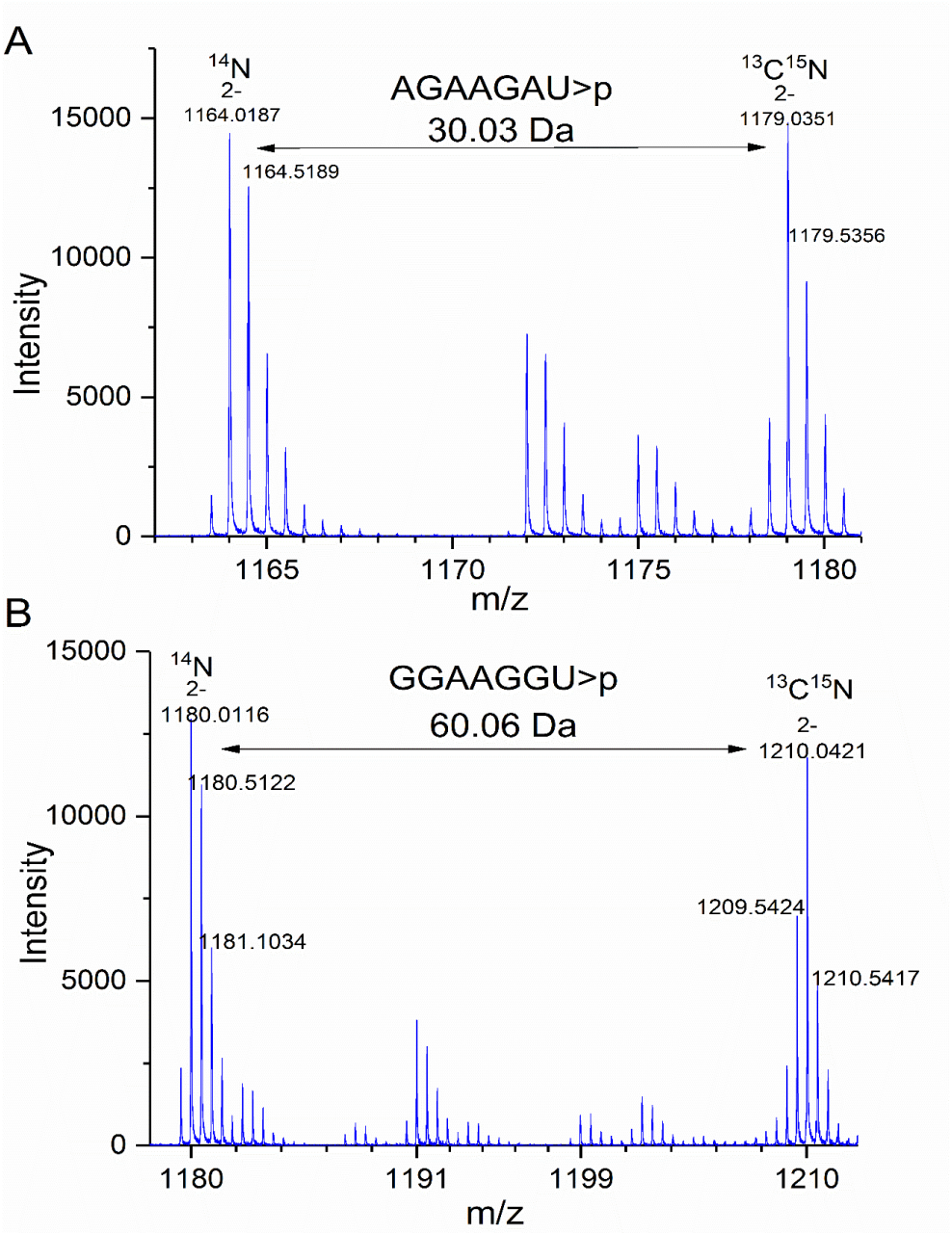

Figure IV-11: Mass spectrum showing the identification of *E. coli* expressing dsRNA (401 bp) using *in vitro* transcribed dsRNA synthesised with $^{13}C_{10}{}^{15}N_5$ enriched Guanosine triphosphate (GTP) in conjunction with an RNase A digestion. The digested oligoribonucleotides from the *in vitro* transcript will have the characteristic15 Da mass increase compared to the same oligoribonucleotides from the *in vivo* dsRNA. (A) Light (1164.0187 m/z) and heavy (1179.0351m/z) isotopic labelled AGAAGAUp oligoribonucleotide fragments from the digested dsRNA sense strand. The 30.03 Da mass difference between the light and heavy monoisotopic corresponds to the number of guanosine on the oligoribonucleotide (B) Light (1180.0116 m/z) and heavy (1210.0421) isotopic labelled GGAAGGUp oligoribonucleotide from the digested dsRNA anti-sense strand; A mass difference of 30.03 Da obtained on the mass spectra signifies that 4 guanosine nucleobases (60 Da) were present, since the masses were -2 charged, the 30.03 Da mass increase was detected on the heavy monoisotope.

4.3.8 Quantitative analysis of dsRNA oligoribonucleotides using stable isotope labelling

The benefits of using stable isotopic labelled reference dsRNA for characterising dsRNA in conjunction with RNase mass mapping have been demonstrated in the previous section. In the current study, these approaches were further applied to a quantitative application in order to rapidly and accurately quantify dsRNA in complex RNA mixtures.

A range of amounts of the *E. coli* ^{15}N purified dsRNA (765 bp) were combined with ^{14}N total RNA (containing 765 bp dsRNA). Following RNase A enzymatic digestion, the digested oligoribonucleotide fragments were analysed using LC-ESI-MS. Relative quantification was then achieved by measuring the ratio and peak areas of both light and heavy samples for five different identified oligoribonucleotides from both the sense and antisense strands.

The mass spectra (Figure IV-12 A) shows the identification of ^{14}N and ^{15}N sense strand oligoribonucleotide (765 bp expressed dsRNA), AAGAU detected in varying amounts of spiked ^{15}N dsRNA. A further example of the mass spectra of the antisense ^{14}N and ^{15}N oligoribonucleotide, GAAGGUp is shown in Figure IV-12 A. Relative quantification was then achieved by measuring the ratio and peak areas of both light and heavy samples for 10 different identified oligoribonucleotides (Figure IV-12 B and C).

The experimental ratios for both sense and antisense strands are shown in Figure IV-12 C, where the standard deviations refer to experimental errors. Average experimental errors were ±0.09 (SD) and 6.1% (CV) for all of the oligoribonucleotides, which were analysed via different dynamic ranges. Spiking in different amounts of the ^{15}N standards enabled the absolute quantification of the dsRNA (see Table IV-8), which was 466.48 ng.

Table IV-8: Quantification of 765 bp dsRNA oligoribonucleotides using stable isotope labelling. Mean and standard deviation information as well the coefficient of variation are included.

Average $^{14}N/^{15}N$ ratio	Quantification of ^{14}N dsRNA (ng/ µL)
0.289±0.04	485.30
0.907±0.11	447.96
3.209±0.12	466.15
Average SD ±0.09	466.47±18.67
Average CV 6.1%	

Table IV-9: Quantification of 401 bp dsRNA oligoribonucleotides using *in vitro* transcript stable isotope labelling. Mean and standard deviation information as well the coefficient of variation are included.

Average $^{14}N/^{15}N$ ratio	Quantification of ^{14}N dsRNA (ng/ µL)
0.277±0.05	640.86
1.069±0.12	618.31
3.453±0.32	614.50
Average SD ±0.16	624.56±14.24
Average CV 10.2%	

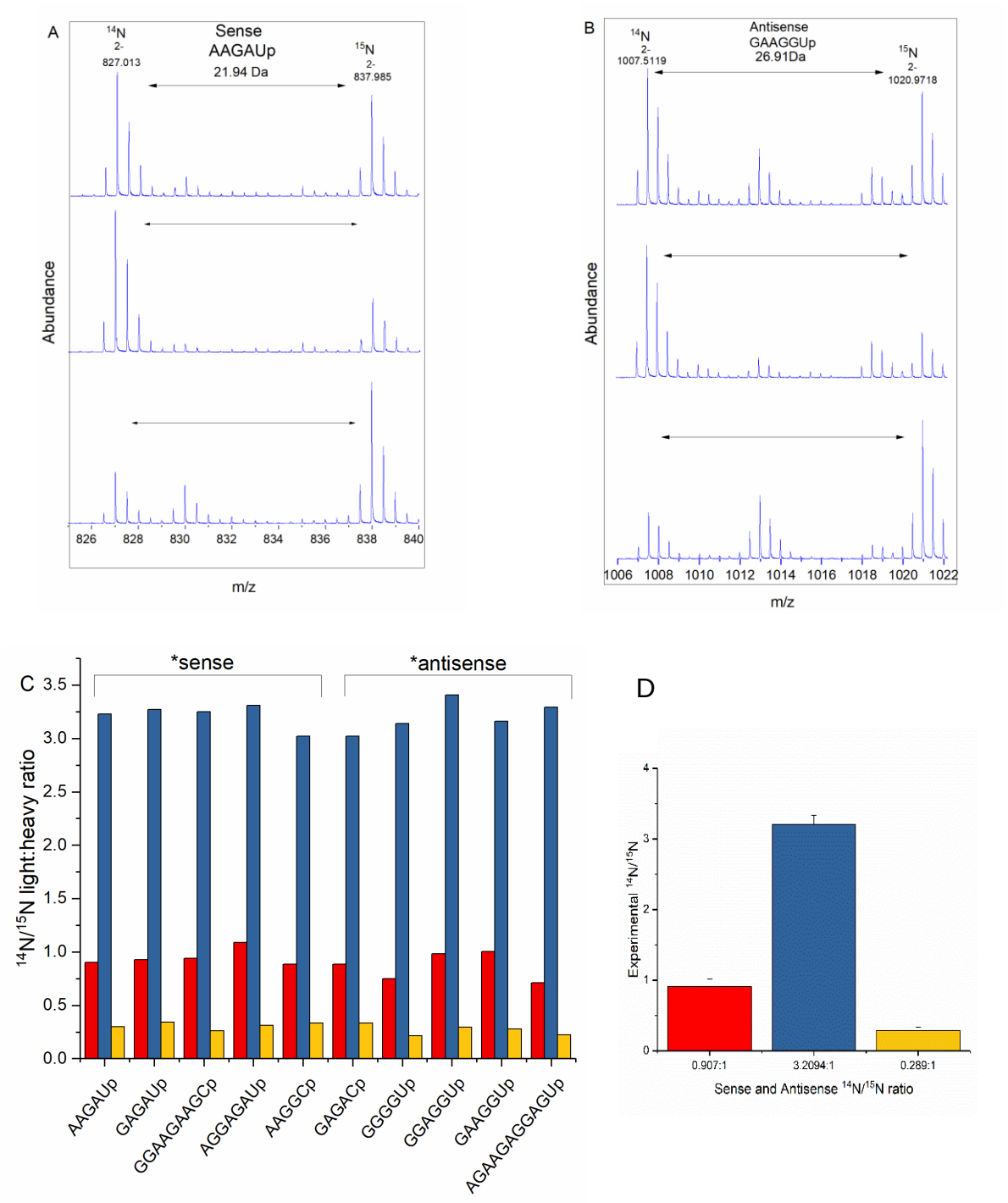

Figure IV-12: Absolute quantification using stable isotope labelling in conjunction with mass spectrometry for the analysis of *E. coli* expressed with 765bp dsRNA. (A) MS spectra of digested oligoribonucleotide AAGAUp (sense strand), (B) GAAGGUp (antisense strand) in a different light and heavy ratios respectively. (C) Light to heavy ratios of ten different oligoribonucleotides. (D) Absolute quantification of experimental masses shown for ten different oligoribonucleotides with the error bars representing standard deviation.

4.3.9 Quantitative analysis of dsRNA oligoribonucleotide using $^{13}C^{15}N$ labelled *in vitro* transcript reference dsRNA

Following quantitative analysis of 765 bp dsRNA using the metabolic isotopic labelling approach in conjunction with LC-MS, we further demonstrated the use of *in vitro* $^{13}C^{15}N$ guanosine containing dsRNA (401 bp) as the internal reference to quantify the same sequence of dsRNA expressed in *E. coli*.

The representative mass spectrum of the doubly charged unique sense and antisense sense strands oligoribonucleotide, AGAAGAUp and GGAAGGUp are shown with varying amounts of spiked isotope labelled standard (Figure IV-13 A). As seen from the examples, the mass separated by 15 Da can be easily distinguished between the sample and reference. A comparison of the five, experimentally observed light and heavy oligoribonucleotides obtained for both sense and antisense strands is shown in Figure IV-13 B/C.

Figure IV-13 C shows the overall quantitative analysis of the experimental ratios for ^{14}N versus ^{15}N oligoribonucleotides, includes information on standard deviations which represent experimental error. It can be observed that the experimental standard deviations indicate an average error of about ± 0.16 (SD) and 10.2% (CV) for different mixed ratios. In summary, the absolute quantification of the amount of dsRNA in the total RNA can be achieved by spiking $^{13}C^{15}N$ guanosine containing IVT dsRNA standards into total RNA mixture (expressing dsRNA). Absolute quantification amount of ^{14}N dsRNA present in total RNA corresponding to 624.56±14.24 ng/µL (Table IV-9).

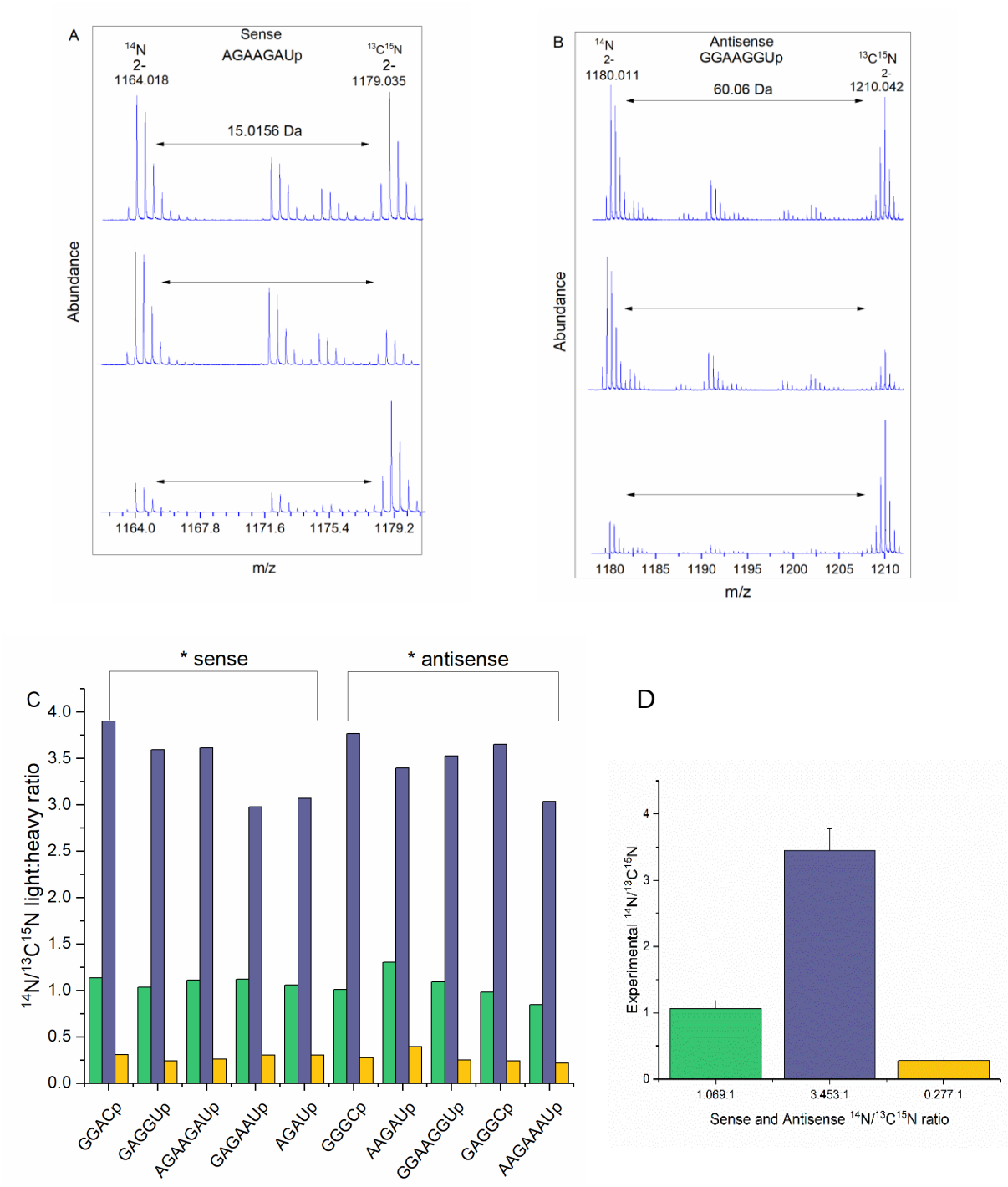

Figure IV-13: Absolute quantification of *in vivo* dsRNA (401 bp) using *in vitro* transcribed dsRNA synthesised with $^{13}C_{10}{}^{15}N_5$ enriched guanosine triphosphate (GTP). (A) Mass spectra of the light and heavy, AGAAGAUp and (B) GGAAGGUp oligoribonucleotides of both sense and antisense strands shown in different light and heavy labelled mixed ratios. (C) Light to heavy ratios of ten different oligoribonucleotides from both sense and antisense strands. (D) Absolute quantification of the experimental masses shown for ten different oligoribonucleotides with the error bars representing standard deviation.

4.3.10 Conclusions

Stable isotopic labelling of dsRNA using both *in vivo* (^{15}N) and *in vitro* ($^{13}C^{15}N$ guanosine) to generate internal standards was used in conjunction with mass spectrometry for the characterisation and quantification of dsRNA in complex RNA mixtures.

From the experiments, several key capabilities of stable isotopic labelling were identified: (1) the method could readily characterise dsRNA fragments based on comparative analysis of light and heavy labelled oligoribonucleotides monoisotopic masses. (2) Possible compositional isomers in either sense or antisense strands of dsRNA could be identified through the determination of the number of heavy atoms on the oligonucleotide; (3) Absolute quantification of dsRNA in a total RNA mixture could be achieved knowing the amount of heavy-labelled dsRNA spiked into light-labelled total RNA (expressing dsRNA), without prior purification of contaminating small RNAs.

These features provide the stable isotope labelling method with a discernible advantage over conventional methods used for rapid nucleic acid quantification such as UV spectrophotometry, which cannot provide quantitative information on individual components in a complex mixture without prior purification. HPLC, another often used method, suffers from limited quantification accuracy due to the presence of abundant tRNA and rRNA or other multiple heterogeneous RNA originating from dsRNA synthesis, which may co-elute with the dsRNA and therefore prevent accurate quantification.

Stable isotope labelled dsRNA standards were synthesised (^{15}N and $^{13}C^{15}N$ guanosine containing) *in vivo* and *in vitro* prior to purification and quantification. The stable isotope dsRNA standards were subsequently mixed into RNA extracted from *E. coli* that were engineered to express dsRNA prior to RNase digestion and LC-ESI-MS analysis. Absolute quantification was performed based on the resulting light and heavy oligonucleotides identified using mass spectrometry. Using this approach, it was determined that 624.6 ng/µL and 466.5 ng/µL of dsRNA was present in 80 µL of total RNA extracted from 10^8 *E. coli* cells expressing 765 bp and 401 bp dsRNA respectively.

Chapter V : Effects of monolith porosity on the analysis of nucleic acids using ion-pair reversed-phase HPLC

5.1 Abstract

Monolithic porous columns are a new generation of powerful stationary phases utilised for the separation of biomolecules. However, the behaviour of monolithic columns is not well understood. This chapter aims to study the performance of monolithic columns with different porosity size distributions (PSD); ProSwift RP-1S (standard PSD), RP-2H (high PSD), and RP-3U (ultra-high PSD) for the analysis of nucleic acids under retentive and non-retentive elution modes using HPLC.

Nucleic acids of different sizes and classes were analysed including dsDNA, oligonucleotides, rRNA, dsRNA, and MS2 ssRNA. Under IP RP HPLC conditions the RP-1S and RP-2H columns demonstrated higher separation efficiencies over the RP-3U column for the analysis of large MW nucleic acids. The RP-3U column was optimal for the analysis of oligonucleotides while the RP-2H column showed the lowest resolution when it was used to analyse small oligonucleotides. The effect of varying flow rates (0.4 mL/min to 1.4 mL/min) was also studied using dsDNA and oligonucleotides on all columns showing that in general higher flow rates significantly improved resolutions regardless of column porosity.

To further study the effects of column porosity, elution times for nucleic acids of different sizes were tested under non-retentive conditions. A general trend where elution time decreased with increasing analyte size was observed on the RP-1S and RP-2H columns. In contrast, this effect was not observed on the RP-3U column. Using the RP-1S and RP-2H columns under varying acetonitrile concentrations did not alter the elution time of smaller oligonucleotides. However, the elution times of larger 18 mer oligonucleotides and ssRNA were affected at high concentrations of acetonitrile (80%). Interestingly on the RP-3U column, variations in ACN concentration did not affect elution times. These results have provided further insight into the behaviour of monolithic columns and the effects of column porosity on the analysis of nucleic acids.

5.2 Introduction

The growing application of nucleic acids in bioscience has driven the demand for improved approaches for their synthesis, purification, and characterisation. Prior to the use of synthetic materials in biological systems, effective techniques for separation, characterisation and quantification of these materials are required. Polyacrylamide gel electrophoresis (PAGE) and liquid chromatography are principal analytical techniques for these purposes. Unfortunately, PAGE involves long analysis times, is labour intensive and leads to poor quantitative accuracy as well as irreproducible results, making the method impractical for analytical purposes. In contrast, high-performance liquid chromatography (HPLC) demonstrates inherent advantages compared to the conventional analytical methods including better efficiency, significant improvements in characterisation and quantitative ability, as well as highly reproducible results.

Ion-pair reversed-phase high-performance liquid chromatography (IP RP HPLC) is a well-established standard analytical platform for nucleic acid separation (Huber et al., 1992). A wide range of reversed-phase columns such as conventional silica-based C18 resins and polymeric resins have been used in IP RP HPLC (Huber et al., 1993). Monolithic columns are a new generation of polymer-based columns which have recently been used for the separation of biomolecules in particular proteins (Xie et al., 1997). However, relevant studies on the application of monolithic columns to analyse nucleic acids have been much less prominent.

Monolithic columns have been successfully applied for efficient and high-resolution separations of nucleic acids using IP RP HPLC. (Premstaller et al., 2000 and Walcher et al., 2002). A wide range of monolithic reversed-phase columns designed with different chemical and physical properties are available. Major factors to be considered when choosing a column include column dimension, pore size distribution, pore structure, and mass transfer properties of the packing material. The different properties of columns show significant impact on the performance of nucleic acids chromatography, by affecting parameters such as cycle time, peak resolution, peak shape, separation efficiency, retention time, and column operational pressure. In addition, since macromolecules such as nucleic acids have low diffusivity rates, choosing a column configuration with favourable mass transfer rates is crucial for their successful separation. The objective of this study was to compare the

chromatographic efficiency of different pore size distributions (PSD) for nucleic acids analysis using ProSwift monolithic columns in 4.6 mm x 50 mm ID (Table V-1).

Table V-1: Specifications of the ProSwift reversed-phase columns used

Parameter	**ProSwift RP-1S**	**ProSwift RP-2H**	**ProSwift RP-3U**
Base matrix	PS-DVB	PS-DVB	PS-DVB
Surface Chemistry	Phenyl	Phenyl	Phenyl
Pore size distribution	1.1 µm Standard permeability	2.2 µm High permeability	5.2 µm Ultra permeability
Bed height	45 mm	43 mm	40 mm
Column volume	0.76 mL	0.73 mL	0.65 mL
Flow rate	0.5-4 mL/min	1-10 mL/min	1-16 mL/min

5.2.1 Morphology of ProSwift reversed-phase monolithic columns

Porous polymeric monolithic media are engineered using *in situ* polymerisation, which is based on a cross-linked material interconnected network in a single cylindrical polymer rod. The morphologies of the ProSwift RP-1S, Rp-2H, and RP-3U monolithic columns can be seen in a scanning electron micrograph (SEM).

Figure V-1 shows fine, moderate, and large pores for the RP-1S, RP-2H, and RP-3U columns respectively. The RP-3U column is further distinguished with interconnected and non-uniform pore sizes.

Small and large aggregates of globules comprise the media in a typical monolith structure and produce structures similar to a cauliflower. The abundant space between the large aggregate globules offers high flow operational capabilities and low back pressure. Between the smaller globules are open or through pores. As a result, the analyte has rapid access to the functionalised surface media. In a conventional bead-based column, mass transfer is controlled by molecular diffusion, in contrast to a monolithic column, where mass convection takes place through the open pores. The presence of mass convection minimises slow mass transfer rates in monolithic columns. Monolithic columns have approximately 60% pore volume which is much higher than porous beads. The pore sizes of monolithic columns are characterised

into two types: large pores, approximately a micron or greater, and small pores, which are specifically engineered to be less than ten to hundreds of nanometres.

Although interstitial volume is absent in monolithic materials, the internal porosity contains micro, meso, and macropores (Hiroyoshi et al., 1996), and as a consequence, all of the eluents must travel through these pores, following the shortest flow path. Polymerisation of the monolith creates mesopores, and the resultant microfollicular configuration lacks diffusive micropores. In principle, the absence of micropores allows an increase in resolution due to the intraparticle convection (Rodrigues et al., 1993). Convective flow is more efficient with species of large molecular weights at high flow rates (Hiroyoshi et al., 1996).

With respect to chromatographic resolution, conventional beads frequently result in poor peak resolutions due to slow analyte mass transfer. In contrast, the unique features of monolithic column morphology lead to rapid mass transfer which minimises widening peak shapes with high resolutions under a wide range of flow rates. This advantage in mass transfer is crucial for high efficiency separation of large biomolecules whose diffusion rates are lower than small molecules. This chapter will explore the influence of pore sizes of ProSwift RP-monolithic columns on nucleic acid analysis using IP RP HPLC, and under isocratic non-retentive HPLC conditions.

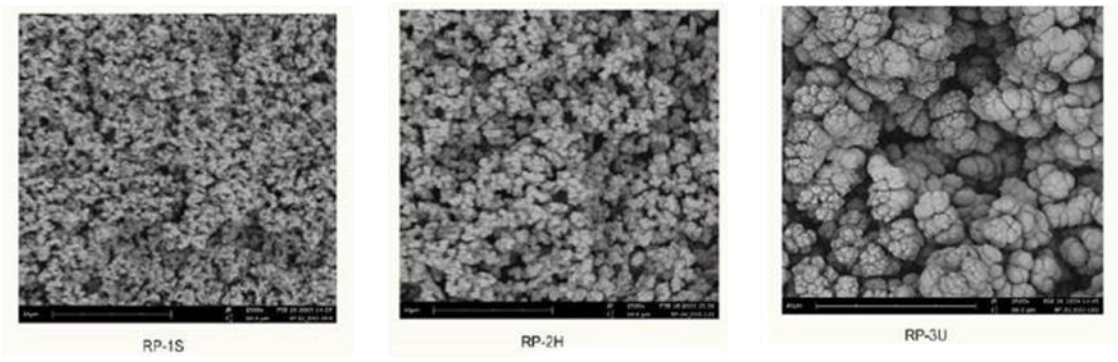

Figure V-1: SEM images of the ProSwift reversed-phase monolithic columns: RP-1S, RP-2H, and RP-3U with pore size distributions: 1.1 µm, 2.2 µm, and 5.2 µm respectively. Morphology of the ProSwift is composed of aggregates of globules, the spaces around the aggregates are through pores which enable fast analyte access (Image reproduced from the Dionex product manual).

5.3 Results and discussion

Part A

5.3.1 Effects of different porosities of monolith RP columns on the analysis of nucleic acids under IP RP HPLC conditions

RP-1S, 2H, and 3U columns were used to analyse dsDNA (fragment size range 80-587 bp) under the same IP RP HPLC gradient condition to compare their performances. The comparative analysis of dsDNA separation is shown in Figure V-2 A-C. The results show that smaller dsDNA fragments (80 and 102 bp) were retained longer on the RP-1S column (Figure V-2 A), while larger fragments (179 bp to 587 bp) were more retentive on the RP-3U column (Figure V-2 C). General trends on the effect of differently sized dsDNA on retention time demonstrate that higher porosities correlate with increased retention times for larger dsDNA fragments (257-587 bp) (RP-3U> RP-2H> RP-1S). The opposite was observed (decreased porosities led to an increase in retention time for smaller sized dsDNA (80-102 bp) (RP-1S> RP-2H> RP-3U). These results may be the consequence of an increase in the functional surface hydrophobicity of the RP-3U column, as the larger dsDNA fragments were shown to be more interactive with the higher porosity monolithic column. This was despite much lower column volume compared to the other columns (see Table V-8), a feature which usually entails lower analyte elution times. However, as the same PS-DVB material is used in all 3 columns, the increase in surface hydrophobicity is unlikely to explain the large differences in retention time seen for the larger dsDNA. Furthermore, the increased hydrophobicity should also increase the retention time of the smaller dsDNA fragments. Therefore, it is proposed that the different porosity of the RP-3U column has a significant impact on the retention of larger dsDNA fragments using IP RP HPLC.

Full width half maximum (FWHM) values were utilised to evaluate the overall peak resolutions of the DNA fragments: 80 bp, 102 bp, 179 bp, and 295 bp across the three columns. The FWHM values obtained for the columns corresponding to the fragments were: 0.10, 0.10, 0.14, 0.14 minutes, 0.12, 0.11, 0.16, 0.18 minutes, and 0.16, 0.14, 0.24, 0.25 minutes for the RP-1S, RP-2H, and RP-3U columns respectively under the same gradient conditions. This result shows that higher resolutions were achieved in the order RP-1S >RP-2H >RP-3U (Figure V-2) i.e. decreasing column porosity is

correlated with increasing dsDNA resolution. The RP-3U column showed a noticeable broadening of the peaks compared to the RP-1S and RP-2H columns. Further analysis to improve the separation efficiency of dsDNA using the RP-3U column was carried out using a steeper gradient. A significant improvement in the resolution of large dsDNA fragments (434-587 bp) was observed.

In summary, the results show that dsDNA separations are sensitive to differences in porosity. Monolithic columns with wide pore-sizes have also been applied to high-efficiency protein separation and were less influenced by changes in porosity (Trojer et al., 2006). It is possible that hydrodynamic properties play a role in separation, and that these disparities in hydrodynamic volume are responsible for the apparent difference in behaviour between protein and DNA separation on the different monoliths. Most proteins fold into globular ellipsoid molecules, while duplex DNA tend to be worm-like filament molecules. Which contain greater hydrodynamic volume than ellipsoid molecules, possibly contributing to their sensitivity to porosity effects (Fernandes et al., 2002).

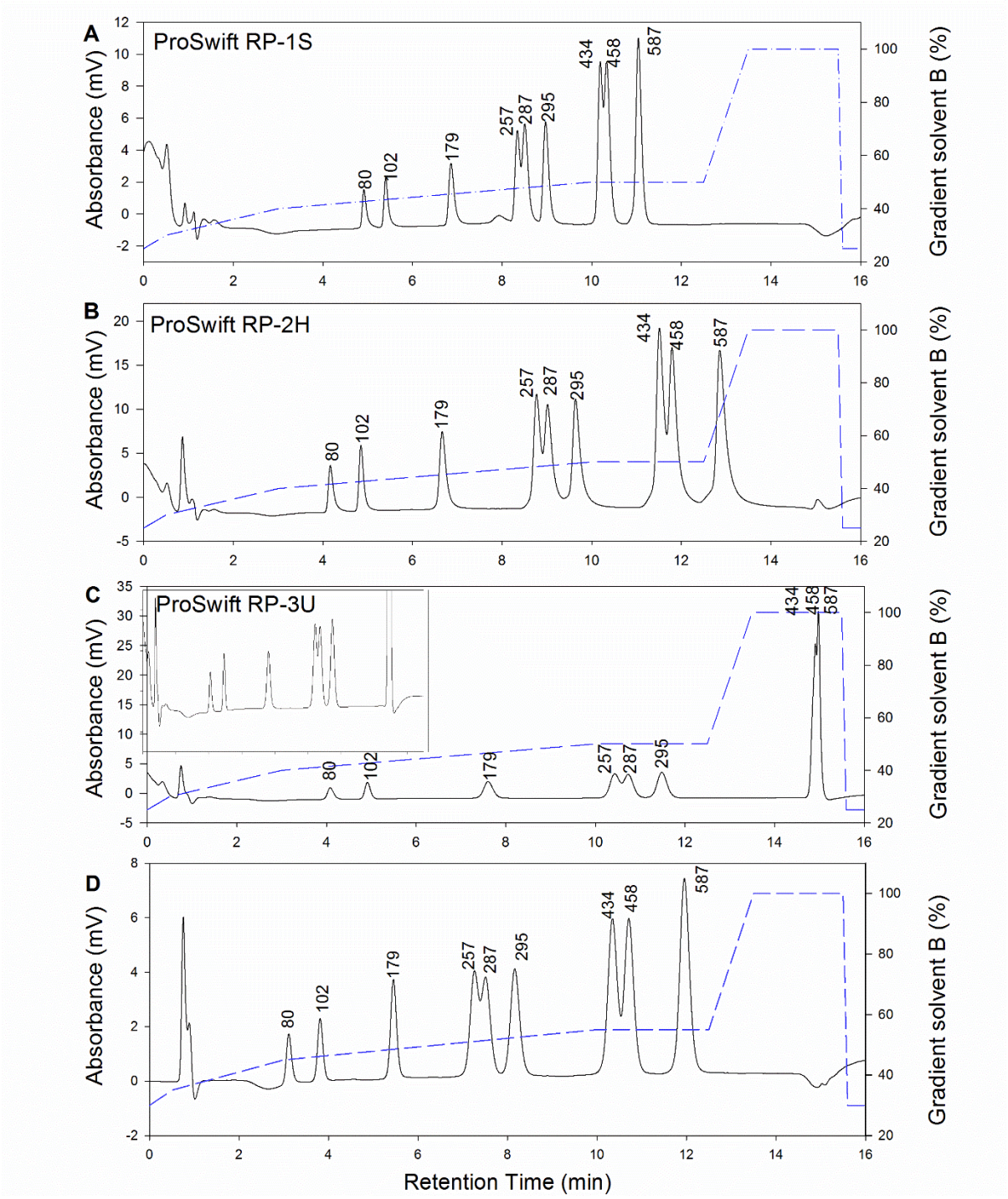

Figure V-2: pUC18 HaeIII digest dsDNA ladder IP RP HPLC analysis performed on ProSwift monolith columns of different porosities. (A) RP-1S, (B) RP-2H, and (C) RP-3U using gradient condition 4 (see Chapter 2.6.5) (D) RP-3U at 50°C with flow rate 0.75 mL/min using gradient condition 5 respectively. The dsDNA fragment sizes are highlighted in base pair.

Following the analysis of dsDNA, a comparative study on RNA separation was performed by analysing total RNA and ribosomal RNA using the polymeric monolith columns (see Figure V-3). Interestingly, using the same gradients on all three columns did not significantly affect the retention time of rRNA in contrast to previous data from the analysis of large dsDNA (see Figure V-2). The results show that the order of elution was RP-3U<RP-2H<RP-1S and this is reflective of the small differences in column volumes of each column (see Table V-1).

The RP-2H column produced optimum resolutions and separation, as seen from both the highest baseline resolution (*R*s) of 4.17 minutes and the narrowest peak shape (FWHM 0.12 and 0.11 minutes for 16S and 23S rRNA respectively) (Figure V-3 B). The RP- 3U column generated relatively good resolutions (*R*s = 3.45 minutes; FWHM of 0.16 and 0.17 minutes for 16S and 23S rRNA respectively, and demonstrated better baseline resolving power (Figure V-3 C) compared to the RP- 1S column. For the RP-1S column, despite good peak shapes (FWHM 0.13 and 0.14 minutes) (Figure V-3 A), its baseline resolution of 2.23 minutes was not as good as the RP-2H and RP-3U columns. In developing HPLC elution method, the anticipation is usually to attain a separation of the peak of interest from other peaks with $Rs \geq 2$ (Snyder and Dolan, 2007). In this study, all three monolithic columns produced high-resolution separation of the 16S and 23S rRNA, with no significant effect on the chromatographic performance when analysing large ribosomal RNA using monolithic columns of different ranges of pore size distribution.

Monoliths of different pore sizes were further compared by analysing a large ssRNA (MS2 RNA, consisting 3569 nucleotides), (Figure V-4 A-C). Using identical gradients for each column, the order of elution time was found to be consistent with data from the analysis of rRNA, in contrast with observations on large dsDNA. The results again showed only small differences in the performance of the RP-1S and RP-2H columns, as well comparable resolutions observed on the RP-3U column (FWHM= 0.11, 0.12, and 0.15 minutes respectively; (Figure V-4 A-C). However, the results show that differences in peak shape were observed, where fronting peaks appeared for the RP-2H and RP-3U columns (Figure V-4 B and C). The fronting peaks may have been caused by an impurity from the MS2 RNA which started co-eluting. This was in contrast to the wide peak shape generated on the RP-1S column, which demonstrated lower

separation efficiency on the smaller porosity monolithic column. Overall, the chromatograms obtained on both the ribosomal RNA and the MS2 RNA clearly demonstrate similar performances for all three columns.

In addition to analysing large MW nucleic acids, 20 mer oligonucleotides were analysed on the different monoliths (Figure V-5 A-D). The results show an optimum resolution on the RP-3U column, as seen from the Gaussian peak with an FWHM of 0.14 minutes (Figure V-5 C). Unexpectedly, a much lower resolution was obtained on the RP-2H column, as the FWHM was not measurable due to poor peak shape. Higher resolution was observed on the RP-1S column (FWHM was 0.17 minutes) (Figure V-5 A) compared to the RP-3U column. Low resolutions were observed on two identical RP-2H columns (Figure V-5 B and C). It is proposed that this may have been due to restrictions on diffusive rates resulting from significant gel porosity of the RP-2H columns, thus reflecting stagnant mass transfer zones and limiting its efficacy for the separation of small molecules such as oligonucleotides under strong retention mode (Nischang and Brüggemann, 2010). In addition, smaller biomolecules such as peptides and oligonucleotides are much more sensitive to changes in porosity compared to larger molecules (Trojer et al., 2006), which might explain the significant differences when observing separation performance oligonucleotide using different monoliths. However, considering the similarity between the pore sizes of the RP 1S and RP 2H columns (1.1 µm and 2.2 µm respectively) and the previous data, it was unexpected that such differences were observed for the analysis of oligonucleotides.

Noticeably, lower retention times for the 20 mer oligonucleotide were observed on the monolithic RP-3U column compared to the RP-1S column under the same chromatographic conditions (Figure V-2 A and C). These results agree with previous data on the analysis of small dsDNA, and rRNA where shorter elution times on the larger pores of the RP-3U column were observed primarily due to the lower dead volumes (0.65 mL and 0.76 mL) of the RP-3U and RP-1S columns respectively. In addition, it is proposed that the smaller molecules will elute faster in larger pores than in smaller pores due to different mass transfer properties.

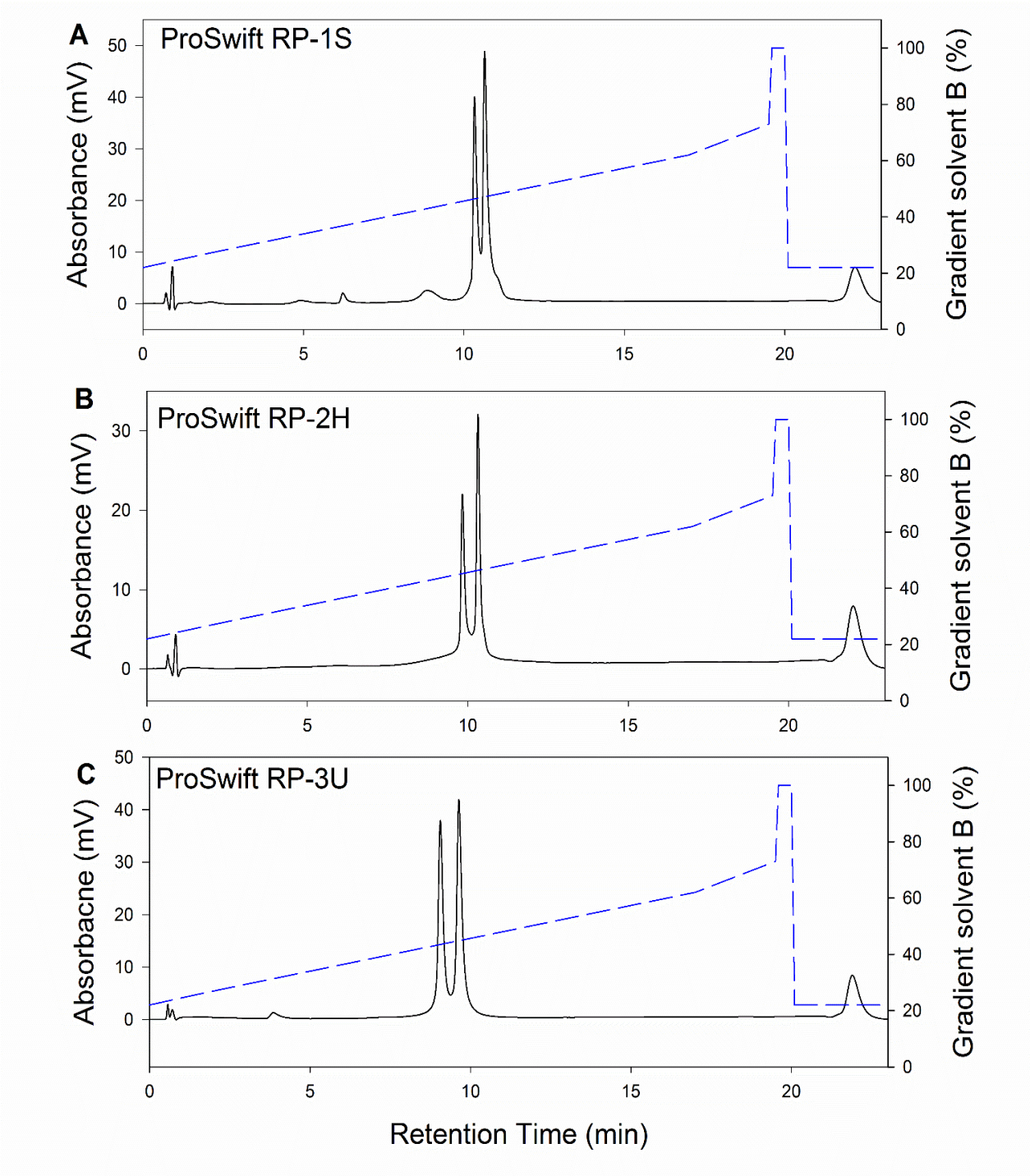

Figure V-3: A comparison of RP-1S, RP-2H, and RP-3U monoliths for the analysis of ribosomal RNAs extracted from *E. coli,* using IP RP HPLC at 50°C. (A) RP-1S (B) RP-2H, and (C) RP-3U monolith columns respectively. The two peaks shown on the chromatogram refer to 16s rRNA and 23s rRNA using gradient 6 (see Chapter 2.6.5).

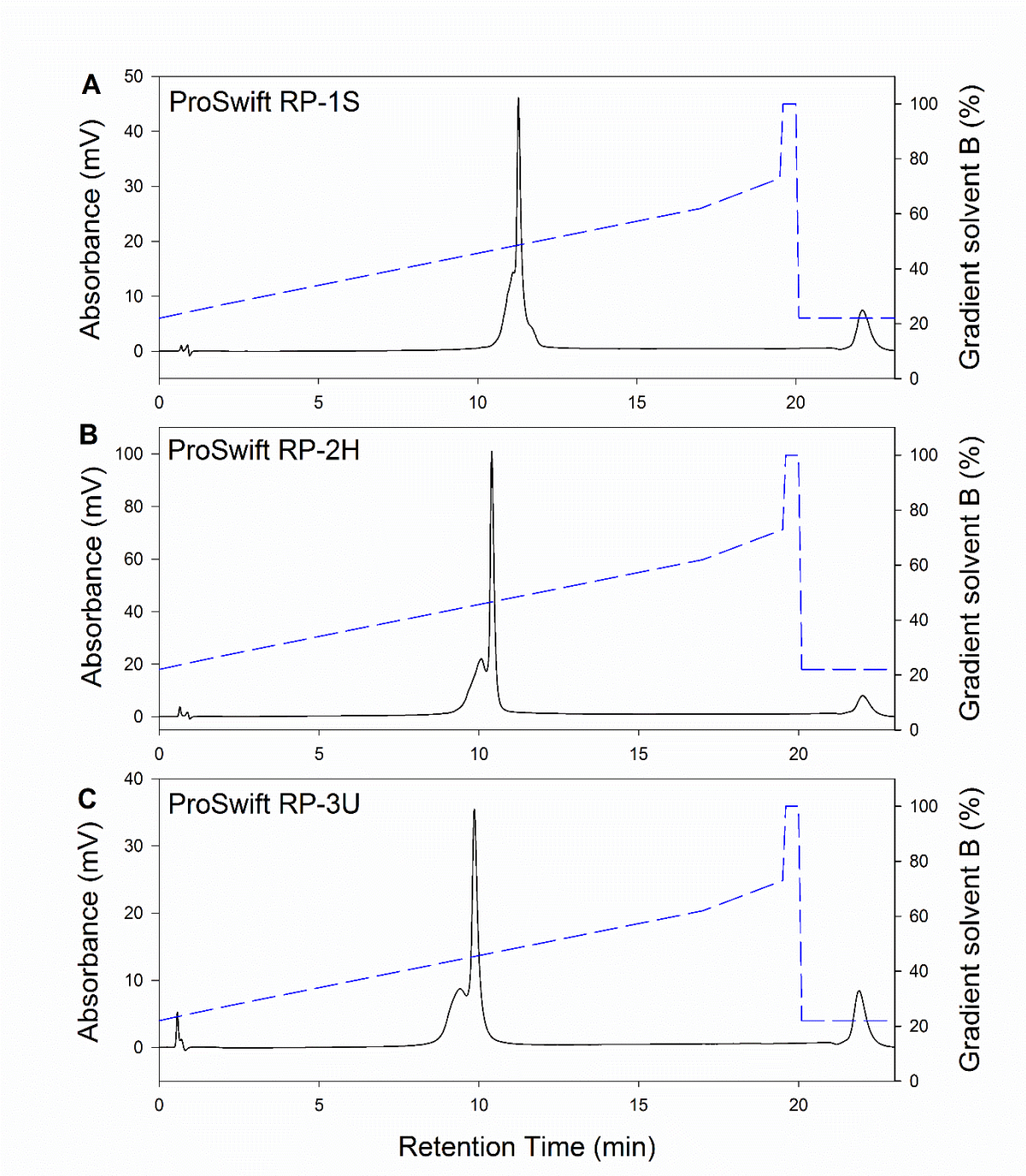

Figure V-4: A comparison of chromatographic performance on the analysis of bacteriophage MS2 RNA using ProSwift monolith columns of different porosities with IP RP HPLC at 50°C. (A) RP-1S (pore size distribution 1.1µm), (B) RP-2H (pore size distribution 2.2 µm), and (C) RP-3U monolith columns (pore size distribution 5.2 µm) respectively, using gradient 6 (See Chapter 2.6.5).

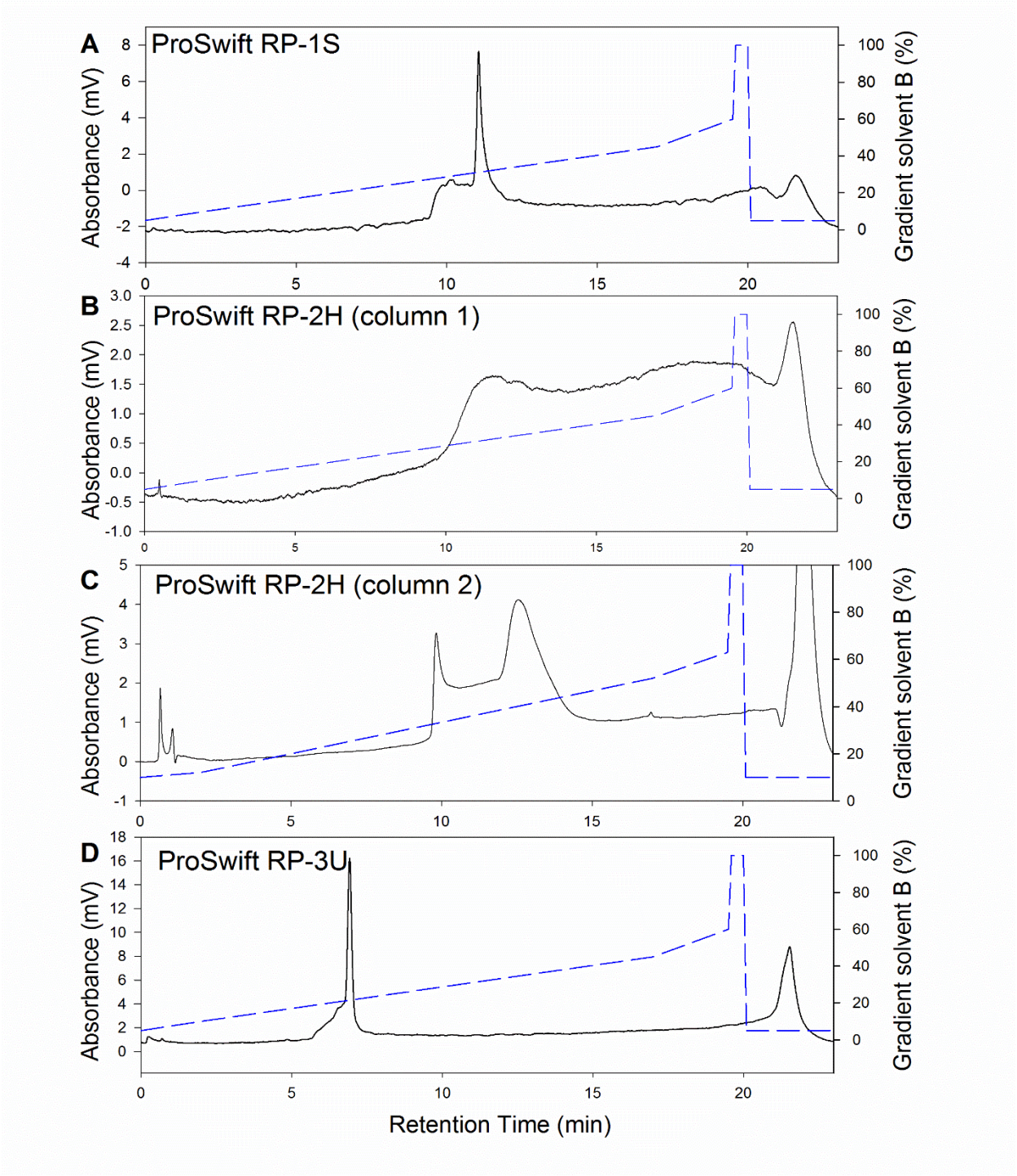

Figure V-5: A comparative analysis of 20 mer oligonucleotides under IP RP HPLC using ProSwift monolithic columns. (A) RP-1S (B) RP-2H column No. 1 (C) RP-2H column No. 2 and (D) RP-3U at 50°C by gradient condition 7, figure C was performed under a steeper gradient condition 8 (see Chapter 2.6.5).

5.3.2 Performance of different monolith columns at various flow rates

The objective of the HPLC method development is to perform analysis in shorter times and to avoid compromising performance in resolution, efficiency, as well as sensitivity. In this respect, the effects of flow rates on monolithic columns (ProSwift RP-1S, RP-2H, and RP-3U) were studied across the range 0.4 mL min^{-1} to 1.4 mL min^{-1} in conjunction with IP RP HPLC for the analysis of 20 mer oligonucleotides and pUC18 *Hae* III DNA ladder.

The results show that for the analysis of 20 mer oligonucleotides using the RP-1S column, an increase in flow rate corresponded with an expected decrease in RT (18.77 to 10.36 minutes) as shown in (Figure V-6 A-F) due to the internal void volume of the column, while FWHM improved from 0.25 to 0.18 minutes (Table V-2). In particular, the fronting peak which was apparent at low flow rates appears to be reduced at higher flow rates. Lower flow rates at 0.4 mL min^{-1} and 0.6 mL min^{-1} also demonstrated peak broadening and peak tailing (Figure V-6 A and B).

The results are consistent with previous data (data not shown) where a broad peak was observed in the analysis of the 20 mer oligonucleotide on the RP-2H column over flow rates ranging from 1.0 mL min^{-1} to 1.4ml min^{-1}. In contrast, using the RP-3U column, a narrow peak was obtained across elevated flow rates (Figure V-7 A-F). In addition, retention time differed only slightly at 1.0, 1.2, and 1.4 mL/min^{-1} (6.92 to 6.66 minutes). Optimum performance was achieved at higher flow rates of 0.8 and 1.0 mL/min^{-1} (FWHM 0.14 minutes) (Figure V-7 C and D; Table V-4). Thus, the RP-3U column clearly demonstrates the highest resolution for the separation of oligonucleotides across a wide range of flow rates (within the range 0.4-1.4 mL/min^{-1}).

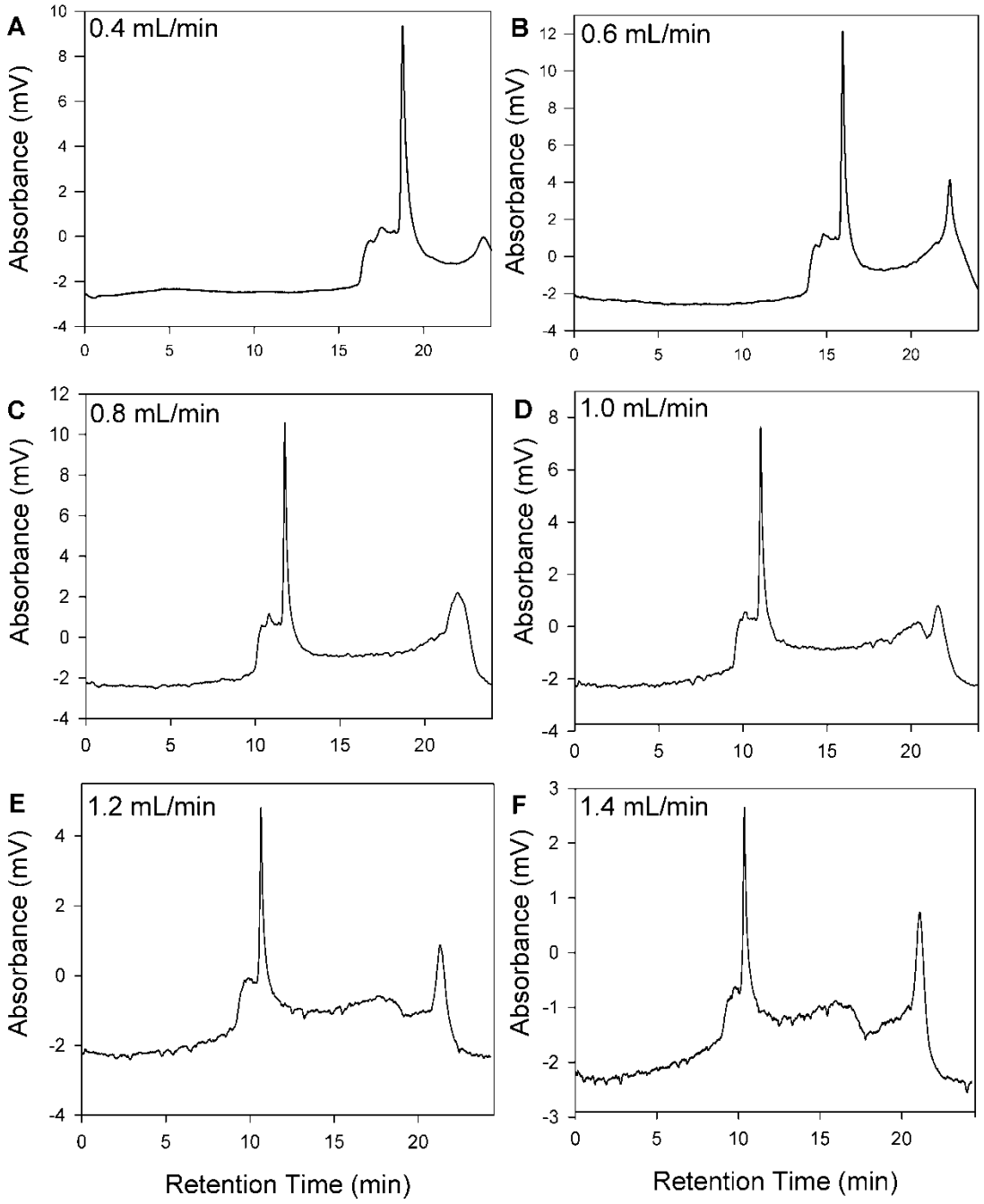

Figure V-6: The effect of increased flow rates on ProSwift RP-1S (1.1 µm pore size) monolith column for the analysis of 20 mer oligonucleotide at 50°C by IP RP HPLC. (A) 0.4 mL min^{-1} (B) 0.6ml min^{-1} (C) 0.8 mL min^{-1} (D) 1.0 mL min^{-1} (E) 1.2ml min^{-1} (F) 1.4 mL min^{-1} using gradient condition 7 (see Chapter 2.6.5).

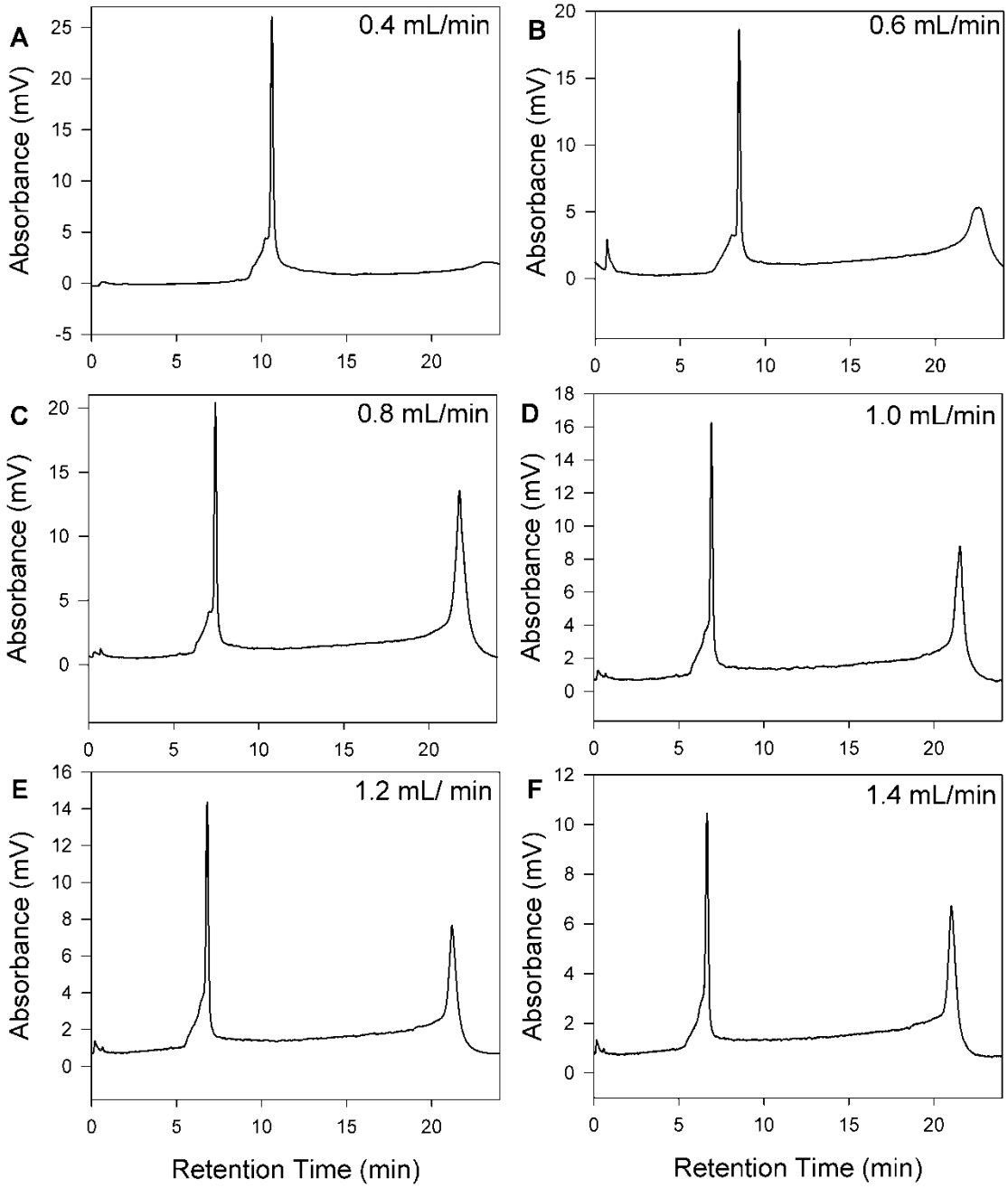

Figure V-7: The effect of different flow rates on ProSwift RP-3U (5.2 µm pore size) monolith column for the analysis of 20 mer oligonucleotide at 50°C by IP RP HPLC. (A) 0.4 mL min^{-1} (B) 0.6ml min^{-1} (C) 0.8 mL min^{-1} (D) 1.0 mL min^{-1} (E) 1.2ml min^{-1} (F) 1.4 mL min^{-1} using gradient condition 7 (see Chapter 2.6.5).

The relationship between retention times and peak resolutions using ProSwift RP-1S, RP-2H, and RP-3U columns for the analysis of 20 mer oligonucleotides at different flow rates. Resolution was not available on the RP-2H column due to lack performance. Comparing these three columns, the RP-3U column at flow rates of 0.8 and 1.0 mL/min provided the optimum peak resolution. The trends produced on the RP-1S and RP-3U columns suggest that higher flow rates may enhance resolutions on porous polymeric monolith columns.

Table V-2: Effect of increasing flow rate using the ProSwift-1S column for 20 mer oligonucleotide analysis

Flow rate (mL/min)	Retention Time (RT)	Full Width Half Maximum (FWHM)
0.4	18.77	0.25
0.6	15.95	0.19
0.8	11.74	0.16
1.0	11.06	0.17
1.2	10.65	0.18
1.4	10.36	0.18

Table V-3: Effect of increasing flow rate using the ProSwift-2H column for 20 mer oligonucleotide analysis

Flow rate (mL/min)	Retention Time (RT)	Full Width Half Maximum (FWHM)
0.4	15.55	*
0.6	13.11	*
0.8	12.20	*
1.0	11.54	*
1.2	11.31	*
1.4	10.91	*

*No resolution excluded

Table V-4: Effect of increasing flow rate using the ProSwift-3U column for 20 mer oligonucleotide analysis

Flow rate (mL/min)	Retention Time (RT)	Full Width Half Maximum (FWHM)
0.4	10.60	0.15
0.6	8.46	0.15
0.8	7.45	0.14
1.0	6.92	0.14
1.2	6.79	0.16
1.4	6.66	0.16

Further analysis into the effect of flow rates using monoliths of the different pores sizes under IP RP HPLC was performed using dsDNA fragments (80-587bp), while the fragments of 102 bp and 295 bp were used to evaluate the peak resolutions (Table V-2-Table V-4).

The results show that due to the combination of a delay in the gradient and the columns' internal volume, it was not practical to operate the flow below 0.8 mL/min. Overall, adjusting flow rates (0.8-1.4 mL/min) did not significantly improve the resolutions obtained for the majority of dsDNA fragments in each column. Similar findings have been reported by Huber's group using a DNAsep column for DNA fragment analysis (Huber et al., 1993). This phenomenon could be the consequence of mass transfer resistance between the column surface and the eluent, resulting in peak broadening or poorer peak shapes at high flow rates. The results are also in contrast with a previous study on peptides and proteins which found that increased flow rates benefit mass transfer rates and show improved resolution and separation (Cabrera et al., 2000 and Thermo product manual, 2014).

The RP-1S column demonstrated a small improvement in resolution with FWHM from 0.07 to 0.05 minutes for 102 bp dsDNA (Figure V-8 B-E and Table V-5). However, the FWHMs were unaltered for 295 bp dsDNA in the same flow rate range. The RP-2H column showed optimal performance at a flow rate of 0.8 mL/min^{-1} (Figure V-9 C and Table V-6). By extending the range of flow rates, good peak resolutions were achieved for fragment sizes ranging from 80 bp-458 bp. The RP-3U column produced a similar peak resolution for 102 bp dsDNA fragments (average FWHM 0.08 minutes) (Table V-7), and much broader peak areas for 295 bp fragments were observed (FWHM 0.30 to 0.25 minutes corresponding to flow rates 0.6-1.4 mL/min^{-1}) (Figure V-10 B-F) in comparison to the RP-1S and RP-2H columns despite the flow rates applied.

In summary, the optimal performance for oligonucleotide analysis when using the RP-1S and RP-3U columns can be obtained at higher flow rates, typically between 0.8 and 1.0 mL/min. Specifically, the RP-3U column can operate at a wider range of flow rates to produce maximum oligonucleotide resolution. As previously observed, the resolution obtained on the RP-2H column was significantly lower compared to that of the RP-1S and RP-3U columns. In addition, the analysis of different-sized dsDNA

fragments using the RP-1S column demonstrated optimal separation at higher flow rates (0.8-1.4 mL/min^{-1}).

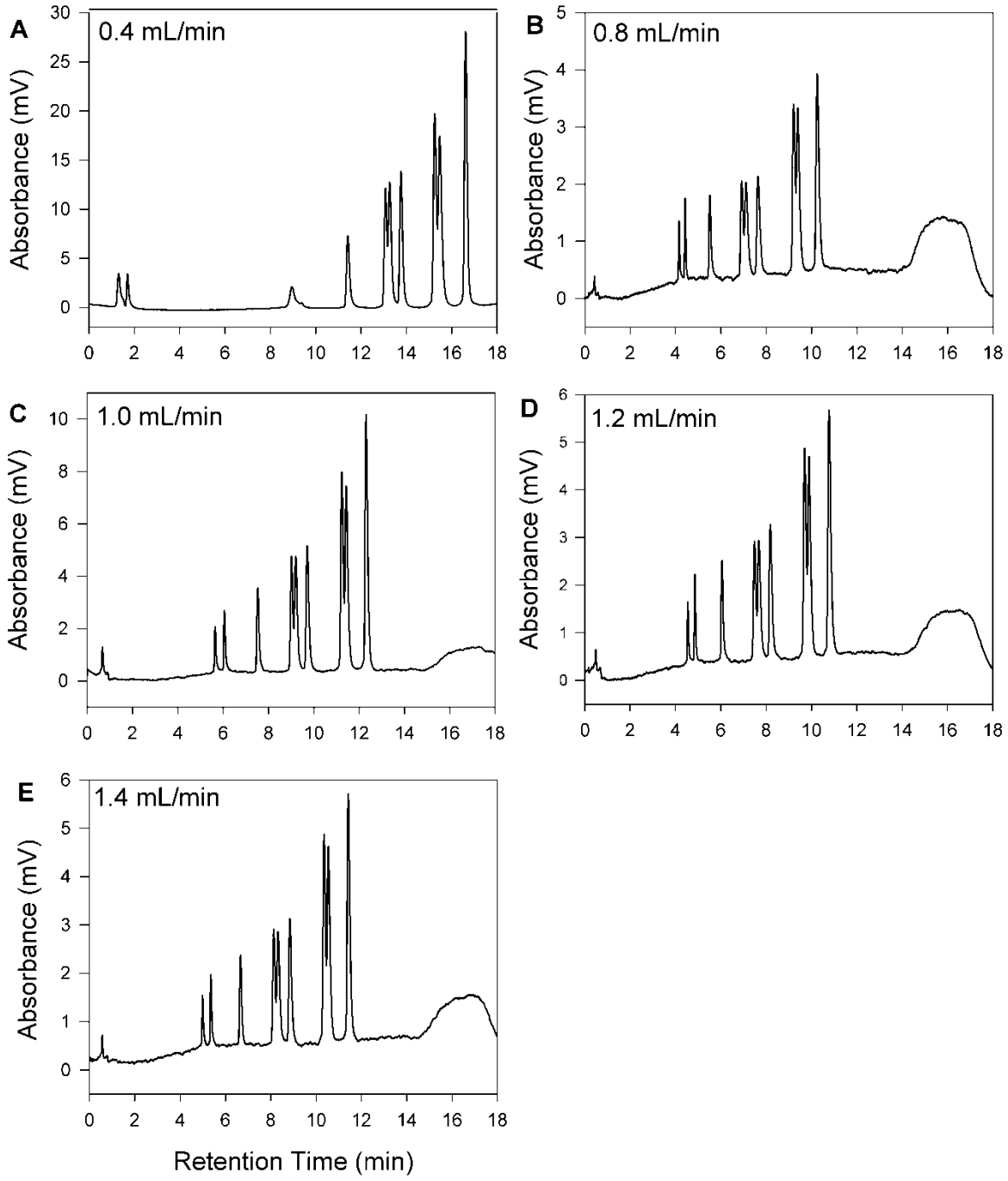

Figure V-8: The effect of different flow rates on the ProSwift RP-1S (1.1 µm pore size) monolithic column for the analysis of pUC18 DNA Hae III digest ladder at 50°C by IP RP HPLC. (A) 0.4 mL min^{-1} (B) 0.8ml min^{-1} (C) 1.0 mL min-^{1} (D) 1.2ml min^{-1} (E) 1.4 mL min^{-1} using gradient condition 9 (see Chapter 2.6.5).

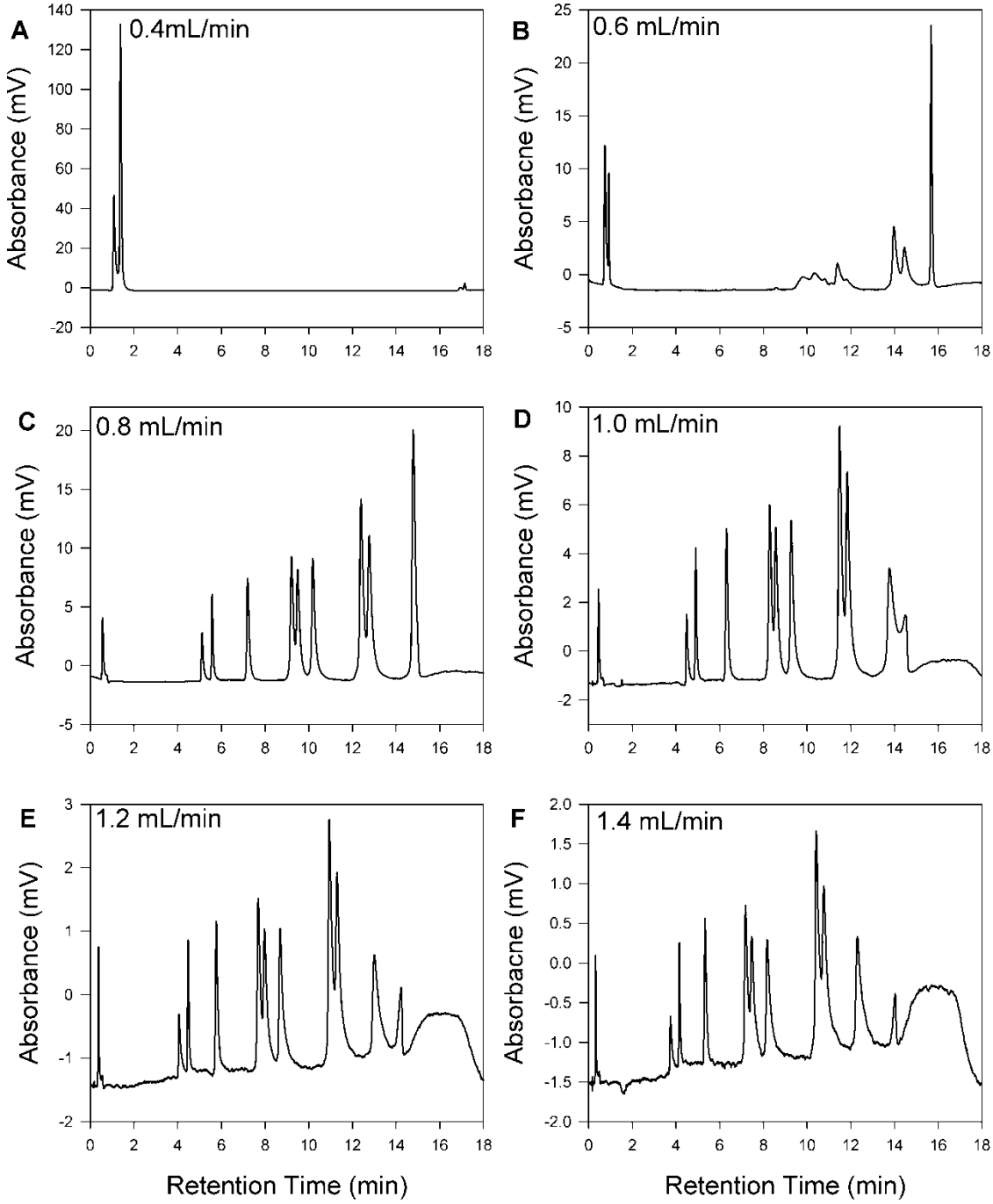

Figure V-9: The effect of different flow rates on the ProSwift RP-2H (2.2 µm pore size) monolithic column for the analysis of pUC18 DNA Hae III digest ladder at 50°C by IP RP HPLC. (A) 0.4 mL min^{-1} (B) 0.6ml min^{-1} (C) 0.8 mL min^{-1} (D) 1.0 mL min^{-1} (E) 1.2ml min^{-1} (F) 1.4 mL min^{-1} using gradient condition 9 (see Chapter 2.6.5).

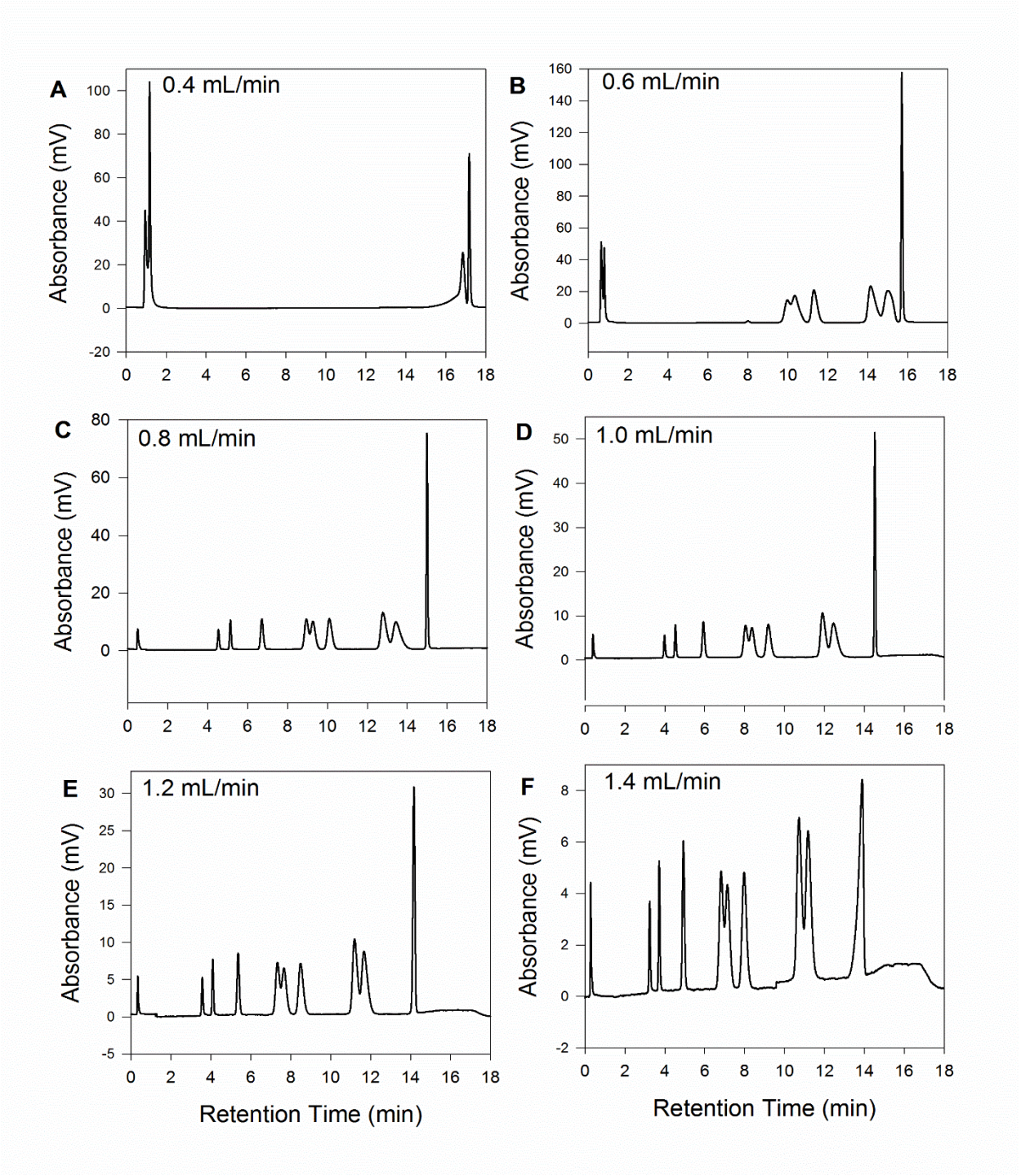

Figure V-10: The effect of different flow rates on ProSwift RP-3U (5.2µm of pore size) monolithic column for the analysis of pUC18 DNA Hae III digest ladder at 50°C by IP RP HPLC. (A) 0.4 mL min^{-1} (B) 0.6 mL min^{-1} (C) 0.8 mL min^{-1} (D) 1.0 mL min^{-1} (E) 1.2 mL min^{-1} (F) 1.4 mL min^{-1}using gradient condition 10 (see chapter 2.6.5).

The relationship between retention times and peak resolutions using monolith columns, ProSwift RP-1S, RP2H, and RP-3U analysing pUC 18 Hae III Digest ladder at different flow rates. The lower flow rates caused delays on elution time. Therefore, the retention time and the resolutions are not available in the RP-2H and RP-3U column at flow rate 0.4 mL/min. dsDNA 102 and 295 bp fragments were used to evaluate the FWHM.

Table V-5: Effect of increasing flow rate using the RP-1S column for pUC18 DNA *Hae* III Digest ladder analysis

Flow Rate (mL/min)	Retention Time (RT)	Full Width Half Maximum (FWHM)	Retention Time (RT)	Full Width Half Maximum (FWHM)
0.4	*	*	13.76	0.14
0.6	*	*	*	*
0.8	6.05	0.07	9.70	0.13
1.0	5.35	0.07	8.84	0.13
1.2	4.86	0.06	8.19	0.13
1.4	4.42	0.05	7.64	0.15

***No resolution excluded

Table V-6: Effect of increasing flow rate using the RP-2H column for pUC18 DNA *Hae* III Digest ladder analysis

Flow Rate (mL/min)	Retention Time (RT)	Full Width Half Maximum (FWHM)	Retention Time (RT)	Full Width Half Maximum (FWHM)
0.4	*	*	*	*
0.6	*	*	*	*
0.8	5.58	0.07	10.19	0.15
1.0	4.90	0.07	9.27	0.15
1.2	4.48	0.06	8.68	0.16
1.4	4.15	0.06	8.18	0.19

*No resolution excluded

Table V-7: Effect of increasing flow rate using the RP-3U column for pUC18 DNA *Hae* III Digest ladder analysis

Flow Rate (mL/min)	Retention Time (RT)	Full Width Half Maximum (FWHM)	Retention Time (RT)	Full Width Half Maximum (FWHM)
0.4	*	*	*	*
0.6	*	*	11.31	0.30
0.8	5.14	0.08	10.10	0.25
1.0	4.53	0.08	9.18	0.25
1.2	4.09	0.08	8.49	0.26
1.4	3.72	0.07	7.97	0.25

*No resolution excluded

5.3.3 Effect of chemical denaturants in conjunction with IP RP HPLC

IP RP HPLC uses a hydrophilic buffer triethylammonium acetate (TEAA) and organic solvent acetonitrile (ACN) as a standard mobile phase for nucleic acid analysis. The analysis is normally performed at room temperature or 50°C using linear gradient elution, a condition referred to as non-denaturing chromatography. Under such conditions, however, long- single-stranded nucleic acids might assume secondary structures, resulting in wide or multiple peaks. IP RP HPLC is often performed at high temperatures (75°C) to overcome these effects; however, even elevated temperatures may not denature long double-stranded nucleic acids.

Recently, the use of urea in conjunction with HPLC for the analysis of long single-stranded oligonucleotides and double-stranded oligonucleotides has been reported as an alternative method for denaturing HPLC (Fueangfung et al., 2014). Urea is a denaturant reagent widely used in biomolecules through the direct binding interaction or by changing the solvent environment by favouring unfolding (Bennion and Daggett, 2003).

A series of experiments were performed to study the effect of using the standard TEAA-ACN mobile phase with a 10% urea solution. A ProSwift RP-1S column (standard pore size) was used to analyse 20 mer oligonucleotides, E. *coli* 16S and 23S ribosomal RNA and bacteriophage MS2 RNA at both denaturing and non-denaturing conditions and column temperatures of 50°C and 75°C. Analysing 20 mer oligonucleotide with the TEAA mobile phase at 50°C produced a sharp peak with FWHM 0.12 minutes, (Figure V-11 A). Potential impurities appeared to co-elute as shown by the multiple peaks appearing at front of the main oligonucleotide peak (FWHM 0.136 minute) in the mobile phase containing urea (Figure V-11 B). The addition of 10% urea resulted in a decrease in retention time (Figure V-11 B), similar to that observed in the absence of urea at 75°C. The addition of 10% urea under denaturing conditions further reduced the retention time (Figure V-11 D). These results are consistent with previous data that showed reduced fragment retention times under denaturing conditions (Gjerde et al., 2009). Comparing the FWHM however, did not show any significant improvement in the resolution of the oligonucleotides. However, for highly complex structures such as oligonucleotides and RNA, the additional denaturing conditions may have a greater effect on resolution. For example, potential

impurities started denaturing, as seen from a hump apart from the main peak on the TEAA buffer (Figure V-11 C). Additionally, the mobile phase containing urea had a significant effect leading to the co-elution of impurities as shown by into two small humps in front of the oligomer (Figure V-11 D).

Performing the same comparative analysis for the analysis of total RNA using 16S and 23S rRNA at 50°C produced very sharp peaks under both mobile phases, as seen from the FWHM of 0.106 and 0.111 minutes, with and without 10% urea respectively (Figure V-12 A and B). FWHM values at 75°C were similar, at 0.106 and 0.108 minutes with and without 10% urea respectively (Figure V-12 C and D). Although the additional 10% urea in TEAA-ACN caused a slight increase in peak resolution, a significant reduction in retention time was observed at both temperatures, indicating a possible reduction in ion pairing with the analyte (or stationary phase) and reduction in overall hydrophobicity.

Finally, analysis of the large bacteriophage MS2 RNA was performed (Figure V-13). Gaussian peaks obtained on the two systems and temperatures (50°C TEAA with FWHM = 0.13 minutes, 50° TEAA and 10% urea with FWHM = 0.10 minutes; 75°C TEAA with FWHM = 0.11 minutes and TEAA and 10% urea with FWHM = 0.09 minutes). The denaturing urea-TEAA buffer system altered the retention time with slightly improved resolutions observed at 50°C and 75°C.

In summary, the experiments performed with urea as an additive to the IP RP HPLC mobile phase showed that it was compatible with an HPLC system, in part because no significant loss of resolution was observed during or after the analysis. However, no significant improvement in the resolution of oligonucleotides or ssRNA was observed.

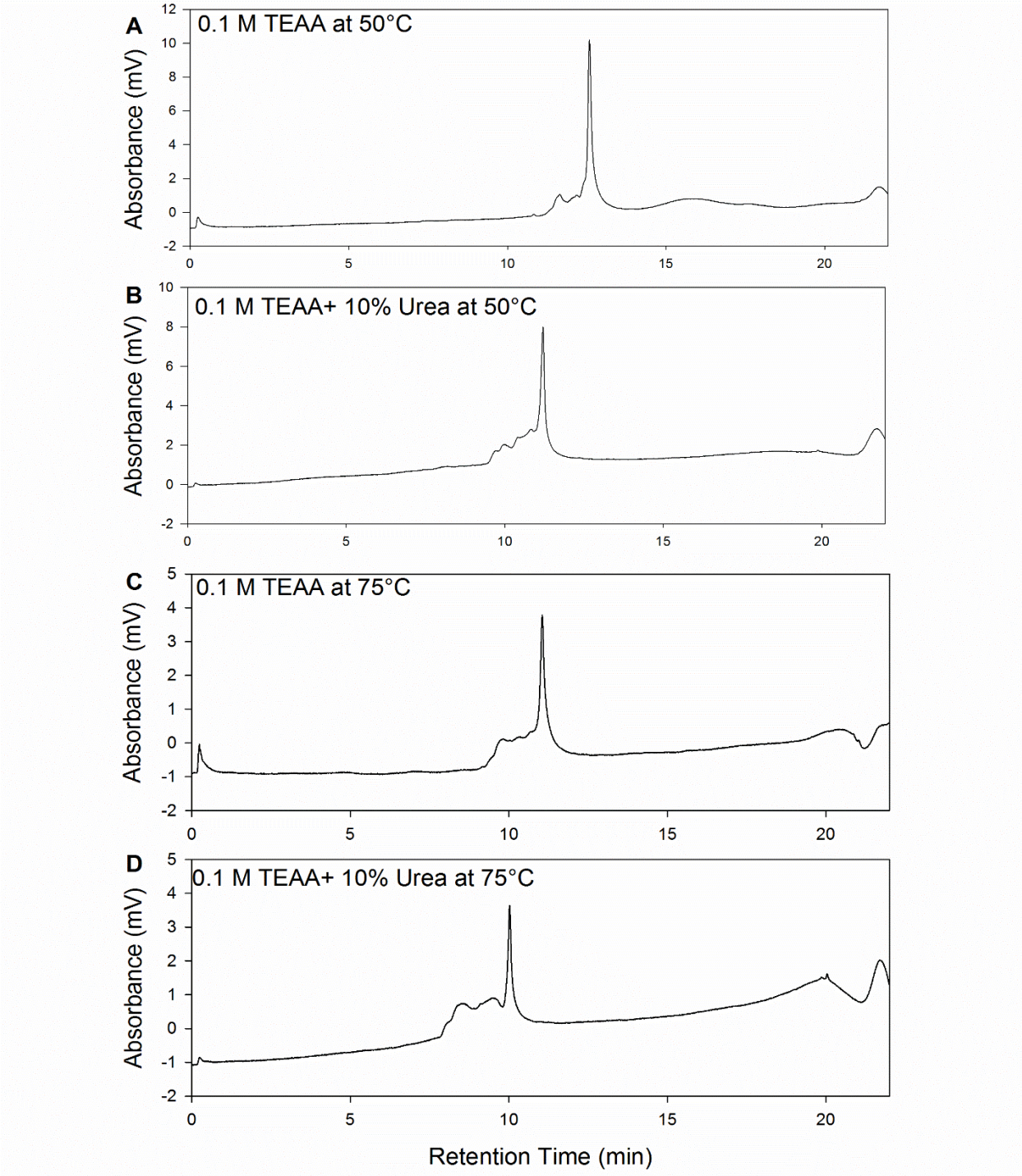

Figure V-11: The analysis of 20 mer oligonucleotides using standard TEAA buffer vs. 10% urea and TEAA under non-denaturing and denaturing temperature conditions by ProSwift RP-1S column. (A) 0.1M TEAA at 50°C (B) 0.1M TEAA and 10% urea at 50°C (C) 0.1M TEAA at 75°C (D) 0.1M TEAA and 10% urea at 75°C under IPRP HPLC using gradient condition 8 (see chapter 2.6.5).

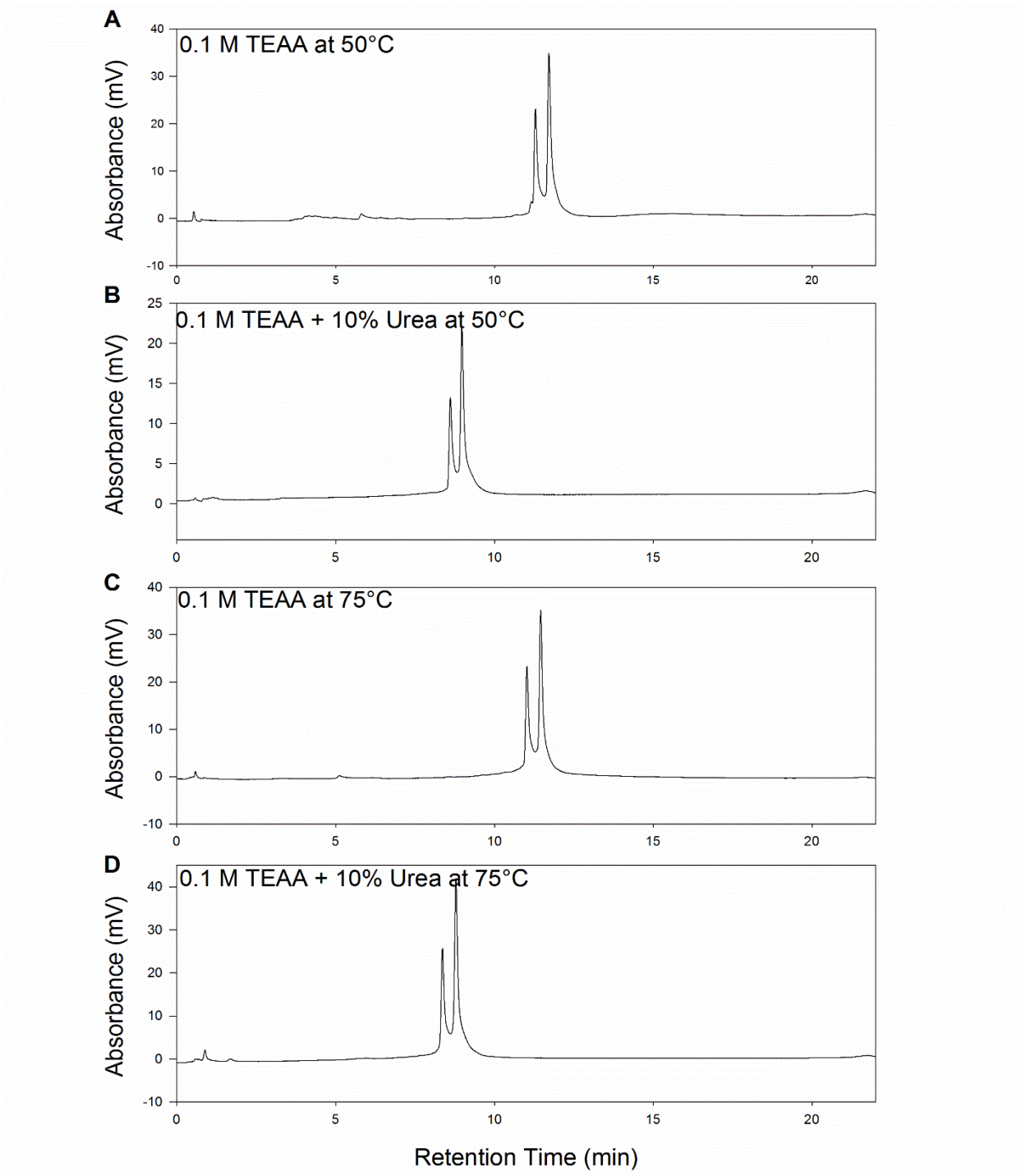

Figure V-12: The analysis of *E. coli* ribosomal RNA 16s and 23s using standard TEAA buffer vs. 10% urea and TEAA under non-denaturing and denaturing temperature conditions by ProSwift RP-1S column. (A) 0.1M TEAA at 50°C (B) 0.1M TEAA and 10% urea at 50°C (C) 0.1M TEAA at 75°C (D) 0.1M TEAA and 10% urea at 75°C under IP RP HPLC using gradient condition 6 (see chapter 2.6.5).

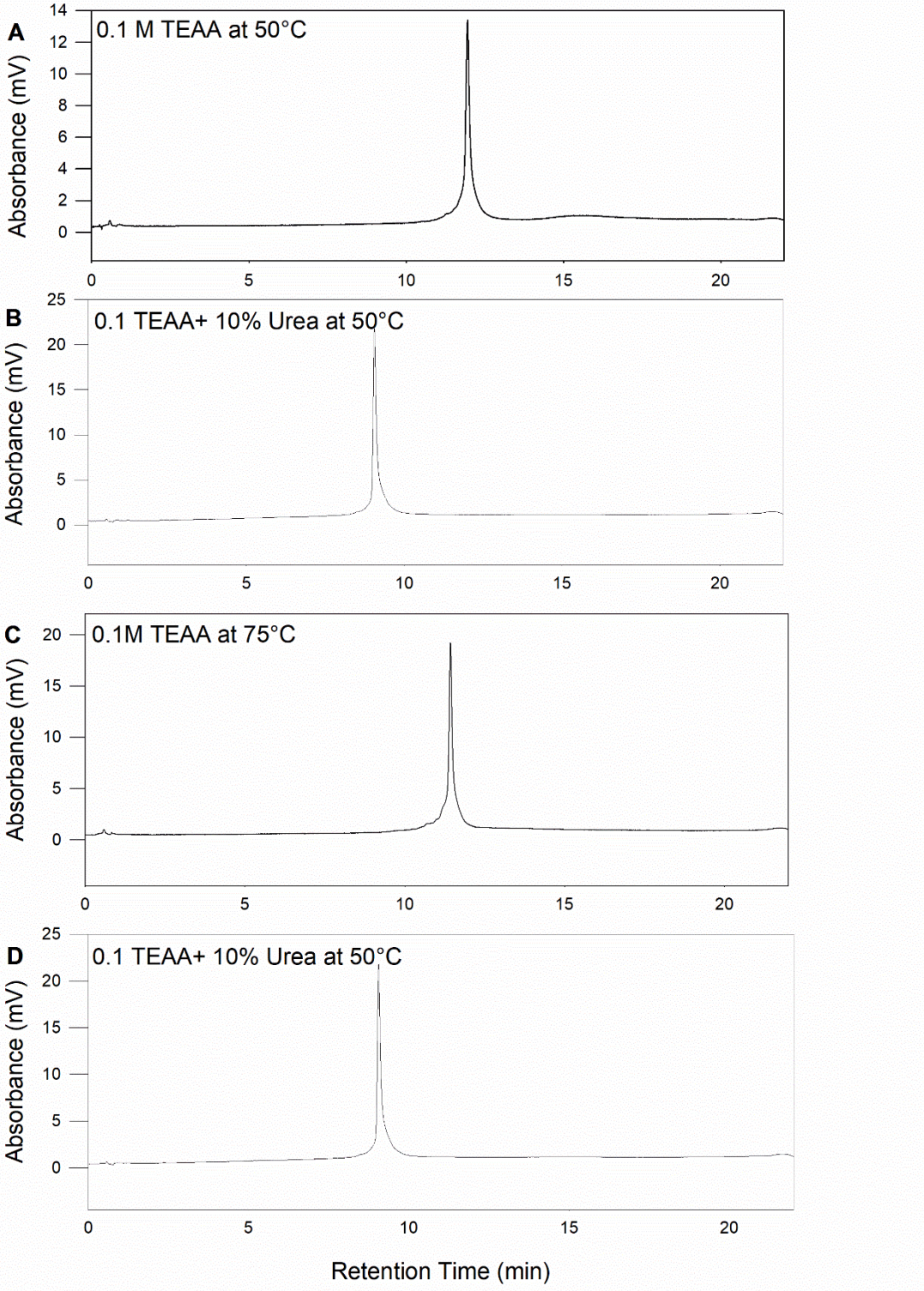

Figure V-13: The analysis of large bacteriophage MS2 RNA using standard TEAA buffer vs. 10% urea and TEAA under non-denaturing and denaturing temperature conditions by ProSwift RP-1S column. (A) 0.1M TEAA at 50°C (B) 0.1M TEAA and 10% urea at 50°C (C) 0.1M TEAA at 75°C (D) 0.1M TEAA and 10% urea at 75°C under IP RP HPLC using gradient condition 6 (see chapter 2.6.5).

Part B

5.3.4 Impact of gel porosity and the matrix of monolith columns

The performance of porous polymer monoliths for the analysis of macromolecules using IP RP HPLC under gradient elution mode was previously studied (see Chapter V part A). However, a lack of fundamental knowledge on gel porosity structure and the function of polymer monolithic media for the analysis of large biomolecules necessitates further investigation (Nischang, 2012). Recently, porous polymeric monolith properties have been studied by measuring the material in a dry state, providing a limited understanding of micro and macro-scale dynamics as well as mass transfer performance for biomolecules (Nischang and Brüggemann, 2010). During the cross-linking stage of the polymeric monolith material, significant gel porosity is formed within the large heterogeneous globular structure. The specific gel porosity is absent in the dry state in polymeric monolith but appears in the scaffold when in a solvated state. Transport phenomena of large molecules remain unknown, as gradient elution mode has restricted spaces which are intended for analyte mass transfer assessment (Nischang, 2012). Using the isocratic elution mode, polymeric monoliths have demonstrated poor performance, possibly due to the large flow through pore heterogeneity (Nischang, 2012). Using non-retained elution conditions, the pore-fluid gel surface area is non-adsorbing and as a consequence, pore structures can be rapidly detected (Trilisky et al., 2009). Characterising different pore size distribution (PSD) is important to understand and predict the behaviour of chromatographic performance.

The primary aim of this experiment was to study the impact of different pore structures of the selected polymeric monolith columns, investigate the presence of micro, meso, and macro-pores, and determine how different sized nucleic acid analytes travel in convective media. Secondary objectives included relating previous IP RP HPLC experimental observations, and performance of the ProSwift RP-1S, RP-2H, and RP-3U with a range of nucleic acids under non-retentive conditions.

The analysis was initially performed to study the effect of elution for a range of different sized nucleic acids under non-retentive isocratic chromatographic mode, using varying percentages of acetonitrile compositions in the mobile phase. The nucleic acids used

were: oligodeoxynucleotides starting from: 3 mer (MW: 806 g/mol), 6 mer (MW: 1763 g/mol), and 18 mer (MW: 5340 g/mol), as well as higher molecular weight MS2 RNA (MW: 1,090,064 g/ mol).

5.3.5 Impact of nucleic acid size and polymeric monolith porosity on elution time

To further study the effect of nucleic acid analytes on the elution performance of the monoliths, nucleic acid analytes of a wide range of sizes were compared under non-retentive isocratic conditions (50% acetonitrile at a flow rate of 1 mL/min) (see Figure V-14). In order to accurately determine the effect of different porosities on elution time in all the non-retentive analyses, it was necessary to compensate for deviations in column internal volume as a result of the column manufacturing process, despite equal dimensions for the RP-1S, RP-2H, and RP-3U columns. This was done through normalisation of the elution times based on the internal column volumes of each column. The normalisation factors and normalised elution times are shown in Table V-8.

Table V-8: Normalisation of elution times of different-sized nucleic acids based on internal column volume.

			Non-Normalisation elution time (min)				Normalisation elution time (min)			
Column	Column volume (mL)	Normalisation factor	MW 806 (g/mol)	MW 1763 (g/mol)	MW 5340 (g/mol)	MW 10,900, 64 (g/mol)	MW 806 (g/mol)	MW 1763 (g/mol)	MW 5340 (g/mol)	MW 10,900,64 (g/mol)
RP-1S	0.76	0.76	0.44	0.43	0.42	0.35	0.44	0.43	0.42	0.35
RP-2H	0.73	0.76/0.73=1.041	0.4	0.383	0.376	0.31	0.416	0.398	0.39	0.384
RP-3U	0.65	0.76/0.65=1.16	0.33	0.33	0.33	0.34	0.385	0.385	0.385	0.394

The results demonstrate that there is a clear relationship between the MW of single-stranded (ss) nucleic acids with elution time in the order: 3 mer>6mer>18 mer oligonucleotides> MS2 RNA for the RP-1S and RP-2H monoliths (Figure V-14). The largest MS nucleic acids had the lowest elution time under all conditions, due to their size, resulting in limited access to the porous structure. These results are consistent with previous data for the analysis of differently-sized protein biomolecules under non-retentive conditions (Nischang, 2014).

In contrast, elution times using the RP-3U column did not appear to show significant differences for all sizes of nucleic acids involved. Nischang (2014) varied protein size of analytes to determine the appearance of porosities on the RP-1S and RP-3U column but the results showed only small variation in apparent porosities exiting at the 50% acetonitrile solvation state. Under the same conditions, however, the RP-1S column demonstrated wide variation in apparent porosities (Nischang, 2014). The current experiment is in good agreement with Nischang's observations, where the size of nucleic acids influenced elution times on the RP-1S and RP-2H columns, indicating the presence of different porosities under non-retentive mode. However, this effect was not apparent on the RP-3U column.

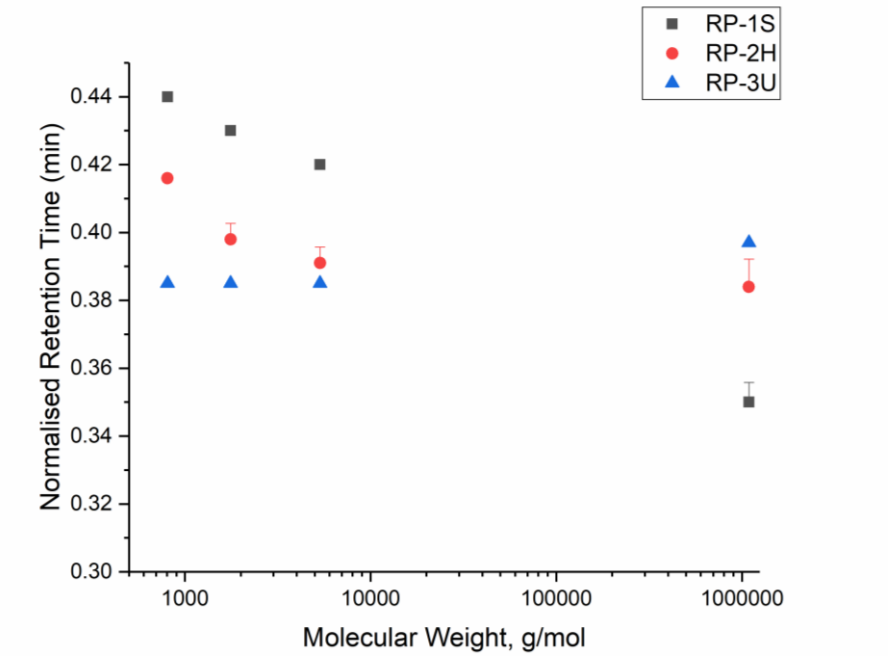

Figure V-14: Retention time against molecular weight of various sizes of nucleic acid analytes; analysis performed using polymeric monolith columns of different porosities. RP-1S (squares), RP-2H (circles), and RP-3U (triangles) under a selected flow rate of 1 mL/min with mobile phase solvent. obile phase consisted of

50/50 acetonitrile and water (v/v) using gradient condition 12 (See chapter 2.6.6). The error bars correspond to the standard deviation (N=3).

5.3.6 Impact of acetonitrile concentration on elution volume

Previous analysis suggested that swelling in porous polymer monolith was observed with increased concentration of acetonitrile. It has been proposed that when the amount of acetonitrile is more than 50% in the eluent, the pores start to close (Nischang, 2014). This phenomenon is expected since the gel porosity of a polymeric monolith can be enhanced through solvation and swelling as more free volume is generated in the polymer monolith (Nischang, 2013). In order to systematically evaluate the effect of a wide range of acetonitrile compositions against a series of nucleic acids on elution time, isocratic elution modes with 20%, 50%, and 80% of acetonitrile/water were tested with the monolith columns (Figure V-15). A general trend where a reduction in retention time is observed: as the percentage of acetonitrile is increased on the RP-1S and RP-2H columns, elution time decreases in the order of 20%>50%>80% acetonitrile.

The results show that changing to a higher percentage of acetonitrile had no significant effect on the elution of smaller-sized oligonucleotides (MW 806 g/mol). This observation appeared on both monolith RP-1S and RP-2H columns (Figure V-15 A and B) and is in good agreement with previous studies involving a wide range of sizes of peptides and proteins, where it was shown that permeation volume is less sensitive to smaller-sized analytes (Nischang, 2014). Interestingly, analytes of higher molecular weight (18 mer oligonucleotides (MW 5340 g/mol) and MS2 RNA (MW 10,900,64 g/mol) seem to be more sensitive to the increasing percentage of acetonitrile (80%), which leads to noticeable variation in elution porosity on the RP-1S column.

Moreover, the analysis on oligonucleotides using the RP-2H monolith column presented comparable trends, peak shapes and peak widths to the RP-1S column under non-retentive mode (Figure V-18 A-D). These results disagree with earlier studies on IP RP HPLC (Figure V-5 A and B), where a dispersion peak was observed on the RP-2H column for oligonucleotides analysis (Figure V-5 B). This conflict could be explained by the solvation state of the porous monolithic material. As swelling occurs during solvation, extra pore space facilitates rapid permeation and diffusion of

smaller molecules within the gel structure (Causon et al., 2012). In contrast to the ion paring elution mode where a lower percentage of acetonitrile is used (non-solvation), oligonucleotides adsorb to the highly permeable functional surface then proceed to move in and out of different pore spaces, before desorbing from the column slowly. The low mass transfer rates cause loss of efficiency. Thus, pore spaces have a considerable impact on the transport and chromatographic behaviour of polymeric monolith columns. It has also been hypothesised that the change in polymer monolith nano-scale gel porosity significantly influences the materials' physio-chemical properties, which is clear when analysing small molecules. In particular, the performance measured in the tests under isocratic elution mode strongly depends on the amount of gel porosity present in the polymer monolith (Nischang et al., 2011).

In contrast, the analysis of nucleic acid elution time on the RP-3U column did not significantly change with the percentage of acetonitrile (Figure V-15), suggesting that increasing ACN concentration does not further alter the gel porosity in the RP-3U column. Notably, nucleic acid analytes with different molecular weights differed negligibly in elution time e.g. the 3mer, 6 mer, and 18 mer oligonucleotides. In addition, for the analysis of large MW MS2 RNA, the elution time increased with increasing percentage of ACN within the range of 20 to 50%. This phenomenon is in agreement with data on the RP-1S column where the larger analyte is more sensitive to changes in ACN content on a polymeric monolith column. The RP-3U morphology shows larger globules and agglomerates of irregular sizes with interconnected pores compared to the RP-1S and RP-2H columns. The results indicate that large flow through channels or macropores are present in the RP-3U column in the solvated state since small-sized analytes experienced similar retentions times.

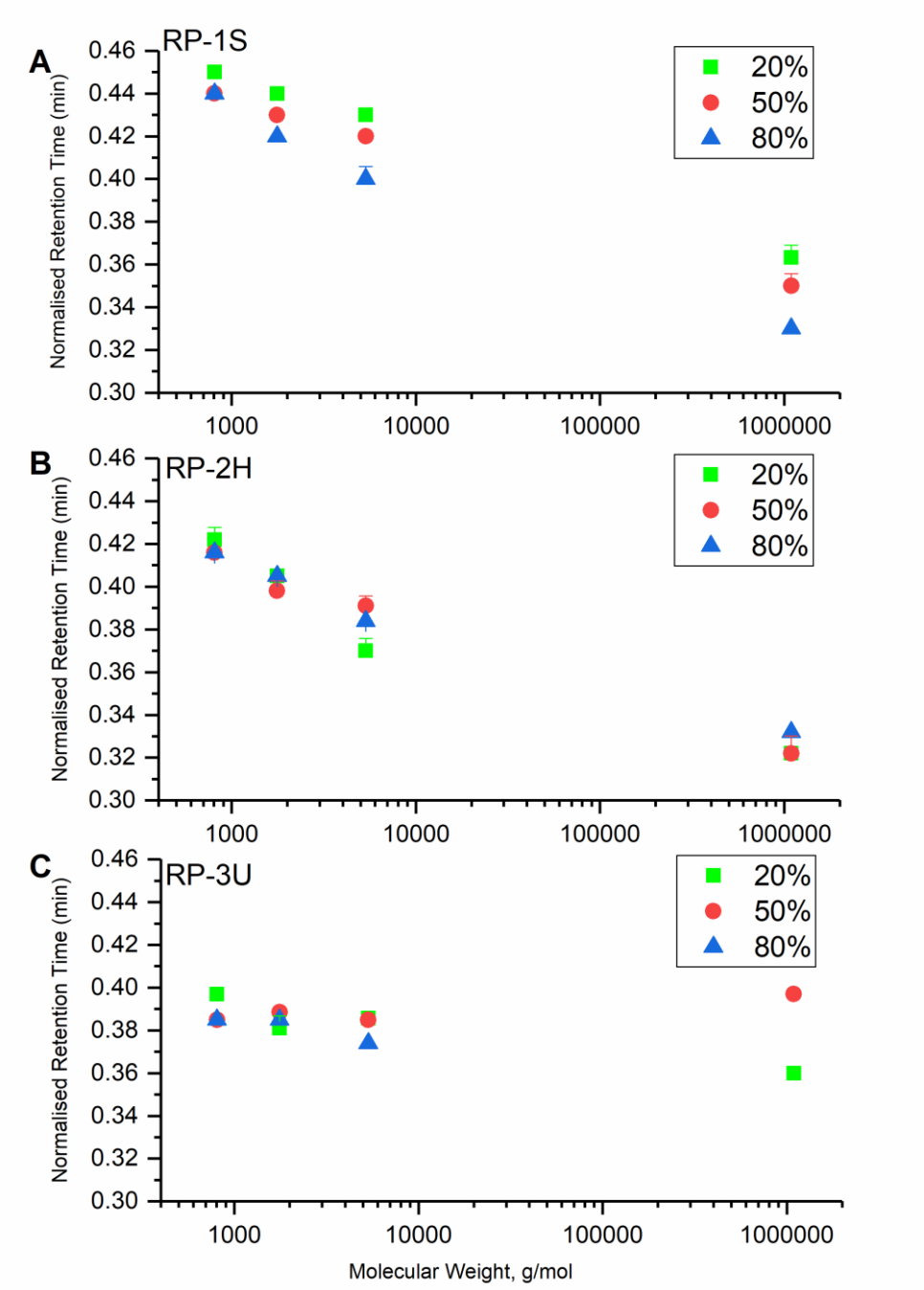

Figure V-15: The effect of molecular weight of different-sized nucleic acids under a binary acetonitrile and water (v/v) environment (20%, 50%, and 80%) on elution time using monolith ProSwift columns (A) RP-1S, (B) RP-2H, and (C) RP-3U. Flow rates were 1 mL/min using gradient condition 13-15 (see Chapter 2.6.6). The error bars correspond to the standard deviation (N=3).

5.3.7 Elution performance under non-retentive conditions at elevated flow rates

The effect of analyte size alongside retention time at various flow rates (0.75 mL/min, 1.0 mL/min, and 1.25 mL/min) were studied under 50% acetonitrile volume in the mobile phase (20% and 80% data are not shown) analysed on the RP-1S, RP-2H, and RP-3U columns (see Figure V-16). The elution time for nucleic acids of a range of MWs on the RP-1S and RP-2H columns show the expected decrease in elution time as MW increases across 3 different flow rates and is consistent with previous data (Figure V-14). In contrast, elution times for the RP-3U column were indistinguishable between all sizes of analytes and at the different flow rates, in agreement with previous data. In terms of individual elution performance under each column, it is evident that the range of analytes studied are more retentive in the finer pore sizes of the RP-1S column, followed by decreased elution times within the medium pore sizes of the RP-2H column, and finally significantly reduced elution volume in the larger pores of the RP-3U column. The ratios are consistent throughout the selected flow rates used in the experiment.

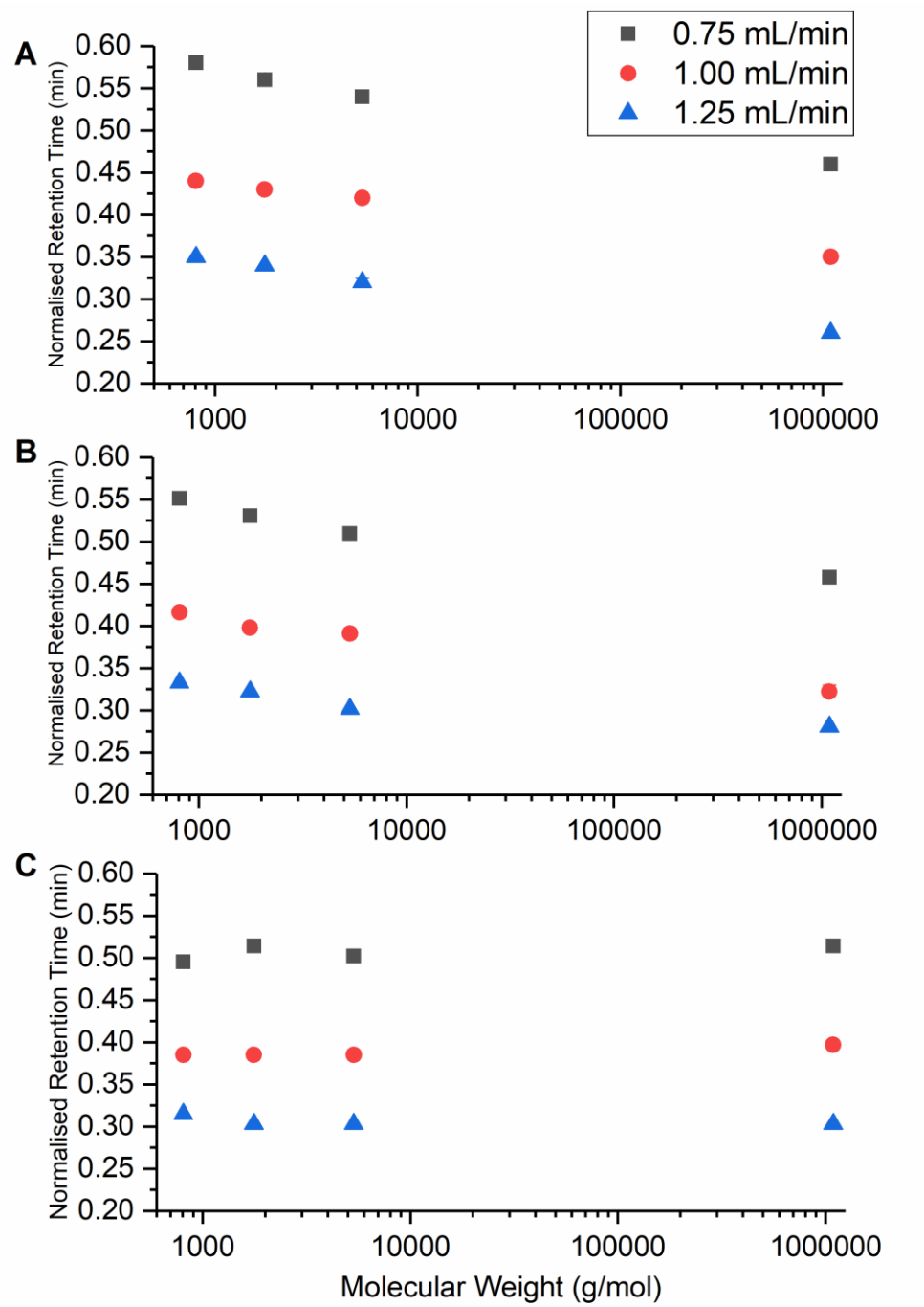

Figure V-16: Retention time versus molecular weight for different nucleic acids analytes with the ProSwift monolithic at flow rates 0.75,1.0, and 1.25 mL. (A) RP-1S, (B) RP- 2H and, (C) RP-3U columns. The mobile phase consisted 50:50 acetonitrile and water and was used with gradient condition 14 (see chapter 2.6.6). The error bars correspond to the standard deviation (N=3).

5.3.8 Effects of analyte concentration on retention time using porous polymeric monolith columns under non-retentive conditions

To further characterise the structural properties of porous polymeric monolithic columns, an experiment was performed with the objective of investigating the effect of analyte concentration versus elution time under non-retentive conditions. Oligonucleotides of lengths 6 mer and 18 mer, as well as large MS2 RNA (used as a standard to compare elution across the columns), were used at concentrations of 500 pmol, 50 pmol, and 5 pmol. Samples were injected with 20%, 50%, and 80% acetonitrile (different solvation state) at flow rates of 1 mL/min^{-1}. As suggested by Trilisky et al., (2009), under solvation state the gel porosity of polymeric monoliths swell, allowing rapid determination of various gel porosities at low elution times.

The results are summarised in Figure V-17 A-C and the specific chromatograms obtained are shown in Figure V-18 A-D. Standard deviations were calculated to measure experimental error, with less than 0.005 of error in the data reported. It can be seen that in the case of 6 mer and 18 mer oligonucleotides, a decrease in analyte concentration reduces elution times (Figure V-18 A-D). This phenomenon is surprising since under non-retentive conditions the mobile phase system is operating in a highly organic environment and thus, adsorption is absent at the monolithic surface. Therefore, any overloading on the stationary phases should not have a direct effect on elution time under such conditions. This finding provides potential evidence for the existence of different gel porosity paths, by showing that higher concentrations of oligonucleotides take longer to travel through pores. Compared to a higher concentration, a low concentration of oligonucleotides of the same size has less overall mass, and can more easily travel through shorter paths, resulting in shorter elution times. In contrast, the results for the RP-3U column show no significant differences in elution time with the analyte concentrations. For example, 6 mer oligonucleotides of 5, 50 and 500 pmol had nearly identical elution times of 0.37, 0.39, and 0.40 minutes respectively (Figure V-18 E).

Altering the percentage of acetonitrile in the mobile phase (i.e. higher ACN content), resulted in a more significant decrease in elution time for the range of analytes observed in the RP-1S column (Figure V-15). This result is consistent with Nischang's findings (2014a) who characterised analytical polymer monoliths using different

percentages of ACN and proteins of a wide range of sizes to investigate apparent elution porosity using the RP-1S column.

In addition, looking at the effect of acetonitrile in the mobile phase to analyse 50 pmol of 18 mer oligonucleotides, different elution times were observed at different concentrations (20-80%) of acetonitrile on the RP-1S column; When using 5 pmol instead at 80% of acetonitrile, a significant decrease in elution time occurred (see Figure V-15 and Figure V-17). Moreover, altering the percentage of ACN on the analysis of 18 mer oligonucleotides using the RP-2H column indicated an apparent variation in elution porosity which was determined by the difference in elution times (Figure V-15 B).

Varying analyte size, analyte concentration, and acetonitrile concentration had insignificant impacts using the RP-3U column (except for the MS2 RNA). This is evident from the trend in Figure V-15 C, which remained flat (signifying similar elution times) for all sizes of analyte despite varying acetonitrile compositions.

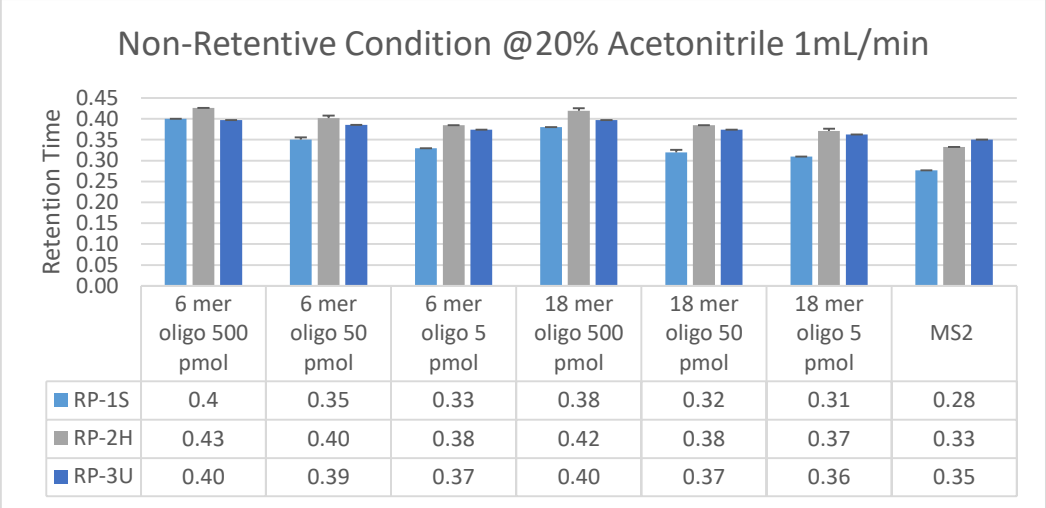

	6 mer oligo 500 pmol	6 mer oligo 50 pmol	6 mer oligo 5 pmol	18 mer oligo 500 pmol	18 mer oligo 50 pmol	18 mer oligo 5 pmol	MS2
RP-1S	0.4	0.35	0.33	0.38	0.32	0.31	0.28
RP-2H	0.43	0.40	0.38	0.42	0.38	0.37	0.33
RP-3U	0.40	0.39	0.37	0.40	0.37	0.36	0.35

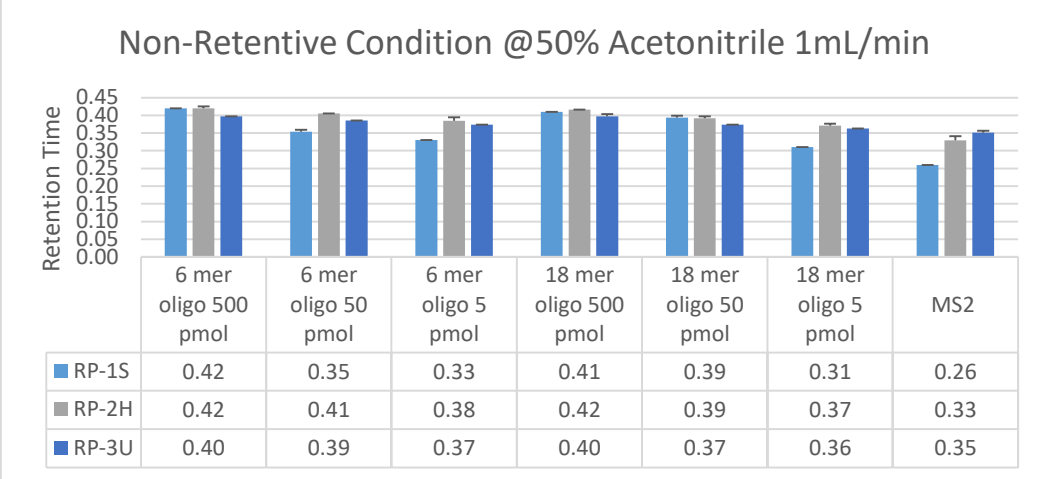

	6 mer oligo 500 pmol	6 mer oligo 50 pmol	6 mer oligo 5 pmol	18 mer oligo 500 pmol	18 mer oligo 50 pmol	18 mer oligo 5 pmol	MS2
RP-1S	0.42	0.35	0.33	0.41	0.39	0.31	0.26
RP-2H	0.42	0.41	0.38	0.42	0.39	0.37	0.33
RP-3U	0.40	0.39	0.37	0.40	0.37	0.36	0.35

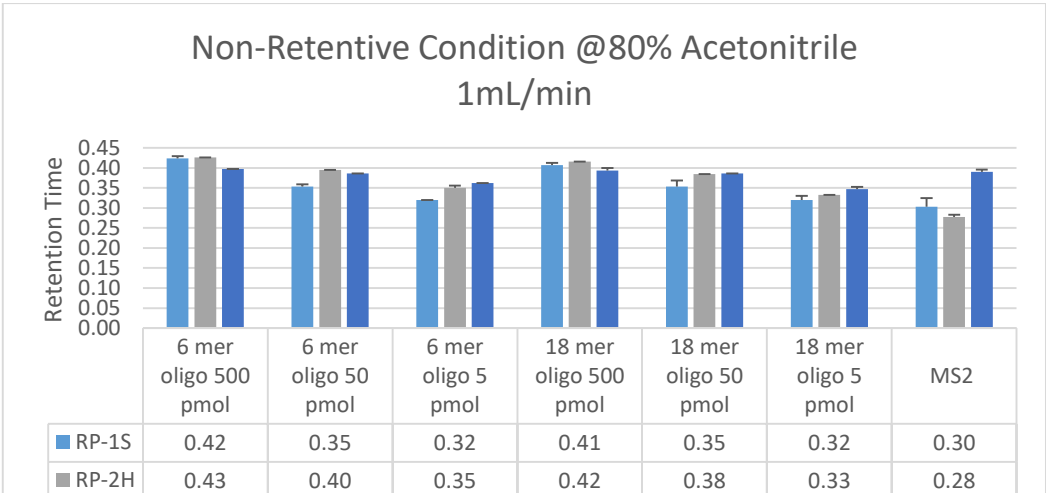

	6 mer oligo 500 pmol	6 mer oligo 50 pmol	6 mer oligo 5 pmol	18 mer oligo 500 pmol	18 mer oligo 50 pmol	18 mer oligo 5 pmol	MS2
RP-1S	0.42	0.35	0.32	0.41	0.35	0.32	0.30
RP-2H	0.43	0.40	0.35	0.42	0.38	0.33	0.28
RP-3U	0.40	0.39	0.36	0.39	0.39	0.35	0.39

Figure V-17: Normalised elution times for different-sized biomolecules analysed using monolith columns RP-1S, RP-2H, and RP-3U under non-retentive conditions (20-80% acetonitrile) (see chapter 2.6.6). The error bars correspond to the standard deviation (N=3).

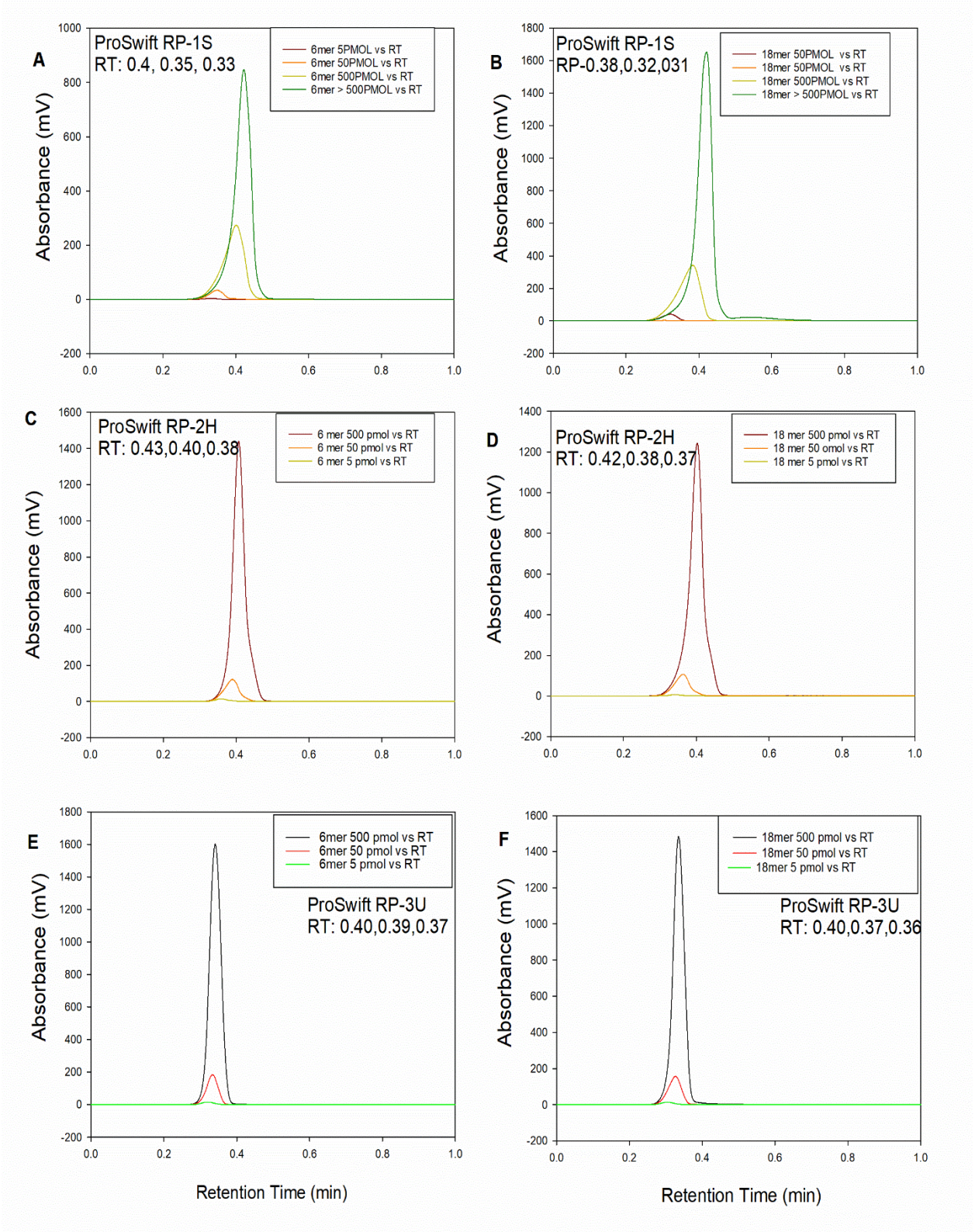

Figure V-18: Comparative analysis of the impact of different sized oligonucleotides at various concentrations on normalised elution times using monolith columns. ProSwift RP-1S, RP-2H, and RP-3U columns and 20% acetonitrile under non-retentive condition using gradient condition 13 (see chapter 2.6.6).

5.4 Conclusions

Three monolithic columns with different pore size distributions were used in conjunction with ion-pair reversed-phase high-performance chromatography (IP RP HPLC) to analyse nucleic acids ranging from small DNA oligonucleotides to large dsDNA fragments and large ssRNA. The results from using identical gradients demonstrated that the relative retention times of the oligonucleotides, rRNA and MS2 RNA, were similar, reflecting the small differences in column volumes across the different monoliths. In contrast, the analysis on the larger dsDNA fragments revealed increased retention times on the RP-3U column and is possibly due to a difference in permeability of these large duplex DNA fragments compared to the other nucleic acids.

The ProSwift RP-1S column with the standard pore size produced an optimal performance for the analysis of a wide range nucleic acids, including DNA oligonucleotides, dsDNA fragments, and ssRNA samples. In contrast, the RP-2H column displayed a much lower resolution for the analysis of oligonucleotides compared to the RP-1S column but showed a comparable performance for the larger MW nucleic acids. These results demonstrate that potentially low diffusion rates of small oligonucleotides may cause significantly low resolution. The porosity of the RP-2H column is one magnitude greater compared to that of RP-1S, yet their performance in terms of peak shape and peak resolution was relatively similar, except when analysing oligonucleotides. Analysis on the RP-3U column demonstrated that it was optimal for the analysis of oligonucleotides, probably due to its much larger pores. In general, the results from the analysis of nucleic acids show that for most nucleic acids except for small oligonucleotides, reducing the practical porosity produces better peak resolutions while increasing the porosity results in peak broadening. The better performance of the RP-1S column could be related to its structural homogeneity, in contrast to the larger, more homogeneous pore structure (consisting of macropores) of the RP-3U column.

Further analysis of the different monoliths was performed under non-retentive conditions to study the effects of polymeric monolith porosity on elution time of a range of different nucleic acids. The results show that under non-retentive chromatographic conditions, the different pore conformations present in the polymeric monolith scaffold on both RP-1S and RP-2H columns affect the elution time of the nucleic acids, with a

general trend of reduced retention time as the MW of the nucleic acid increase. In contrast, on the RP-3U column, no significant effect of MW on retention time was observed, demonstrating that the RP-3U column lacks the different types of pores required for accessibility by the range of nucleic acids.

These results further suggest the existence of macropores on the RP-3U column. The finer porous structure on the RP-1S column clearly demonstrates better efficiency compared to the RP-2H and RP-3U columns, which may be associated with the structural homogeneity in the solvated state of the RP-1S column. Accordingly, the RP-2H column illustrates a structure moderately balanced between the homogeneity and heterogeneity, whereas the RP-3U column has the most pronounced heterogeneous structure. Even though the stationary phases used in this study consist of the same fundamental material, their distinct morphological properties alter the availability of stationary phase surface area, directly affecting their capability and performance. In the current study, we showed the significance of sorbent pore size for a range of nucleic acid applications using retentive and non-retentive HPLC analysis.

Chapter VI : Final discussion and future work

The overall aim of this thesis was to develop analytical methods focused on ion-pair reversed-phase chromatography and mass spectrometry for the analysis of nucleic acids. This chapter is subdivided into three sections and covers the improvements and limitations of the developed techniques, possible applications, as well as the scope for future experiments.

6.1 Optimisation of electrospray-ionisation mass spectrometry for the analysis of oligonucleotides

The difficulty in balancing the need for high resolution and adequate MS sensitivity is one of the main limitations in unleashing the full potential of LC-ESI-MS in oligonucleotide analysis. Other issues, such as the formation of RNA-metal ion adducts and performance issues with larger oligonucleotides are also significant (Huber and Krajete, 1999). The physiochemical properties of a mobile phase are understood to have a significant impact on the electrospray desorption efficacy of oligonucleotides. Chapter III aimed to study the roles of these properties in the desorption process of the oligonucleotides through experiments using various alkylamine ion-paring reagents.

Several relevant factors were found to significantly influence the performance of an ESI-MS system including boiling point, water solubility, Henry's law constant (k_H,cc (aq/gas)), organic modifier use, pH value of the system, and the hydrophobicity content of the oligonucleotides. The optimal buffer system was found to consist of 5 mM TBA and 80 mM HFIP, demonstrated the highest ion abundance and minimal cation adduction and, responded efficiently with increasing the concentration of HFIP. This result was inferred to be the effect of TBA's low k_H,cc (aq/gas) value, which led to highly efficient ionisation of oligonucleotides. The k_H,cc (aq/gas) value was also found to have an effect on charge state distribution: higher values (e.g. in HA) led to lower charge state distributions while lower values (e.g. TBA) led to higher charge state distributions. Additionally, the IP hydrophobicity also had a significant effect on ESI-MS sensitivity, in agreement with McGinnis et al., (2013). The increased IP

hydrophobicity leads to the reduction of surface tension in ESI droplets, providing greater sensitivity for the ESI-MS system (Oberacher, Oefner, et al., 2001). These results and the knowledge of how the relevant parameters affect ESI-MS performance allows for a more systematic approach to future evaluations. For example, tripropylamine (TPA), and dimethylbutylamine are hypothetically better ion-pairing reagents than TEA due to their higher hydrophobicity. Further experiments could focus on systematically evaluating and combining the ion-pairing reagents TPA and DMBA with different organic modifiers such as HFIP and TFE for the comparative analysis of different sequence oligonucleotides. The optimal ion-pairing reagent for each oligonucleotide should be considered on a case-by-case basis, as the choice is dependent on the sequence of oligonucleotide under investigation each time, as suggested by Basiri et al., (2017). Finally, the optimal ESI-MS mobile phase could be paired with an on-line LC separation system to investigate the compatibility between both instruments.

In addition, it should be noted that significant standard deviation was observed for the datasets in experiment section 3.3.1, which can be explained by instrument drift resulting from the running of replicate samples on different days. Issues with data variability are quite common in ESI-MS signal intensity studies, and have been reported by Basiri et al., (2017). There are several ways that the experiments performed could be improved in future studies; one would be using an oligonucleotide and a buffer as a reference and compare other buffer combinations with the same oligonucleotides to report the ratio of MS signal intensities as suggested by Basiri et al., (2017), who found that it resulted in much better reproducibility of results with minimal variability between the experiments.

One possible application of the results of this experiment is the generation of a predictive model to identify a subset effective mobile phases. Basiri et al., (2017) have already created a model which predicts the performance of IP reagents from their experiments. Such a model may be expanded to include a wider class of nucleic acids and IP reagents while accounting for the parameters which were found to be important. Initially, the available IP reagents could be sorted according to their suitability to the sequence or type of analyte. They can then be paired with an appropriate organic modifier to produce effective mobile phase combination according to their specific

physiochemical properties. Results from future work should be stored in a database to improve the model. Thus, by combining the results of these experiments with a predictive model it is possible to benefit researchers in this field, through improved efficiency and reduced processing times.

6.2 Purification and quantification of dsRNA extracted from microbial cells

RNA interference has received significant interest from the biopharmaceutical industries for its application to study various biological systems including the ability to analyse specific gene functions. The specificity of RNAi is a highly attractive feature in drug development and a wide range biotherapeutics, including antisense oligonucleotides and siRNAs, are emerging to treat a variety of important diseases. Meanwhile, researchers in agriculture are discovering ways to use novel RNAi-based methods to prevent disease in beneficial insects as well as for insect management by acting as an alternative to chemical insecticides. The potential for RNAi applications has led to a huge increase in demand for RNA-related products such as dsRNA. However, technologies with the capacity to synthesize large quantities of dsRNA by in-vitro transcription or in bacterial systems are stifled by the lack of efficient and high-throughput systems capable of rapid extraction, purification, and analysis of dsRNA. Chapter IV presented a study on various RNA extraction methods to extract high yields of dsRNA engineered from *E. coli* cells in conjunction with stable isotope labelling for the quantitative analysis of dsRNA using LC-ESI-MS.

A variety of guanidine isothiocyanate-phenoL/chloroform based extraction methods were utilised to compare dsRNA extraction quantities and qualities. A high yield of dsRNA extraction was achieved in a rapid manner using the DNAzol method without performing complicated steps and the use of phenol-chloroform for phase separation. Although DNAzol obtained the maximum yield of dsRNA compared to the other methods used in this experiment, a number of major drawbacks were found in other extraction methods such as: complicated, labour-intensive, and time-consuming procedures which may lead to degradation of RNA; procedures requiring the use of hazardous chemicals; relatively low yields of dsRNA despite large quantities of total RNA extracted; and compatibility issues between extracted RNA and downstream analysis. The discovery of an efficient nucleic acid extraction method such as that

presented in this thesis is a crucial development step and could potentially benefit molecular biology as well as provide the required materials for downstream production and disease diagnostics.

Using a modified protocol DNAzol, (a DNA extraction reagent) resulted in efficient dsRNA extraction. In addition, it was demonstrated that modifying the TRIzol method by using phenol at neutral pH also increased the extraction yield of dsRNA compared to traditional phenol based RNA extractions at acidic pH.

The finding that dsRNA can be extracted using neutral pH solutions greatly expands the pool of possible solutions available for dsRNA extraction, removing the restriction to only acidic solutions, and allowing the use of neutral pH solutions. The lifting of this restriction increases the chance of finding dsRNA extraction methods with improved performance in yield, quality, and processing time. However, future extraction development should manage the possibility of contaminating genomic DNA is present in the extracted dsRNA sample at neutral pH by considering further solid phase extraction or DNase treatment steps, which can efficiently remove the contamination.

In addition to RNA extraction, stable isotope labelling approaches were also employed in conjunction with mass spectrometry for the absolute quantification of dsRNA. Stable isotope labelling approach by *in vivo* and *in vitro* labelling of dsRNA in conjunction with mass spectrometry were successfully demonstrated for the characterisation and quantification of dsRNA in complex total RNA mixtures. Rapid characterisation was achieved via the discrimination between light and heavy isotope oligonucleotide fragments. The isotope labelling approach allowed the development of a procedure for the absolute quantification of dsRNA when a known amount of reference dsRNA is spiked into an unknown amount of sample followed by the analysis of various peak ratios of the selected oligonucleotides.

This method overcomes the drawbacks present in conventional methods used in quantitative analysis such as UV spectrophotometry and HPLC, which requires prior purification of the dsRNA and are unable to quantify dsRNA in complex mixtures. Stable isotope labelling has added the benefit of not altering any biophysical or biochemical properties of the oligonucleotide sample.

6.3 Effects of monolith porosity on the analysis of nucleic acids using ion-pair reversed-phase HPLC

A wide range of monolithic reversed-phase columns has been designed with various chemical and physical properties for different analytical purposes. Differences in column properties such as pore size distribution and pore structure can lead to significant differences in chromatographic performance. To understand these effects, chapter V reports on the performance of polymeric monolith columns of different pore size distribution (PSD), i.e. ProSwift RP-1S (standard PSD), RP-2H (high PSD), and RP-3U (ultra-high PSD) on the analysis of nucleic acids centred on the retentive and non-retentive HPLC modes. Using polymeric monolith columns with IP RP HPLC, it was possible to separate nucleic acids of a wide-range of sizes (from small oligonucleotides to large DNA fragments as well as RNA) with high resolution. For nucleic acids with larger molecular weights, higher resolutions were achieved in the descending order RP-1S>RP-2H>RP-3U, suggesting that lower porosity may be better suited for the analysis of nucleic acids. On the other hand, a higher porosity demonstrated high-resolution separations of small oligonucleotides. In terms of scale, although the porosity of the RP-2H column is only one magnitude greater than the RP-1S column, a significantly lower resolution of oligonucleotides was observed. The results demonstrated that using identical gradients, the relative retention time of oligonucleotides and ssRNA was similar, reflecting the small differences in column volumes across the different monoliths. Interestingly, the results revealed that larger dsDNA fragments showed an increased retention time on the RP-3U column highlighting possible different permeability of these large duplex DNA fragments compared to the other nucleic acids.

Finally, under non-retentive mode the elution times on the RP-1S and RP-2H columns were significantly affected by the nucleic acid size and analyte concentrations, while the RP-3U column did not display similar characteristics. The understanding of the effect of column porosity developed from these experiments may be beneficial in further studies on column behaviour as well as column design. A potential application is that column manufacturers can design more suitable columns by basing it on parameters such as the size of the analyte being studied and choosing an appropriate porosity.

In summary, these results might be attributed to structural homogeneity, as a better separation performance was observed on the RP-1S column in contrast to the RP-3U column, which has a larger and more homogenous pore structure (mesopore). In addition, the results observed under non-retentive chromatographic mode reveal the different pore conformations (which experienced different elution times for a wide range of analyte sizes) present in the polymeric monolith scaffold of the three columns. This hypothesis is consistent with previous work on the analysis of a range of biomolecules using the RP-1S and RP-3U columns (Nischang, 2014). In summary, these results have provided further insight into the characteristics and behaviour of monolithic reversed-phase columns for the analysis of nucleic acids. The results demonstrate the impacts of nucleic acid size, retention, and mobile phase composition on the performance of porous polymer monoliths while highlighting their unique inherent column characteristics.

Further experiments may provide further insight into the different monoliths by further studying flow velocity and plate height as additional variables in a similar approach as Nischang (2014) who previously characterised polymeric monolith columns by using different sizes of proteins to determine their plate height curves under non-retentive conditions. These results suggest that flow velocity and molecular weight of the analyte have a significant impact on column performance. It is proposed that further analysis evaluating column performance should be carried out by measuring the height equivalent to a theoretical plate value against various combinations of nucleic acids and flow rates under a non-retentive mode.

6.4 Final remarks

This thesis presented several analytical methods centred on ion-pair reversed-phase chromatography and mass spectrometry, which have been developed to facilitate high-throughput analysis of nucleic acids demanded by the bio-therapeutic and agritech markets. Impurities from the oligonucleotide synthesis process can often be present together with the target oligonucleotides and may lead to negative effects. A mobile phase optimised for oligonucleotide characterisation was determined based on several key parameters such as hydrophobicity and the Henry's Law constant of the alkylamine reagents. The results provide key insight into how such parameters affect

analytical performance and may help oligonucleotide producers choose mobile phases optimised to their needs at product characterisation stage. The modification of an existing DNA extraction method to enable the extraction of dsRNA through the use of neutral pH solutions at high yields was successfully demonstrated. Stable isotope labelling was also developed and utilised for the accurate quantification of dsRNA. Together these tools can further provide siRNA oligonucleotide therapeutic manufacturers and the agritech industry with improved methods for the purification and characterisation of nucleic acid products to be part of highly efficient (bio) manufacturing processes. High-resolution nucleic acid separations were achieved using a range of different monoliths. Moreover, a comparative analysis of monolith column porosities delivered a better understanding of the interplay between porosity and analyte size and their relation to HPLC performance. Both column manufacturers and their customers stand to benefit by applying this knowledge to choose better-suited columns based on the analyte type. There may also be potential new opportunities using alternative monolith column porosities apart from those studied here. Overall, the main industries that utilise RNA-pharmaceutical companies performing drug development for antisense and other therapeutic oligonucleotides, agricultural companies researching next-generation RNAi insecticides, and other biotechnology sectors can use the insights and methods from this research to significantly improve multiple aspects of their analytical operations.

References

Aalto, A. P., Sarin, L. P., Van Dijk, A. A., Saarma, M., Poranen, M. M., Arumae, U., et al. (2007). Large-Scale Production of dsRNA and siRNA Pools for RNA Interference Utilizing Bacteriophage 6 RNA-Dependent RNA Polymerase. *RNA*, 13(3), 422–429.

Alberts, B., Bray, D., Lewis, J., Raff, M., Roberts, K. & Watson, J. D. (1989). *Molecular Biology of the Cell*. GARLAND PUBLISHING INC.

Alberts, B., Johnson, A., Lewis, J., Raff, M., Roberts, K. & Walter, P. (2002). *Molecular Biology of the Cell*. New York: Garland Science.

Altman, S. & Stark, B. C. (1974). Separation of E. Coli tRNA-Tyr Precursor RNA from E. Coli tRNA by Hydroxyapatite Chromatography. *Analytical biochemistry*, 59(2), 547–54.

Amado, R. G., Mitsuyasu, R. T., Rosenblatt, J. D., Ngok, F. K., Bakker, A., Cole, S., et al. (2004). Anti-Human Immunodeficiency Virus Hematopoietic Progenitor Cell-Delivered Ribozyme in a Phase I Study: Myeloid and Lymphoid Reconstitution in Human Immunodeficiency Virus Type-1-Infected Patients. *Human gene therapy*, 15(3), 251–62.

Amarnath, V. & Broom, A. D. (1977). Chemical Synthesis of Oligonucleotides. *Chemical Reviews*, 77(2), 183–217.

Apffel, A., Chakel, J. A., Fischer, S., Lichtenwalter, K. & Hancock, W. S. (1997). Analysis of Oligonucleotides by HPLC-Electrospray Ionization Mass Spectrometry. *Analytical chemistry*, 69(7), 1320–5.

Avison, M. . (2008). *Measuring Gene Expression*. Abingdon, UK: Taylor & Francis.

Bailey, J. M. & Davidson, N. (1976). Methylmercury as a Reversible Denaturing Agent for Agarose Gel Electrophoresis. *Analytical biochemistry*, 70(1), 75–85.

Banerjee, S. & Mazumdar, S. (2012). Electrospray Ionization Mass Spectrometry: A Technique to Access the Information beyond the Molecular Weight of the Analyte. *International Journal of Analytical Chemistry*, 2012, 1–40.

Basiri, B. & Bartlett, M. G. (2014). LC–MS of Oligonucleotides: Applications in

Biomedical Research. *Bioanalysis*, 6(11), 1525–1542.

Basiri, B., Murph, M. M. & Bartlett, M. G. (2017). Assessing the Interplay between the Physicochemical Parameters of Ion-Pairing Reagents and the Analyte Sequence on the Electrospray Desorption Process for Oligonucleotides. *Journal of the American Society for Mass Spectrometry*, 28(8), 1647–1656.

Baum, J. A., Bogaert, T., Clinton, W., Heck, G. R., Feldmann, P., Ilagan, O., et al. (2007). Control of Coleopteran Insect Pests through RNA Interference. *Nature biotechnology*, 25(11), 1322–6.

Beaucage, S. L. & Caruthers, M. H. (1981). Deoxynucleoside phosphoramidites—A New Class of Key Intermediates for Deoxypolynucleotide Synthesis. *Tetrahedron Letters*, 22(20), 1859–1862.

Bennion, B. J. & Daggett, V. (2003). The Molecular Basis for the Chemical Denaturation of Proteins by Urea. , 2003 (Track II).

Berhane, B. T. & Limbach, P. A. (2003). Stable Isotope Labeling for Matrix-Assisted Laser Desorption/ionization Mass Spectrometry and Post-Source Decay Analysis of Ribonucleic Acids. *Journal of mass spectrometry : JMS*, 38(8), 872–8.

Bernstein, E., Caudy, A. A., Hammond, S. M. & Hannon, G. J. (2001). Role for a Bidentate Ribonuclease in the Initiation Step of RNA Interference. *Nature*, 409(6818), 363–6.

Bidlingmeyer, A. W. (1980). Separation of Ionic Compounds by Reversed-Phase Liquid Chromatography An Update of Ion-Pairing Techniques. *Journal of Chromatographic Science*, 18(10), 525–539.

Bidlingmeyer, B. A., Deming, S. N., Price, W. P., Sachok, B. & Petrusek, M. (1979). Retention Mechamism for Reversed-Phase Ion-Pair Liquid Chromatography. *Journal of Chromatography A*, 186, 419–434.

Bleicher, K. & Bayer, E. (1994). Analysis of Oligonucleotides Using Coupled High Performance Liquid Chromatography-Electrospray Mass Spectrometry. *Chromatographia*, 39(7–8), 405–408.

Boom, R., Sol, C. J. A., Salimans, M. M. M., Jansen, Wertheim-van Dillen, P, M. E. & Noordaa, J. Van Der. (1990). Rapid and Simple Method for Purification of Nucleic

Acids. *Americam Society for microbiology*, 28(3), 495–503.

Brenner, S., Barnett, L., Katz, E. R. & Crick, F. H. C. (1967). UGA: A Third Nonsense Triplet in the Genetic Code. *Nature*, 213(5075), 449–450.

Brenner, S., Jacob, F. & Meselson, M. (1961). An Unstable Intermediate Carrying Information from Genes to Ribosomes for Protein Synthesis. *Nature*, 190(4776), 576–581.

Brenner, S., Stretton, A. O. W. & Kaplan, S. (1965). Genetic Code: The 'Nonsense' Triplets for Chain Termination and Their Suppression. *Nature*, 206(4988), 994–998.

Burnett, J. & Rossi, J. (2012). RNA-Based Therapeutics: Current Progress and Future Prospects. *Chemistry & biology*, 19(1), 60–71.

Cabrera, K., Lubda, D., Eggenweiler, H.-M., Minakuchi, H. & Nakanishi, K. (2000). A New Monolithic-Type HPLC Column For Fast Separations. *Journal of separation science*, 23(1), 93–99.

Causon, T. J., Hilder, E. F. & Nischang, I. (2012). Impact of Mobile Phase Composition on the Performance of Porous Polymeric Monoliths in the Elution of Small Molecules. *Journal of Chromatography A*, 1263, 108–112.

Cech, N. B. & Enke, C. G. (2001). Practical Implications of Some Recent Studies in Electrospray Ionization Fundamentals. *Mass spectrometry reviews*, 20(6), 362–87.

Chen, B. & Bartlett, M. G. (2013). Evaluation of Mobile Phase Composition for Enhancing Sensitivity of Targeted Quantification of Oligonucleotides Using Ultra-High Performance Liquid Chromatography and Mass Spectrometry: Application to Phosphorothioate Deoxyribonucleic Acid. *Journal of Chromatography A*, 1288, 73–81.

Chen, B., Mason, S. F. & Bartlett, M. G. (2013). The Effect of Organic Modifiers on Electrospray Ionization Charge-State Distribution and Desorption Efficiency for Oligonucleotides. *Journal of the American Society for Mass Spectrometry*, 24(2), 257–264.

Chirgwin, J.M., Przybyla, A.E., MacDonald, R.J. & Rutter, W. J. (1979). Isolation of

Biologically Active Ribonucleic Acid from Sources Enriched in Ribonuclease.o Title. *Biochemistry*, 18, 5294–5299.

Cibiel, A., Pestourie, C. & Ducongé, F. (2012). In Vivo Uses of Aptamers Selected against Cell Surface Biomarkers for Therapy and Molecular Imaging. *Biochimie*, 94(7), 1595–606.

Cohen, M. G., Purdy, D. A., Rossi, J. S., Grinfeld, L. R., Myles, S. K., Aberle, L. H., et al. (2010). First Clinical Application of an Actively Reversible Direct Factor IXa Inhibitor as an Anticoagulation Strategy in Patients Undergoing Percutaneous Coronary Intervention. *Circulation*, 122(6), 614–22.

Corey, D. R. (2007). Chemical Modification: The Key to Clinical Application of RNA Interference? *The Journal of clinical investigation*, 117(12), 3615–22.

Crooke, S. T. (1999). Molecular Mechanisms of Action of Antisense Drugs. *Biochimica et biophysica acta*, 1489(1), 31–44.

Cummings, M, R. (2014). *Human Heredity: Principles and Issues*. Boston: Brooks/Cole, a division of Cengage Learning.

Dean, N. M. & Bennett, C. F. (2003). Antisense Oligonucleotide-Based Therapeutics for Cancer. *Oncogene*, 22(56), 9087–9096.

Deleavey, G. F. & Damha, M. J. (2012). Designing Chemically Modified Oligonucleotides for Targeted Gene Silencing. *Chemistry & biology*, 19(8), 937–54.

Dellinger, D. J., Betley, J. R., Wyrzykiewicz, T. K. & Caruthers, M. H. (2005). Synthesis of DNA Using a New Two-Step Cycle, in: *Oligonucleotide Synthesis*, (pp. 1–16). Methods in Molecular Biology. Humana Press.

Dickman, M. J. (2011). Ion Pair Reverse-Phase Chromatography: A Versatile Platform for the Analysis of RNA. *Chromatography Today*, (March), 22–26.

Dickman, M. J. (2005). Effects of Sequence and Structure in the Separation of Nucleic Acids Using Ion Pair Reverse Phase Liquid Chromatography. *Journal of chromatography. A*, 1076(1–2), 83–9.

Dickman, M. J., Conroy, M. J., Grasby, J. A. & Hornby, D. P. (2002). RNA Footprinting

Analysis Using Ion Pair Reverse Phase Liquid Chromatography. *Rna*, 8(2), 247–251.

Donovan, W.P. and Kushner, S. R. (1986). Polynucleotide Phosphorylase and Ribonuclease II Are Required for Cell Viability and mRNA Turnover in Escherichia Coli K-12. *Proc. Natl Acad. Sci.*, 83, 120–124.

Doudna, J. a & Cech, T. R. (2002). The Chemical Repertoire of Natural Ribozymes. *Nature*, 418(6894), 222–8.

Duan, C.-G., Wang, C.-H. & Guo, H.-S. (2012). Application of RNA Silencing to Plant Disease Resistance. *Silence*, 3(1), 5.

Dykxhoorn, D. M., Novina, C. D. & Sharp, P. A. (2003). Killing the Messenger: Short RNAs That Silence Gene Expression. *Nature Reviews Molecular Cell Biology*, 4(6), 457–467.

Eeltink, S., Wouters, S., Dores-sousa, J. L. & Svec, F. (2017). Advances in Organic Polymer-Based Monolithic Column Technology for High-Resolution Liquid Chromatography-Mass Spectrometry Profiling of Antibodies, Intact Proteins, Oligonucleotides, and Peptides. *Journal of Chromatography A*, (2016), 1–14.

Ellington, A. D. & Szostak, J. W. (1990). In Vitro Selection of RNA Molecules That Bind Specific Ligands. *Nature*, 346(6287), 818–822.

Emmerechts, G., Barbé, S., Herdewijn, P., Anné, J. & Rozenski, J. (2007). Post-Transcriptional Modification Mapping in the Clostridium Acetobutylicum 16S rRNA by Mass Spectrometry and Reverse Transcriptase Assays. *Nucleic acids research*, 35(10), 3494–503.

Emmerechts, G., Maes, L., Herdewijn, P., Anné, J. & Rozenski, J. (2008). Characterization of the Posttranscriptional Modifications in Legionella Pneumophila Small-Subunit Ribosomal RNA. *Chemistry & biodiversity*, 5(12), 2640–53.

Farand, J. & Gosselin, F. (2009). De Novo Sequence Determination of Modified Oligonucleotides. *Analytical chemistry*, 81(10), 3723–30.

Fenn, J. B., Mann, M., Meng, C. K., Wong, S. F. & Whitehouse, C. M. (1989). Electrospray Ionization for Mass Spectrometry of Large Biomolecules. *Science*

(New York, N.Y.), 246(4926), 64–71.

Fernandes, M. X., Ortega, A., Martínez, M. C. L. & Torre, J. G. De. (2002). Calculation of Hydrodynamic Properties of Small Nucleic Acids from Their Atomic Structure. , 30(8), 1782–1788.

Fire, A., Xu, S., Montgomery, M. K., Kostas, S. A., Driver, S. E. & Mello, C. C. (1998). Potent and Specific Genetic Interference by Double-Stranded RNA in Caenorhabditis Elegans. *Nature*, 391(6669), 806–11.

Floyd, R. W., Stone, M. P. & Joklik, W. K. (1974). Separation of Single-Stranded Ribonucleic Acids by Acrylamide-Agarose-Urea Gel Electrophoresis. *Analytical biochemistry*, 59(2), 599–609.

Fueangfung, S., Yuan, Y. & Fang, S. (2014). Nucleosides , Nucleotides and Nucleic Acids Denaturing Reversed-Phase HPLC Using a Mobile Phase Containing Urea for Oligodeoxynucleotide Analysis. *Nucleosides, Nucleotides and Nucleic Acids*, 33, 487–488.

Gilar, M. (2001). Analysis and Purification of Synthetic Oligonucleotides by Reversed-Phase High-Performance Liquid Chromatography with Photodiode Array and Mass Spectrometry Detection. *Analytical Biochemistry*, 298(2), 196–206.

Gjerde, D. ., Hoang, L. & Hornby, D. (2009). *RNA Purification and Analysis*. Weinheim: WILEY-VCH Verlag GmbH & Co. KGaA.

Glisin,V., Crkvenjakov,R. and Byus, C. (1974). Ribonucleic Acid Isolated by Cesium Chloride Centrifugation. *Biochemisity*, 13, 2633–2637.

Goda, S. K. & Minton, N. P. (1995). No A Simple Procedure for Gel Electrophoresis and Northern Blotting of RNA. *Nucleic Acids Research*, 23(16), 3357–3358.

Gong, L. & McCullagh, J. S. O. (2014). Comparing Ion-Pairing Reagents and Sample Dissolution Solvents for Ion-Pairing Reversed-Phase Liquid Chromatography/electrospray Ionization Mass Spectrometry Analysis of Oligonucleotides. *Rapid Communications in Mass Spectrometry*, 28(4), 339–350.

Gordon, K. H. J. & Waterhouse, P. M. (2007). RNAi for Insect-Proof Plants. *Nature Biotechnology*, 25(11), 1231–1232.

Greig, M. & Griffey, R. H. (1995). Utility of Organic Bases for Improved Electrospray Mass Spectrometry of Oligonucleotides. *Rapid communications in mass spectrometry : RCM*, 9(1), 97–102.

Guerrier-Takada, C., Gardiner, K., Marsh, T., Pace, N. & Altman, S. (1983). The RNA Moiety of Ribonuclease P Is the Catalytic Subunit of the Enzyme. *Cell*, 35(3 Pt 2), 849–57.

Guo, Y., Srinivasula, S. M., Druilhe, A., Fernandes-Alnemri, T. & Alnemri, E. S. (2002). Caspase-2 Induces Apoptosis by Releasing Proapoptotic Proteins from Mitochondria. *The Journal of biological chemistry*, 277(16), 13430–7.

Haasnoot, J., Westerhout, E. M. & Berkhout, B. (2007). RNA Interference against Viruses: Strike and Counterstrike. *Nature Biotechnology*, 25, 1435.

Hiroyoshi, M., Nakanishi, K., Soga, N., Ishizuka, N. & Tanaka, N. (1996). Octadecylsilylated Porous Silica Rods as Separation Media for Reversed-Phase Liquid Chromatography. *Analytical Chemistry*, 68(19), 3498–3501.

Hoffman, N. E. & Liao, J. C. (1977). Reversed Phase High Performance Liquid Chromatographic Separations of Nucleotides in the Presence of Solvophobic Ions. *Analytical chemistry*, 49(14), 2231–4.

Hoffmann, E. D. & Stroobant, V. (2007). *Mass Spectrometry: Principles and Applications* (D. Hoffmann, Edmond and V. Stroobant, Eds.). Chichester, West Sussex: WILEY-VCH Verlag GmbH & Co. KGaA.

Hölzl, G., Oberacher, H., Pitsch, S., Stutz, A. & Huber, C. G. (2005). Analysis of Biological and Synthetic Ribonucleic Acids by Liquid Chromatography-Mass Spectrometry Using Monolithic Capillary Columns. *Analytical chemistry*, 77(2), 673–80.

Horvath, C., Melander, W., Molnar, I. & Molnar, P. (1977). Enhancement of Retention by Ion-Pair Formation in Liquid Chromatography with Nonpolar Stationary Phases. *ANALYTICAL CHEMISTRY*, 49(December), 2295–2305.

Hossain, M. & Limbach, P. A. (2007). Mass Spectrometry-Based Detection of Transfer RNAs by Their Signature Endonuclease Digestion Products. , 295–303.

Huang, Z., Jayaseelan, S., Hebert, J., Seo, H. & Niu, L. (2013). Single-Nucleotide

Resolution of RNAs up to 59 Nucleotides by High-Performance Liquid Chromatography. *Analytical biochemistry*, 435(1), 35–43.

Huber, C., Oefner, P., Presuss, E. & Bonn, G. . (1993). High-Resolution Liquid Chromatography of DNA Fragments on Non-Porous Poly(styrene-Divinylbenzene) Particles. *Nucleic Acids Research*, 21(5), 1061–1066.

Huber, C. G. (1998). Micropellicular Stationary Phases for High-Performance Liquid Chromatography of Double-Stranded DNA. *Journal of Chromatography A*, 806(1), 3–30.

Huber, C. G. & Buchmeiser, M. R. (1998). On-Line Cation Exchange for Suppression of Adduct Formation in Negative-Ion Electrospray Mass Spectrometry of Nucleic Acids. *Analytical chemistry*, 70(24), 5288–95.

Huber, C. G. & Krajete, A. (1999). Analysis of Nucleic Acids by Capillary Ion-Pair Reversed-Phase HPLC Coupled to Negative-Ion Electrospray Ionization Mass Spectrometry. *Analytical chemistry*, 71(17), 3730–9.

Huber, C. G. & Oberacher, H. (2002). Analysis of Nucleic Acids by on-Line Liquid Chromatography-Mass Spectrometry. *Mass spectrometry reviews*, 20(5), 310–43.

Huber, C. G., Oefner, P. J. & Bonn, G. K. (1992). High-Performance Liquid Chromatographic Separation of Detritylated Oligonucleotides on Highly Cross-Linked Poly-(Styrene-Divinylbenzene) Particles. *Journal of Chromatography A*, 599(1–2), 113–118.

Huber, C. G., Oefner, P. J. & Bonn, G. K. (1993). High-Resolution Liquid Chromatography of Oligonucleotides on Nonporous Alkylated Styrene-Divinylbenzene Copolymers. *Analytical Biochemistry*, 212(2), 351–358.

Huber, C. G., Oefner, P. J. & Bonn, G. K. (1995). Rapid and Accurate Sizing of DNA Fragments by Ion-Pair Chromatography on Alkylated Nonporous Poly(styrene-Divinylbenzene) Particles. *Analytical Chemistry*, 67(3), 578–585.

Huck, C. W. and & Bonn, G. K. (2005). Poly(Styrene-Divinylbenzene) Based Media for Liquid Chromatography. *Chem. Eng. Technol*, 28(12), 1457–1469.

Ivleva, V. B., Yu, Y.-Q. & Gilar, M. (2010). Ultra-Performance Liquid Chromatography/tandem Mass Spectrometry (UPLC/MS/MS) and UPLC/MS E

Analysis of RNA Oligonucleotides. *Rapid Communications in Mass Spectrometry*, 24(17), 2631–2640.

Ivleva, V. B., Yu, Y. Q. & Gilar, M. (2008). *UPLC Synapt MS/MS Method for Structural Characterisation of siRNA Oligonucleotides*. Waters Corporation.

Jacob, F. & Monod, J. (1961). Genetic Regulatory Mechanisms in the Synthesis of Proteins. *Journal of Molecular Biology*, 3(3), 318–356.

Jilge, G., Unger, K. K., Esser, U., Schäfer, H.-J., Rathgeber, G. & Müller, W. (1989). Evaluation of Advanced Silica Packings for the Separation of Biopolymers by High-Performance Liquid Chromatography. *Journal of Chromatography A*, 476, 37–48.

Karas, M. (1996). Matrix-Assisted Laser Desorption Ionization MS: A Progress Report. *Biochemical Society Transactions*, 24(3), 897–900.

Karas, M. & Hillenkamp, F. (1988). Laser Desorption Ionization of Proteins with Molecular Masses Exceeding 10,000 Daltons. *Analytical Chemistry*, 60(20), 2299–2301.

Keefe, A. D., Pai, S. & Ellington, A. (2010). Aptamers as Therapeutics. *Nature reviews. Drug discovery*, 9(7), 537–50.

Kennerdell, J. R. & Carthew, R. W. (1998). Use of dsRNA-Mediated Genetic Interference to Demonstrate That Frizzled and Frizzled 2 Act in the Wingless Pathway. *Cell*, 95(7), 1017–26.

Kim, S. H., Suddath, F. L., Quigley, G. J., McPherson, A., Sussman, J. L., Wang, A. H., et al. (1974). Three-Dimensional Tertiary Structure of Yeast Phenylalanine Transfer RNA. *Science (New York, N.Y.)*, 185(4149), 435–40.

Knox, J. H. & Jurand, J. (1976). Separation of Catecholamines and Their Metabolites by Adsorption, Ion-Pair and Soap Chromatography. *Journal of chromatography*, 125(1), 89–101.

Kobayashi, H., Eckhardt, S. G., Lockridge, J. A., Rothenberg, M. L., Sandler, A. B., O'Bryant, C. L., et al. (2005). Safety and Pharmacokinetic Study of RPI.4610 (ANGIOZYME), an Anti-VEGFR-1 Ribozyme, in Combination with Carboplatin and Paclitaxel in Patients with Advanced Solid Tumors. *Cancer chemotherapy*

and pharmacology, 56(4), 329–36.

Kowalak, J. A., Pomerantz, S. C., Crain, P. F. & Mccloskeyl, J. A. (1993). A Novel Method for the Determination of Post- Transcriptional Modification in RNA by Mass Spectrometry. , 21(19), 4577–4585.

Kraak, J. C. & Bijster, P. (1977). Determination of Amitriptyline and Some of Its Metabolites in Blood by High-Pressure Liquid Chromatography. *Journal of chromatography*, 143(5), 499–512.

Kruger, K., Grabowski, P. J., Zaug, A. J., Sands, J., Gottschling, D. E. & Cech, T. R. (1982). Self-Splicing RNA: Autoexcision and Autocyclization of the Ribosomal RNA Intervening Sequence of Tetrahymena. *Cell*, 31(1), 147–57.

Kung, A., Kilby, P. M., Portwood, D. E. & Dickman, M. J. (2018). Quantification of dsRNA Using Stable Isotope Labeling Dilution Liquid Chromatography/mass Spectrometry. *Rapid Communications in Mass Spectrometry*, 32(7), 590–596.

Lanford, R. E., Hildebrandt-Eriksen, E. S., Petri, A., Persson, R., Lindow, M., Munk, M. E., et al. (2010). Therapeutic Silencing of microRNA-122 in Primates with Chronic Hepatitis C Virus Infection. *Science (New York, N.Y.)*, 327(5962), 198–201.

Larsen, B. S. & McEwen, C. N. (Eds.). (1998). *Mass Spectrometry of Biological Materials*. New York: Marcel Dekker.

Lee, R. C., Feinbaum, R. L. & Ambros, V. (1993). The C. Elegans Heterochronic Gene Lin-4 Encodes Small RNAs with Antisense Complementarity to Lin-14. *Cell*, 75(5), 843–54.

Lehrach, H., Diamond, D., Wozney, J. M. & Boedtker, H. (1977). RNA Molecular Weight Determinations by Gel Electrophoresis under Denaturing Conditions, a Critical Reexamination. *Biochemistry*, 16(21), 4743–4751.

Levin, D. S., Shepperd, B. T. & Gruenloh, C. J. (2011). Combining Ion Pairing Agents for Enhanced Analysis of Oligonucleotide Therapeutics by Reversed Phase-Ion Pairing Ultra Performance Liquid Chromatography (UPLC). *Journal of chromatography. B, Analytical technologies in the biomedical and life sciences*, 879(19), 1587–95.

Li, X., Zhang, M. & Zhang, H. (2011). RNA Interference of Four Genes in Adult

Bactrocera Dorsalis by Feeding Their dsRNAs. *PLoS ONE*, 6(3).

Liang, J. C., Bloom, R. J. & Smolke, C. D. (2011). Engineering Biological Systems with Synthetic RNA Molecules. *Molecular cell*, 43(6), 915–26.

Limbach, P. A., Crain, P. F. & McCloskey, J. A. (1995). Characterization of Oligonucleotides and Nucleic Acids by Mass Spectrometry. *Current opinion in biotechnology*, 6(1), 96–102.

Lin-Chao, S. and Bremer, H. (1986). Effect of the Bacterial Growth Rate on Replication Control of Plasmid pBR322 in Esherichia Coli. *Mol. Gen. Genet*, 203, 143–149.

Maa, Y. & Horvath, C. (1988). RAPID ANALYSIS OF PROTEINS AND PEPTIDES BY REVERSED-PHASE CHROMATOGRAPHY WITH POLYMERIC MICROPELLICULAR SORBENTS. *Journal of Chromatography*, 445, 71–86.

Macpherson, J. L., Boyd, M. P., Arndt, A. J., Todd, A. V, Fanning, G. C., Ely, J. A., et al. (2005). Long-Term Survival and Concomitant Gene Expression of Ribozyme-Transduced CD4+ T-Lymphocytes in HIV-Infected Patients. *The journal of gene medicine*, 7(5), 552–64.

Mamyrin, B. A., Karataev, V. I., Shmikk, D. V & Zagulin, V. A. (1973). The Mass-Reflectron, a New Nonmagnetic Time-of-Flight Mass Spectrometer with High Resolution. *Sov. Phys. - JETP*, 37(1), 45–48.

Mao, Y.-B., Cai, W.-J., Wang, J.-W., Hong, G.-J., Tao, X.-Y., Wang, L.-J., et al. (2007). Silencing a Cotton Bollworm P450 Monooxygenase Gene by Plant-Mediated RNAi Impairs Larval Tolerance of Gossypol. *Nature Biotechnology*, 25(11), 1307–1313.

Maori, E., Paldi, N., Shafir, S., Kalev, H., Tsur, E., Glick, E., et al. (2009). IAPV, a Bee-Affecting Virus Associated with Colony Collapse Disorder Can Be Silenced by dsRNA Ingestion. *Insect Molecular Biology*, 18(1), 55–60.

McCarthy, S. M., Gilar, M. & Gebler, J. (2009). Reversed-Phase Ion-Pair Liquid Chromatography Analysis and Purification of Small Interfering RNA. *Analytical biochemistry*, 390(2), 181–8.

McGinnis, A. C., Grubb, E. C. & Bartlett, M. G. (2013). Systematic Optimization of Ion-Pairing Agents and Hexafluoroisopropanol for Enhanced Electrospray Ionization

Mass Spectrometry of Oligonucleotides. *Rapid Communications in Mass Spectrometry*, 27(23), 2655–2664.

McMaster, G. K. & Carmichael, G. G. (1977). Analysis of Single- and Double-Stranded Nucleic Acids on Polyacrylamide and Agarose Gels by Using Glyoxal and Acridine Orange. *Proceedings of the National Academy of Sciences of the United States of America*, 74(11), 4835–8.

Melnikova, I. (2007). RNA-Based Therapies. *Nature Reviews Drug Discovery*, 6(11), 863–864.

Michienzi, A., Castanotto, D., Lee, N., Li, S., Zaia, J. A. & Rossi, J. J. (2003). RNA-Mediated Inhibition of HIV in a Gene Therapy Setting. *Annals of the New York Academy of Sciences*, 1002, 63–71.

Misra, V. K. & Draper, D. E. (1998). On the Role of Magnesium Ions in RNA Stability. *Biopolymers*, 48(2–3), 113–35.

Monia, B. P., Lesnik, E. A., Gonzalez, C., Lima, W. F., McGee, D., Guinosso, C. J., et al. (1993). Evaluation of 2′-Modified Oligonucleotides Containing 2′-Deoxy Gaps as Antisense Inhibitors of Gene Expression. *Journal of Biological Chemistry*, 268(19), 14514–14522.

Mooers, B. H. & Singh, A. (2011). The Crystal Structure of an oligo(U):pre-mRNA Duplex from a Trypanosome RNA Editing Substrate. *Rna*, 17, 1870–1883.

Moras, D., Comarmond, M. B., Fischer, J., Weiss, R., Thierry, J. C., Ebel, J. P., et al. (1980). Crystal Structure of Yeast tRNAAsp. *Nature*, 288(5792), 669–674.

Morris, H. R., Paxton, T., Dell, A., Langhorne, J., Berg, M., Bordoli, R. S., et al. (1996). High Sensitivity Collisionally-Activated Decomposition Tandem Mass Spectrometry on a Novel Quadrupole/Orthogonal-Acceleration Time-of-Flight Mass Spectrometer. *Rapid Communications in Mass Spectrometry*, 10(8), 889–896.

Muddiman, D. C., Cheng, X., Udseth, H. R. & Smith, R. D. (1996). Charge-State Reduction with Improved Signal Intensity of Oligonucleotides in Electrospray Ionization Mass Spectrometry. *Journal of the American Society for Mass Spectrometry*, 7(8), 697–706.

Murgha, Y. E., Rouillard, J.-M. & Gulari, E. (2014). Methods for the Preparation of Large Quantities of Complex Single-Stranded Oligonucleotide Libraries. *PloS one*, 9(4), e94752.

Murray, J. B., Collier, A. K. & Arnold, J. R. P. (1994). A General Purification Procedure for Chemically Synthesized Oligoribonucleotides. *Analytical Biochemistry*, 218(1), 177–184.

Ngô, H., Tschudi, C., Gull, K. & Ullu, E. (1998). Double-Stranded RNA Induces mRNA Degradation in Trypanosoma Brucei. *Proceedings of the National Academy of Sciences of the United States of America*, 95(25), 14687–92.

Nischang, I. (2012). On the Chromatographic Efficiency of Analytical Scale Column Format Porous Polymer Monoliths : Interplay of Morphology and Nanoscale Gel Porosity. *Journal of Chromatography A*, 1236, 152–163.

Nischang, I. (2013). Porous Polymer Monoliths : Morphology , Porous Properties , Polymer Nanoscale Gel Structure and Their Impact on Chromatographic Performance. *Journal of Chromatography A*, 1287, 39–58.

Nischang, I. (2014). Impact of Biomolecule Solute Size on the Transport and Performance Characteristics of Analytical Porous Polymer Monoliths. *Journal of Chromatography A*, 1354, 56–64.

Nischang, I. & Brüggemann, O. (2010). On the Separation of Small Molecules by Means of Nano-Liquid Chromatography with Methacrylate-Based Macroporous Polymer Monoliths. *Journal of Chromatography A*, 1217(33), 5389–5397.

Nischang, I., Teasdale, I. & Brüggemann, O. (2011). Porous Polymer Monoliths for Small Molecule Separations : Advancements and Limitations. , 2289–2304.

Nolte, A., Ott, K., Rohayem, J., Walker, T., Schlensak, C. & Wendel, H. P. (2013). Modification of Small Interfering RNAs to Prevent off-Target Effects by the Sense Strand. *New biotechnology*, 30(2), 159–65.

Null, A. P., Nepomuceno, A. I. & Muddiman, D. C. (2003). Implications of Hydrophobicity and Free Energy of Solvation for Characterization of Nucleic Acids by Electrospray Ionization Mass Spectrometry. *Analytical Chemistry*, 75(6), 1331–1339.

Nwokeoji, A. O., Kilby, P. M., Portwood, D. E. & Dickman, M. J. (2016). RNASwift: A Rapid, Versatile RNA Extraction Method Free from Phenol and Chloroform. *Analytical Biochemistry*, 512, 36–46.

Nwokeoji, A. O., Kung, A., Kilby, P. M., Portwood, D. E. & Dickman, M. J. (2017). Purification and Characterisation of dsRNA Using Ion Pair Reverse Phase Chromatography and Mass Spectrometry. *Journal of Chromatography A*, 1484, 14–25.

Oberacher, H. & Huber, C. G. (2002). Capillary Monoliths for the Analysis of Nucleic Acids by High-Performance Liquid Chromatography–electrospray Ionization Mass Spectrometry. *Trends in analytical chemistry*, 21(3), 166–174.

Oberacher, H., Oefner, P. J., Parson, W. & Huber, C. G. (2001). On-Line Liquid Chromatography Mass Spectrometry: A Useful Tool for the Detection of DNA Sequence Variation This Work Was Financially Supported by the Austrian Science Fund (P-14133-PHY) and the National Institutes of Health (HG01932). The Suggestion of Dr. *Angewandte Chemie (International ed. in English)*, 40(20), 3828–3830.

Oberacher, H., Parson, W., Hölzl, G., Oefner, P. J. & Huber, C. G. (2004). Optimized Suppression of Adducts in Polymerase Chain Reaction Products for Semi-Quantitative SNP Genotyping by Liquid Chromatography-Mass Spectrometry. *Journal of the American Society for Mass Spectrometry*, 15(12), 1897–906.

Oberacher, H., Parson, W., Mühlmann, R. & Huber, C. G. (2001). Analysis of Polymerase Chain Reaction Products by On-Line Liquid Chromatography−Mass Spectrometry for Genotyping of Polymorphic Short Tandem Repeat Loci. *Analytical Chemistry*, 73(21), 5109–5115.

Oberacher, H. & Pitterl, F. (2009). On the Use of ESI-QqTOF-MS/MS for the Comparative Sequencing of Nucleic Acids. *Biopolymers*, 91(6), 401–9.

Oefner, P. J. & Huber, C. G. (2002). A Decade of High-Resolution Liquid Chromatography of Nucleic Acids on Styrene-Divinylbenzene Copolymers. *Journal of chromatography. B, Analytical technologies in the biomedical and life sciences*, 782(1–2), 27–55.

Offord, c. (2016). Oligonucleotide Therapeutics Near Approval. *The scientist*.

Overington, J. P., Al-Lazikani, B. & Hopkins, A. L. (2006). How Many Drug Targets Are There? *Nature reviews. Drug discovery*, 5(12), 993–6.

Palli, S. R. (2014). RNA Interference in Colorado Potato Beetle: Steps toward Development of dsRNA as a Commercial Insecticide. *Current Opinion in Insect Science*, 6, 1–8.

Pasquinelli, A. E. & Ruvkun, G. (2002). Control of Developmental Timing by Micrornas and Their Targets. *Annual review of cell and developmental biology*, 18, 495–513.

Paul, W. (1990). Electromagnetic-Traps-for-Charged-and-Neutral-Particles-Paul.pdf. *Review of modern physics*, 62(3), 531–540.

Paulines, M. J. & Limbach, P. A. (2017). Stable Isotope Labeling for Improved Comparative Analysis of RNA Digests by Mass Spectrometry. , 551–561.

Phongsisay, V., Perera, V. N. & Fry, B. N. (2007). Evaluation of Eight RNA Isolation Methods for Transcriptional Analysis in Campylobacter Jejuni. *Journal of Microbiological Methods*, 68(2), 427–429.

Pinder, J. C., Staynov, D. Z. & Gratzer, W. B. (1974). Electrophoresis of RNA in Formamide. *Biochemistry*, 13(26), 5373–8.

Pollack, A. (2013). F.D.A. Approves Genetic Drug to Treat Rare Disease. *The New York Times*.

Popova, A. M. & Williamson, J. R. (2014). Quantitative Analysis of rRNA Modi Fi Cations Using Stable Isotope Labeling and Mass Spectrometry.

Premstaller, A., Oberacher, H. & Huber, C. (2000). High-Performance Liquid Chromatography-Electrospray Ionization Mass Spectrometry of Single- and Double-Stranded Nucleic Acids Using Monolithic Capillary Columns. *Analytical chemistry*, (18), 4386–93.

Rayleigh, Lord. (1882). XX. On the Equilibrium of Liquid Conducting Masses Charged with Electricity. *Philosophical Magazine Series 5*, 14(87), 184–186.

Rodrigues, A. E., Lu, Z. P. & Loureiro, J. M. (1993). Peak Resolution in Linear Chromatography Convection Effects of Intraparticle. *Journal of Chromatography*

A, 653, 189–198.

Roehr, B. (1998). Fomivirsen Approved for CMV Retinitis. *Journal of the International Association of Physicians in AIDS Care*, 4(10), 14–6.

Ronnee, Y. & Cummings, M. (2012). *Human Genetics and Society*.

Rozing, G. P. & Goetz, H. (1989). Fast Separation of Biological Macromolecules on Non-Porous, Microparticulate Columns. *Journal of Chromatography*, 476, 3–19.

Sanghvi, Y. S. (2011). A Status Update of Modified Oligonucleotides for Chemotherapeutics Applications. *Current Protocols in Nucleic Acid Chemistry*, (SUPPL.46).

Saurabh, S., Vidyarthi, A. S. & Prasad, D. (2014). RNA Interference: Concept to Reality in Crop Improvement. *Planta*, 239(3), 543–564.

Scherer, L. J. & Rossi, J. J. (2003). Approaches for the Sequence-Specific Knockdown of mRNA. *Nature biotechnology*, 21(12), 1457–65.

Sheehan, D., Lunstad, B., Yamada, C. M., Stell, B. G., Caruthers, M. H. & Dellinger, D. J. (2003). Biochemical Properties of Phosphonoacetate and Thiophosphonoacetate Oligodeoxyribonucleotides. *Nucleic Acids Research*, 31(14), 4109–4118.

Shevchenko, A., Chernushevich, I., Ens, W., Standing, K. G., Thomson, B., Wilm, M., et al. (1997). Rapid 'de Novo' Peptide Sequencing by a Combination of Nanoelectrospray, Isotopic Labeling and a Quadrupole/time-of-Flight Mass Spectrometer. *Rapid communications in mass spectrometry : RCM*, 11(9), 1015–24.

Sinha, N. D., Kuchimanchi, S. N., Miranda, G. & Shaikh, S. (2006). Manufacture of Therapeutic Oligonucleotides: Development of New Reagents and Processes. *Indian Journal of Chemistry Section B*, 45(10), 2297.

Škeříková, V. & Urban, J. (2013). Highly Stable Surface Modification of Hypercrosslinked Monolithic Capillary Columns and Their Application in Hydrophilic Interaction Chromatography. *Journal of Separation Science*, 36(17), 2806–2812.

Skopp, R. N. & Lane, L. C. (1988). Agarose Gel Electrophoresis of Denatured RNA with Silver Staining. *Analytical biochemistry*, 169(1), 132–7.

Smith, J. D. (1975). Mutants Which Allows Accumulation of tRNATyr Precursor Molecules. *Brookhaven symposia in biology*, (26), 1–11.

Snead, N. M. & Rossi, J. J. Biogenesis and Function of Endogenous and Exogenous siRNAs. *Wiley Interdisciplinary Reviews: RNA*, 1(1), 117–131.

Snyder, L. . & Dolan, J. . (2007). *High-Performance Gradient Elution: The Practical Application of the Linear*. Hoboken: John Wiley & Sons.

Soller, M. (2006). Pre-Messenger RNA Processing and Its Regulation: A Genomic Perspective. *Cellular and Molecular Life Sciences*, 63(7–8), 796–819.

Sprinzl, M., Wagner, T., Lorenz, S. & Erdmann, V. A. (1976). Regions of tRNA Important for Binding to the Ribosomal A and P Sites. *Biochemistry*, 15(14), 3031–3039.

Stead, M. B., Agrawal, A., Bowden, K. E., Nasir, R., Mohanty, B. K., Meagher, R. B., et al. (2012). RNAsnap???: A Rapid, Quantitative and Inexpensive, Method for Isolating Total RNA from Bacteria. *Nucleic Acids Research*, 40(20), 1–9.

Swiderski, P. M., Bertrand, E. L. & Kaplan, B. E. (1994). Polystyrene Reverse-Phase Ion-Pair Chromatography of Chimeric Ribozymes. *Analytical Biochemistry*, 216(1), 83–88.

Tanaka, N., Kobayashi, H., Nakanishi, K., Minakuchi, H. & Ishizuka, N. (2001). Monolithic LC Columns. *Analytical chemistry*, 73(15), 420A–429A.

Taoka, M., Nobe, Y., Hori, M., Takeuchi, A., Masaki, S., Yamauchi, Y., et al. (2015). A Mass Spectrometry-Based Method for Comprehensive Quantitative Determination of Post-Transcriptional RNA Modifications : The Complete Chemical Structure of Schizosaccharomyces Pombe Ribosomal RNAs. , 43(18),e115.

Taoka, M., Nobe, Y., Yamaki, Y., Yamauchi, Y., Ishikawa, H., Takahashi, N., et al. (2016). The Complete Chemical Structure of Saccharomyces Cerevisiae rRNA : Partial Pseudouridylation of U2345 in 25S rRNA by snoRNA snR9. , 44(18), 8951–8961.

Taoka, M., Yamauchi, Y., Nobe, Y., Masaki, S., Nakayama, H., Ishikawa, H., et al. (2009). An Analytical Platform for Mass Spectrometry-Based Identification and Chemical Analysis of RNA in Ribonucleoprotein Complexes. , 37(21), e140.

Thiel, K. W. & Giangrande, P. H. (2009). Therapeutic Applications of DNA and RNA Aptamers. *Oligonucleotides*, 19(3), 209–22.

Timmons, L., Court, D. L. & Fire, A. (2001). Ingestion of Bacterially Expressed dsRNAs Can Produce Specific and Potent Genetic Interference in Caenorhabditis Elegans. *Gene*, 263(1–2), 103–112.

Timmons, L. & Fire, A. (1998). No Title. *Nature*, 395(6705), 854–854.

Trilisky, E. I., Koku, H., Czymmek, K. J. & Lenhoff, A. M. (2009). Relation of Structure to Performance Characteristics of Monolithic and Perfusive Stationary Phases. , 1216, 6365–6376.

Trojer, L., Lubbad, S. H., Bisjak, C. P. & Bonn, G. K. (2006). Capillary Columns as Novel Styrene Stationary Phases for Biopolymer Separation. , 1117, 56–66.

Tsang, S. S., Yin, X., Guzzo-Arkuran, C., Jones, V. S. & Davison, A. J. (1993). Loss of Resolution in Gel Electrophoresis of RNA: A Problem Associated with the Presence of Formaldehyde Gradients. *BioTechniques*, 14(3), 380–1.

Unger, K, K., Janzen, R. & Jilge, G. (1987). Packings and Stationary Phases for Biopolymer Separations by HPLC. *Chromatographia*, 24(1), 144–154.

Unger, K. K. & Janzen, R. (1986). Packings and Stationary Phases in Preparative Column Liquid Chromatography. *Journal of chromatography*, 373(2), 227–64.

Unger, K. K., Skudas, R. & Schulte, M. M. (2008). Particle Packed Columns and Monolithic Columns in High-Performance Liquid Chromatography-Comparison and Critical Appraisal. *Journal of chromatography. A*, 1184(1–2), 393–415.

Voinnet, O., Vain, P., Angell, S. & Baulcombe, D. C. (1998). Systemic Spread of Sequence-Specific Transgene RNA Degradation in Plants Is Initiated by Localized Introduction of Ectopic Promoterless DNA. *Cell*, 95(2), 177–87.

Wacker, W. E. C. (1969). THE BIOCHEMISTRY OF MAGNESIUM*. *Annals of the New York Academy of Sciences*, 162(2), 717–726.

Waghmare, S. P. & Dickman, M. J. (2011). Characterization and Quantification of RNA Post-Transcriptional Modifications Using Stable Isotope Labeling of RNA in Conjunction with Mass Spectrometry Analysis. *Analytical Chemistry*, 83(12), 4894–4901.

Walcher, W., Oefner, P., Zolla, L. & Huber, C. G. (2002). Monolithic Capillary Columns for Liquid Chromatography – Electrospray Ionization Mass Spectrometry in Proteomic and Genomic Research. , 782, 111–125.

Waterhouse, P. M., Graham, M. W. & Wang, M. B. (1998). Virus Resistance and Gene Silencing in Plants Can Be Induced by Simultaneous Expression of Sense and Antisense RNA. *Proceedings of the National Academy of Sciences of the United States of America*, 95(23), 13959–64.

Watts, J. K. & Corey, D. R. (2012). Silencing Disease Genes in the Laboratory and the Clinic. *The Journal of Pathology*, 226(2), 365–379.

Wei, X. (2013). Coupling Activators for the Oligonucleotide Synthesis via Phosphoramidite Approach. *Tetrahedron*, 69(18), 3615–3637.

Wieland, M., Berschneider, B., Erlacher, M. D. & Hartig, J. S. (2010). Aptazyme-Mediated Regulation of 16S Ribosomal RNA. *Chemistry & biology*, 17(3), 236–42.

Wincott, F., DiRenzo, a, Shaffer, C., Grimm, S., Tracz, D., Workman, C., et al. (1995). Synthesis, Deprotection, Analysis and Purification of RNA and Ribozymes. *Nucleic acids research*, 23(14), 2677–84.

Wittmer, D. P., Nuessle, N. O. & Haney, W. G. (1975). Simultaneous Analysis of Tartrazine and Its Intermediates by Reversed Phase Liquid Chromatography. *Analytical chemistry*, 47(8), 1422–3.

Wong-Staal, F., Poeschla, E. M. & Looney, D. J. (1998). A Controlled, Phase 1 Clinical Trial to Evaluate the Safety and Effects in HIV-1 Infected Humans of Autologous Lymphocytes Transduced with a Ribozyme That Cleaves HIV-1 RNA. *Human gene therapy*, 9(16), 2407–25.

Wu, H., Lima, W. F. & Crooke, S. T. (1999). Properties of Cloned and Expressed Human RNase H1. *Journal of Biological Chemistry*, 274(40), 28270–28278.

Wu, Z., Gao, W., Phelps, M. A., Wu, D., Miller, D. D. & Dalton, J. T. (2004). Favorable Effects of Weak Acids on Negative-Ion Electrospray Ionization Mass Spectrometry. *Analytical chemistry*, 76(3), 839–47.

Xie, S. F., Svec, F. & Fréchet, J. M. J. (1997). Rigid Porous Polyacrylamide-Basedmonolithic Columns Containing Butyl Methacrylate as a Separation Mediumfor the Rapid Hydrophobic Interaction Chromatography of Proteins. *Chromatography A*, 65–72.

Yang, L., Zhang, X., Ye, M., Jiang, J., Yang, R., Fu, T., et al. (2011). Aptamer-Conjugated Nanomaterials and Their Applications. *Advanced Drug Delivery Reviews*, 63(14–15), 1361–1370.

Ylmaz, M., Ozic, C. & Gok, L. (2012). Principles of Nucleic Acid Separation by Agarose Gel Electrophoresis, in: Sameh Magdeldin (Ed.), *Gel Electrophoresis - Principles and Basics*, (pp. 33–40). Rijeka: InTech.

Appendix

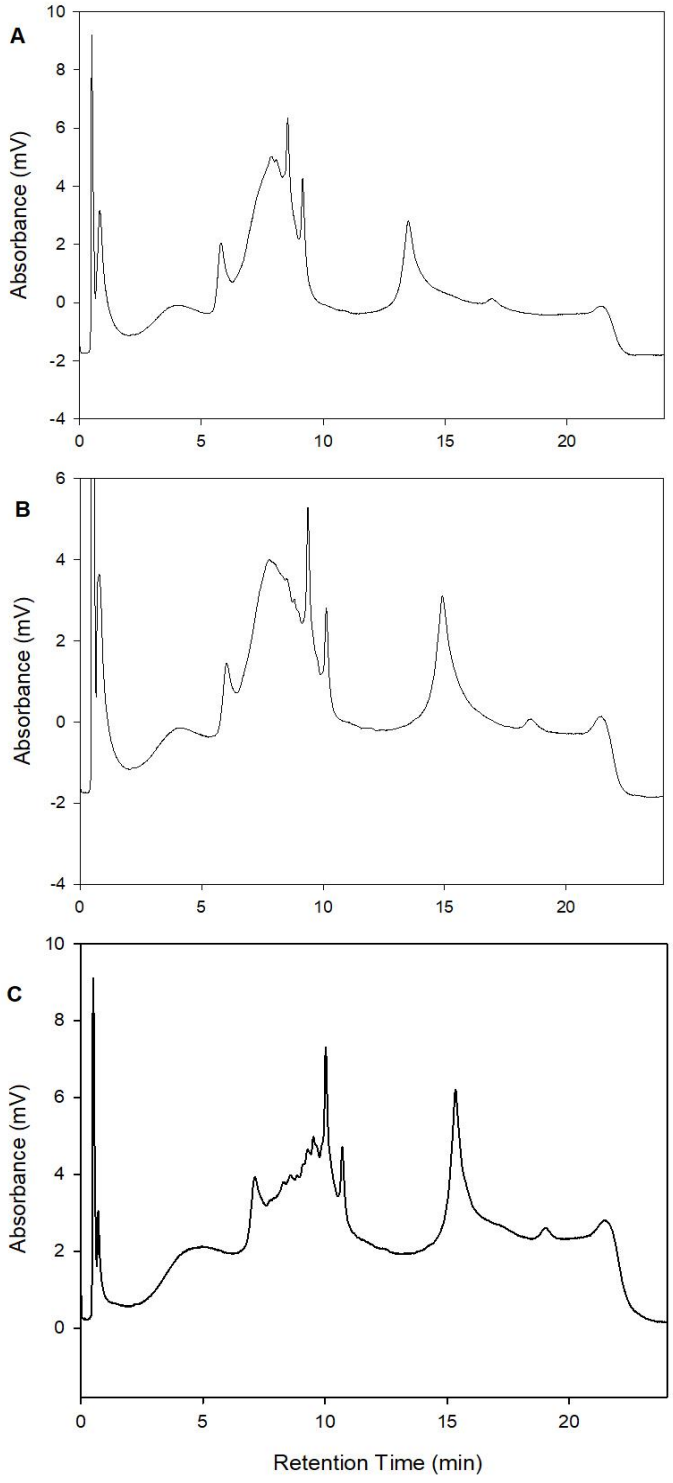

Appendix A1 The IP RP HPLC analysis of *E. coli* expressed with 765 bp dsRNA extracted using TRIzol Max performed in biological triplicate under gradient condition 12 (see chapter 2, 2.6.5.1).

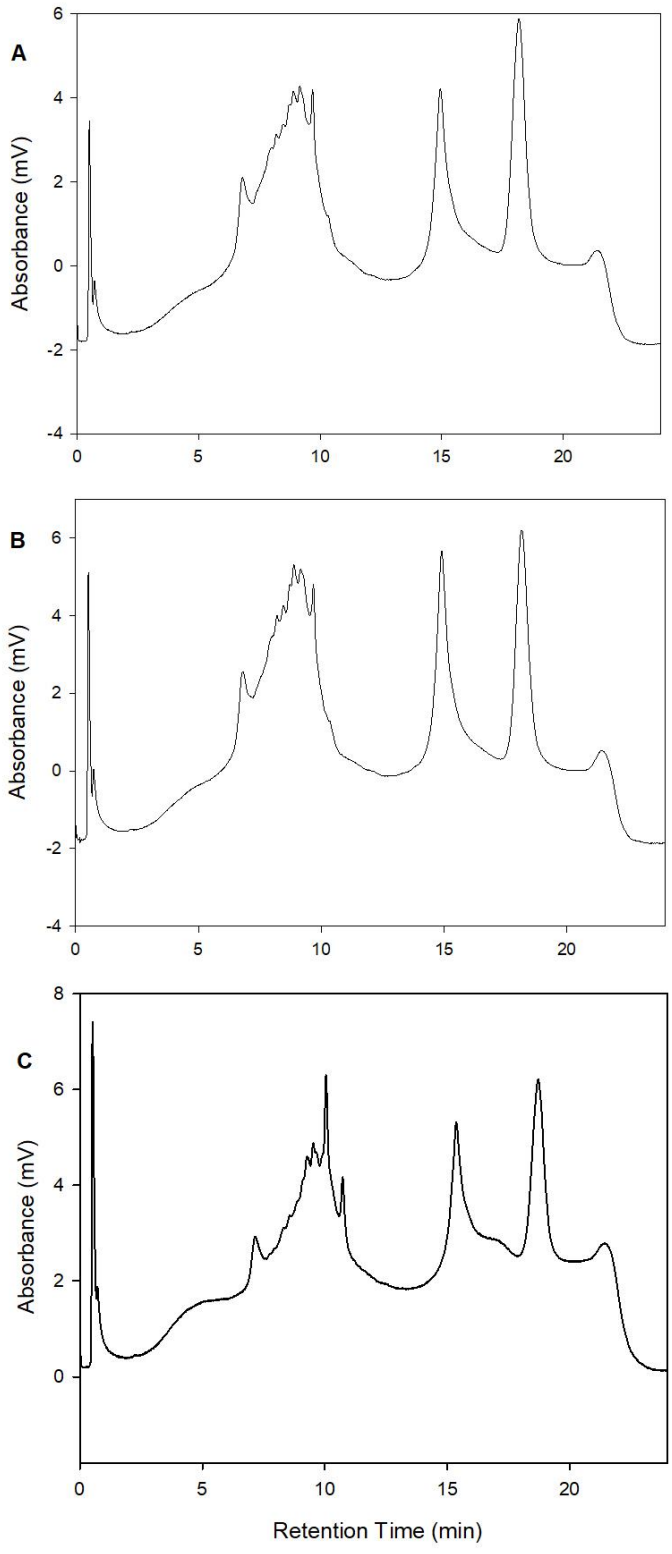

Appendix A2 The IP RP HPLC analysis of *E. coli* expressed with 765 bp dsRNA extracted using DNAzol performed in biological triplicate under gradient condition 12 (see chapter 2, 2.6.5.1).

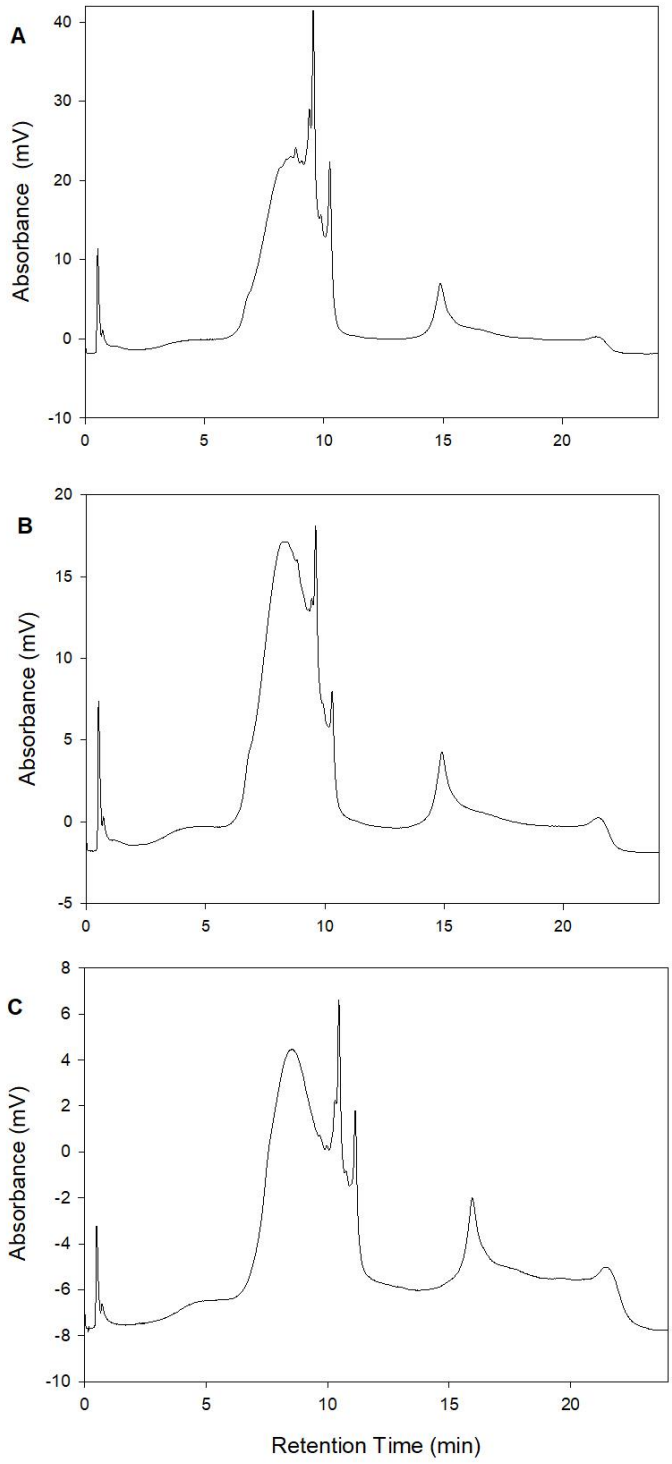

Appendix A3 The IP RP HPLC analysis of *E. coli* expressed with 765 bp dsRNA extracted using RNAzol performed in biological triplicate under gradient condition 12 (see chapter 2, 2.6.5.1).